11-5-2003

Characterization and Formation of Particulate Nitrate in a Coastal Area

Melissa Cheryl Foster Evans
University of South Florida

Characterization and Formation of Particulate Nitrate in a Coastal Area

by

Melissa Cheryl Foster Evans

A dissertation submitted in partial fulfillment
of the requirements for the degree of
Doctor of Philosophy
Department of Chemistry
College of Arts and Sciences
University of South Florida

Co-Major Professor: Noreen D. Poor, Ph.D.
Co-Major Professor: Julie P. Harmon, Ph.D.
Scott W. Campbell, Ph.D.
Milton D. Johnston, Jr., Ph.D.

Date of Approval:
November 5, 2003

Keywords: mineral dust, modeling, nitric acid, sea salt, Tampa Bay

Dedication

To my loving husband.

Acknowledgements

Several people deserve special thanks for their contribution to this dissertation. I would like to extend my deepest gratitude to my advisor and co-major professor, Noreen D. Poor, for her unending support, motivation and guidance throughout this project. I feel extremely fortunate to have had the opportunity to work with such a dedicated individual.

I would like to thank my other co-major professor Julie P. Harmon, for her willingness to support me as I studied outside the department. I am extremely grateful for my committee members. Many thanks to Scott W. Campbell for his valuable insight, gentle spirit and encouragement. I am especially appreciative for his gift in teaching and devotion to students. Thanks to Milton D. Johnston, Jr., for his guidance and expertise. Thanks to Yehia Y. Hammad for serving as my defense chair and for his knowledge and instruction in aerosol science.

Many other individuals deserve thanks for their contribution to this project. I am grateful for the many graduate and undergraduate students I have had the pleasure of working with and for the assistance I have had from the Environmental Protection Commission of Hillsborough County.

I extend my gratitude to my family and friends for their unconditional love, encouragement and support.

This research was funded by the Florida Department of Environmental Protection and the Tampa Bay Estuary Program.

Table of Contents

List of Tables

List of Figures

List of Symbols and Abbreviations

α	mass accommodation coefficient
(ads)	adsorbed
ADS	annular denuder system
(aq)	aqueous phase
avg	average
B_x	fitting coefficient for electrolyte x
ºC	degree Centigrade
$\bar{c}$	molecular speed
C	concentration
cm	centimeter(s)
CRH	crystallization relative humidity
d	day(s)
$\bar{d}$	mean difference between data sets
D_a	particle aerodynamic diameter
den	denuded
D_g	particle geometric diameter
D_{HNO_3}	diffusion coefficient of nitric acid
dichot	dichotomous sampler

D_p	particle diameter
D_{p50}	particle diameter collected with 50% efficiency
DRH	deliquescent relative humidity
F	flux
F_{aq}	mass fraction of the aqueous phase
f_i	mass fraction of species *i*
FP	filter pack
F_{solid}	mass fraction of the solid phase
FTIR	Fourier transform infrared spectroscopy
(g)	gas phase
g	gram(s)
γ	uptake coefficient
$\gamma_{measured}$	measured uptake coefficient
γ_{net}	net uptake probability
$\gamma_{NH_4^+,NO_3^-}$	mean mixed activity coefficient of NH_4NO_3
γ_{rxn}	surface reaction probability
ha	hectare(s)
I_{NO_3}	nitrate accumulation rate
i	integer
k_{eq}	equilibrium coefficient
kg	kilogram(s)
kg-N	kilograms of nitrogen

kg-S	kilograms of sulfur
K_i	kernel function for species *i*
km	kilometer(s)
k_s	surface rate constant
(l)	liquid phase
L	liter(s)
m	meter(s)
m	molality
Max	maximum
MBL	marine boundary layer
M_i	molar mass of species *i*
min	minute(s)
Min	minimum
mL	milliliter(s)
MΩ	megohm
MOUDI	Micro-Orifice Uniform Deposit Impactor
mTorr	milliTorr(s)
μ	air viscosity
μeq	microequivalent(s)
μg	microgram(s)
μm	micrometer(s)
μmol	micromole(s)
MW	molecular weight

N	nitrogen
n	number of samples or observations
p	gas phase partial pressure
PM	particulate matter
PM_{10}	particulate matter less than 10 μm in diameter
$PM_{2.5}$	particulate matter less than 2.5 μm in diameter
$PM_{10-2.5}$	particulate matter ($2.5 < D_p < 10$ μm diameter)
PTFE	polytetrafluoroethylene
q	volumetric flow rate
r	correlation coefficient
RB	relative bias
RH	relative humidity
ρ_{aq}	density of aqueous phase
ρ_o	standard density (1 g cm^{-3})
ρ_p	particle density
ρ_s	density of solute
ρ_{solid}	density of the solid phase
ρ_w	density of water
RP	relative precision
RT	residence time
s	second(s)
(s)	solid phase

σ	standard deviation
S_-	Wilcoxon's signed rank test negative value
S_+	Wilcoxon's signed rank test positive value
S	sulfur
SD	standard deviation
soln	solution
St	Stokes number
t	paired t-test value
T	time
$t_{crit\ 95\%}$	$t_{critical}$ at the 95% confidence interval
$t_{critical}$	paired t-test critical value
$T_{critical}$	Wilcoxon's signed rank test critical value
$t_{obtained}$	paired t-test obtained value
$T_{obtained}$	Wilcoxon's signed rank test obtained value
TTU	Texas Tech University
TD	traveling distance of a particle
Tg	teragram(s) (10^{12} gram)
TSP	total suspended particulate matter
TT	traveling time of a particle
UD	undenuded
V_d	deposition velocity
V_i	molar volume of *i*
V_o	average air velocity

v/v	volume/volume
W	nozzle diameter
WS	wind speed
w_s	mass fraction of solute
w_w	mass fraction of water
w/v	weight/volume
w/w	weight/weight
{X}	thermodynamic activity of species X
X_i	mole fraction of *i*
yr	year(s)
$Z_{critical}$	Grubbs' outlier test critical value
$Z_{obtained}$	Grubbs' outlier test obtained value

Characterization and Formation of Particulate Nitrate in a Coastal Area

Melissa Cheryl Foster Evans

ABSTRACT

Particulate nitrates play important roles in the atmosphere. They consist mainly of NH_4NO_3 and $NaNO_3$, products from the reactions of gaseous HNO_3 with gaseous NH_3 and sea salt, respectively. The gas-to-particle phase conversion of nitrate changes its deposition characteristics and ultimately changes the transport and deposition rates of the locally produced species. Studies were conducted to develop background information on the particle concentrations and size distributions and the chemistry and kinetics behind the interactions.

The predominant nitrate species in the Tampa Bay area was identified as coarse mode $NaNO_3$. NH_4NO_3 was not detected as it has high volatility at ambient temperatures. Spatial distribution sampling determined a gradient of NaCl and $NaNO_3$ with increased distance from the coastal shore and an increase in the gas-to-particle conversion of nitric acid along a predominant air mass trajectory.

The EQUISOLV II thermodynamic equilibrium model was evaluated. It was determined that the model can be used to predict gas and size-distributed

particulate matter concentrations. The model was also used to examine the gas-to-particle partitioning of nitric acid to nitrate by NaCl and $CaCO_3$. Both sodium and calcium partitioned nitrate to the particle phase. The magnitude of the partitioning was directly dependent on the equilibrium coefficients.

The fine mode percentage of the total nitrate was determined using two methods. The results were used to expand the current data set to account for the coarse mode nitrate, and they indicated that particle nitrate accounted for 9% of the total nitrogen deposition flux to Tampa Bay.

The formation of particle nitrate was examined using a nitrate accumulation model. Results indicated that the equilibrium time for particles less than 10 μm in diameter was significantly less than their atmospheric residence time, with fastest conversion occurring under the highest relative humidity conditions.

This information is vital in the development of atmospheric nitrogen dry deposition estimates, which are used to assess water quality and nutrient loading. These data can be used to determine air-monitoring strategies and to develop models that account for the coarse particle nitrogen species.

Introduction

Eutrophication

The atmospheric deposition of nitrogen is a major concern for the Tampa Bay, Florida region (Tampa Bay National Estuary Program, 1996). Nitrogen is a primary limiting nutrient in marine waters (Conley, 2000; de Wit and Bendoricchio, 2001; Nixon et al., 1996) for phytoplankton growth (Pryor and Sorensen, 2000) and is a fundamental building block for plant cells (Pryor and Barthelmie, 2000a). Excess amounts of nitrogen can pollute the bay by accelerating phytoplankton growth (Burian et al., 2001; Tampa Bay National Estuary Program, 1996). These algal blooms, or increased abundance of phytoplankton, have implications for water quality, human health, and ecosystem health and productivity (Pryor and Barthelmie, 2000b). The algal blooms inhibit sufficient light penetration required for seagrass growth and result in seagrass death. This has a dramatic impact on the local environment, as the seagrasses serve as a protective habitat and feeding grounds for fish and shellfish. Partial or complete oxygen depletion (hypoxia or anoxia) is often seen following the algal blooms as the algae begin to decay (Burian et al., 2001; de Leeuw et al., 2001). The condition associated with excess nitrogen, algal blooms, oxygen depletion

and the degradation of water quality is known as eutrophication (Paerl, 2001; Tampa Bay National Estuary Program, 1996).

Research has indicated that approximately 29% (or 980 metric tons-N yr^{-1}) of the bay's total nitrogen loading comes from atmospheric deposition of pollutants directly to the surface of the bay (Burian et al., 2001; Patwardhan and Donigian Jr., 1995; Tampa Bay National Estuary Program, 1996; Zarbock et al., 1996). These estimates are actually much higher if deposition to the watershed is included, since much of this nitrogen will eventually enter the bay in stormwater runoff (Tampa Bay National Estuary Program, 1996). EPA estimates that as much as 67% of Tampa Bay's total nitrogen could come from the atmosphere (Patwardhan and Donigian Jr., 1995). Other major sources of nitrogen loading include point sources (19%) and fertilizer application (14%) (Patwardhan and Donigian Jr., 1995; Zarbock et al., 1996).

Dry and wet deposition are the two main processes by which nitrogen is transferred to surface waters. Dry deposition is the transfer of gaseous species and particles in the absence of precipitation and is determined by meteorological conditions, atmospheric conditions and particle and gas properties. In wet deposition, gaseous species and particles are transferred to the surface via precipitation (rain, fog, sleet and snow).

Dry deposition fluxes are difficult to measure and are often calculated under the assumption that the dry deposition flux is directly proportional to the concentration of the species (Caffrey et al., 1998; Poor et al., 2001; Seinfeld and Pandis, 1998),

$$F = V_d \times C \times 3.15576 \quad \text{(Equation 1)}$$

where F (kg ha^{-1} yr^{-1}) is the dry particle or gas deposition flux, V_d (cm s^{-1}) is the deposition velocity and C (μg m^{-3}) is the concentration of nitrogen. The V_d depends on particle size or Henry's constant for gaseous species, meteorological conditions and the characteristics of the depositing surface (Caffrey et al., 1998). Wet deposition fluxes are estimated using:

$$F = C \times P \quad \text{(Equation 2)}$$

where F (kg ha^{-1} yr^{-1}) is the wet deposition flux, C (μg m^{-3}) is the concentration and P (m yr^{-1}) is the precipitation rate (Luo et al., 2003).

Aerosols

Aerosols are defined as a suspension of liquid or solid particles in a gas (McMurry, 2000; Wayne, 2000). They are an extremely important component of our atmosphere; however, they are only partially understood. They play important roles in many biogeochemical cycles, acting as reaction sites and as carriers for many sorbed species (Dentener et al., 1996). Particles also contribute to smog episodes and light and radiation scattering (Seinfeld and Pandis, 1998). Aerosols are produced by natural and anthropogenic activities. Natural sources include sea spray, mineral dust, forest fires and volcanic emissions (Wayne, 2000). Anthropogenic activities predominantly include the burning of fossil fuels and biomasses and contribute mostly to the submicron (less than 1 μm diameter) particle concentrations. These particles are primary

pollutants, as they are emitted directly into the atmosphere (Finlayson-Pitts and Pitts Jr., 2000). Secondary pollutant or aerosol formation includes the gas-to-particle conversion of emitted primary pollutants, such as the oxidation of SO_2 to sulfate compounds.

There are two main size classifications of particles based on observed modes: (a) fine, those with a diameter less than 2.5 μm and (b) coarse, those with a diameter greater than 2.5 μm (Seinfeld and Pandis, 1998). This size distinction is important, as the two classes differ in their modes of production and removal, chemical composition, deposition and optical properties (Seinfeld and Pandis, 1998). Within the fine particle category are two distinct modes: (a) the nuclei mode, particles with a diameter of 0.005 to 0.1 μm and (b) the accumulation mode, diameter of 0.1 to 2.5 μm. Due to their size, nuclei mode particles compose a very small mass percent of all particulate matter. They are formed from combustion sources and nucleation of atmospheric species and are removed from the mode primarily through coagulation with larger particles. Accumulation mode particles comprise a significant amount of aerosol mass and surface area. These particles are formed through nuclei particle coagulation and from the growing of existing particles due to the condensation of gases. As indicated by its name, the accumulation mode has very inefficient removal mechanisms, resulting in long residence times (Seinfeld and Pandis, 1998). Mechanical processes generate the coarse mode particles. These particles have large gravitational settling velocities, allowing them to settle out of the atmosphere in a relatively short amount of time.

Sea Salt

Sea salt particles are considered to be the dominant particles originating from natural sources (Roth and Okada, 1998). They are the largest source of tropospheric particulate matter (Weis and Ewing, 1999) and are the principal constituent of the coarse particle mode (Fitzgerald, 1991). The global emission rate of sea salt is estimated at 1000 to 2000 Tg yr^{-1} (Jaenicke, 1993). Sea salts, which are primarily composed of NaCl, play an important role in our atmosphere, as they provide a reactive surface for many pollutants. Particulate sulfates can be formed from the gas-to-particle conversion of biogenically emitted SO_2 on sea salt particles. Heterogeneous chemical reactions with acidic species (i.e. HNO_3) result in the emission of volatile HCl, creating a source for HCl in the atmosphere (Roth and Okada, 1998).

Sea salts are produced at the ocean's surface by the mechanical wave action and the bursting of entrained air bubbles (Allen et al., 1996; de Leeuw et al., 2001; O'Dowd et al., 1997). The mechanical generation of aerosols results in a wide size range of particles produced from 0.1 to 100 μm in diameter (Andreas et al., 1995; O'Dowd et al., 1997). The majority of sea salt particles are found in the coarse mode with a diameter greater than 1 μm (Plate and Schulz, 1997). The coarse mode makes up over 95% of the total mass but only contributes to 5-10% of the total particle number (Seinfeld and Pandis, 1998).

Sea salt, as a primary component of marine aerosol, can affect the climate by scattering and absorbing radiation (Fitzgerald, 1991). Research has shown

that sea salt particles can be responsible for up to 75% of light scattering by aerosols (Clegg and Toumi, 1998; Murphy et al., 1998). The concentration of sea salt aerosol is a function of wind speed, relative humidity and turbulence (de Leeuw, 1986; Lovett, 1978; O'Dowd et al., 1997).

The relative humidity in the marine boundary layer is often above the deliquescent point of sea salt, the relative humidity point at which the substance absorbs atmospheric moisture to produce a saturated aqueous solution (Pilinis et al., 1989). The sorbed waters are unbound, and their quantity is governed by thermodynamic equilibrium. The deliquescent relative humidity for sodium chloride is 76% (Seinfeld and Pandis, 1998). Consequently, most sea salt aerosols exist as concentrated aqueous droplets of salt. The available surface waters allow for the scavenging of atmospheric gases, chemical transformations and volatilization of products (Erickson III et al., 1999).

Sea salts enriched in sulfur (as sulfate) are considered aged sea salts, with sulfur being greater than 20% (by weight) and sodium plus chloride greater than 60% (Ebert et al., 2000). Freshly emitted sea salts are primarily composed of sodium and chloride. These particles are categorized as fresh sea salts, distinguished as having sodium and chloride making up over 85% of the total mass. Over 90% of a fresh sea salt particle is 1:10 (by weight) magnesium and sodium chlorides (Laskin et al., 2002). Processing through reactions with other species results in the replacement of chloride with nitrate in both salts.

$NaCl_{(aq,s)} + HNO_{3(g)} \rightarrow NaNO_{3(aq,s)} + HCl_{(g)}$ (Reaction 1)

$MgCl_{2(aq,s)} + 2\ HNO_{3(g)} \rightarrow Mg(NO_3)_{2(aq,s)} + 2\ HCl_{(g)}$ (Reaction 2)

Magnesium and sodium are untouched by these reactions and are therefore used as signature elements for particle apportionment. Sea salt particles are primarily processed during the daytime hours, as gaseous NO_2 is photochemically converted into reactive gaseous HNO_3. Laskin et al. (2002) reported that daytime sea salt particles in Houston, Texas were found to be almost completely processed, or converted $NaNO_3$ particles. They noted by 8:00 a.m. chloride started to disappear from the particle composition and four to five hours later was completely eliminated. However, nighttime sea salt particles were found to be almost completely unprocessed, and their composition was close to that of seawater.

Mineral Dust

Mineral dust aerosols are formed from wind-blown soils. It is estimated that 1000 to 3000 Tg of mineral aerosol are emitted annually into the atmosphere (Dentener et al., 1996; Grassian, 2002). Mineral dusts play an important role as a sink for nitric acid, converting it into a coarse mode species, $Ca(NO_3)_2$.

$CaCO_{3(s)} + 2\ HNO_{3(g)} \rightarrow Ca(NO_3)_{2(aq,s)} + CO_{2(g)} + H_2O_{(g,aq)}$ (Reaction 3)

Dentener et al. (1996) stated, however, that the uptake of HNO_3 can take place only in mineral dust aerosols with a high enough alkalinity to overcome the acidity associated with uptake. The alkalinity of the mineral dust is to a great

extent determined by the concentration of $CaCO_3$. Soils in arid regions of the United States can contain 3 to 8% by weight Ca^{2+} (Dentener et al., 1996).

Sodium

A significant amount of particulate sodium exists in our atmosphere, as the "emission sources of sodium are widely spread on the Earth's surface" (Ooki et al., 2002). Sodium along with chloride is one of the largest trace components of sea spray, which accounts for 36% of the global sodium emissions (Ooki et al., 2002; Seinfeld and Pandis, 1998). Land-based mineral dust emissions contribute 42% of the total sodium emissions (Ooki et al., 2002; Seinfeld and Pandis, 1998). According to the 1987 California Air Resources Board emissions inventory, land-based sodium emissions were estimated at 5 metric tons day^{-1} (Jacobson, 1997). Land-based sources include paved road dust and diesel emissions.

Sodium can be found in the coarse and fine particle modes. Refuse incineration is considered to be the most significant source of fine particle sodium in urban air (Ooki et al., 2002). In Japan, refuse incineration accounted for 24-43% of the total sodium emissions and for 79-91% of the total anthropogenic sodium emissions (Ooki et al., 2002).

In marine environments, sodium is primarily seen in the coarse fraction. It is often used as an indicator for primary aerosols, as it is a conservative nonreactive species (Ten Brink, 1998).

Chloride

The primary source for particulate chloride is sea salt, as NaCl. Land-based sources for particulate chloride include biomass burning, fossil fuel burning, chemical manufacturing and soil dust (Jacobson, 1997). Gaseous chloride is also emitted through coal combustion (over 98%) and waste incineration (Saxena et al., 1994). Chloride is mainly distributed in the coarse mode, as NaCl. However, combustion sources contribute to fine mode chloride.

HCl can also be produced through the reaction of nitric acid with sodium chloride (Reaction 1). The production of HCl gas is termed a chloride-depletion process with respect to particulate chloride because chloride changes phase from particle to gas (Cheng et al., 2000). This reaction with sea salt plays a role in the halogen release over the marine boundary layer (Aristarain and Delmas, 2002), which may be linked to ozone depletion (Pryor and Sorensen, 2000). In freshly produced sea salt, Cl^-:Na^+ molar ratio is 1.17 (Zhuang et al., 1999a). Chloride depletion can be calculated using the estimated quantities of chloride compared to the experimental quantities.

$$\%Cl^- - dep = \frac{(1.174[Na^+] - [Cl^-])}{(1.174[Na^+])} \times 100\% \qquad \text{(Equation 3)}$$

Chloride depletion has been found to decrease with increasing particle size, suggesting a surface mechanism for the loss (Jordan et al., 2000). Two factors have been noted that affect the extent of chloride depletion. They include

relative humidity and the competition of Ca^{2+} with Na^{+} for the acidic gases (Zhuang et al., 1999a).

As nitric acid is taken up by the sea salt particle, it forces HCl into the gas phase. This process is due to the Henry's constant and the binary activity coefficient of both HNO_3 and HCl. The binary activity coefficient for dissolved HCl increases exponentially at high molalities, whereas the activity coefficient of dissolved nitric acid remains moderately low at high molalities (Jacobson, 1997; Jacobson et al., 1996). As HCl is released or degassed from the sea salt particle, the pH of the aerosol increases due to the loss of H^{+} (Brimblecombe and Clegg, 1988).

Nitrate

The primary oxidized reactive nitrogen compounds of concern are nitric acid (HNO_3) and particulate nitrate (NO_3^{-}). These compounds are considered secondary pollutants, as they are not directly emitted into the atmosphere (Blanchard, 1999). Nitric acid is produced through the gas phase oxidation of NO_x ($NO_X = NO + NO_2$) (Zhuang et al., 1999b), which is emitted directly into the atmosphere from anthropogenic activities, including the combustion of fossil fuels. Natural sources for nitrogen oxides include soil, volcanic emissions and lightning; they make up less than 10% of the total emissions (Erisman et al., 1998).

During daylight hours, HNO_3 is produced by NO_2 reaction with a hydroxyl radical (Blanchard et al., 2000; Seinfeld and Pandis, 1998):

$$\bullet OH + NO_2 \rightarrow HNO_3 \qquad \text{(Reaction 4)}$$

At night, HNO_3 is produced through a multi-step process (Blanchard et al., 2000; Seinfeld and Pandis, 1998):

$$O_3 + NO_2 \rightarrow \bullet NO_3 + O_2 \qquad \text{(Reaction 5)}$$

$$NO_2 + \bullet NO_3 \leftrightarrow N_2O_5 \qquad \text{(Reaction 6)}$$

$$N_2O_5 + H_2O \rightarrow 2\ HNO_3 \qquad \text{(Reaction 7)}$$

During atmospheric chemical processes, these oxides are transformed into more water-soluble and thermally stable pollutants (nitrates), which are subject to wet or dry atmospheric deposition (Ali-Mohamed and Jaffar, 2000; Mamane and Mehler, 1987; Pilinis and Seinfeld, 1987; Pio and Harrison, 1987; Russell and Cass, 1984; Watson et al., 1994).

Because there is no primary source for coarse particle nitrate, it is assumed to originate from atmospheric reactions of gaseous nitrogen species with coarse particles (Evans and Poor, 2001; Pakkanen et al., 1996b). Sea salt and mineral dust particles play an important role in the incorporation of nitrate aerosols in the coarse mode (greater than 2.5 μm). The oxidized nitrogen species (nitrous and nitric acids) can react with NaCl on the surface of sea salt aerosols or $CaCO_3$ on mineral dust to form $NaNO_3$ or $Ca(NO_3)_2$ and HCl (Reactions 1 and 3) (Clarke et al., 1999; de Leeuw et al., 2001; Dentener et al., 1996; Evans and Poor, 2001; Goodman et al., 2000; Pakkanen et al., 1996a; Tabazadeh et al., 1998; Ten Brink and Spoelstra, 1998; Zhuang et al., 1999b).

Because $NaNO_3$ is formed on the surface of an existing coarse mode sea salt or mineral dust particle, $NaNO_3$ and $Ca(NO_3)_2$ will be collected in the coarse mode (de Leeuw et al., 2001). The production of coarse mode nitrogen from gaseous HNO_3 greatly affects its deposition rate. Larger particles have a higher "efficiency of precipitational scavenging via inertial impaction" (de Leeuw et al., 2001) and a change in gravitational settling velocities, V_d, as compared to gas phase species. This change in deposition rate may change current nitrogen loading estimates when accounting for coarse nitrate particles (Torseth et al., 2000).

Ammonium

Ammonia, NH_3, is the predominant alkaline atmospheric gas (Seinfeld and Pandis, 1998) and is a primary pollutant. Over 90% is emitted from agricultural practices as animal waste and fertilizer loss (Erisman et al., 1998; Seinfeld and Pandis, 1998).

Other ammonia sources include landfills, wastewater treatment plants, industry and combustion. Industrial sources release ammonia during the manufacturing of ammonia-based products, such as fertilizer. It is also used to make nitric acid and to remove NO_X from industrial coal boiler flue gases (Chang et al., 2003).

Ammonia is readily absorbed by water and soil surfaces, resulting in a relatively low residence time of approximately 10 days (Seinfeld and Pandis,

1998). In 1994, the total global ammonia emissions were estimated at 45 Tg-N yr^{-1} (Dentener and Crutzen, 1994; Seinfeld and Pandis, 1998). Annual national (U.S.A.) ammonia emissions were estimated in 1997 to be 4.47 Tg-N yr^{-1} (Gilliland et al.).

Both ammonia and the ammonium ion, NH_4^+, contribute to nutrient loadings as sources for nitrogen. Processes in which this nitrogen is converted into secondary aerosols include the reactions of ammonia with nitric and sulfuric acids. Fine particulate nitrate and ammonium are produced from the heterogeneous chemical reactions of nitric and sulfuric acids and ammonia, producing ammonium nitrate (NH_4NO_3) (Reaction 8) and ammonium bisulfate (NH_4HSO_4) (Reaction 9) or ammonium sulfate ($(NH_4)_2SO_4$) (Reaction 10) (Paerl, 2001; Seinfeld and Pandis, 1998; Wall et al., 1988).

$NH_{3(g)} + HNO_{3(g, aq)} \leftrightarrow NH_4NO_{3(aq, s)}$ (Reaction 8)

$NH_{3(g)} + H_2SO_{4(aq)} \rightarrow NH_4HSO_{4(aq, s)}$ (Reaction 9)

$NH_{3(g)} + NH_4HSO_{4(aq, s)} \rightarrow (NH_4)_2SO_{4(aq, s)}$ (Reaction 10)

The ammonium nitrate reaction exists in equilibrium and is reversible. This reaction usually occurs in fogs and clouds. Ammonium nitrate is quite unstable (Watson et al., 1994) and is easily forced back into its reactive gaseous components. Production of NH_4NO_3 can range from 1 to 90 percent per hour, depending on the time of day and meteorological conditions, mainly temperature and relative humidity (Calvert and Stockwell, 1983; Watson et al., 1994).

It is important to note that ammonium nitrate is a major secondary component of suspended particles in urban areas (Watson et al., 1994). With

increasing relative humidity, ammonium nitrate adsorbs water, resulting in particle growth and increased light scattering. A wintertime study in Denver, CO, found ammonium nitrate concentrations as high as 28 μg m^{-3}, contributing to 180 Mm^{-1} light extinction (Watson et al., 1994).

Ammonium may also be seen in the coarse mode aerosol. Ammonia may neutralize with acidic species on sea salt particles, or physical processes may transfer the NH_4NO_3, NH_4HSO_4 and $(NH_4)_2SO_4$ to the coarse mode (Cheng et al., 2000; Yeatman et al., 2001)

Sulfate

Sulfur dioxide, SO_2, is a primary pollutant and is the "predominant anthropogenic sulfur-containing air pollutant" (Seinfeld and Pandis, 1998). In 1995, global sulfur emissions were estimated at 98-120 Tg-S yr^{-1}, with approximately 80 Tg-S yr^{-1} emitted as SO_2 (Berresheim et al., 1995; Seinfeld and Pandis, 1998).

Sulfuric acid, H_2SO_4, is produced when SO_2 is oxidized in the presence of hydroxyl radicals and water vapor, forming sulfuric acid droplets (Watson et al., 1994). These droplets are then readily neutralized by ammonia (Reactions 9-10), forming fine particulate species (Allen and Miguel, 1995). The reaction of ammonia with sulfuric acid occurs in two stages (Harrison, 1993; Mehlmann and Warneck, 1995). In an environment with low concentrations of ammonia, sulfate and nitrate compete for available ammonia. However, sulfate preferentially

scavenges ammonia and tends to drive the unstable ammonium nitrate to the gas phase, resulting in very low particulate ammonium nitrate levels. Significant amounts of ammonium nitrate are formed only when the concentrations of ammonia exceed that of sulfate by a molar ratio of two or more (Watson et al., 1994). Below this ratio, the aerosol phase will be acidic and sulfate may exist as ammonium bisulfate (Seinfeld and Pandis, 1998). Transformation rates range from 0.01 to 5 percent per hour of the SO_2 concentration (Calvert and Stockwell, 1983), being most active during daylight hours (Watson et al., 1994).

Coarse mode sulfate arises from the reaction of sulfuric acid with sea salt or mineral dust particles (Wall et al., 1988; Zhuang et al., 1999a).

$H_2SO_{4(aq)} + 2\ NaCl_{(aq,s)} \rightarrow Na_2SO_{4(aq,s)} + 2\ HCl_{(g)}$ (Reaction 11)

$H_2SO_{4(aq)} + CaCO_{3(aq,s)} \rightarrow CaSO_{4(aq,s)} + H_2O_{(g,aq)} + CO_{2(g)}$ (Reaction 12)

The sulfate formed from the reaction with sea salt is termed non-sea salt sulfate, as it was not part of the initial particle originating from the sea (Zhuang et al., 1999b). This reaction is also important as it leads to particulate chloride depletion.

It has also been found that coarse mode sulfate is formed through the heterogeneous oxidation of SO_2 by O_3 in freshly formed sea salt particles. Because these particles contain water and are alkaline, this process proceeds rapidly. It has been noted that the conversion of SO_2 to sulfate is strongly dependent on the amount of available surface waters and water volume of the particle (Chameides and Stelson, 1992; Sievering et al., 1995; Zhuang et al., 1999a).

Particle Diameter

Atmospheric particles are usually categorized by their diameters, implying the particles are spherical. Many atmospheric particles, however, have irregular shapes and are not easily categorized by their geometric radii or diameters. Equivalent or effective diameters are often used as they depend on physical, rather than geometric, properties (Finlayson-Pitts and Pitts Jr., 2000).

The most common effective diameter used is the aerodynamic diameter, D_a, which is the "diameter of a spherical particle with a standard density of 1000 kg m^{-3} (density of a water droplet) that has the same settling velocity as the particle" (Hinds, 1999). The aerodynamic diameter is used to correct for particle morphology as it standardizes for shape (a sphere), density and settling velocities. It is the primary particle property for characterizing filtration and respiratory deposition (Finlayson-Pitts and Pitts Jr., 2000; Hinds, 1999) and can be calculated using:

$$D_a = D_g \sqrt{\frac{\rho_p}{\rho_o}} \qquad \text{(Equation 4)}$$

where D_a is the aerodynamic diameter, D_g is the geometric diameter, ρ_p is the particle density, and ρ_o is the standard density.

Another type of diameter used is the Stokes diameter, D_s, which is the "diameter of a sphere having the same density and settling velocity as the particle" (Hinds, 1999). The Stokes diameter standardizes for settling velocity,

whereas the aerodynamic diameter standardizes for both settling velocity and density.

The term “diameter” in this work represents the aerodynamic diameter of atmospheric particles unless otherwise stated. As will be discussed later, the particles in the area of interest were determined to be predominantly in the metastable or deliquescent state. Their densities were near that of the standard density, allowing the assumption that the aerodynamic diameter approximated the geometric diameter.

Deposition Velocities

The significance in the gas-to-particle conversion of gaseous HNO_3 to particle NO_3^- relates to the deposition velocities of the substances. The dry deposition velocity of HNO_3 is relatively high wih respect to fine particulate matter. However, since most of the NO_3^- particles formed in the Tampa Bay area are in the coarse size range (diameter greater than 2.5 μm), the conversion may have an increased significance. To determine if the phase change results in increased or decreased nitrogen loadings to the Tampa Bay watershed, the deposition velocities of the formed species were reviewed.

Typical dry deposition velocities for gaseous HNO_3 are reported as 4 and 1 cm s^{-1} for over land and over open water, respectively (Seinfeld and Pandis, 1998). Particle dry deposition velocities over water can be calculated using a combination of the NOAA Buoy and Williams models (Bhethanabotla, 2002; Poor

et al., 2001; Valigura, 2001; Williams, 1982). The NOAA Buoy model is an iterative bulk exchange model for momentum, heat and moisture; and the Williams model is a two-layer multiple-path model for the dry deposition of particles to surface waters. The combined or integrated NOAA Buoy-Williams model includes the effects of wave breaking, particle hygroscopic growth and turbulent heat flux. The model calculates the over water dry deposition velocities on the basis of turbulent heat transfer and gravitational settling of particles. Table 1 lists the average over water deposition velocity and one standard deviation for the MOUDI ten particle size ranges using May 2002 meteorology.

Particle Range (μm)	Geometric Mean D_{p50} (μm)	Average Deposition Velocity (cm s^{-1})
18-30	23	1.7 ± 0.17
3.2-18	7.6	0.21 ± 0.12
1.8-3.2	2.4	0.02 ± 0.01
1.0-1.8	1.3	0.01 ± 0.01
0.56-1.0	0.75	0.01 ± 0.01
0.32-0.56	0.42	0.01 ± 0.01
0.18-0.32	0.24	0.01 ± 0.01
0.10-0.18	0.13	0.02 ± 0.02
0.056-0.10	0.075	0.03 ± 0.03
0.01-0.056	0.024	0.07 ± 0.07

Table 1. Average over water deposition velocities and their respective standard deviations for the MOUDI ten particle size ranges calculated using May 2002 meteorological data.

The geometric mean of each size bin was used as the D_{p50} for the model input. The geometric mean can be calculated by:

$$Geometric\ Mean = \sqrt[n]{(x_1)(x_2)...(x_n)} \qquad \text{(Equation 5)}$$

Sampling

It is essential to collect accurate measurements of atmospheric gases and particulate species in order to understand the processes occurring in our environment. These species are difficult to collect, as they exist at trace levels in multiple phases. Many species are partitioned between the gaseous and particulate phases. Numerous methods have been developed to facilitate collection of atmospheric species. They include filtration (Allen et al., 1989; Appel et al., 1980; Okita et al., 1976; Spicer et al., 1982), diffusion denuders (Forrest et al., 1982; Harrison and Kitto, 1990; Possanzini et al., 1983) and spectroscopy (Platt et al., 1980).

Filtration Methods

Filtration sampling is the most widely used technique for sampling atmospheric gaseous and particulate species due to its low cost and simplicity (Kitto and Colbeck, 1999). Many types of filters have been used, the most popular being glass fiber, quartz fiber, PTFE (polytetrafluoroethylene) Teflon® membrane and nylon filters. PTFE Teflon is a choice of many scientists, as it is inert towards chemical species (Kitto and Colbeck, 1999) and contains low blank analyte levels. Quartz fiber filters are typically used for organic sampling, as they

can be heated to remove blank analytes. Nylon filters have the ability to adsorb acidic gaseous species, making them ideal for nitric and hydrochloric acid collection (Dasch et al., 1989; Grosjean, 1982; Hering et al., 1988; Spicer et al., 1982). In addition to these filters, impregnated filters may also be used. Nitric acid has been collected using sodium chloride- (Appel et al., 1980; Forrest et al., 1980; Karakas and Tuncel, 1997), potassium carbonate- (Kim and Allen, 1997) and tetrabutyl ammonium hydroxide-impregnated filters (Huebert and Lazrus, 1980). SO_2 has been collected using potassium hydroxide- (Nodop and Hanssen, 1986) and various carbonate- (Karakas and Tuncel, 1997; Kim and Allen, 1997) impregnated filters. Ammonia has been collected using a variety of acid-impregnated filters, including citric, oxalic and phosphoric acids (Harrison and Kitto, 1990; Karakas and Tuncel, 1997; Masia et al., 1994).

Filters are deployed in the field for atmospheric gaseous and particulate species collection in a filter pack. Filter packs can be set up using a single filter or multiple filters, allowing for the collection of multiple species in both the gas and particle phases. A multiple filter setup is used to collect and determine the volatilization of particulates, gas-particle reactions and particle-particle reactions (Kitto and Colbeck, 1999).

Under changing temperature, relative humidity and acidity, unstable species, such as ammonium nitrate and ammonium chloride, may volatilize into their parent gases:

$NH_4NO_{3(s)} \leftrightarrow NH_{3(g)} + HNO_{3(g)}$ (Reaction 13)

$NH_4Cl_{(s)} \leftrightarrow NH_{3(g)} + HCl_{(g)}$ (Reaction 14)

Gas-particle artifacts can form from the interaction of incoming reactive gases with pre-collected aerosols. Examples of these types of interferences include:

$2\ NH_{3(g)} + H_2SO_{4(aq)} \rightarrow (NH_4)_2SO_{4(aq,s)}$ (Reaction 15)

$2\ HNO_{3(g)} + CaCO_{3(aq,s)} \rightarrow Ca(NO_3)_{2(aq,s)} + H_2O_{(g,aq)} + CO_{2(g)}$ (Reaction 16)

$HNO_{3(g)} + NaCl_{(aq,s)} \rightarrow NaNO_{3(aq,s)} + HCl_{(g)}$ (Reaction 17)

Particle-particle interactions may result in the loss of a species of interest. Examples of this type of reaction include:

$NH_4NO_{3(s)} + H_2SO_{4(aq)} \rightarrow NH_4HSO_{4(aq,s)} + HNO_{3(g)}$ (Reaction 18)

$2\ NaCl_{(aq,s)} + H_2SO_{4(aq)} \rightarrow 2\ HCl_{(g)} + Na_2SO_{4(aq,s)}$ (Reaction 19)

All of these processes can result in a sampling bias, over- or under-estimation, of the measurements. To minimize these effects, filter packs are often coupled with denuder samplers, which remove the reactive gas phase species prior to the filter pack. Like the previous filter pack setup, multiple filters can be used in conjunction with denuders.

Denuder Methods

In denuders, atmospheric gaseous components are removed from the airstream by diffusion to the walls of the instrument, leaving the particulate matter untouched. There are several types of denuders including cylindrical, annular, honeycomb and others. In this work, annular denuders were used. These consisted of concentric etched glass tubes contained within a Teflon-coated

stainless steel cylindrical housing. The walls of the denuders are coated with a solution designed to react with the species desired to be collected. In order to be efficient, a denuder must maintain stable and laminar gas flow, have an infinitely large collection capacity with a large sink for the species, and not generate or destroy the species of interest inside the denuder (Kitto and Colbeck, 1999).

A typical configuration of an annular denuder system (ADS) includes an inlet, a series of coated denuders and a filter pack. There are many types of inlets, including cyclones and elutriators, and they are generally Teflon-coated. When using a cyclone inlet in marine environments, the interior wall of the ADS cyclone may become coated by sea salt particles. It has been found that sea salt aerosols react with acids in the atmosphere, such as H_2SO_4 and HNO_3, forming sulfates and nitrates (Li-Jones et al., 2001). The reaction between HNO_3 and sea salts within the cyclone may result in a substantial loss of HNO_3 (Appel et al., 1988; Vossler et al., 1988). This reaction leads to the misapportionment of both nitrate and chloride ions, as HCl is released into the vapor phase. Under marine conditions, it has been suggested that the ADS be used with a different type of inlet device such as a small impactor (Li-Jones et al., 2001). In an impactor, large sea salt particles will be deposited within a relatively small area on the impaction surface, making the area of sea salt exposed to the sample air stream smaller. Because they were readily available, 2.5-μm Teflon-coated cyclones were chosen for the ADS assembly inlet device during the course of these experiments. These cyclones were cleaned on a regular basis to prevent the buildup of sea salt.

As mentioned, the walls of the denuders should be coated with solutions appropriate for the target species to be collected. Typical species collected include HCl, HNO_2, HNO_3, SO_2 and NH_3. The first four species are acidic and are easily collected using basic coating solutions. Ammonia sampling uses acidic coating solutions. The criteria for choosing the proper denuder coating are: (1) the coating must be very selective, (2) it must be a good sink for the species to be determined, (3) it must have high collection efficiency, and (4) it must be unreactive towards products resulting from the primary reaction between species and the coating layer (Perrino et al., 1990).

In previous work, a coating solution of NaCl or NaF was used for the collection of HNO_2 and HNO_3 (Allegrini et al., 1987; Allegrini et al., 1994), with a collection efficiency for HNO_3 greater than 97%. There are several problems associated with using NaCl. First, excess chloride from the coating solution in ion chromatography (IC) analysis can overwhelm the analytical column, creating a masking peak that invalidates the nitrite and nitrate analysis (from HNO_2 and HNO_3, respectively). Second, when HNO_3 reacts with NaCl, gaseous HCl is formed. As a result, atmospheric HCl will be mixed with the coating solution reaction byproduct HCl and, therefore, cannot be quantified in a subsequent denuder in series. Third, the collection efficiency for HNO_2 on NaCl- and NaF-coated denuders is poor. It has been shown that HNO_2 was almost entirely released from those denuders; only to be captured by the subsequent Na_2CO_3-coated denuder (Perrino et al., 1990).

Na_2CO_3- and glycerol-coated (1% + 1% w/w in 50:50 methanol-water solution) denuders can be used for the collection of SO_2, HNO_2, HNO_3 and HCl (Allegrini et al., 1987; Allegrini et al., 1994; Vossler et al., 1988). Perrino et al. (2001) determined the collection efficiency for SO_2 collection to be greater than 99.9% of incoming SO_2 with deposition of particulate SO_4^{2-} at 0.5-2%. Breakthrough was tested using a second backup Na_2CO_3-coated denuder. The backup denuder showed collection of less than 0.1% of SO_2. Na_2CO_3 has been proven to be a good sink for HNO_2, with a removal constant near infinity.

Difficulty arrives in the quantification of NO_2^- (from HNO_2) when collecting HNO_3 on the same denuder. HNO_3 is collected and analyzed as NO_3^-, whereas HNO_2 is partially oxidized during sampling and is analyzed as both NO_2^- and NO_3^-. Exposure to gaseous NO can cause an increase in NO_2^- formation on the Na_2CO_3-coated denuders. This interferent amount can be taken into account by using the differential technique (Febo et al., 1989; Perrino et al., 1990).

For these experiments, Na_2CO_3 was used as the basic denuder coating. Collection efficiencies have been determined to be greater than 99.5% for HCl, greater than 98.5% for HNO_2, greater than 97% for HNO_3 and greater than 99% for SO_2 on Na_2CO_3-coated denuders (Allegrini et al., 1987; Perrino et al., 2001).

Acid-coated denuders are used to determine ambient ammonia concentrations. The following acids were considered: citric, oxalic, phosphoric and phosphorus. The collection efficiencies of oxalic acid, citric acid and phosphorus acid (H_3PO_3) have been compared (Perrino and Gherardi, 1999). The data indicated the collection efficiencies of oxalic and phosphorus acid were

equivalent (>99%). However, the efficiency of citric acid had great variation from the values that were expected for a perfect sink, with a negative bias of approximately 20% (McCulloch and Shendrikar, 2000). Phosphorus and oxalic acids yielded very good reproducibility in determining ammonia. The drawbacks of oxalic acid are its toxicity and desorbing potential. Perrino and Gherardi (1999) found significant amounts of oxalate releasing from the denuder into the incoming air stream and displacing nitrate ion on the Teflon filter, causing an excess of nitrate ions on the backup filter. Their conclusion indicated that both oxalic and phosphorus acid proved to be suitable for ammonia determination, but only the latter is able to assure a correct determination of ammonium salts on the backup filter packs. After direct discussion with Dr. Perrino, it has concluded that the performances of phosphoric and phosphorus acid are very similar. In these experiments, both citric and phosphoric acid coating solutions were used.

Cascade Impactors

Many instruments have been developed for the collection of PM_{10}, particulate matter with an aerodynamic diameter less than 10 μm. Cascade (or inertial) and virtual impactors are the methods of choice for collecting particles 10 μm and smaller (Spurny, 1999). Both devices size segregate particles based on their aerodynamic diameter. The micro-orifice uniform deposit impactor (MOUDI) and Andersen Mark II sampler are examples of cascade impactors. Virtual

impactors are used in instruments like the dichotomous or trichotomous sampler, where only two or three size fractions, respectively, are collected.

Impaction methods have been used for particle collection for quite some time. In the early twentieth century, dust particles were collected through impaction to evaluate occupational environments (Hinds, 1999). Since the 1960s, cascade impactors have been developed to measure the particle size distributions. The collected particle mass distributions were determined by weighing the impaction plates before and after sampling.

All cascade (or inertial) impactors are composed of two basic parts: an impaction nozzle and an impaction plate. Together, they make up a collection stage. Cascade impactors can have multiple stages, allowing for particles to be collected in multiple size bins. The airstream enters the impactor through the impaction nozzle, or jet, which directs the airstream towards the flat impaction plate. The plate is placed perpendicular to the airstream, deflecting the airflow to a near 90° bend (Figure 1). Due to the inertia and size, some particles are unable to follow the bend in the airflow and collide or impact on the impaction plate, whereas the smaller particles follow the bend in the airstream and are not collected on the impaction plate. As a result, the impactor separates particles by size. The larger particles are removed from the airstream and collected on the impaction plates, leaving the smaller particles in the remainder of the airflow to be collected on latter stages.

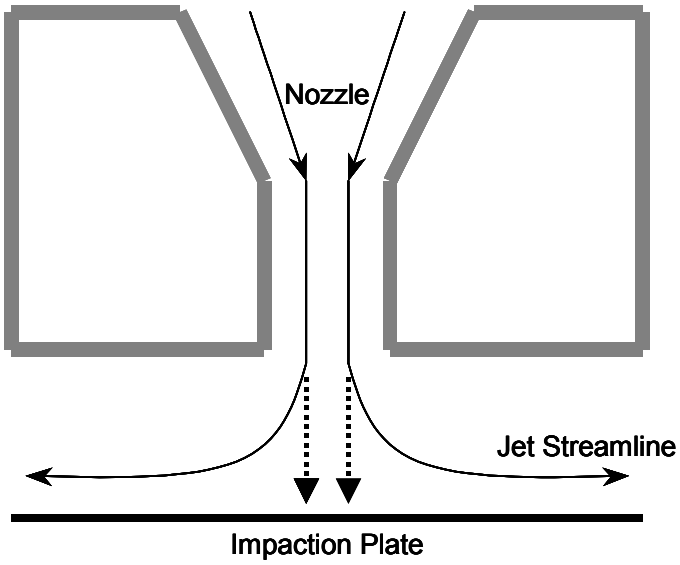

Figure 1. Cross-sectional view of an impactor stage (adapted from Hinds, 1999).

Impactors have been used in parallel to collect particles in multiple size bins. However, this is uncommon due to the complexity of maintaining multiple flow rates required. The use of impactors in series has been developed and is commonly practiced to collect multiple size bin particles. Stages are arranged in order of decreasing cutoff diameters, collecting the largest particles first. The device is referred to as a cascade impactor, with each separate unit called an impactor or collection stage. The smaller particles are collected by continually decreasing the nozzle diameters, keeping the volumetric flow rate the same for all stages. Each stage in a cascade impactor is fitted with a plate, and a final backup collection filter is placed at the exit of the instrument to collect those remaining particles.

When in operation, each collection plate may be used as is, coated, or have a filter placed on top. Uncoated plates are used for the collection of liquid

particles as they stick when impacted onto the collection plate. Hard, solid particles have a tendency to bounce once impacted and end up collected in a lower stage. To reduce particle bounce, impaction stages may be coated with a thin film of oil or grease. Filters are used for the collection of both liquid and solid particles and are placed on top of the collection plate. They are preferred because they minimize sample contamination by being easily removed and replaced without the requirement of thorough cleaning of each impaction plate.

The Stokes number parameter, *St*, predicts whether a particle will impact or follow the airstream out of the impaction region (Hinds, 1999; Marple et al., 1991). The Stokes number can be defined as:

$$St = \frac{\rho_p C V_o D_p^{\,2}}{9 \mu W} \qquad \text{(Equation 6)}$$

where ρ_p is the particle density, C is the slip correction factor (also known as the Cunningham correction factor, C_c), V_o is the average air velocity at the nozzle, D_p is the particle diameter, μ is the air viscosity, and W is the nozzle diameter. V_o can be determined using:

$$V_o = \frac{4 q}{\pi W^2} \qquad \text{(Equation 7)}$$

where q is the volumetric flow rate through the nozzle. The Stokes number is the primary parameter that governs the size of particles collected in an inertial impactor.

Each collection stage in a cascade impactor has a cut point diameter, in which 50% of the particles greater than a certain size are collected and those smaller continue with the airstream. The Stokes number is used to characterize

the collection efficiency of each impaction stage (Hinds, 1999). The cut points for each impaction plate are defined by the particle diameter that is collected with 50% efficiency, D_{p50}.

$$D_{p50} = \sqrt{\frac{9\,\mu W}{\rho_p C V_o}}\sqrt{St_{50}} \qquad \text{(Equation 8)}$$

where $\sqrt{St_{50}}$ is the dimensionless particle size defining the value of $\sqrt{St}$ corresponding to D_{p50} (Hinds, 1999).

Particle concentrations collected using a cascade impactor are calculated by dividing the mass collected by the volume of air sampled.

$$PM_{Stg(i)} = \frac{Mass_{Stg(i)}}{Volume_{total}} \qquad \text{(Equation 9)}$$

where $PM_{Stg(i)}$ (μg m^{-3}) is the particulate concentration from stage (i) of the impactor, $Mass_{Stg(i)}$ (μg) is the mass collected and $Volume_{total}$ (m^{-3}) is the volume of air through the impactor.

Virtual Impactors

Virtual impactors are used in the dichotomous sampler to separate particles into two size fractions. Unlike a traditional impactor, particles are collected on filters the air is drawn through, instead of impacting on a plate. Ambient air is drawn through the virtual impactor and is split into major and minor airstreams. During typical operation of a dichotomous sampler, the total flow rate

is 16.7 L min^{-1}, with respective 15.0 and 1.67 L min^{-1} directed onto the $PM_{2.5}$ and $PM_{10-2.5}$ filters.

Particles are separated in a similar fashion to that of a traditional impactor. Larger particles, those with enough inertia, are drawn into a collection probe and are carried by the minor flow. Smaller particles are carried away from the nozzle and continue with the major flow stream. All particles are collected onto a filter through which the air flows. Due to the complexity of controlling multiple more airflows, virtual impactors are used for the collection of one or two stages. A trichotomous sampler has been developed using virtual impactors, allowing the collection of particles in three size bins.

The traditional cutpoint for a dichotomous sampler is 2.5 μm, naming the collective $PM_{2.5}$ bin "fine" and the $PM_{10-2.5}$ bin "coarse". $PM_{2.5}$ concentrations can be calculated using

$$PM_{2.5} = \frac{Mass_{2.5}}{Volume_{2.5}} \qquad \text{(Equation 10)}$$

where $PM_{2.5}$ (μg m^{-3}) is the concentration of particulate matter, $Mass_{2.5}$ (μg) is the collected mass and $Volume_{2.5}$ (m^{-3}) is the volume of air (Poor et al., 2002). The $PM_{10-2.5}$ concentrations are calculated using

$$PM_{10-2.5} = \frac{Mass_{10-2.5}}{Volume_{total}} - PM_{2.5}\frac{Volume_{10-2.5}}{Volume_{total}} \qquad \text{(Equation 11)}$$

where $PM_{10-2.5}$ (μg m^{-3}) is the concentration of particulate matter, $Mass_{10-2.5}$ (μg) is the collected mass and $Volume_{total}$ and $Volume_{10-2.5}$ (m^{-3}) are the volumes of air (Poor et al., 2002). This equation serves to correct for the $PM_{2.5}$ collected on the $PM_{10-2.5}$ filter.

Models

Models are tools used to "provide the necessary framework for integration of our understanding of individual atmospheric processes and study of their interactions" (Seinfeld and Pandis, 1998). Models are needed because of the complexity of the atmosphere, with numerous processes occurring simultaneously. Atmospheric sampling provides a "snapshot of atmospheric conditions at a particular time and location" (Seinfeld and Pandis, 1998) and helps identify the state of the atmosphere. Models are used to extend our snapshot to understand processes on a local or regional scale.

Thermodynamic models have been developed over the past twenty years using thermodynamic equilibrium principles to predict the composition and physical state of atmospheric aerosols. The basis for these models is the assumption that gas and aerosol volatile species are in equilibrium (Ansari and Pandis, 1999; Bassett and Seinfeld, 1983; Pilinis and Seinfeld, 1987; Stelson and Seinfeld, 1982). Current thermodynamic equilibrium models include EQUIL (Bassett and Seinfeld, 1983), KEQUIL (Bassett and Seinfeld, 1984), MARS (Saxena et al., 1986), SEQULIB (Pilinis and Seinfeld, 1987), AIM (Wexler and Seinfeld, 1991), SCAPE (Kim et al., 1993a; Kim et al., 1993b), SCAPE2 (Kim and Seinfeld, 1995; Meng et al., 1995), MARS-A (Binkowski and Shankar, 1995), EQUISOLV (Jacobson et al., 1996), AIM2 (Clegg et al., 1998), ISORROPRIA (Nenes et al., 1998), GFEMN (Ansari and Pandis, 1999) and EQUISOLV II (Jacobson, 1999a). During the development of many of these models,

maintaining computer efficiency was a primary endeavor. As a result, assumptions were made to simplify problems and allow the use of these equilibrium models in atmospheric chemical transport models (Ansari and Pandis, 1999).

Most of these equilibrium models solve for equilibrium using the iterative Gibbs free energy minimization method (Jacobson, 1999a). The following table taken from Jacobson 1999 summarizes the equilibrium models, the system solved and their solution method.

Model Name	Reference	System Solved	Solution Method
AIM	Wexler and Seinfeld (1991)	NH_4^+-Na^+-NO_3^--SO_4^{2-}-Cl^-	Iterative Gibbs free energy minimization method
AIM2	Clegg et al. (1998)	NH_4^+-Na^+-NO_3^--SO_4^{2-}-Cl^-	Iterative Gibbs free energy minimization method
EQUIL	Bassett and Seinfeld (1983)	NH_4^+-NO_3^--SO_4^{2-}	Iterative Gibbs free energy minimization method
EQUISOLV	Jacobson et al. (1996)	NH_4^+-Na^+-NO_3^--SO_4^{2-}-Cl^-	Mass-flux iteration method
EQUISOLV II	Jacobson (1999a)	NH_4^+-Na^+-NO_3^--SO_4^{2-}-Cl^--Ca^{2+}-Mg^{2+}-K^+-CO_3^{2-}	Analytical equilibrium iteration + mass-flux iteration
GFEMN	Ansari and Pandis (1999)	NH_4^+-Na^+-NO_3^--SO_4^{2-}-Cl^-	Iterative Gibbs free energy minimization method
ISORROPRIA	Nenes et al. (1999)	NH_4^+-Na^+-NO_3^--SO_4^{2-}-Cl^-	Iterative bisection + bisection-Newton for H^+
KEQUIL	Bassett and Seinfeld (1984)	NH_4^+-NO_3^--SO_4^{2-}	Iterative Gibbs free energy minimization method
MARS	Saxena et al. (1986)	NH_4^+-NO_3^--SO_4^{2-}	Iterative Newton-Raphson method
MARS-A	Binkowski and Shankar (1995)	NH_4^+-NO_3^--SO_4^{2-}	Iterative Newton-Raphson method
SCAPE	Kim et al. (1993)	NH_4^+-Na^+-NO_3^--SO_4^{2-}-Cl^-	Iterative bisection + bisection-Newton for H+
SCAPE2	Kim and Seinfeld (1995), Meng et al. (1995)	NH_4^+-Na^+-NO_3^--SO_4^{2-}-Cl^--Ca^{2+}-Mg^{2+}-K^+-CO_3^{2-}	Iterative bisection method
SEQUILIB	Pilinis and Seinfeld (1987)	NH_4^+-Na^+-NO_3^--SO_4^{2-}-Cl^-	Iterative bisection method

Table 2. Equilibrium models, species treated and numerical method used to solve equilibrium (Jacobson, 1999a).

The primary thermodynamic equilibrium model used throughout this work was the EQUISOLV II (Jacobson, 1999a), which solves for thermodynamic equilibrium through analytical equilibrium iterations and mass flux iterations. The model can be used over a range of temperatures as it corrects equilibrium constants, deliquescent relative humidities and activity coefficients for

temperature dependence. This model is very versatile as it can be used for NH_4^+, Na^+, NO_3^-, SO_4^{2-}, Cl^-, Ca^{2+}, Mg^{2+}, K^+ and CO_3^{2-} systems.

The Aerosol Inorganics Model (AIM2 - Model III) (Clegg et al., 1998) was used for model comparison. AIM2 solves for thermodynamic equilibrium by minimizing the Gibbs free energy of the system through the use of sequential quadratic programming algorithms. This model is limited to a single particle bin, NH_4^+, Na^+, NO_3^-, SO_4^{2-} and Cl^- systems and 25°C environments.

Kinetics

Heterogeneous Reactions

Heterogeneous chemical reactions are those occurring between gases and either solids or liquids in the atmosphere (Finlayson-Pitts and Pitts Jr., 2000). These reactions occur on many different types of surfaces including ice crystals, liquid aerosols, sea salts, soot, metal oxides, clouds and surface waters as well as a number of other surface types (Kolb et al., 1995).

There are a few common terms used to describe heterogeneous reactions. The surface reaction probability (γ_{rxn}) is the fraction of collisions between the gas and condensed phases that leads to the irreversible uptake of the gaseous species due to chemical reaction. γ_{rxn} is also known as the reaction probability. The mass accommodation coefficient (α) is the fraction of collisions between the gas and condensed phases that result in the uptake of the gaseous

species by the condensed phase. It is the fundamental parameter that measures the rate at which molecules cross the interface between the gas and condensed phases (Kolb et al., 1995). The mass accommodation coefficient is not the net uptake because it does not include the reversible effect of evaporation of the gaseous species from the condensed phase; however, it determines the maximum rate of mass transport. α is also referred to as the sticking coefficient for the uptake on solid surfaces. The overall or net uptake probability (γ_{net}) is the net rate of uptake normalized to the rate of collisions. When determining uptake coefficients experimentally $(\gamma_{measured})$, $\gamma_{measured} = \gamma_{net}$ (Finlayson-Pitts and Pitts Jr., 2000).

Several types of instrumentation have been used to experimentally determine heterogeneous chemistry kinetics. The most common instrumentation is the Knudsen cell (Caloz et al., 1997; Fenter et al., 1997; Finlayson-Pitts and Pitts Jr., 2000). It has been used over the last 30 years for kinetic measurements of both homogeneous and heterogeneous systems. According to Caloz et al. (1997), the technique is well adapted for heterogeneous reactions because the reactant interacts with the substrate without boundary layer effects and because the collision frequency between the gaseous reactant and substrate can be accurately determined. The Knudsen cell is comprised of a chamber containing a reactive surface through which the reactant gas is allowed to pass. It is typically coupled with a mass spectrometer, which detects the gas phase concentration. The condensed phase is loaded on a sample plate, which is either placed in a separate chamber or covered with a lid, depending if the

Knudsen cell is dual or single chambered. The reactant gas enters the cell through a valve where it evenly disperses. The gas is often allowed to flow through the system prior to exposure to the condensed phase for some time to minimize loss of the reactant gas to the cell walls. When the reactant gas is exposed to the condensed phase, the surface takes up the gas reducing the concentration of the gas in the cell. This change in gas concentration is detected by the mass spectrometer, allowing the net uptake of the gas by the surface to be determined.

The major limitation for Knudsen cells is that they are operated at low pressures (<10 mTorr) to increase the mean free path of the gas molecules (Davies and Cox, 1998; Finlayson-Pitts and Pitts Jr., 2000). Reactions can be studied only under dry and very low relative humidity conditions. This limits environmental applications, as the humidity in coastal areas is often greater than 60%.

Other types of instrumentation have been developed which are not limited to low relative humidity conditions. The aerosol flow tube has been used to determine rate constants for gas-phase reactions (Finlayson-Pitts and Pitts Jr., 2000), and it has been recently adapted to study heterogeneous reactions (Abbatt and Washewsky, 1998; Hu and Abbatt, 1997).

The aerosol flow tube can be used in one of two ways. The walls of the flow tube can be coated with the condensed phase of interest. However, it is often difficult to coat the walls of the flow tube. In the second method, the condensed phase is generated as an aerosol that can be aqueous or solid and

passed through the flow tube along with the reactant gas phase. The exit orifice of the flow tube is connected to a detection device, which is typically a mass spectrometer. The exiting gas is analyzed in a similar fashion to that in a Knudsen cell apparatus. The aerosol flow reactor is not constrained to low pressure, and it is very versatile for a wide range of relative humidity conditions.

Sea Salt

Understanding the kinetics behind the uptake of nitric acid by sea salt is essential in modeling the gas phase nitric acid to particulate nitrate conversion and its effects on nitrogen deposition. Past studies have focused on determining the uptake of nitric acid by NaCl, a major component of sea salt (77% w/w) (Beichert and Finlayson-Pitts, 1996; De Haan and Finlayson-Pitts, 1997; Ghosal and Hemminger, 1999; Zangmeister and Pemberton, 1998; Zangmeister and Pemberton, 2001). However, other research has suggested that the reaction probabilities, the fractional loss of a species from the gas phase due to reaction with a surface (Jacobson, 1999b), for sea salt are at least an order of magnitude faster than those for sodium chloride. Other measurements have suggested that NaCl may not be the most reactive component of sea salt (De Haan and Finlayson-Pitts, 1997; Langer et al., 1997)

Under most marine conditions, sea salt is present in the form of deliquescent aerosol particles (Guimbaud et al., 2002a). However, the majority of laboratory studies investigating the kinetics behind the HNO_3 and sea salt

interaction were performed on solid crystals or thin films at low relative humidity conditions. A model describing the step-by-step process of the uptake of nitric acid and conversion to nitrate has been proposed (Laskin et al., 2002). HNO_3 and other nitrogen oxide gases are first taken up into the surface adsorbed water of a sea salt particle. Even at conditions well below the deliquescent point at ambient temperature, NaCl (and sea salt) has significant amounts of adsorbed water on its surface, which is associated with its steps, edges and defect sites (Beichert and Finlayson-Pitts, 1996; Davies and Cox, 1998; Finlayson-Pitts and Hemminger, 2000). Nitric acid dissolves and remains inactive until the particle becomes significantly acidified. This happens by the further uptake of acids or the drying of the particle. As it dries, the particle becomes more concentrated in all components, including acids. When the acidity reaches ~pH 1.7, HCl begins to degas, $NaNO_3$ precipitates and additional HNO_3 is taken up (Beichert and Finlayson-Pitts, 1996; Finlayson-Pitts and Hemminger, 2000). A thermodynamic model (Clegg et al., 1998) predicts that HCl evaporates faster than HNO_3, leaving the dried particles deficient in chloride rather than nitrate.

The reaction between HNO_3 and NaCl has been widely studied (Beichert and Finlayson-Pitts, 1996; Finlayson-Pitts and Hemminger, 2000; Langer et al., 1997; Ten Brink, 1998; Vogt and Finlayson-Pitts, 1994; Zangmeister and Pemberton, 1998). NaCl is a hygroscopic salt; its deliquescent relative humidity (DRH) is 75% (Seinfeld and Pandis, 1998). Below the deliquescent point, the aerosol exists as a metastable supersaturated liquid droplet until the efflorescence point, or crystallization relative humidity, is reached (~37% RH), at

which point the salt begins to crystallize (Davies and Cox, 1998). Studies have been done at different relative humidities to determine the effect of water on the HNO_3 absorption. At 30% relative humidity, dry aerosol NaCl was reacted with gaseous HNO_3. Reaction analysis revealed the absence of measurable substitution of chloride by nitrate, providing evidence that HNO_3 does not react with dry NaCl (Ten Brink, 1998). However, this absence of nitrate detection does not provide enough evidence to exclude the possibility of a small surface interaction of HNO_3 with NaCl (Ten Brink, 1998; Vogt et al., 1996). It is possible that the detection limits were too high at the time of experimentation. The experiment was repeated at 80% relative humidity, and it resulted in a substantial amount of nitrate formation (Ten Brink, 1998). The experiment was repeated again, this time at 50% RH (below the 75% DRH of NaCl). The formation of nitrate was observed, contradicting the results reported at 30% RH. After further analysis, it was concluded that these particles were formed from NaCl droplets that were “dried”. The aerosols, in actuality, were not thoroughly “dry” aerosols but supersaturated droplets due to the hysteresis effect of aerosol water (Seinfeld and Pandis, 1998; Tang, 1980).

Evidence suggests that the reaction probability significantly increases with the presence of adsorbed surface water (Beichert and Finlayson-Pitts, 1996; Langer et al., 1997). The water layers create a quasi-liquid layer allowing the surface molecules to deliquesce and increase ionic mobility. This greatly facilitates the uptake and reaction of HNO_3 with the NaCl solution (Zangmeister and Pemberton, 1998). $NaNO_3$ is formed on the surface of the salt particle.

Without the further uptake of additional water molecules, the reaction rate of additional $NaNO_3$ formation is greatly decreased or stops due to the formation of a protective layer or film on the particle's surface (Allen et al., 1996). Upon the exposure to increased relative humidity, the particle adsorbs additional water molecules, increasing the ionic (nitrate) mobility (Finlayson-Pitts and Hemminger, 2000). The components of the particle are then allowed to rearrange, regenerating the NaCl reactive surface. A two-step model has been developed representing this process:

$HNO_{3(g)} + NaCl_{site} \rightarrow NO_3^-{}_{(ads)} + HCl_{(g)}$ (Reaction 20)

$NO_3^-{}_{(ads)} + H_2O_{(l)} \rightarrow NaCl_{site} + NaNO_{3(s)}$ (Reaction 21)

where $NaCl_{site}$ is the unreacted surface site and $NO_3^-{}_{(ads)}$ is the newly formed immobile $NaNO_3$ that is blocking the NaCl reactive site (Finlayson-Pitts and Hemminger, 2000; Ghosal and Hemminger, 1999).

The availability of surface waters on NaCl appears to govern the uptake of HNO_3 (Beichert and Finlayson-Pitts, 1996; De Haan and Finlayson-Pitts, 1997; Ten Brink, 1998). Beichert (1996) did not observe the uptake of HNO_3 on single crystals. He proposed the explanation that a single crystal is relatively free of defects and does not readily hold adsorbed water. The measured dry HNO_3 uptake by a NaCl single crystal was approximately two orders of magnitude less than that on finely ground NaCl powders.

The uptake coefficient for a given reaction is the probability that a molecule is removed from the gas phase upon colliding with a particle surface (Guimbaud et al., 2002a). It is "simply a measure of how likely the molecule will

be taken up by the surface, through either adsorption or reaction, on a per collision basis" (Grassian, 2002).

The uptake coefficients for gaseous HNO_3 on NaCl and sea salt have been determined experimentally. For NaCl, the uptake coefficient was characterized by the value of $\gamma > 0.2$ (Abbatt and Washewsky, 1998). This value was determined using the aerosol kinetics flow tube technique at room temperature with deliquescent NaCl at 75% relative humidity. The rate of uptake was determined to be independent of particle size for deliquescent particles (Guimbaud et al., 2002b; Ten Brink, 1998). Abbatt and Waschewsky (1998) report that this elevated uptake coefficient is driven by the very high solubility of HNO_3 in aqueous salt solution but limited by the gas-diffusion rate.

Other uptake coefficients for HNO_3 on NaCl have been reported, ranging from 10^{-4} to 10^{-2}, depending on the amount of water on the salt surface (Abbatt and Washewsky, 1998; Beichert and Finlayson-Pitts, 1996; Fenter et al., 1994; Laux et al., 1994; Vogt and Finlayson-Pitts, 1994). Low-pressure Knudsen cell flow reactors are other tools used to determine heterogeneous kinetics of these types of interactions. However, the Knudsen cell flow reactor is limited to very low relative humidity conditions (Davies and Cox, 1998). Beichert and Finlayson-Pitts (1996) determined a constant steady-state uptake of $\gamma = (1.4 \pm 0.6) \times 10^{-2}$ for particles 0.5 and 4 μm at room temperature. Fenter et al. (1994) determined a value of $\gamma = (2.8 \pm 0.3) \times 10^{-2}$.

The value determined by Abbatt and Waschewsky (1998) was used in the modeling and is considered a lower limit for the uptake of HNO_3 by NaCl as the average relative humidity for the Tampa Bay coastal area is approximately 80%.

For sea salt, the uptake coefficient was estimated to be $\gamma = 0.50 \pm 0.20$ for deliquescent sea salt at 55% relative humidity (Guimbaud et al., 2002a). This value was also determined using an aerosol flow tube technique. The difference between the coefficients for sea salt (which is primarily NaCl) and NaCl lie in the composition of sea salt. Sea salt contains hygroscopic hydrates, such as $MgCl_2 \cdot 6H_2O$, which provide additional surface waters for the uptake and reaction of HNO_3 (De Haan and Finlayson-Pitts, 1997).

Other uptake coefficient values for HNO_3 on sea salt have been reported. Knudsen cell flow reactor studies resulted in a steady-state HNO_3 uptake rate of $\gamma \cong 0.2$ (De Haan and Finlayson-Pitts, 1997).

Mineral Dust

The irreversible reactions between nitrogen oxides and mineral dust surfaces have been investigated (Dentener et al., 1996; Grassian, 2002). The research indicated that mineral dust aerosols provide an important sink for HNO_3 (Goodman et al., 2000), and these particles may have a significant impact on the chemistry of the troposphere (Dentener et al., 1996). Mineral aerosols are composed of metallic and nonmetallic oxides, silicates and carbonates.

Carbonates are of special interest as they may be especially effective in removing gaseous HNO_3 from the atmosphere (Reaction 3).

Grassian (2002) studied the uptake of gaseous HNO_3 by $CaCO_3$ using in situ FTIR spectroscopic methods. Her results indicate the dependence of water vapor on the HNO_3 uptake. Under dry conditions, exposure of $CaCO_3$ to HNO_3 resulted in very little changes to the solid particle. However, when the $CaCO_3$ particle was exposed to HNO_3 in the presence of 20% relative humidity, several changes were noted. Spectral absorption bands indicated the presence of the formation of $Ca(NO_3)_2$, the formation of gas-phase CO_2 and the presence of OH stretching vibrations from the adsorbed water. The quantity of adsorbed water increased with the increased $Ca(NO_3)_2$ formation. This is related to the solubility and hygroscopicity of the particle; calcium nitrate is more hygroscopic and approximately 100 times more soluble than calcium carbonate (Lide, 1991). The formation of $Ca(NO_3)_2$ allows more water to adsorb onto the particle surface.

Morphological studies of the surface of the calcium carbonate particles have been conducted using transmission electron microscopy. Unreacted calcium carbonate particles have a smooth shape. However, those particles exposed to nitric acid at 20% RH had irregular shape with jagged edges. Smooth $CaCO_3$ particles were seen to become more irregular with increased exposure to nitric acid. The jagged edges also resulted in an increase in the surface area of the particle. Similar studies were conducted using NaCl crystals. Upon exposure to HNO_3, the micrographs indicated a physical change in

morphology indicating the formation of $NaNO_3$ (Allen et al., 1996; Allen et al., 1998; Grassian, 2002).

Due to the presence of water vapor and the particle's ability to adsorb water, the reaction between nitric acid and carbonaceous mineral dust particles is not limited to the surface but can continue within the bulk of the particle (Goodman et al., 2000; Grassian, 2002). The adsorbed water is thought to be involved with the subsequent reactivity of the particle. This uptake of nitric acid and formation of $Ca(NO_3)_2$ has been found to be irreversible.

For $CaCO_3$, the uptake coefficients have been determined under a few different conditions (Goodman et al., 2000; Grassian, 2002; Hanisch and Crowley, 2001). At 0% and 20% relative humidities, they were estimated to be $\gamma = 2.4 \times 10^{-4}$ and $\gamma = 2.5 \times 10^{-3}$, respectively (Goodman et al., 2000; Grassian, 2002). Hanisch and Crowley determined the uptake coefficients for "dry" heated and "damp" unheated $CaCO_3$ to be $\gamma = (10 \pm 2.5) \times 10^{-2}$ and $\gamma = (18 \pm 4.5) \times 10^{-2}$, respectively. The value estimated under "damp" conditions by Hanisch and Crowley (2001) is thought to be more relevant under atmospheric conditions. Their reported value is considered a lower limit for the uptake of HNO_3 by $CaCO_3$.

Statement of the Problem

The atmospheric deposition of nitrogen has had a detrimental environmental impact on the water quality and biodiversity in Tampa Bay as well as other regions around the world. Nitrogen is deposited through wet and dry deposition processes in the form of both gaseous and particulate species. The dominant nitrogen-containing gaseous forms include nitric acid and ammonia; nitrate and ammonium are the dominant particulate species.

In the Tampa Bay area, gaseous ammonia and nitric acid and fine particle ammonium and nitrate (less than 2.5 μm in diameter) have been monitored since 1996. Research in coastal regions, however, has revealed the dominance of nitrate in the coarse mode (greater than 2.5 μm). By virtue of their increased mass, the coarse particles may have a greater local environmental impact than the fine particles as they have greater deposition velocities and shorter residence times.

The purpose of this study was to investigate the formation of particulate nitrate species in a coastal urban environment through the use of ambient monitoring and modeling. The goals of this study were:

- To characterize ambient air nitrate concentrations and particle size distributions through a network of sampling campaigns

- To determine the retention of nitric acid by nylon filters
- To determine the spatial distribution of particles along an air mass trajectory
- To evaluate the use of a thermodynamic equilibrium model for predicting ambient aerosol phases and concentrations
- To expand the current data set (from 1996 to the present) to account for coarse mode nitrate formation and its contribution to the local nitrogen deposition estimates
- To determine if macroparticles, those with a diameter greater than 10 μm, contain nitrogen
- To determine the partitioning of nitric acid gas to particles nitrate by NaCl and $CaCO_3$ (mineral dust)
- To model the formation of particulate nitrate on NaCl, sea salt and mineral dust particles, with a focus on macroparticle formation, and to determine the environmental implications

This knowledge will be useful in developing more accurate estimates of the atmospheric contribution of nitrogen to Tampa Bay. The need and importance of coarse particle nitrate monitoring will be addressed as well as the chemistry behind the formation of these particles.

Methods and Experimental

Instrumentation

Cascade Impactors

Two sampling systems were used throughout these experiments to collect size-segregated particulate matter. The Andersen impactor (Mark-II Cascade Impactor, Thermo Andersen) had eight fractionated stages with nominal cut-points of 10, 9.0, 5.8, 4.7, 3.3, 2.1, 1.1, 0.7, 0.4 μm and a backup filter. The flow rate was factory set at 28.3 L min^{-1} and was verified using a dry gas meter. Custom-cut 81-mm quartz filters (Pall Gelman Sciences) were used as the collection media. Quartz was chosen for its low SO_2 absorption (Batterman et al., 1997) and low blank analyte concentrations.

Four different non-rotating Micro-Orifice Uniform Deposit Impactors (MOUDI™, MSP Corporation) (Marple et al., 1991) were used during May 2002. Two MOUDIs (MDI-242 and MDI-245) had ten fractionated stages with nominal cut-points of 18, 10, 5.6, 3.2, 1.8, 1.0, 0.56, 0.32, 0.18, 0.10, 0.056 μm and a backup filter. One MOUDI (MDI-020) had eight fractionated stages with nominal cut-points of 18, 3.2, 1.8, 1.0, 0.56, 0.32, 0.18, 0.10, 0.056 μm and a backup

filter. Nominal cut-points for the MDI-079 MOUDI were 18, 10, 5.6, 3.2, 1.8, 1.0, 0.56, 0.32, 0.18 μm and a backup filter. Each MOUDI was equipped with Pall Gelman Sciences Teflo™ PTFE membrane filters. To prevent an excess pressure drop, 2-μm pore size filters were used for all backup filters. The flow rate for the MOUDIs was set at 30 L min^{-1} and was verified using a dry gas meter. Teflo filters were chosen for their low blank analyte concentrations and their inertness towards the species of interest.

Annular Denuder System

The annular denuder system (ADS) consisted of (a) a Teflon-coated cyclone inlet to remove particles 2.5 μm or greater in diameter, (b) annular denuders to quantitate acidic and basic gases, and (c) a filter pack for particle collection. The denuders are a series of concentric glass tubes that have been etched and coated with chemicals to adsorb gaseous species of interest. During operation, ambient air is drawn in through the cyclone, passed through the denuders, and then filtered. The filter pack typically held a single Teflon PTFE or Nylasorb® nylon membrane filter. A series of filters or impregnated filters may be used to collect species that may have volatilized off the denuders of preceding filters.

A typical deployment setup for the ADS included (a) a denuder housing, to protect the ADS from the harsh elements, (b) rigid air tubing, to prevent the line from collapsing, and (c) a pump, typically encased in a weatherproof housing.

Flow rates can vary from system to system depending on the type of equipment purchased. In these experiments, the flow rate was set at 10 L min^{-1}. The flow rate was checked using a dry gas meter.

Dichotomous Sampler

The Rupprecht and Patashnick Partisol®-Plus Dichotomous Model 2025 Sequential Air Sampler was an automated monitoring device allowing for the collection of $PM_{2.5}$ and $PM_{10\text{-}2.5}$ (Poor et al., 2002). The $PM_{2.5}$ and $PM_{10\text{-}2.5}$ fractions are termed the "fine" and "coarse" particulate matter fractions, respectively. The combined flow rate for the instrument was 16.7 L min^{-1}, which was split, directing 15.0 L min^{-1} and 1.7 L min^{-1} of ambient air onto the fine and coarse filters, respectively. The inlet apparatus was approximately 2.5 meters above ground level. Samples were collected using Whatman® PTFE 46.2-mm filters, integrating over 24 hours.

Total Suspended Particulate Collection

An inverted filter pack from URG Corporation was used to collect total suspended particulate matter (TSP) to determine the concentration of macroparticles (greater than 10 µm in diameter). The filter pack was attached to a burette stand and placed on a platform, with the inlet approximately 2.5 m above the ground. The ambient airflow was 28.3 L min^{-1}, sufficient to collect

particles up to approximately 80 μm in diameter. Samples were collected daily on Whatman 46.2-mm PTFE filters, integrating over 24 hours.

Filters

Several different types of filters were used during the course of the experiments. The instrumentation limited the size of filters required for sample collection, and the types of experiment governed the type of filter used. The dichotomous, macroparticle and MOUDI samplers used 47-mm filter media, where the filter media included: Pall Gelman Sciences Nylasorb membrane, Whatman PTFE and Teflo filters. The PTFE filters were inert towards the species of interest and had the advantage of low HNO_3 adsorption, hence the minimization of nitrate bias. Nylasorb membrane filters were used to prevent volatilization and loss of particles. The Andersen cascade impactor used custom cut 81-mm quartz fiber filters, purchased from Pall Gelman Sciences.

Due to the presence of background analytes, lab blanks were used to correct for background concentration. Field and trip blanks were also collected for all media types.

Because the nature of environmental work is similar to trace analysis, filters and equipment were treated with special care to avoid contamination. While working with the instrumentation and filters, powderless gloves were worn and clean tweezers were used. All equipment and glassware were washed, double rinsed in deionized water and allowed to air dry.

Filter Extraction

Filters were removed from the sampling apparatus using tweezers while wearing powderless gloves. Filters were placed into 15-mL centrifuge tubes, and 5-15 mL of >18 MΩ-cm deionized water was added. The volume of water depended on the type and size of filter to be extracted. For 47-mm Nylasorb and Teflon PTFE filters prior to May 2002, 10.0 mL of deionized water was used. For 81-mm quartz filters, 15.0 mL of deionized water was used. For all MOUDI samples collected during May 2002, 5.0 mL of deionized water was used. Smaller aliquots of water were used to lower detection limits during specified sampling events.

The deionized water was added to the centrifuge tubes using a calibrated pipettor. The filters were then sonicated for 45 min. The extract was decanted into vials for ion chromatography analysis, leaving ~0.5 mL for pH analysis. If samples were not analyzed that day, they were stored at 4°C until analysis.

Denuder Preparation and Extraction

Preparation

The denuder coatings chosen for these experiments were sodium carbonate (Na_2CO_3) and either citric ($C_6H_8O_7$) or phosphoric (H_3PO_4) acid. A Na_2CO_3 coating removes acidic atmospheric gases, such as HCl, HNO_2, HNO_3 and SO_2 (Allegrini et al., 1994). Citric and phosphoric acids capture ammonia (Allegrini et al., 1994).

Alkaline denuders were coated with Na_2CO_3 and glycerol (1% + 1% w/w) in a 50:50 v/v water-methanol solution (Allegrini et al., 1987; Allegrini et al., 1994; Vossler et al., 1988). Collection efficiencies were determined to be >99.5% for HCl, >98.5% for HNO_2, >97% for HNO_3 and >99% for SO_2 (Allegrini et al., 1987; Perrino et al., 2001).

Acidic denuders were coated with either citric or phosphoric acid (1% w/v) in an 80% v/v methanol solution (Allegrini et al., 1994). The collection efficiency for ammonia was determined to be >99% with negligible deposition of particulate NH_4^+ (Allegrini et al., 1987; Perrino et al., 2001; Vossler et al., 1988).

Prior to coating, each denuder was rinsed with deionized water for one minute followed by approximately 5 mL of the coating solution. The coating solution was then decanted and the denuder filled with ~10 mL of the fresh coating solution. The denuder was shaken or placed on a rotating table for 10 min. The solution was then decanted, and the denuders were dried using either

filtered compressed air or zero air (Vossler et al., 1988). The compressed air was filtered through silica gel, activated carbon and acid-coated glass beads. The acid coating was used on the beads to capture any ammonia.

Extraction

Denuders were extracted using 10.0 mL of >18 MΩ-cm deionized water. Denuders were capped and either shaken or placed on a rotating table for 10 min. The extract was decanted into vials for analysis by ion chromatography.

The filters from the ADS filter pack were removed using tweezers and placed into 15 mL centrifuge tubes. 10.0 mL of >18 MΩ-cm deionized water was added to each tube, which were then capped and sonicated for 30 min (Vossler et al., 1988). An aliquot of the filter extract was taken for pH analysis. The remainder was filtered using a Pall Gelman Sciences 0.45 µm syringe tip filter and placed into vials for analysis by ion chromatography. Lab blanks were used to correct for background concentrations.

Sample Analysis

Ion Chromatography Analysis

Prior to June 2001, samples were analyzed using a Dionex 2000i ion chromatograph. After June 2001, samples were analyzed using a Dionex DX-

600 ion chromatograph. In both systems, cations (Na^+, NH_4^+, K^+, Mg^{2+} and Ca^{2+}) were analyzed using CS12G guard and CS12A analytical columns. Prior to June 2001, anions (F^-, Cl^-, NO_2^-, NO_3^-, PO_4^{3-} and SO_4^{2-}) were analyzed using AS4G guard and AS4A analytical columns. Post June 2001, AS14G and AS14A columns separated the anions. For both cations and anions, isocratic elution and self-regenerating suppressors were used.

Calibration curves were used to determine the concentration of each analyte. Curves were created using external standards from SPEX CERTIPREP®. Three check standards were run for every ten samples for verification. These standards were prepared from a separate batch of standards from which the curves were run.

pH Analysis

pH of samples was taken using an Accumet® AR50 pH meter fitted with a Thermo Orion pH probe. The pH meter was calibrated using four points: 4.00, 5.00, 6.00 and 7.00. Prior to analysis, samples were brought to room temperature. Measurements were taken with ~0.5 mL of sample. The pH probe was rinsed with deionized water, blotted using Kimwipes® and place into the sample. The pH was allowed to stabilize. The sample was stirred, and the pH was allowed to re-stabilize. The pH was then recorded. The probe filling solution was replaced every 30 days, and calibration was checked daily.

Trajectory Analysis

Incoming air masses to the Tampa Bay area were classified using backward trajectories obtained from the National Oceanographic and Atmospheric Administration's Air Resources Laboratory (NOAA ARL) website (Draxler and Hess, 1998; HYSPLIT4, 1997). The Hybrid Single-Particle Lagrangian Integrated Trajectory (HYSPLIT) model plots the trajectory of an air mass on a three-dimensional grid using archived two-hour meteorological data and Lagrangian and Eulerian calculations. Trajectories were plotted for each 24-hour sampling period at each sampling site (Table 3).

Site	Street Address	City	Latitude	Longitude
Azalea Park	7200 22nd Ave. N.	St. Petersburg	27N 47' 03"	82W 44' 24"
Gandy	5121 Gandy Blvd.	Tampa	27N 53' 33"	82W 32' 15"
Sydney	Dover & Sydney Rds.	Dover	27N 57' 56"	82W 13' 56"

Table 3. Addresses and coordinates for each sampling site.

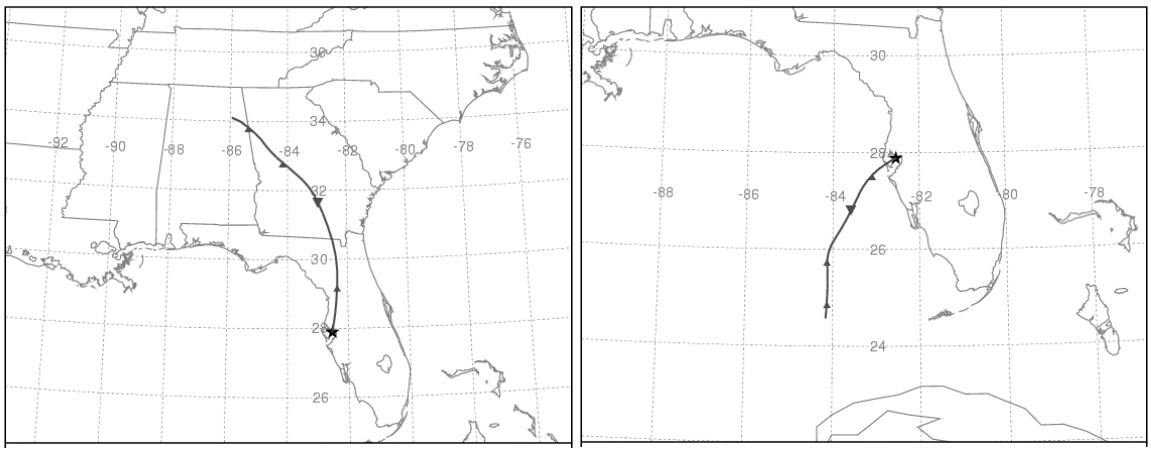

Figure 2. 24-hour backward trajectories for (a) terrestrial or land origin (October 17, 2001) and (b) marine origin (October 25, 2001) (HYSPLIT4, 1997).

Terrestrial or land air masses consisted of masses that originated from the north, swept across the state of Florida, or swirled around Tampa (as moderately stagnant air). Marine air masses were those that spent the majority of their path over the Gulf of Mexico or the Atlantic Ocean.

Error Analysis

MOUDI

Error was estimated for the MOUDI samplers using collocated instrument data from the May 2002 Sydney site intensive monitoring period. Two instruments were deployed side-by-side. The flow rates of each instrument were adjusted so they were identical at 30 L min^{-1}. Instrument A was comprised of twelve collection bins and instrument B only ten. The three smallest bins of instrument A collected the same diameter particles as the smallest bin of instrument B. Bins nine through twelve of instrument A were summed and then compared to bin ten of instrument B. This resulted in ten comparable bins for May 2-20, 2002. On May 21, 2002, the instruments were exchanged and rotated at the collection sites. Instrument C was collocated with instrument B. However, instrument C did not contain the same cut-points as instrument B. The only way to compare these instruments would have been to sum all of the bins. Because

of this, samples collected after May 20, 2002, were not used in the error estimation.

Figures 3-11 display the size distributions for the collocated measurements. Size distributions for fluoride, nitrite and phosphate were not created because these analytes were near the detection limits.

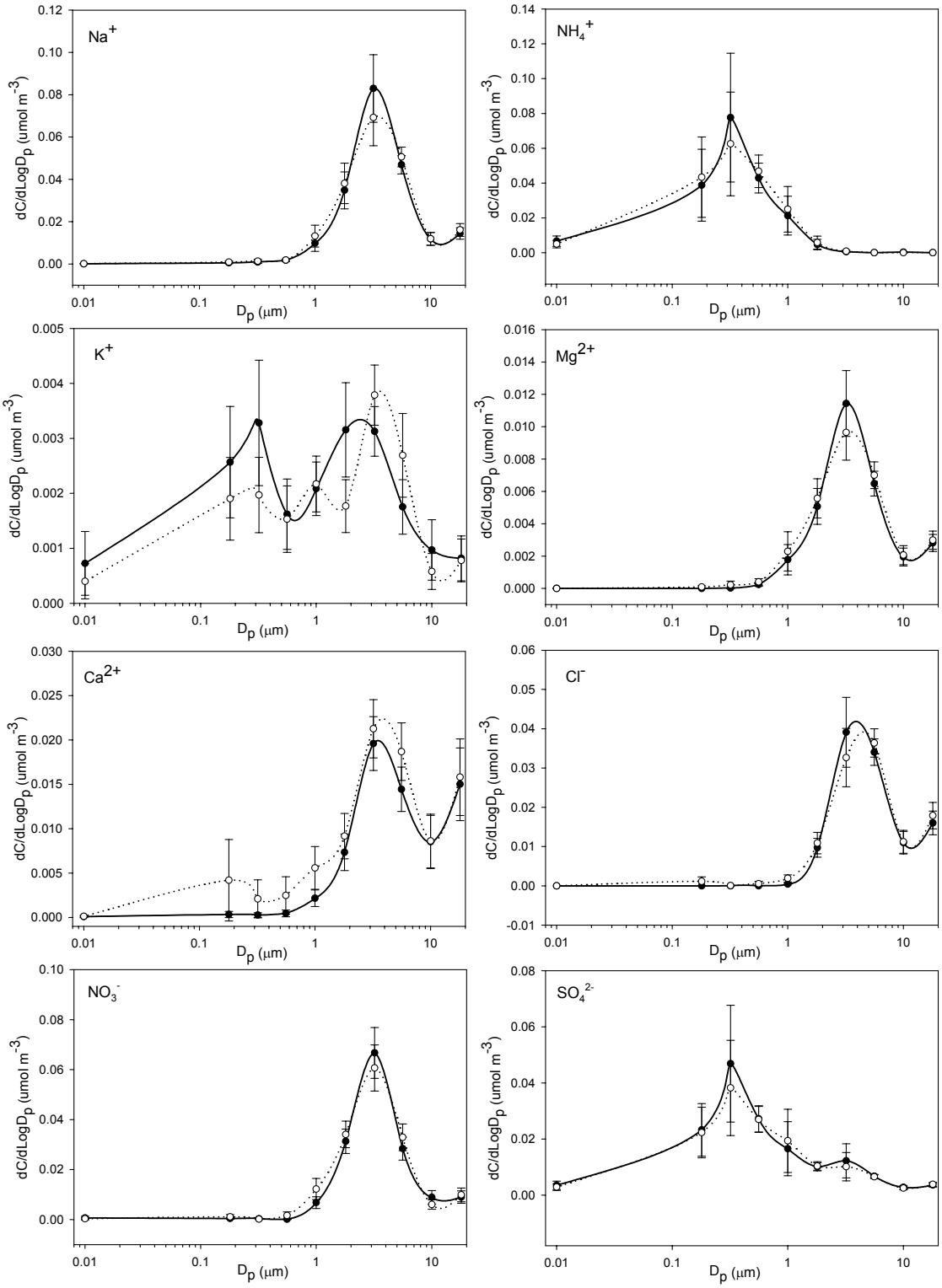

Figure 3. Comparison of collocated measurements of instrument A (●) and instrument B (○) for May 4, 2002.

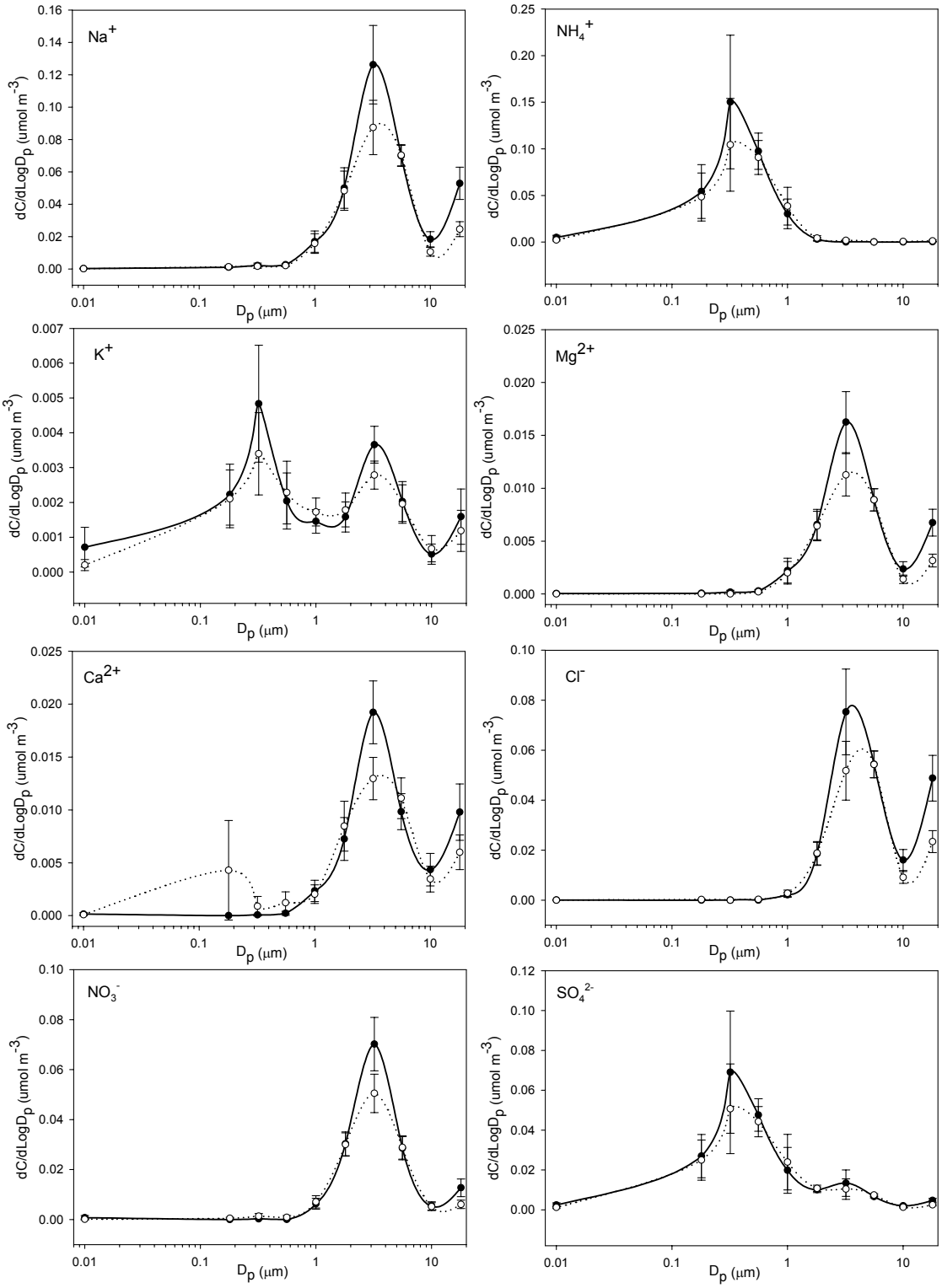

Figure 4. Comparison of collocated measurements of instrument A (●) and instrument B (○) for May 6, 2002.

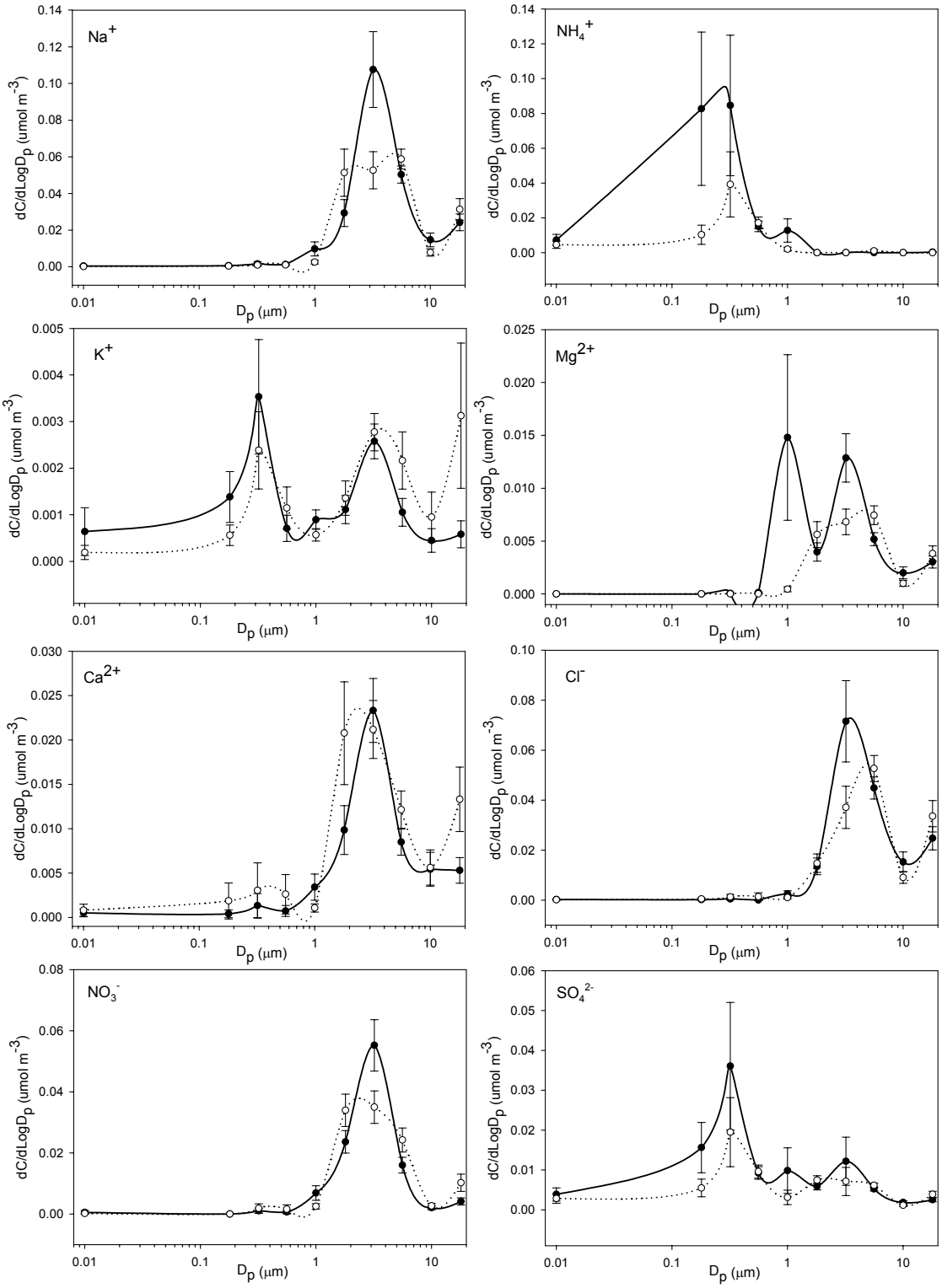

Figure 5. Comparison of collocated measurements of instrument A (●) and instrument B (○) for May 10, 2002.

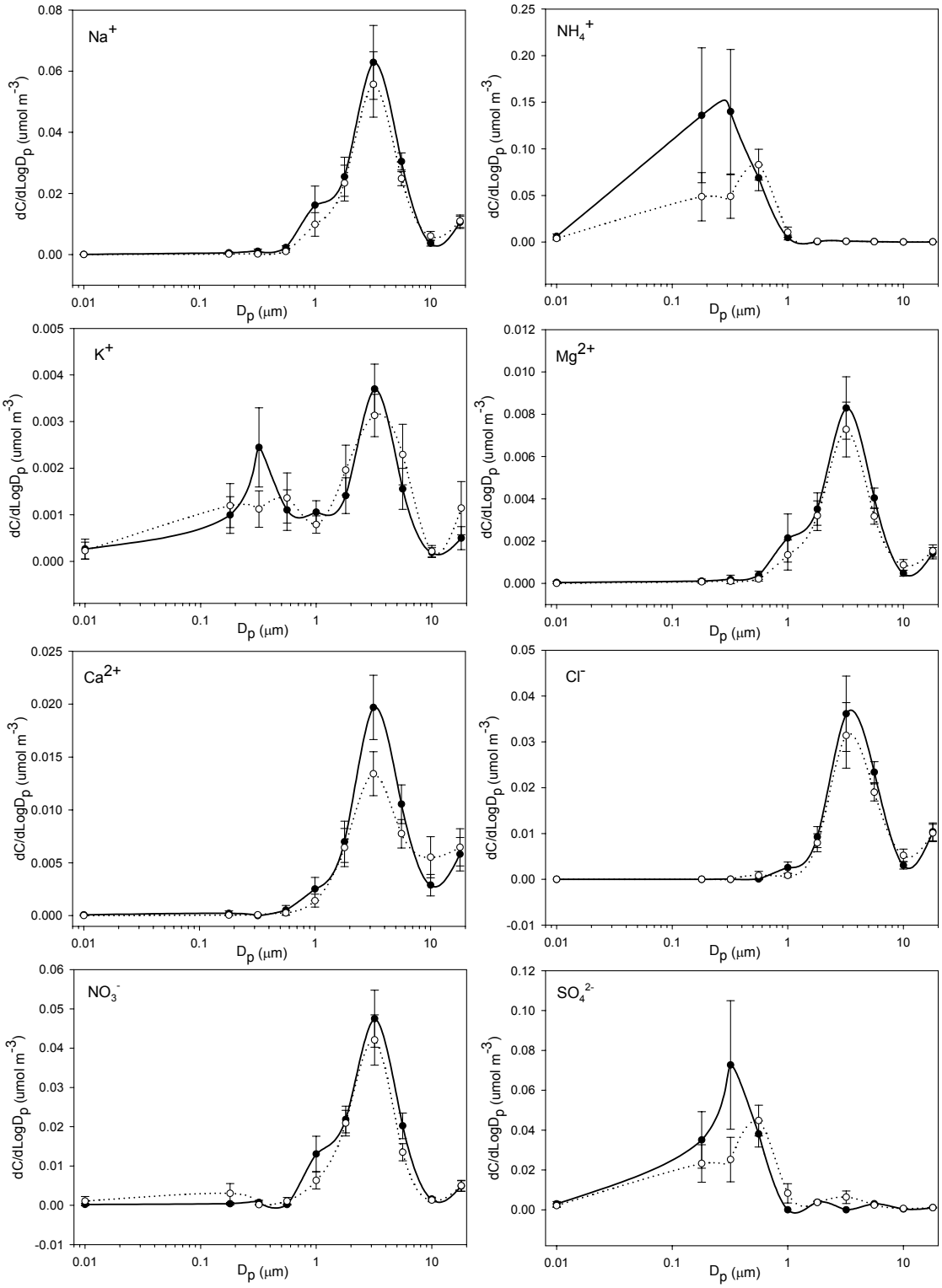

Figure 6. Comparison of collocated measurements of instrument A (●) and instrument B (○) for May 14, 2002.

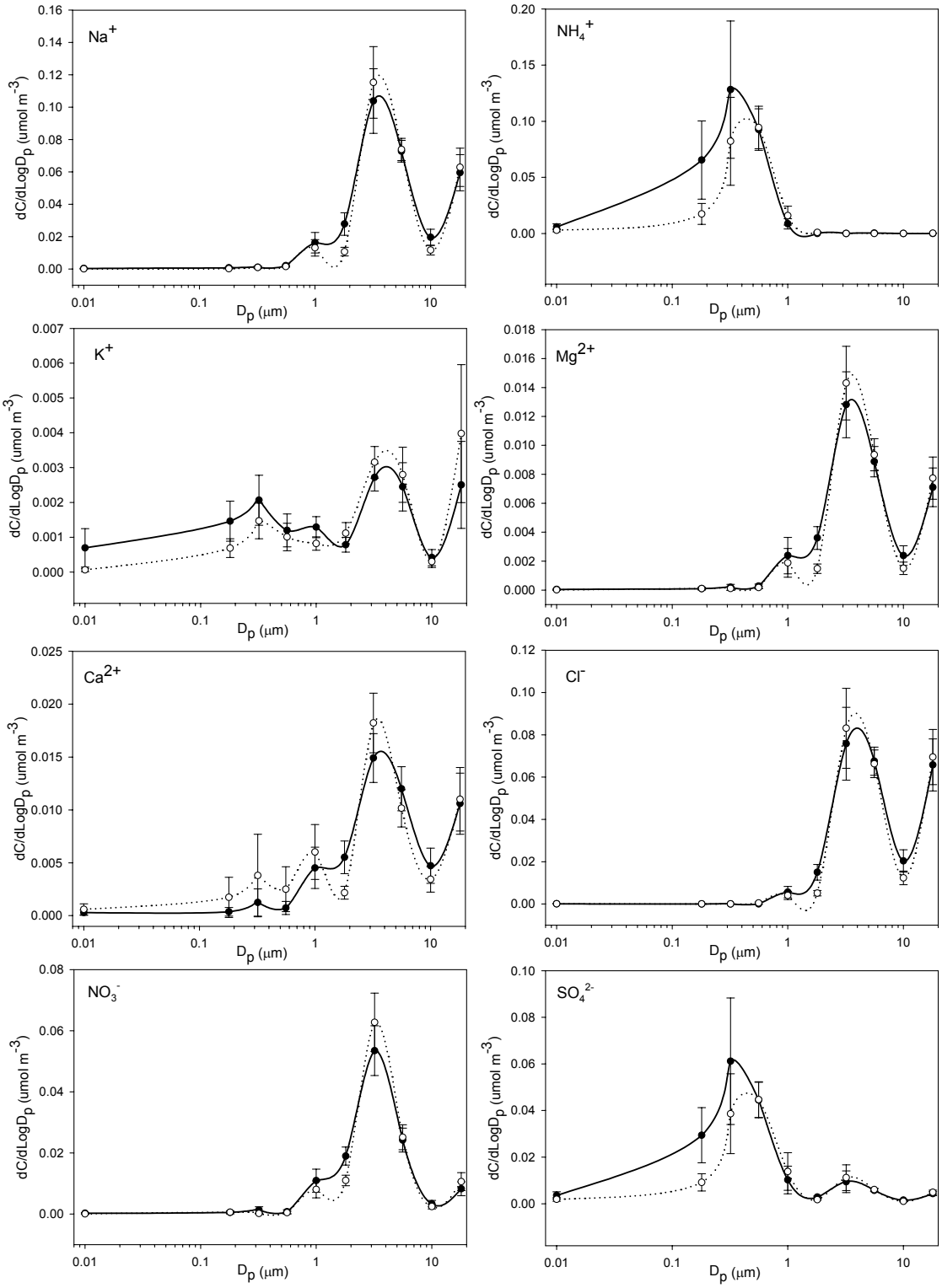

Figure 7. Comparison of collocated measurements of instrument A (●) and instrument B (○) for May 15, 2002.

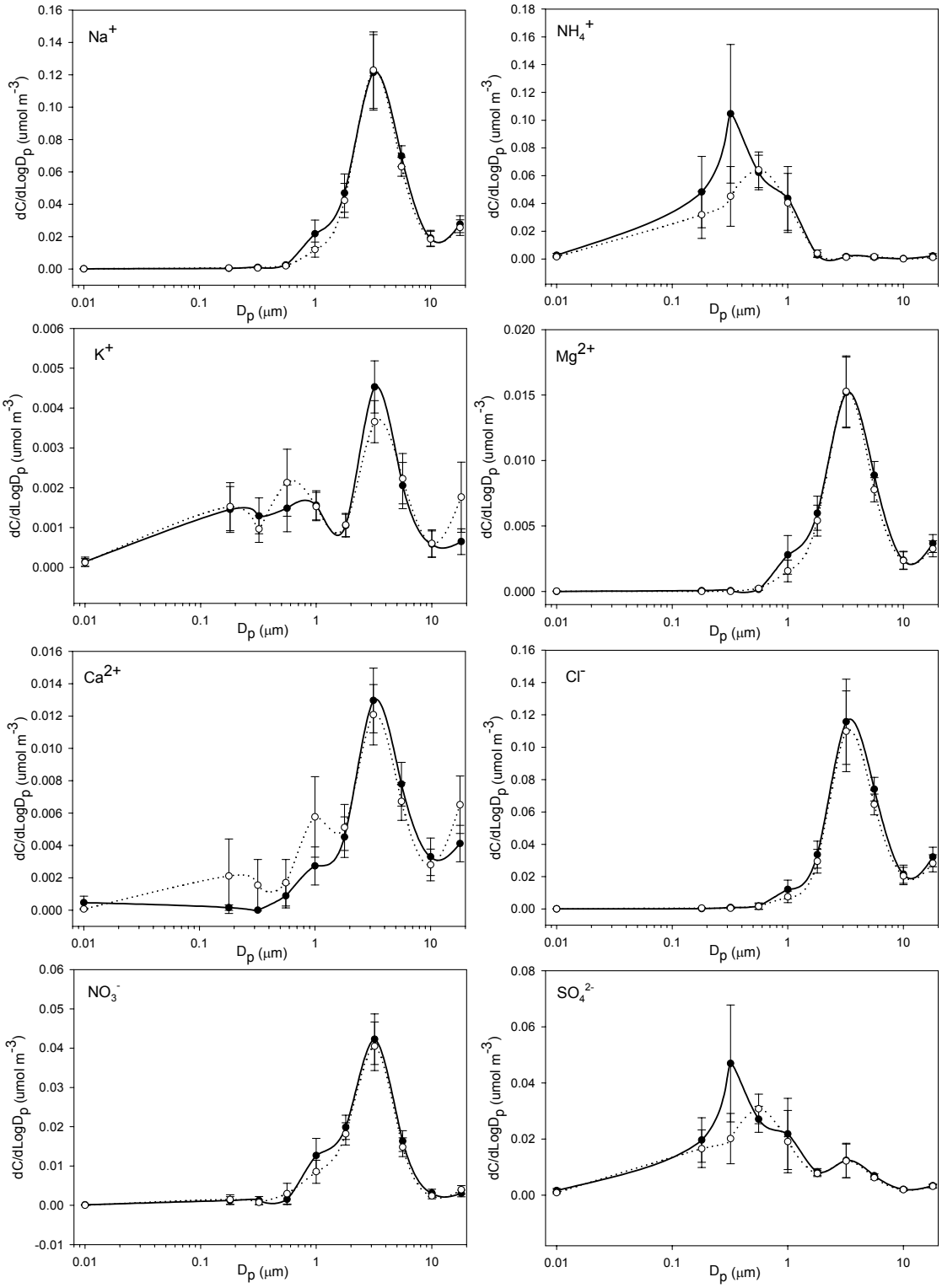

Figure 8. Comparison of collocated measurements of instrument A (●) and instrument B (○) for May 16, 2002.

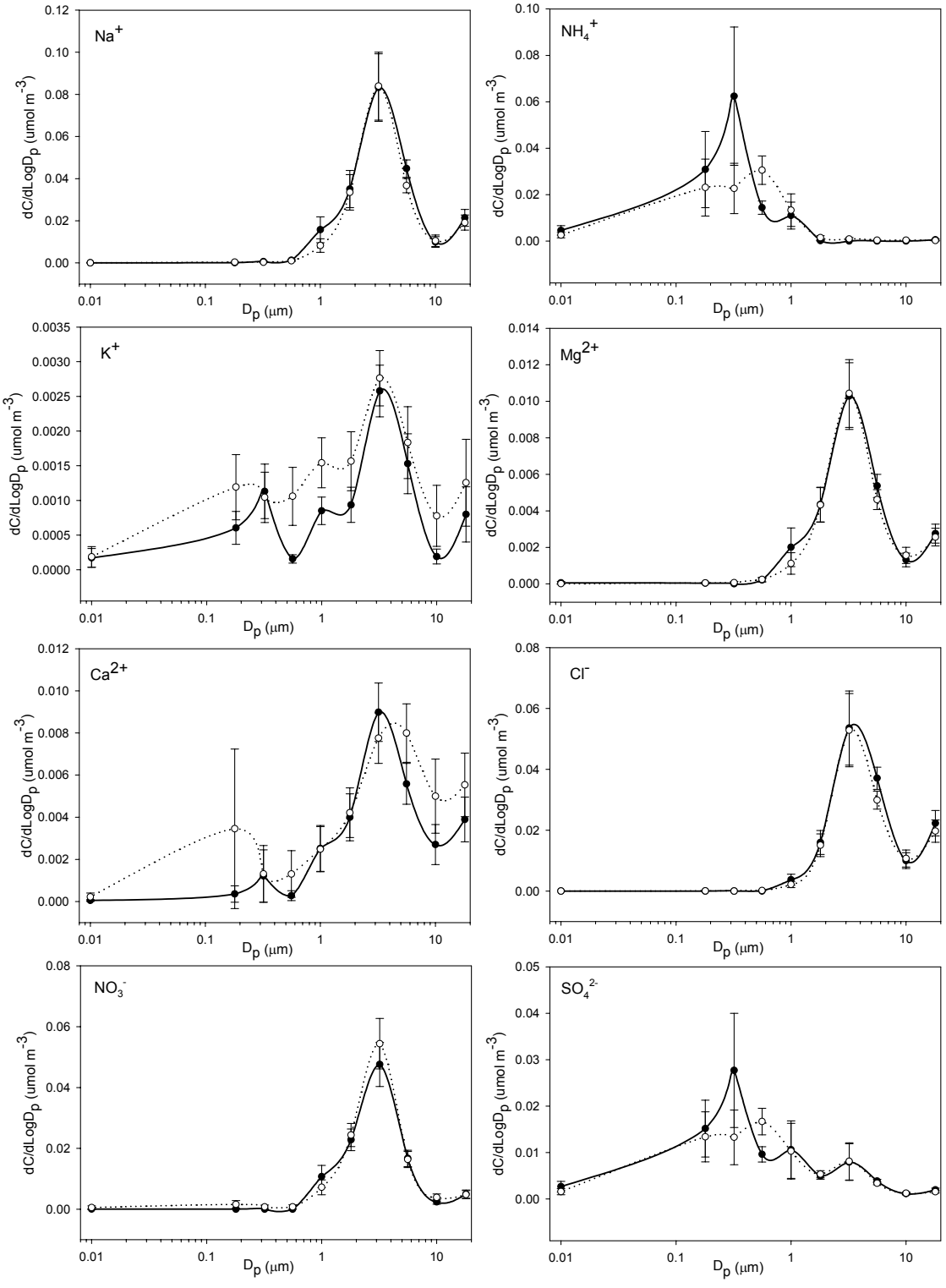

Figure 9. Comparison of collocated measurements of instrument A (●) and instrument B (○) for May 17, 2002.

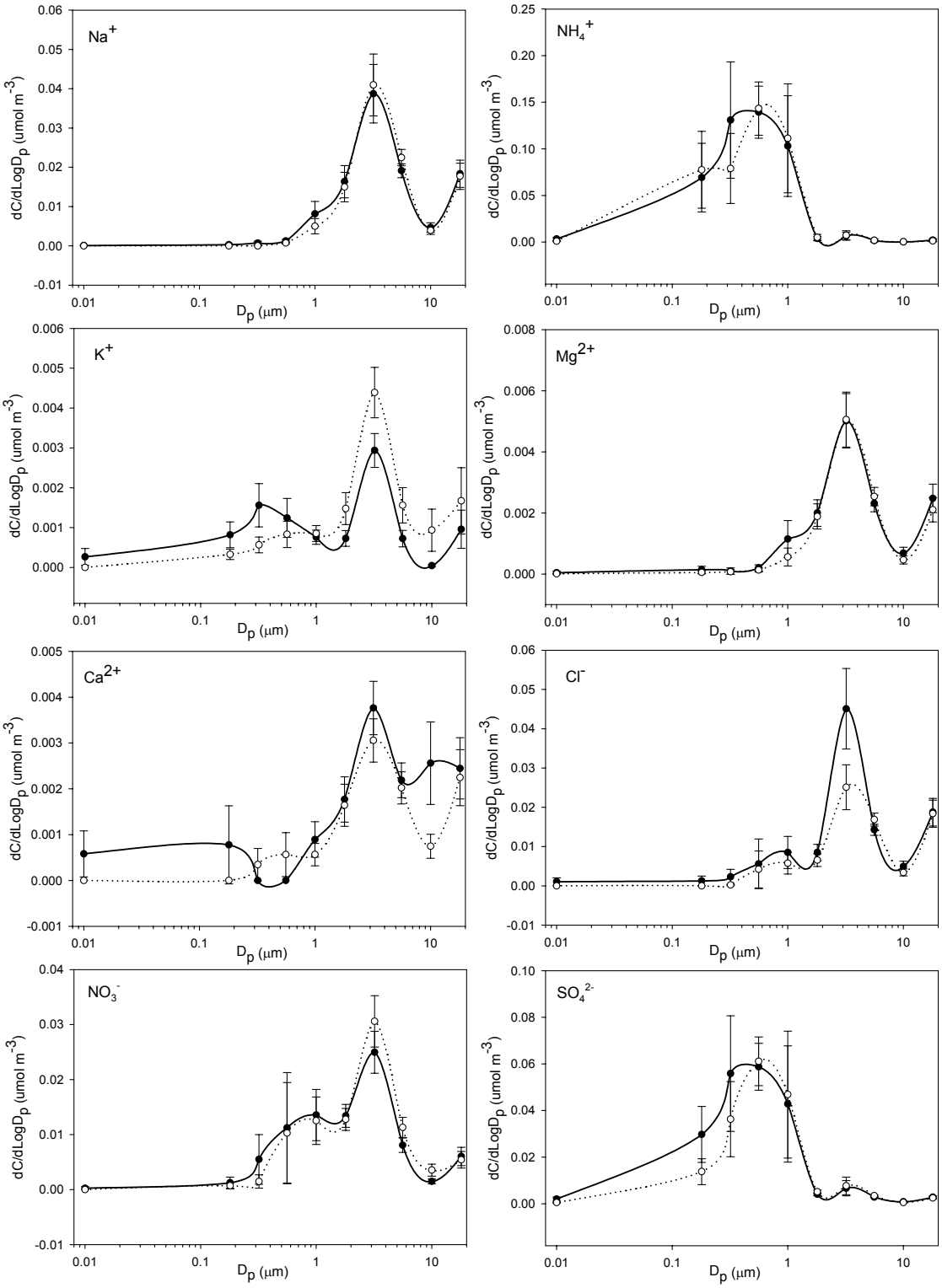

Figure 10. Comparison of collocated measurements of instrument A (●) and instrument B (○) for May 19, 2002.

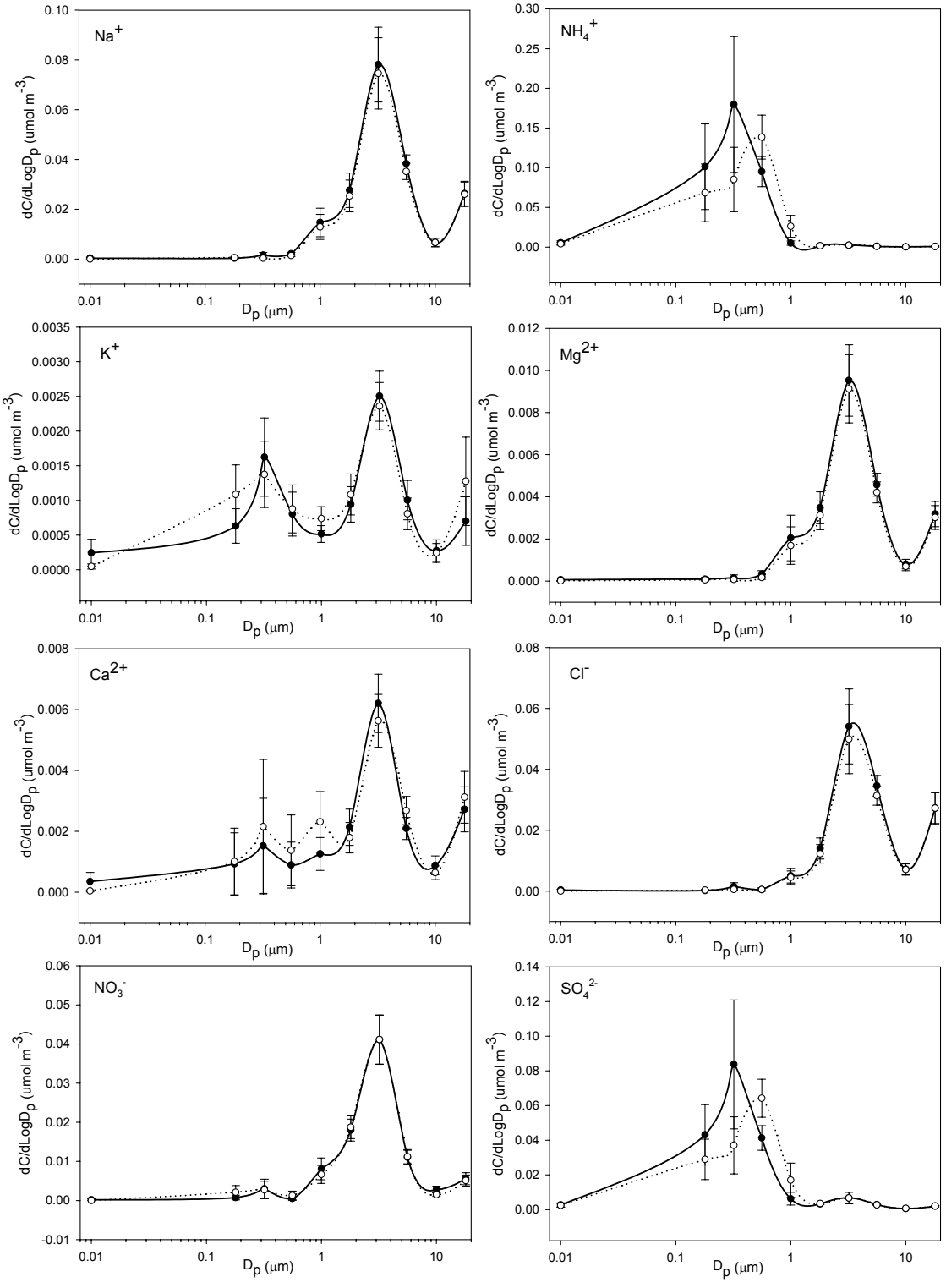

Figure 11. Comparison of collocated measurements of instrument A (●) and instrument B (○) for May 20, 2002.

Relative bias and relative precision were calculated for the error analysis period using Equations 12-14 (Poor et al., 2002). The relative precision was calculated for each analyte in each size bin (Table 4).

$$RB_i = \frac{2(y_i - x_i)}{(y_i + x_i)} \qquad \text{(Equation 12)}$$

$$RB = \frac{1}{n}\sum_i RB_i \qquad \text{(Equation 13)}$$

$$RP = \sqrt{\frac{1}{n}\sum_i \left(\frac{RB_i}{\sqrt{2}}\right)^2} \qquad \text{(Equation 14)}$$

Geo Mean (μm)	Bin Max (μm)	Na^+	NH_4^+	K^+	Mg^{2+}	Ca^{2+}	F^-	Cl^-	NO_2^-	NO_3^-	PO_4^{3-}	SO_4^{2-}	AVG
23	30	19%	77%	50%	19%	27%	73%	19%	92%	28%	19%	20%	40%
13	18	26%	100%	57%	28%	35%	103%	26%	116%	31%	48%	24%	54%
7.5	10	9%	82%	28%	12%	17%	70%	10%	90%	16%	50%	9%	36%
4.2	5.6	19%	68%	14%	18%	15%	65%	23%	98%	15%	56%	50%	40%
2.4	3.2	25%	64%	27%	22%	28%	83%	25%	98%	16%	13%	14%	38%
1.3	1.8	39%	53%	23%	53%	43%	82%	48%	75%	34%	77%	58%	53%
0.75	1.0	28%	20%	40%	50%	85%	47%	112%	97%	90%	1%	17%	53%
0.42	0.56	71%	48%	35%	106%	103%	47%	85%	96%	82%	82%	44%	73%
0.24	0.32	73%	53%	39%	86%	110%	47%	99%	109%	83%	67%	40%	73%
0.042	0.18	98%	45%	80%	124%	87%	47%	96%	100%	109%	67%	42%	81%
Average		41%	61%	39%	52%	55%	66%	54%	97%	50%	48%	32%	54%

Table 4. Relative precision for the MOUDI instrument during May 2002.

Relative precision improves at higher analyte concentration. Chloride is predominantly a coarse mode species. When analyzing the relative precision for chloride in the coarse particle bins, the relative precision is, on average, 20%. When analyzing the chloride in the fine particle bins, however, the relative precision is near 100%. Analyte concentrations of F^-, NO_2^- and PO_4^{3-} were near

the detection limits during the sampling period, resulting in higher relative precision values.

The relative precision values listed in Table 4 were used to place error bars on the MOUDI measurements.

Annular Denuder System

Error estimation for the annular denuder system (ADS) was done using collocated measurement data from August 1996 through November 2002. The Environmental Protection Commission of Hillsborough County collected data on a one-in-six day measurement cycle at the Gandy monitoring site. The relative bias and precision were calculated using Equations 12-14. The values are reported in Table 5.

	Number of Samples (n)	Relative Precision (%)
HCl	19	37%
HNO_3	304	24%
NH_3	305	15%
SO_2	303	14%
NO_3^-	280	23%
NH_4^+	278	28%
SO_4^{2-}	281	26%

Table 5. Relative precision for the annular denuder system measurements.

Grubbs' Outlier Test

The Grubbs' outlier test (GraphPad Software, 2000) is also called the extreme studentized deviate (ESD) method. The test computes a $Z_{obtained}$ value,

$$Z = \frac{|\, mean - value \,|}{SD} \qquad \text{(Equation 15)}$$

where the *mean* was the arithmetic mean of the data set, *value* was the numerical value in question and *SD* was the standard deviation of the data set. Both the mean and the standard deviation were calculated using all of the values, including the outlier value in question. The $Z_{obtained}$ value was compared to a $Z_{critical}$. The null hypothesis was rejected if $|Z_{obtained}| > |Z_{critical}|$, and the value in question was identified as an outlier.

Paired t-Test

The paired t-test was used to compare the means of two groups of data. The test assumes the sampled data set was taken from a Gaussian bell-shaped distributed population. A null hypothesis was developed stating the two data sets were not statistically different. The difference between each pair of measurements was calculated. The mean, $\bar{d}$, and the standard deviation, *SD*,

of the differences were then calculated and used to obtain a t-value (Glover and Mitchell, 2002; Pagano and Gauvreau, 2000),

$$t = \frac{\bar{d}}{\left(\frac{SD}{\sqrt{n}}\right)} \qquad \text{(Equation 16)}$$

where n was the number of observations. The null hypothesis was accepted if $|t_{obtained}| < |t_{critical}|$, indicating the data sets were not statistically different.

Wilcoxon's Signed Rank Test

The Wilcoxon's signed rank test is a non-parametric test used to test the differences between two paired data sets taken from a non-Gaussian distributed population. Values were ranked according to the absolute value of their size from the smallest to the largest (Ott, 1993; Pagano and Gauvreau, 2000). The ranks were summed as:

$$S = \frac{n(n+1)}{2} \qquad \text{(Equation 17)}$$

where n was the number of observations. Ranks were then summed according to their association with positive or negative values.

$$T_{obtained} = min(S_+, S_-) \qquad \text{(Equation 18)}$$

The smaller of the two values (S_+ or S_-) was used as the test statistic. $T_{critical}$ can be obtained from a table. The null hypothesis was accepted if $|T_{obtained}| < |T_{critical}|$ indicating the paired data sets were not statistically different.

Experimental Studies

Preliminary Dichotomous Studies

Local air quality and particulate matter size distributions depend on the local environment and meteorological conditions. Particulate ammonium and nitrate can be found in the fine fraction as NH_4NO_3, as seen in California's urban environment (Grosjean, 1982); and nitrate can be almost exclusively in the coarse fraction as $NaNO_3$, as seen in Hong Kong's maritime environment (Zhuang et al., 1999a; Zhuang et al., 1999b). Previous measurements of coarse particulate matter in urban coastal Tampa have only included mass determination; they have not included inorganic species determination through chemical analysis. The main focus of this experiment was to develop a background understanding of the inorganic aerosol distribution for the Tampa area.

Experimental

Samples were collected at the Gandy Bridge sampling site, adjacent to Tampa Bay, with the help of the Environmental Protection Commission of

Hillsborough County. The samples were collected during a seven-day period from October 5-12, 2000, using a dichotomous sampler. The sampler was equipped with Nylasorb membrane filters, integrating over 24 hours. After sampling, the filters were brought back to the laboratory where they were extracted and analyzed.

Results and Discussion

Samples were analyzed to determine which particulate species dominated the coarse and fine size fractions. Results indicated the following: sodium, calcium, chloride and nitrate were the species dominating the coarse size fraction (Figure 12). The remainder, ammonium, potassium, fluoride, sulfate and hydronium, were primarily found in the fine fraction. The coarse percent of a species was calculated by:

$$Coarse\ \%\ [Na^+] = \frac{[Na^+_{coarse}]}{([Na^+_{coarse}] + [Na^+_{fine}])} \times 100\% \qquad \text{(Equation 19)}$$

The high concentrations of sodium and chloride in the coarse fraction can be attributed to the presence of sea salt at the bayside Gandy site. Calcium was also found predominantly in the coarse mode. The Ca^{2+}:Na^+ molar ratios for this sampling period averaged to be 0.41, where the ratio to that in seawater is 0.044 (Zhuang et al., 1999a). The excess calcium in the coarse fraction, which was not accounted for by sea salt, can be attributed to mineral dust ($CaCO_3$) particles (Zhuang et al., 1999a).

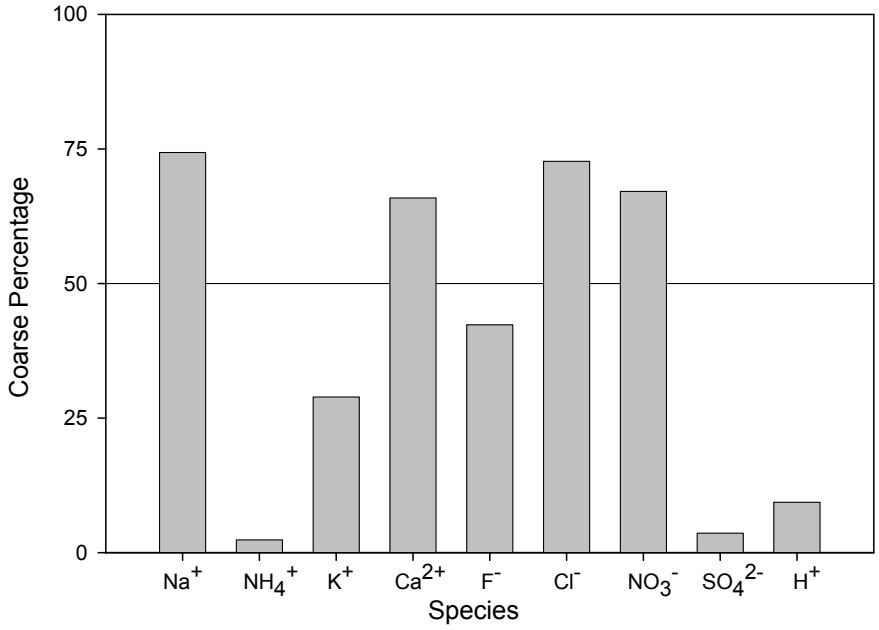

Figure 12. Coarse percentage for dichotomous samples collected during October 5-12, 2000.

About two-thirds, or 67%, of nitrate was found in the coarse fraction. Coarse mode nitrate is assumed to be predominantly $NaNO_3$, a product from the reaction with sea salt. The presence of nitrate in the fine fraction was not thought to be NH_4NO_3, as this species is very volatile and unlikely to form in warm, humid environments (Allen et al., 1989; Grosjean, 1982). Instead, the presence of fine mode nitrate can be attributed to two reasons: (1) the filter media used for collection was Nylasorb membrane filters. These nylon filters have a tendency to adsorb nitric acid from the air stream, potentially biasing the nitrate concentration. In the dichotomous sampler, the air stream was split by a virtual

impactor, 1.67 L min^{-1} of the incoming air was directed onto the coarse filter, with the remaining 15 L min^{-1} directed onto the fine filter (Poor et al., 2002). This increase in airflow on the fine filter greatly increased the potential for bias during the sampling period. (2) The distribution of coarse mode nitrate may extend into the fine (<2.5 μm) fraction. This theory will be examined using size distribution studies.

Size Distribution Determination

Cascade impactors are instruments used to obtain a clearer understanding of particle size distributions. These instruments separate particles by their aerodynamic diameter into multiple size bins instead of simply coarse and fine particle bins. The purpose of this experiment was to determine the size distribution of nitrate and ammonium particles.

Experimental

An Andersen cascade impactor was deployed during a three-day period, January 11-13, 2001. The instrument was equipped with custom-cut quartz fiber filters, integrating over 72 hours. For instrument comparison, a dichotomous sampler was collocated with the Andersen impactor. The dichotomous sampler was equipped with Nylasorb membrane filters, integrating over 24 hours.

Results

Table 6 shows the range and three-day averaged concentrations for the dichotomous fine and coarse size fractions. Table 7 shows the total concentrations for the Andersen cascade impactor samples for the three-day integrated period based on size fraction.

Dichotomous Particle Concentrations (μg m^{-3})				
	Fine (D_p<2.5 μm)		Coarse (2.5<D_p<10 μm)	
	Min-Max	3-Day Avg	Min-Max	3-Day Avg
H^+	0.03-0.16	0.10	0.00-0.15	0.05
Cl^-	0.00-0.07	0.03	0.01-0.46	0.18
NO_3^-	0.67-1.8	1.2	0.00-1.8	0.91
SO_4^{2-}	4.6-5.4	5.1	0.00-0.00	0.00
Na^+	0.00-0.91	0.40	0.16-2.0	1.12
NH_4^+	1.0-1.3	1.1	0.00-0.05	0.02
K^+	0.03-0.06	0.04	0.00-0.00	0.00
Mg^{2+}	0.00-0.05	0.02	0.04-0.19	0.12
Ca^{2+}	0.00-0.31	0.10	0.16-0.38	0.26

Table 6. Total and averaged daily concentrations of dichotomous samples collected January 11-13, 2001.

Cascade Impactor Particle Concentrations (μg m^{-3})									
	Size ranges, μm								
	0.0-0.4	0.4-0.7	0.7-1.1	1.1-2.1	2.1-3.3	3.3-4.7	4.7-5.8	5.8-9.0	9.0-10
H^+	0.00	0.002	0.002	0.001	0.00	0.001	0.005	0.00	0.002
Cl^-	0.00	0.00	0.00	0.00	0.00	0.00	0.00	0.068	0.00
NO_3^-	0.02	0.51	0.15	0.23	0.39	0.68	0.40	0.64	0.43
SO_4^{2-}	0.69	2.9	3.4	1.1	0.36	0.34	0.22	0.24	0.30
Na^+	0.068	0.092	0.15	0.23	0.27	0.55	0.33	0.53	0.33
NH_4^+	0.11	0.47	0.59	0.16	0.00	0.00	0.00	0.00	0.00
K^+	0.011	0.020	0.026	0.059	0.00	0.020	0.009	0.090	0.015
Mg^{2+}	0.028	0.029	0.002	0.028	0.029	0.050	0.035	0.050	0.035
Ca^{2+}	0.029	0.00	0.072	0.24	0.063	0.15	0.18	0.12	0.12

Table 7. Concentrations for the Andersen cascade impactor for January 11-13, 2001.

Size distributions were calculated from the Andersen cascade impactor data. The data was fit to a normalized distribution by dividing the experimental analyte concentration, $C_{experimental}$, by the difference in the Log_{10} diameter for the bin maximum and minimum.

$$\frac{dC}{dLogD_p} = \frac{C_{\text{experimental}}}{Log_{10}(D_p \max) - Log_{10}(D_p \min)} \qquad \text{(Equation 20)}$$

Sodium and nitrate had bimodal distributions (Figure 13), both peaking between 3-4 and 9-10 μm. Ammonium and sulfate were both of a single mode (Figure 14), peaking around 0.65 μm.

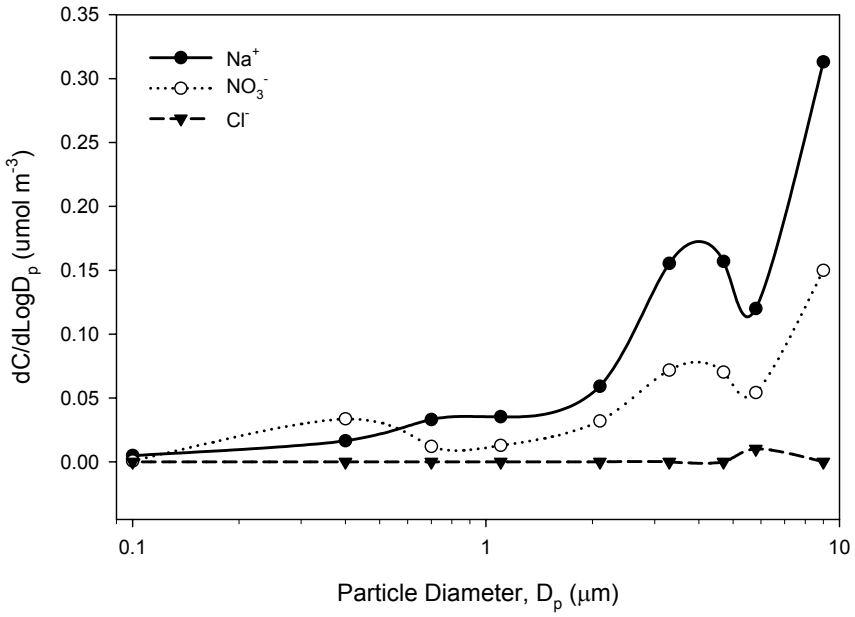

Figure 13. Normalized particle size distributions of sodium, nitrate and chloride using Andersen instrument from January 11-13, 2001.

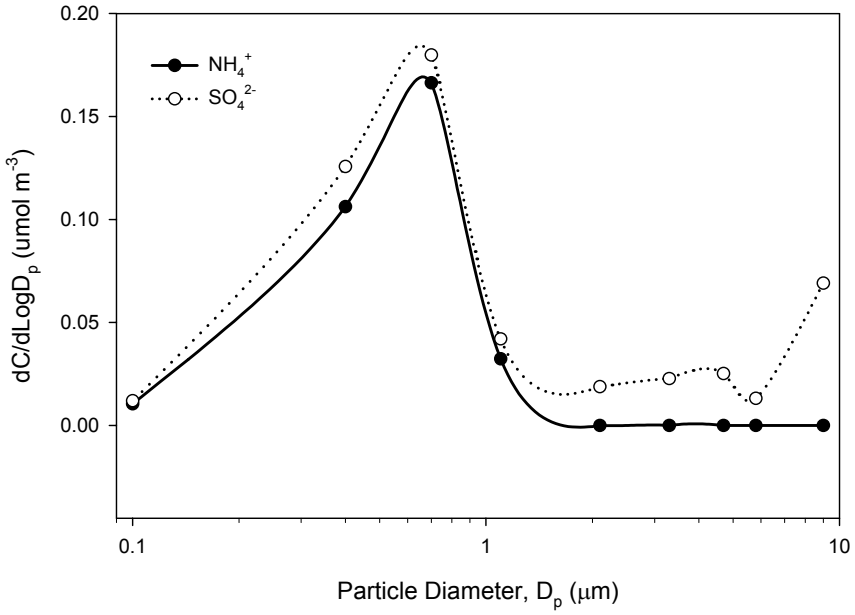

Figure 14. Normalized particle size distributions of ammonium and sulfate using the Andersen instrument from January 11-13, 2001.

Discussion

Coarse mode nitrate can be attributed to the adsorption and reaction of gaseous HNO_3 with calcium and magnesium in mineral dust and sodium in sea salt particles (Jordan et al., 2000). Reactions with the calcium or magnesium do not appear to be the major pathway under the sodium-rich marine conditions. The fine mode nitrate may be due to the gas-to-particle conversion and neutralization of HNO_3 and NH_3, forming NH_4NO_3. During the sampling times, the environmental conditions did not favor the formation of volatile NH_4NO_3. As a result, very little nitrate was assumed to be associated with ammonium.

The formation of fine mode sulfate results from the condensation and neutralization of sulfuric acid with ammonia. During the sampling period, the majority of the sulfate and ammonium was collected in the fine size fractions. Figure 14 shows a strong 1:1 molar ratio of ammonium to sulfate. It appears that these constituents are present in the form of NH_4HSO_4, leaving the fine aerosol slightly acidic.

The dichotomous and size-fractioned samples revealed the presence of chloride in the coarse fraction. The major source of chloride is sea salt, as NaCl. Seawater has a molar ratio of Cl^-:Na^+ of 1.16 (Aherne and Farrell, 2002), but the molar ratios of Cl^-:Na^+ for the coarse and fine fractions were 0.10 and 0.05, respectively. This indicated a deficiency of chloride relative to the sodium concentration. The loss of chloride was attributed to the reactions of NaCl with HNO_3 and H_2SO_4, producing gaseous HCl.

Chloride depletion was calculated using Equation 3. The percentage of chloride depletion for this sampling period ranged from 86 to 100%, results are reported in Table 8.

	% Cl-depletion
Andersen Fine ($D_p > 2.1$ μm)	100%
Dichot Fine ($D_p > 2.5$ μm)	94%
Andersen Coarse ($2.1 < D_p < 10.0$ μm)	99%
Dichot Coarse ($2.5 < D_p < 10.0$ μm)	86%

Table 8. Average chloride depletion, in percentage, for January 11-13, 2001.

One factor for determining the extent of chloride depletion is the relative humidity. The water content of the hygroscopic salts increases with relative humidity. The additional surface waters play a role in the uptake of nitric acid and the gas-particle nitrate equilibrium (Guimbaud et al., 2002b). During this sampling period, the relative humidity was greater than 90%, and the air mass was of marine origin. High chloride depletion was expected.

In Table 9, the dry deposition flux (Equation 1) was calculated for three particle diameters. The nine different size bins of the cascade impactor were assigned to one of the three particle diameter categories. Concentrations were the nitrate particle concentration sums for all stages in that size range. As the square of the particle diameter increases, its gravitational settling velocity increases. Results in Table 9 indicate that 5.8 to 10.0 μm particles accounted for 60% of the total nitrogen flux for particles less than 10.0 μm.

Particle Diameter (μm)	Particle D_p Range (μm)	Particle Conc. (μg-N m^{-3})	Settling Velocity (cm s^{-1})	Flux (kg-N ha^{-1} yr^{-1})	Percent of Flux
1.0	0.0-3.3	1.3	0.017	0.071	23%
4.7	3.3-5.8	0.24	0.069	0.053	17%
9.0	5.8-10.0	0.24	0.25	0.19	60%
			Sum of Flux	0.31	100%

Table 9. Dry deposition flux for particulate nitrogen (nitrate + ammonium) for January 11-13, 2001.

Previous research has modeled the dry deposition settling velocities for different nitrogen containing species (Poor et al., 2001). Over a three-year averaged study, gaseous ammonia and nitric acid accounted for 53% and 40% of the 7.3 kg-N ha^{-1} yr^{-1} of total nitrogen deposition, respectively. Particulate nitrate only accounted for 3.5%, but this estimate only accounted for fine mode particulate nitrogen compounds. As seen from Table 9, coarse mode nitrate would account for 60% of particle nitrogen deposition for particles less than 10 μm. New estimates need to be developed to account for coarse particle nitrate.

Evidence of Macroparticles

In recent years, research has confirmed the presence of coarse particle nitrogen. Coarse particles of $NaNO_3$ can form, for example, when a marine air mass laden with sodium chloride mixes with an anthropogenic air mass rich in nitric acid. These particles are typically less than 10 μm in diameter. The

purpose of this investigation was to determine if rapidly depositing atmospheric particles or particle aggregates with diameters 10 to 80 μm contain nitrogen.

Experimental

Macroparticles are those with a diameter greater than 10 μm. They were investigated during an intensive six-week period during October and November 2001. Particles up to 10 μm were collected using the dichotomous sampler, collecting coarse and fine species. Total suspended particulates (TSP) were collected using the TSP sampler, or simply an inverted filter pack. In both instruments, Whatman PTFE Teflon membrane filters were used as the collecting media and were integrated over 24 hours. An annular denuder system was collocated with the samplers to collect ambient gaseous nitric acid and fine particulate matter.

Results and Discussion

Macroparticle concentrations were first determined by simply subtracting the dichotomous (coarse + fine) concentration from the TSP concentration (Equation 21).

$$[NO_3^-]_{TSP} - [NO_3^-]_{dichotomous} = [NO_3^-]_{macro} \qquad \text{(Equation 21)}$$

Figure 15 represents the daily macroparticle concentrations of Na^+, Cl^- and NO_3^-. All values greater than zero indicate the presence of that species in

the greater than 10 μm size fraction. Na^+ and Cl^- concentrations were significantly correlated (r=0.75) but not Na^+ and NO_3^- (r=0.26). NO_3^- concentrations were plotted to visualize the correlations with Ca^{2+} (r=0.69). These correlations pointed to macroparticle NO_3^- as possibly $Ca(NO_3)_2$ rather than $NaNO_3$.

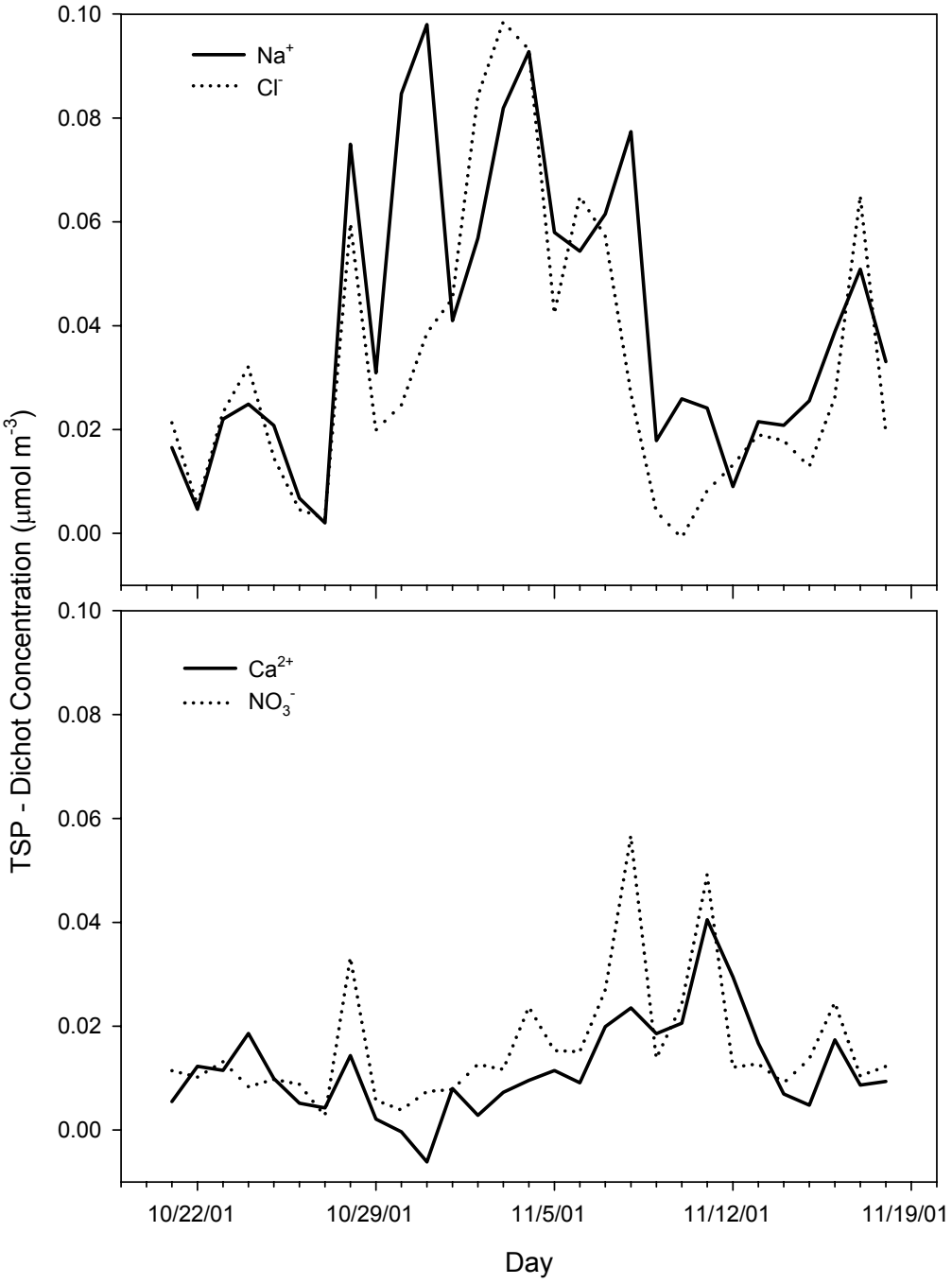

Figure 15. Daily macroparticle concentrations of (a) Na^+ and Cl^- and (b) Ca^{2+} and NO_3^- (October-November 2001).

Due to the nature of coarse particulate matter sampling, ambient gas species may play a role in the final result of the species collected. In this study, gaseous HNO_3 was not denuded from the airflow of neither the TSP nor the dichotomous samplers, and the potential existed for HNO_3 to react with coarse particles that had accumulated on the filter (Perrino et al., 1988). In the dichotomous sampler, however, the airflow through the coarse filter was low at 1.67 L min^{-1} (as compared to the 28.3 L min^{-1} of the TSP sampler) thus reducing the nitric acid bias associated with coarse particle interactions.

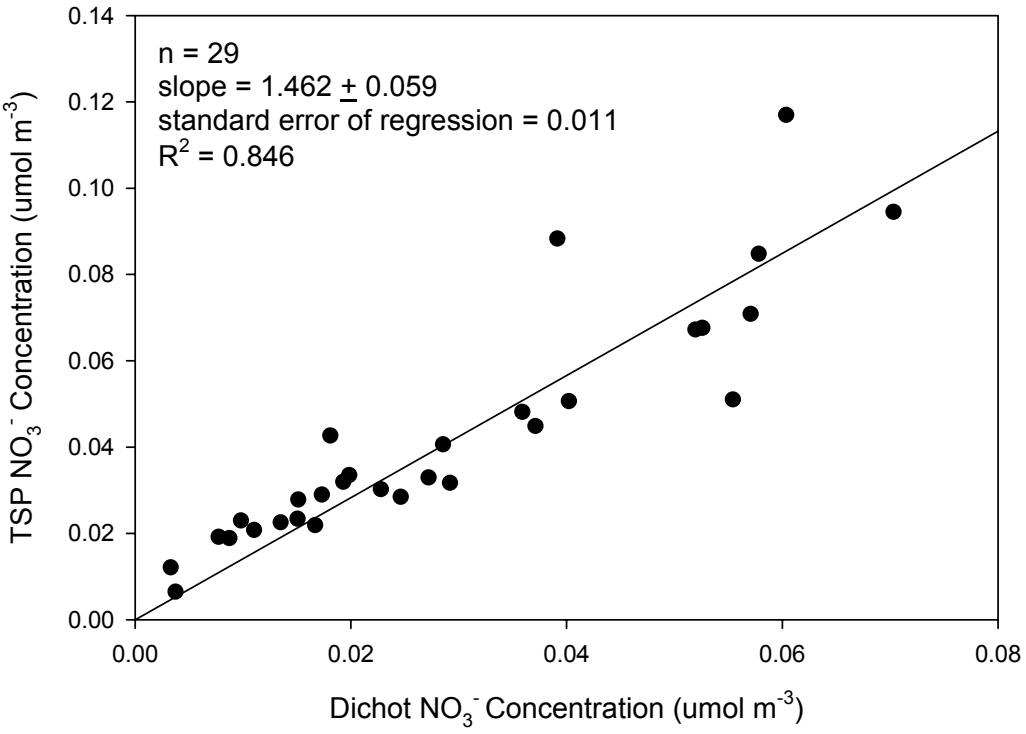

Figure 16. Simple linear regression for TSP NO_3^- versus dichotomous total NO_3^- using daily concentrations (October-November 2001).

To estimate the HNO_3 bias between the TSP and dichotomous samplers, TSP NO_3^- was plotted against the dichotomous NO_3^- (Figure 16). From the linear regression, it was found that the dichotomous total NO_3^- concentrations explained ~85% of the variability in the TSP NO_3^- concentrations. The daily TSP NO_3^- concentrations were ~46% higher than the dichotomous total NO_3^- concentrations. The slope of the regression curve was defined as the possible nitric acid bias between the two methods. For each sampling day, the macroparticle concentrations were corrected for this bias (Equation 22).

$$[NO_3^-]_{TSP} - 1.46[NO_3^-]_{dichotomous} = [NO_3^-]^*_{macro} \quad \text{(Equation 22)}$$

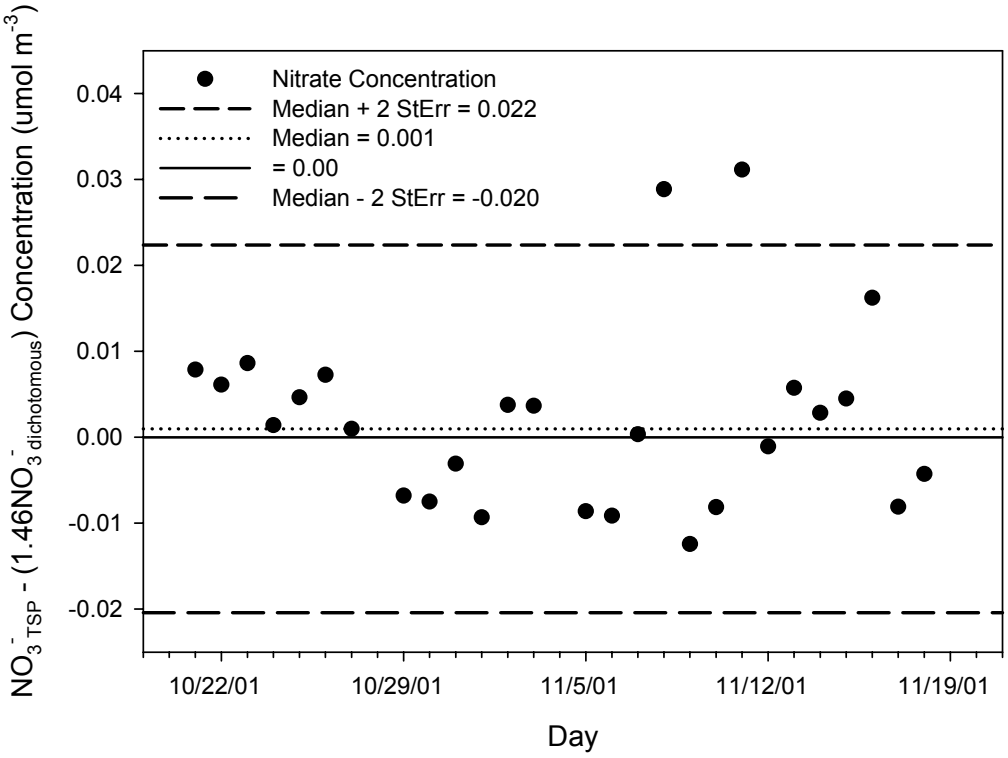

Figure 17. Daily macroparticle nitrate concentrations with correction for the nitric acid bias.

The mean and standard error of the nitrate macroparticle concentrations were plotted in Figure 17 after correction for the nitric acid bias. The mean and standard error excluded the two statistical outliers. All but two concentrations were within two times the standard error of the regression about zero. These two concentrations offer tentative evidence of ambient nitrate macroparticles.

The formation of $NaNO_3$ and $Ca(NO_3)_2$ on the filter was likely dependent on the air velocity through the filter, the particle number and size, the relative humidity and the ambient nitric acid concentration; and it may not be well modeled with a linear regression. It was postulated that relative humidity played a role, providing an aqueous layer for the chemical conversion (Ten Brink, 1998).

Trends were addressed to find an affiliation for the macroparticle nitrate. Ammonium-to-sulfate ratios have been used as an indicator of an air mass age. NH_4^+:SO_4^{2-} molar ratios near 2.0 indicate an aged air mass, whereas those less than or equal to 1.0 represent a relatively fresh air mass, as NH_3 has not been completely neutralized with sulfate. The two days of possible macroparticle formation were consistent with NH_4^+:SO_4^{2-} molar ratios of near 2.0, suggesting an aged air mass. The air mass origin on these days was predominantly from terrestrial sources, with higher than average Ca^{2+} concentrations and HNO_3 concentrations. This suggested that the macroparticle NO_3^- was affiliated with mineral dust particles, possibly as $Ca(NO_3)_2$.

The nitrate affiliated with the mineral dust Ca^{2+} particles may also be a product of depositing HNO_3 reacting on previously settled soil dust. There was a minimum amount of rain during the sampling period, leaving the potential for

water-soluble species to exist on the ground. The bayside sampling site was located <100 m from a major roadway. Re-suspended soil or road dust was a possible source of macroparticle Ca^{2+} and NO_3^-. A 20-μm particle re-suspended to a height of 100 m could travel more than 30 km before re-depositing to the surface. Other possible sources for macroparticle nitrate include dust from local agricultural areas. These particles may be more enriched with nitrate than those from other sources.

Retention of Nitric Acid by Nylon Filters

Several techniques have been used to measure gaseous HNO_3 and particulate NO_3^- concentrations in the atmosphere. Some of these techniques include filter pack (FP) methods (Anlauf et al., 1986; Perrino et al., 1988; Spicer, 1986; Torseth et al., 2000) and annular denuder systems (ADS) (Torseth et al., 2000; Tsai et al., 2000; Vossler et al., 1988). Filter packs have been the method of choice for a number of government agencies, such as U.S. Environmental Protection Agency National Dry Deposition Network (NDDN) and U.S. Clean Air Status and Trends Network (CASTNet) (Kim and Allen, 1997; Sickles II and Hodson, 1999) because they have low maintenance problems, light weight, low cost and the same collection efficiency as other methods (Karakas and Tuncel, 1997). The ADS was designed to collect HNO_3 and particulate NO_3^-, differentiating between the vapor phase HNO_3 and HNO_3 produced from the dissociation of NH_4NO_3 during sampling (Vossler et al., 1988).

Several studies have indicated the potential for nylon filters to adsorb gaseous nitric acid (Karakas and Tuncel, 1997; Perrino et al., 1988), but most of these studies were performed in environments where conditions were suitable for the formation of NH_4NO_3. This experimental study was done in a coastal environment where the average relative humidity and temperature were above the deliquescent relative humidity (Seinfeld and Pandis, 1998) and dissociation temperatures (Stelson et al., 1979) for NH_4NO_3, thus avoiding the issues of formation and dissociation.

$PM_{2.5}$ cyclone inlets were chosen to avoid the collection of sea salt particles, which have bimodal diameters greater than 3 μm (Evans and Poor, 2001). HNO_3 can be liberated from sea salt particles by the reaction of nitrate salts ($NaNO_3$) with H_2SO_4 and HCl (Appel et al., 1984).

Experimental

Ambient gas and particulate concentrations were collected using two separate channels on an annular denuder system (ADS) from URG Corporation. Channel one consisted of a Teflon-coated $PM_{2.5}$ cyclone inlet, two 242-mm denuders and a filter pack, in series. The denuders were prepared as stated in the methods section using citric acid as the acidic denuder coating solution. The filter pack was equipped with a Whatman nylon or Nylasorb nylon filter. The second channel consisted of a Teflon-coated $PM_{2.5}$ cyclone inlet and a filter pack,

in series. The filter pack was equipped with a Whatman nylon or Nylasorb nylon filter. Denuders and filters were extracted and analyzed.

The samples were collected during a six-week period in the fall of 2001. The sampling site was located on the property of the State of Florida Fish and Wildlife Conservation Commission, which is on the eastern side of the Gandy Bridge on Tampa Bay. The samples were integrated over 24 hours with an ambient airflow of 10 L min^{-1}, which was checked daily using a dry gas meter. During the first three weeks, 47-mm, 1-μm pore size Whatman nylon filters were used. Pall Gelman Nylasorb 47-mm, 1-μm pore size were used during the second three-week period.

When using a cyclone inlet in marine environments, the interior wall of the ADS cyclone may be become coated by sea salt particles. It has been found that sea salt aerosols react with acids, such as H_2SO_4 and HNO_3, in the atmosphere forming sulfates and nitrates (Li-Jones et al., 2001). The reaction between HNO_3 and sea salts within the cyclone may result in a substantial amount of HNO_3 loss. This reaction leads to the misapportionment of both NO_3^- and Cl^-, as HCl is released into the vapor phase. To prevent nitric acid loss within the cyclone, the cyclones were thoroughly cleaned with deionized water and dried between deployments.

Results and Discussion

Two channels on the ADS were used to collect (a) HNO_3 and "denuded" particulate matter (PM) nitrate. The term denuded is used to describe the $PM_{2.5}$ fraction of nitrate of which the HNO_3 and other reactive gases have been removed, or denuded, prior to collection of the particulate matter; and (b) "undenuded" PM NO_3^-. Undenuded refers to the second channel of collection in which both HNO_3 and $PM_{2.5}$ NO_3^- are collected on the filter. In theory if nylon substrates prove to be 100% efficient in HNO_3 collection, the sum of analytes collected on both the denuder and denuded filter will equal the sum of analytes on the undenuded filter.

The reason for using two different types of nylon filters was the availability of the media types at the time of sampling. Pall Gelman Sciences had halted production of the Nylasorb nylon filter, and they were unavailable for purchase. As an alternative, nylon filters were purchased from Whatman. One major drawback for the use of the Whatman filters was the presence of existing analytes, especially nitrates. Both types of filters were treated identically from deployment to analysis. Data correction by blank subtraction is common for this type of analysis, but was a major factor in the Whatman filters. Pall Gelman Sciences certifies their filters with respect to nitrate concentrations.

The temperature and relative humidity (RH) values for the sampling period are listed in Table 29 (Appendix 1). Experimental HNO_3, denuded PM nitrate and undenuded (UD) nitrate concentrations are given in Table 10.

Whatman (μmol m^{-3})				Nylasorb (μmol m^{-3})			
	HNO_3 gas	den PM NO_3^-	UD HNO_3 + NO_3^-		HNO_3 gas	den PM NO_3^-	UD HNO_3 + NO_3^-
10/10/01	0.009	0.009	0.017	11/1/01	0.007	0.017	0.020
10/11/01	0.007	0.007	0.010	11/2/01	0.006	0.014	0.016
10/12/01	0.007	0.011	0.015	11/3/01	0.006	0.012	0.013
10/13/01	0.008	0.010	0.014	11/4/01	0.019	0.007	0.008
10/14/01	0.007	0.008	0.014	11/5/01	0.008	0.015	0.023
10/15/01	0.023	0.013	0.022	11/6/01	0.010	0.002	0.028
10/16/01	0.012	0.011	0.020	11/7/01	0.033	0.017	0.031
10/17/01	0.013	0.007	0.014	11/8/01	0.023	0.029	0.052
10/18/01	0.012	0.010	0.018	11/9/01	0.059	0.037	0.047
10/19/01	0.010	0.015	0.019	11/11/01	0.090	0.033	0.085
10/20/01	0.007	0.011	0.015	11/12/01	0.032	0.011	0.043
10/21/01	0.014	0.008	0.010	11/13/01	0.015	0.009	0.012
10/24/01	0.012	0.008	0.008	11/14/01	0.026	0.007	0.009
10/26/01	0.043	0.004	0.023	11/15/01	0.009	0.010	0.018
10/27/01	0.011	0.003	0.008	11/16/01	0.038	0.011	0.026
10/28/01	0.009	0.010	0.015	11/17/01	0.038	0.016	0.019
10/30/01	0.026	0.010	0.015	11/18/01	0.011	0.019	0.022
10/31/01	0.006	0.012	0.016	11/19/01	0.024	0.041	0.049

Table 10. Experimental nitric acid, denuded nitrate and undenuded nitrate concentrations for October - November 2001.

The Grubbs' outlier test (GraphPad Software, 2000) was performed for the Whatman nylon filter data set, and no outliers were detected. All data points were included in the linear regression analysis (Figure 18) (GraphPad Software, 2000).

From the linear regression (Figure 18), the sum of HNO_3 plus the denuded PM NO_3^- can be estimated to be 37% greater than that collected on the undenuded NO_3^- fraction. These filters do not appear to be completely efficient in adsorbing gaseous nitric acid.

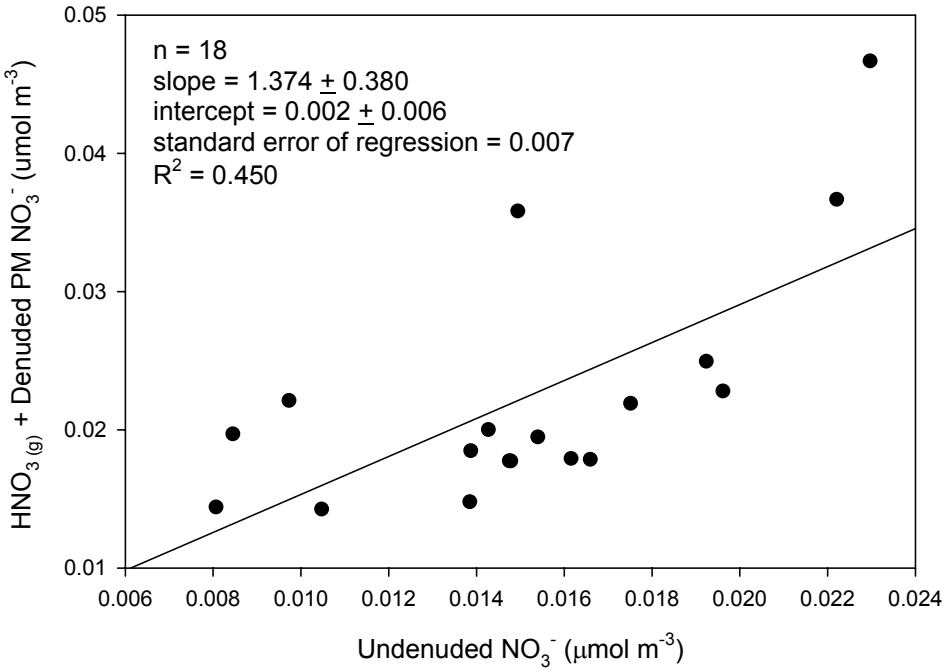

Figure 18. HNO_3 + Denuded PM NO_3^- vs. Undenuded NO_3^- for Whatman nylon filters.

The paired t-test (GraphPad Software, 2000) was performed to determine the statistical significance of the data set. The test was based on a two-tailed test at the 95% confidence interval. The two data sets were not statistically different if $|t_{obtained}|<|t_{critical}|$. For the Whatman nylon filters data set, the $t_{obtained}$ = 4.6 ($t_{crit\ 95\%}$ = 2.1). The test resulted in a rejection of the null hypothesis, indicating the data sets for the (HNO_3 + denuded NO_3^-) compared to the undenuded NO_3^- (gas plus particulate) were statistically different.

A linear regression was created for the Nylasorb nylon filters. The Grubbs' outlier test was performed, not detecting any outliers (GraphPad

Software, 2000). All data points were included in the linear regression analysis (Figure 19).

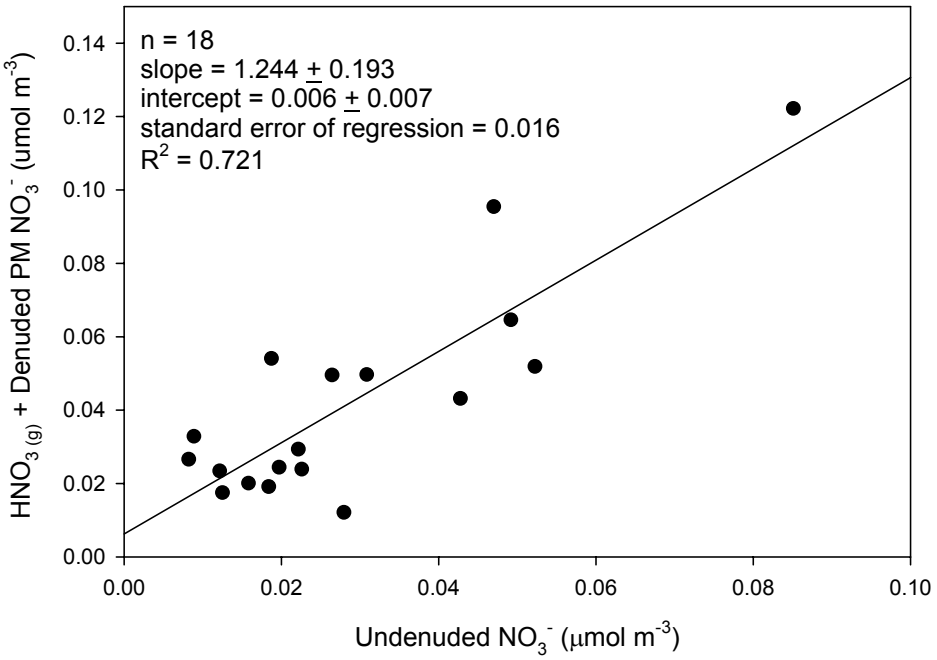

Figure 19. $HNO_{3\ (g)}$ + Denuded PM NO_3^- vs. Undenuded NO_3^- for Nylasorb nylon filters.

The paired t-test (GraphPad Software, 2000) was performed to determine the statistical significance of the data set. The test was based on the 95% confidence interval. For the Nylasorb nylon filter data set, $t_{obtained} = 3.5$ ($t_{crit\ 95\%} = 2.1$). The data sets (HNO_3 + denuded PM NO_3^-) compared to the undenuded NO_3^- (gas + particulate) were statistically different.

To determine the collection efficiency of both the Whatman and Nylasorb nylon filters, the particulate matter fraction was subtracted from the undenuded nitrate (Equation 23), leaving only the adsorbed nitric acid fraction to compare.

$$[HNO_3]_{adsorbed} = [NO_3^-]_{undenuded} - [NO_3^-]_{PM} \qquad \text{(Equation 23)}$$

The adsorbed nitric acid, $[HNO_3]_{adsorbed}$, from both filter types was compared to the nitric acid collected on the denuders through a linear regression (Figures 20-21).

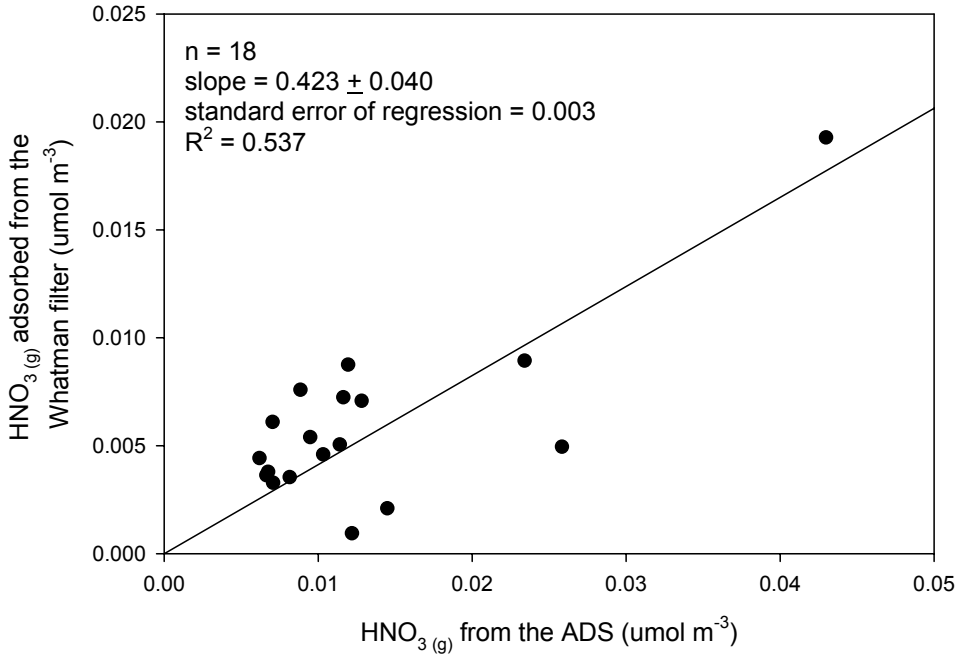

Figure 20. Nitric acid from the ADS compared to that adsorbed by the Whatman nylon filters.

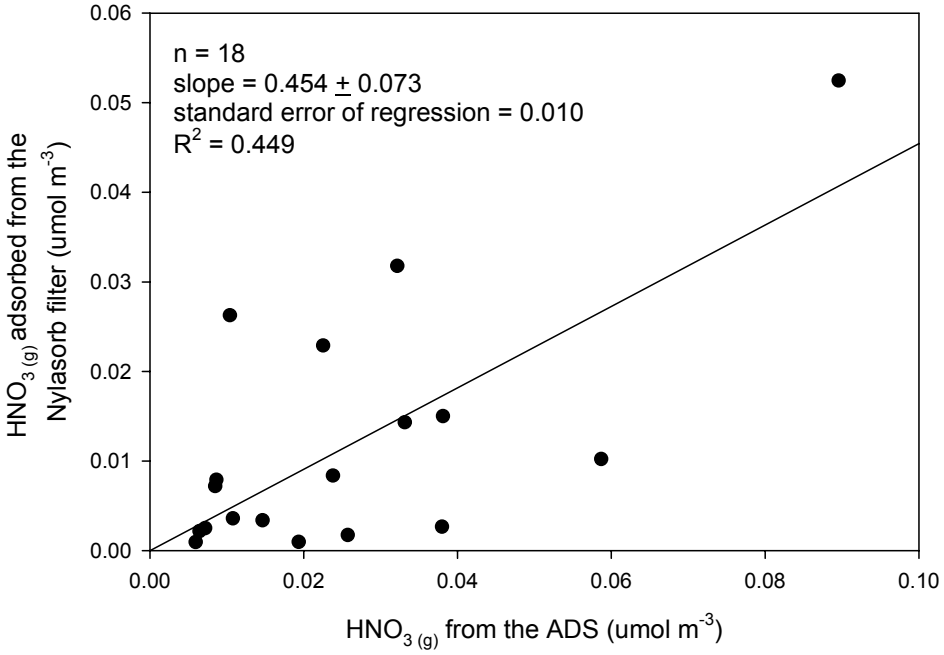

Figure 21. Nitric acid from the ADS compared to that adsorbed by the Nylasorb nylon filters.

The Whatman and Nylasorb filters appear to have collected only 42% and 45% of the total nitric acid, respectively. To verify this was correct, the t-test was performed comparing the HNO_3 adsorbed by each filter type to the linear regression slope times the HNO_3 collected by the ADS.

For the Whatman filter type, where the regression slope was 0.42, $t_{obtained}$ = 0.55 ($t_{crit\ 95\%}$ = 2.1). The t-test resulted in a non-statistical difference between the two sets, further indicating the collection efficiency of the Whatman nylon filters to be approximately 42%.

For the Nylasorb nylon filters, where the regression slope was 0.45, $t_{obtained}$ = 0.20 ($t_{crit\ 95\%}$ = 2.1). The t-test resulted in a non-statistical difference between

the two data sets. This indicated the collection efficiency of the Nylasorb nylon filters to be approximately 45%.

A similar study has been done looking at the uptake of nitrous acid (HNO_2) and NO_X by nylon surfaces (Perrino et al., 1988). The collection efficiencies of HNO_2 on nylon filters was determined experimentally at different flow rates. Efficiencies ranged from 25% at 12 L min^{-1} to 80% at 2 L min^{-1}. At 10 L min^{-1}, the collection efficiency ranged from 30-40%.

The results from Perrino et al. (1988) are comparable to those reported here with nitric acid, HNO_3. Both the Whatman and Nylasorb nylon filter media resulted in a collection efficiency of approximately 40%.

Size Distributed Trajectory Study

As freshly emitted sea salt particles mix with the urban plume, sodium nitrate particles begin to form. With transport, this gas-to-particle conversion of nitric acid on the sea salt particles is expected to reach equilibrium and contribute to particulate nitrate deposition within the Tampa Bay area watershed. A trajectory study was completed looking at the transformation and deposition of particles as an air mass moves throughout the Tampa Bay area.

Experimental

Three monitoring sites were established during May 2002, taking advantage of monitoring already in progress. At each site, a MOUDI sampler, an ADS and various meteorological instrumentation were deployed. Collected data included 23-hour integrated, size-segregated inorganic particulate species concentrations, 12-hour integrated acidic and alkaline gas concentrations, wind speed, wind direction, ambient temperature, relative humidity, and water temperature.

The Azalea Park site is located in the southwester corner of Pinellas County, with close proximity to the Gulf of Mexico (Figure 22). The Gandy Bridge site is located on the eastern side of the Gandy Bridge, adjacent to Tampa Bay. The third site, Sydney, is located in a semi-rural area, approximately 20 km from Tampa Bay. The three sites span over a 55 km distance, providing sufficient travel distance for particle conversion and some deposition.

There are many sources of error and uncertainties in this type of experimental fieldwork. They need to be addressed in order to determine if there was a real difference in particle concentrations and flux between the sampling sites. The greatest uncertainty lies in the pump flow control. Each pump was set at a 30 L min^{-1} flow rate and was checked weekly using a dry gas meter. The pumps were not installed in a climate-controlled shelter but were deployed in the field open to the elements. With continual changes to ambient temperature and pressure, the flow rate was assumed to change. During May 2002, the daily

temperature ranged from 18 to 33ºC, with an 8 to 10ºC difference between the daily minimum and maximum temperatures. Applying a 10ºC temperature change to the ideal gas law resulted in a 3% change to the 30 L min^{-1} volumetric flow rate, which was within the range of the quality assurance protocol flow restriction guidelines of 5%.

The overall error of the MOUDI samplers was estimated during this time period and was averaged at 54%, ranging from 1 to over 100% (Table 4). The average size- and species-dependent error was applied to each data set and was seen in the following particle size distributions. In order to determine a real or significant change in the particle concentrations, the entire data range with its error needs to be compared. As a result, minor changes in concentration cannot be considered significant as the data points may, in actuality, be of identical value. In this study, trends were used to determine significant changes in the particle concentration and flux. Ten percent was assigned as the minimum difference values needed before they were considered significantly different from one another.

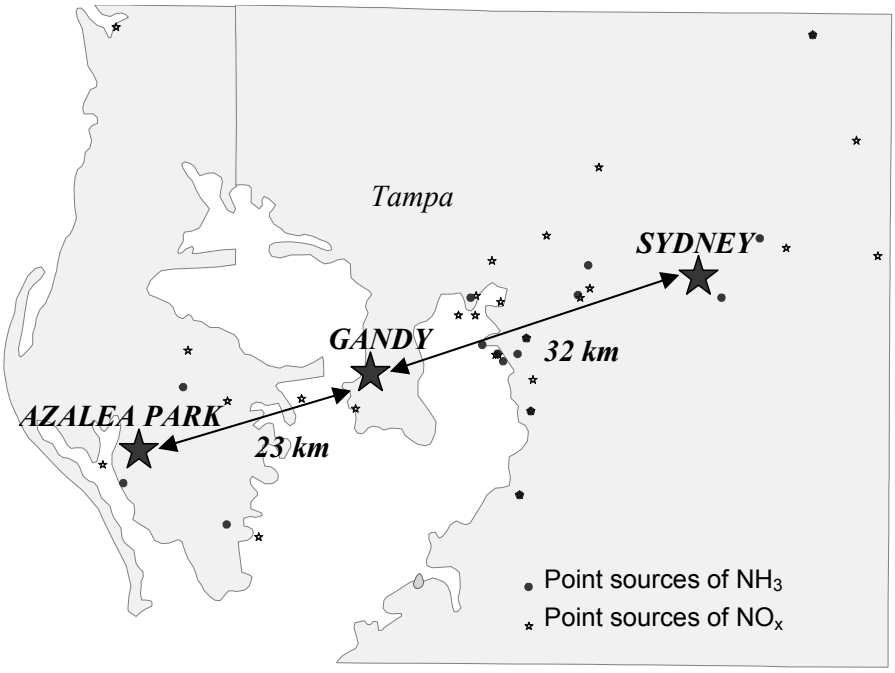

Figure 22. Map of sampling sites during the May 2002 intensive period.

Results and Discussion

Four specific days during the May 2002 intensive were investigated as they represented the predominant air mass pattern during the sampling period. May 4, 2002, represents a southwestern air origin day (Figure 23a), originating from the Gulf of Mexico and the southwestern Florida region. The air came into the area from the west, crossing the sites eastward in order from Azalea to Sydney. May 14, 2002, represents a northwestern air day (Figure 23b), originating from the northern states, coming across the Gulf of Mexico for only a short period of time. The air on May 6, 2002, originated from the Atlantic Ocean (Figure 23c). The air mass traveled across the state before reaching the Tampa Bay area. The air traveled in towards the west, reaching the Sydney site first and

then traveling onwards past Gandy towards Azalea. On May 20, 2002, the air originated in the Atlantic Ocean area near North and South Carolina (Figure 23d). The air traveled over the ocean for some time and then proceeded to cross the state, reaching the Sydney site first, followed by Gandy and Azalea.

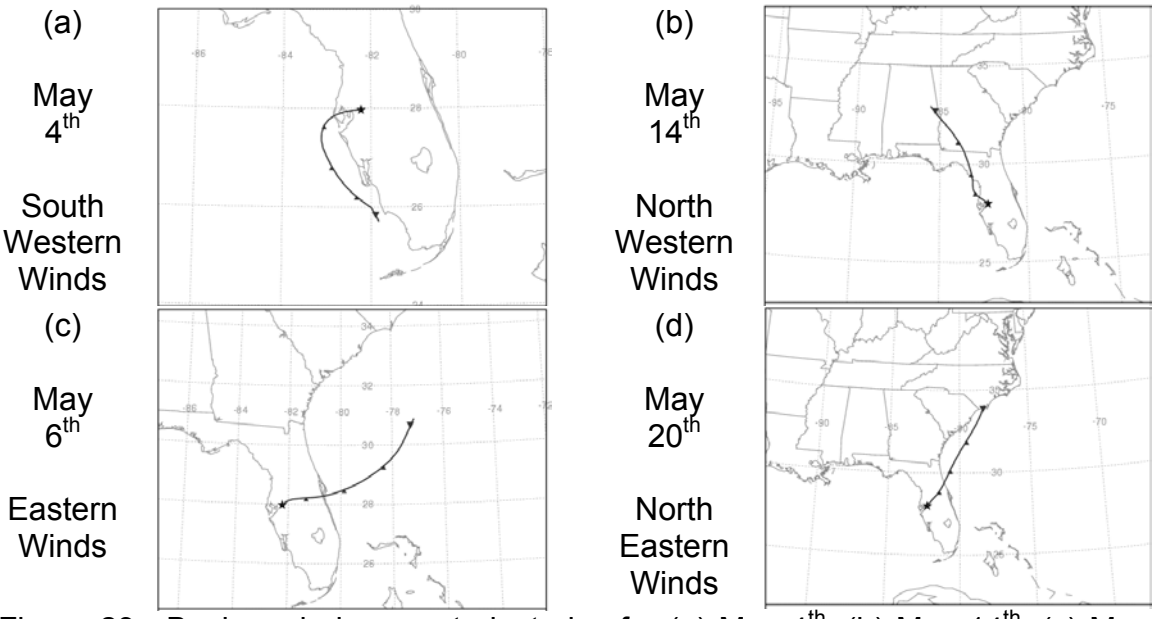

Figure 23. Backward air mass trajectories for (a) May 4th, (b) May 14th, (c) May 6th and (d) May 20th, 2002.

Many interesting things can be looked at for each episode. Ammonium to sulfate molar ratios can be used to determine the approximate age of an air mass. Ratios near 1.0 indicate a fresh marine air mass, however those near 2.0 indicate an aged or pollution-laden air mass. Chloride to sodium and nitrate to sodium molar ratios and chloride depletion can be used to determine the extent of the reaction between sea salt and nitric acid. The trends of the magnitudes of concentrations can be used to indicate particulate deposition and re-suspension.

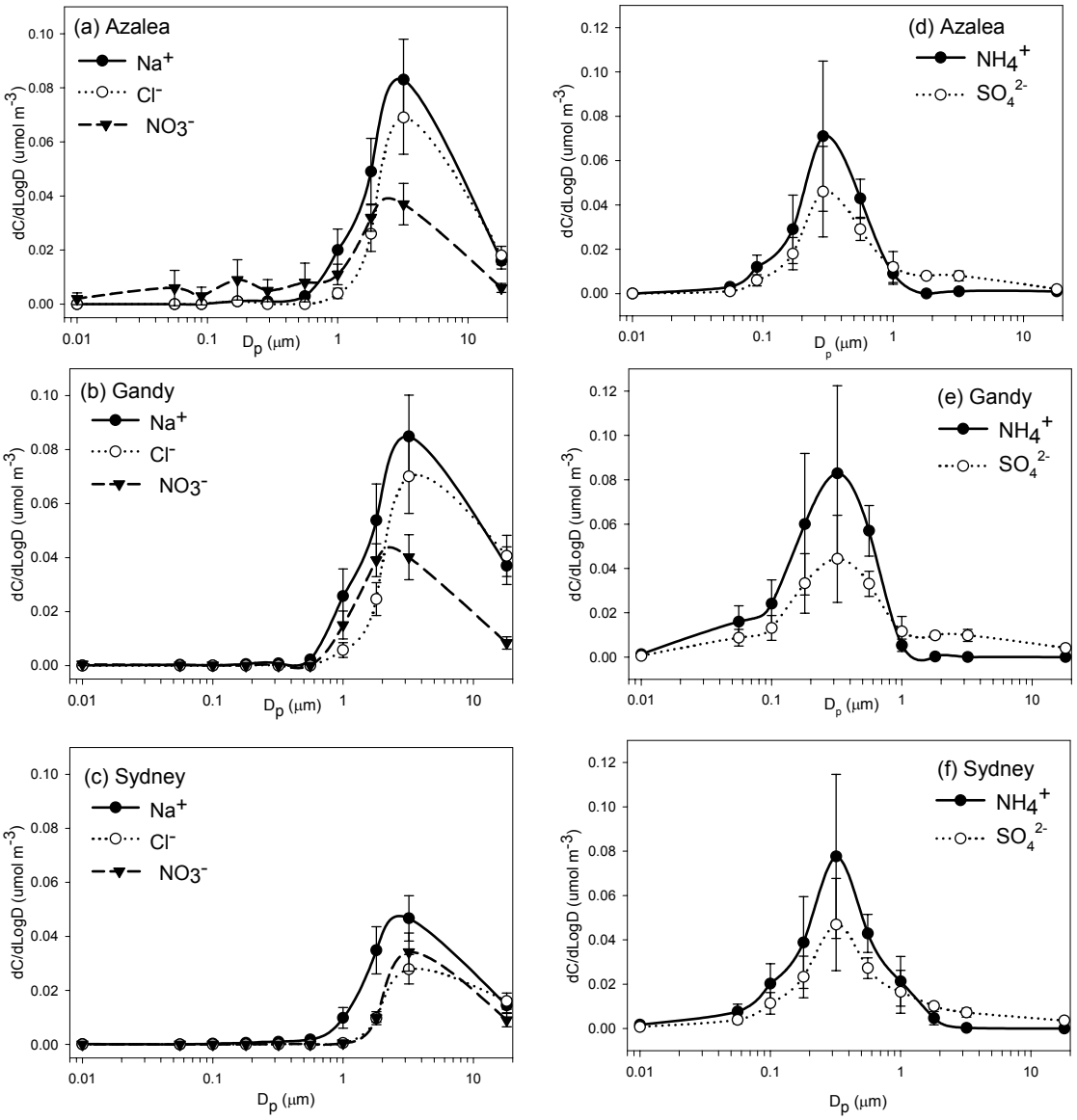

Figure 24. Size distributions for each sampling site on May 4, 2002.

	Azalea	Gandy	Sydney
Cl^-:Na^+	0.77	0.75	0.55
NO_3^-:Na^+	0.48	0.50	0.75
Cl^--dep %	35%	36%	54%
NH_4^+:SO_4^{2-}	1.6	1.8	1.7

Table 11. Ion ratios for May 4, 2002.

On May 4, 2002, the air mass originated from the Gulf of Mexico and southwestern Florida region (Figure 23a). Upon arrival, the NH_4^+:SO_4^{2-} ratio was 1.57, indicating a moderately fresh or slightly aged air parcel (Figure 24d-f and Table 11). As the air mass traveled eastward, towards Gandy, the ratio increased. However, as the air parcel traveled towards Sydney, the ratio decreased slightly. This may be attributed to the increased SO_2 and SO_4^{2-} concentrations over urban Tampa. As the air parcel moved through the downtown area, it is possible that additional sulfate was picked up.

Upon the arrival at the Azalea site, the chloride to sodium ratio was 0.77 (Figure 24a-c and Table 11). As the air mass traveled throughout the area, this ratio steadily decreased, reaching 0.55 at the Sydney site. Nitrate to sodium ratios increased from 0.48 to 0.75 as the air picked up urban NO_X or nitric acid, converting it to particulate nitrate. In agreement with the above trends, chloride depletion increases from 35% to 54% from Azalea to Sydney. Combined, these three indicators represent the adsorption and conversion of gaseous nitric acid to particulate nitrate. As predicted by Reaction 1, HCl is released during the process. This is seen through a steady increase in the percentage of chloride depletion.

On May 14, 2002, winds originated from the northern states, approaching the Tampa area from the northwestern direction (Figure 23b). When this air mass arrived, the ammonium to sulfate ratio was 1.90 (Figure 25d-f and Table 12). This is indicative of an aged air mass. As the air mass crossed Tampa Bay, the ratio remained unchanged (ratio values of 1.9 and 1.8 are not significantly

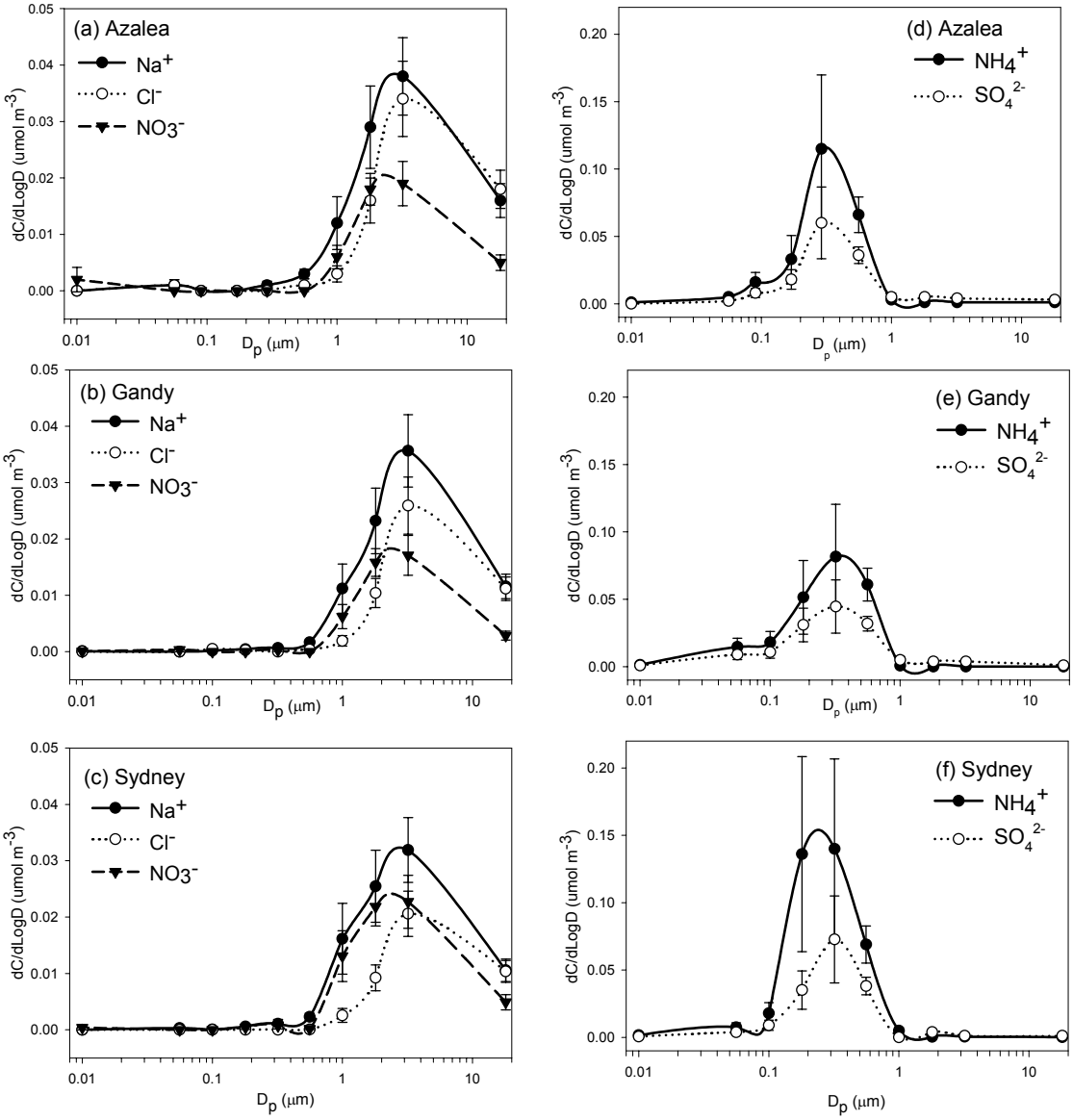

Figure 25. Size distributions for each sampling site on May 14, 2002.

	Azalea	Gandy	Sydney
Cl^-:Na^+	0.81	0.66	0.56
NO_3^-:Na^+	0.50	0.50	0.73
Cl^--dep %	31%	44%	52%
NH_4^+:SO_4^{2-}	1.9	1.8	2.3

Table 12. Ion ratios for May 14, 2002.

different) and then continued to increase, reaching over 2.3 at the Sydney site. There was a significant increase in the ammonium concentration from the Gandy to Sydney sites. There are anhydrous ammonia loading docks and a large wastewater treatment plant located at the Port of Tampa, which lies between the Gandy and Sydney sites. This increase in ammonium may be due to activities at these facilities. The concentration of sulfate was seen to only increase slightly.

When the air first reaches the Azalea site on May 14, 2002, the nitrate to sodium ratio is 0.50 (Figure 25a-c Table 12). As the air travels through urban Tampa and picks up nitric acid, the nitrate to sodium ratio continues to increase, reaching 0.73 at the Sydney site. Coupled with the chloride to sodium ratios and chloride depletion indicators, an uptake and transformation of nitric acid to particulate nitrate was seen. All three indicators reveal an increase in the uptake and conversion to nitrate. It appears that some sea salt deposition is occurring between the Gandy and Sydney sites, as the concentration of sodium decreases between these monitoring locations.

On May 6, 2002, the air mass originated in the Atlantic Ocean, traveling west across the state before reaching the Tampa Bay area. Upon arrival to the Sydney site, the NH_4^+:SO_4^{2-} ratio was over 2.0 (Figure 26d-f Table 13). This is indicative of the air aging as it traveled across the state. The ratio continued to remain over 2.0 as the air traveled past the Gandy and Azalea sites.

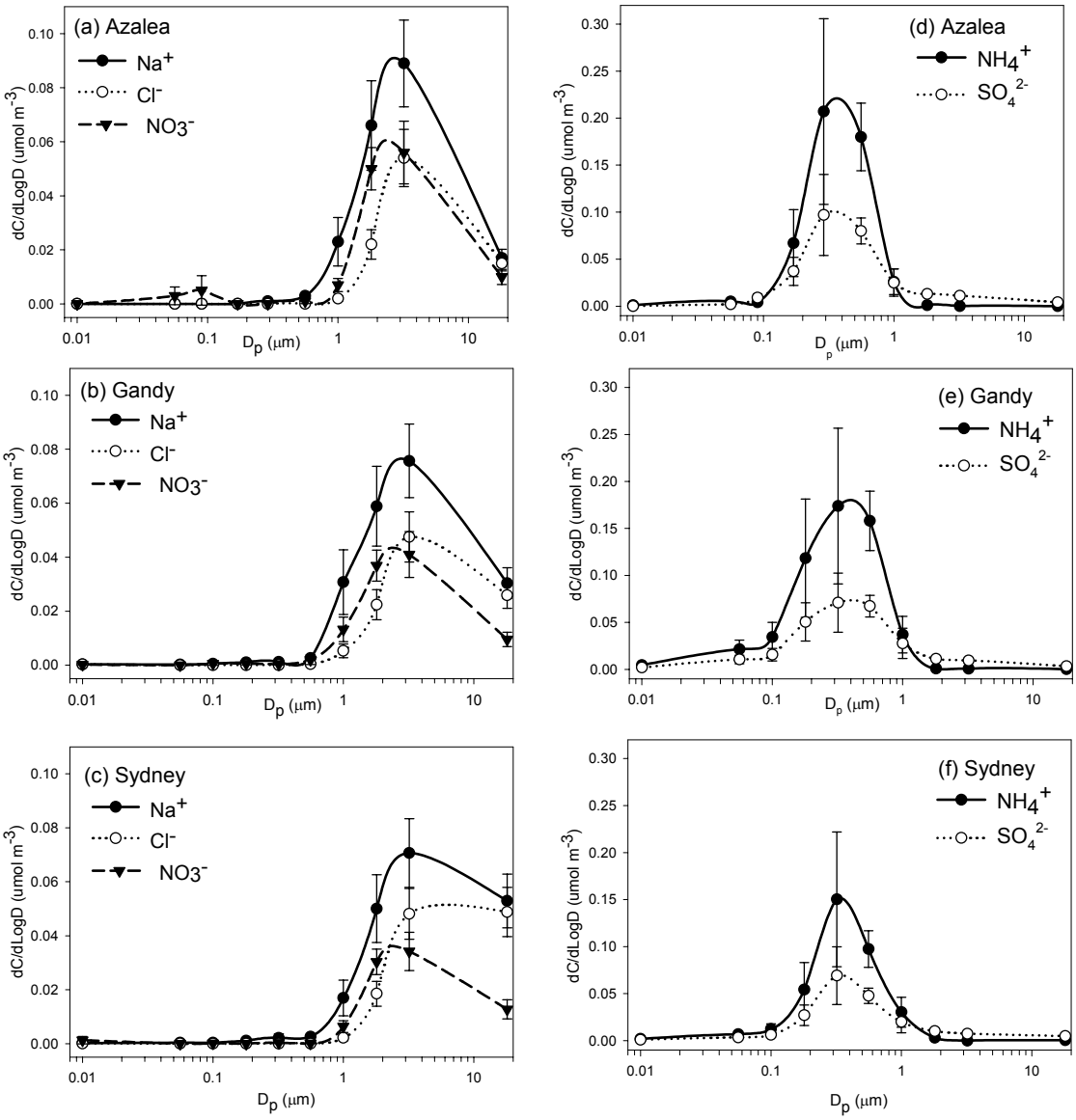

Figure 26. Size distributions for each sampling site on May 6, 2002.

	Azalea	Gandy	Sydney
Cl^-:Na^+	0.53	0.56	0.64
NO_3^-:Na^+	0.63	0.53	0.46
Cl^--dep %	55%	52%	46%
NH_4^+:SO_4^{2-}	2.1	2.4	2.1

Table 13. Ion ratios for May 6, 2002.

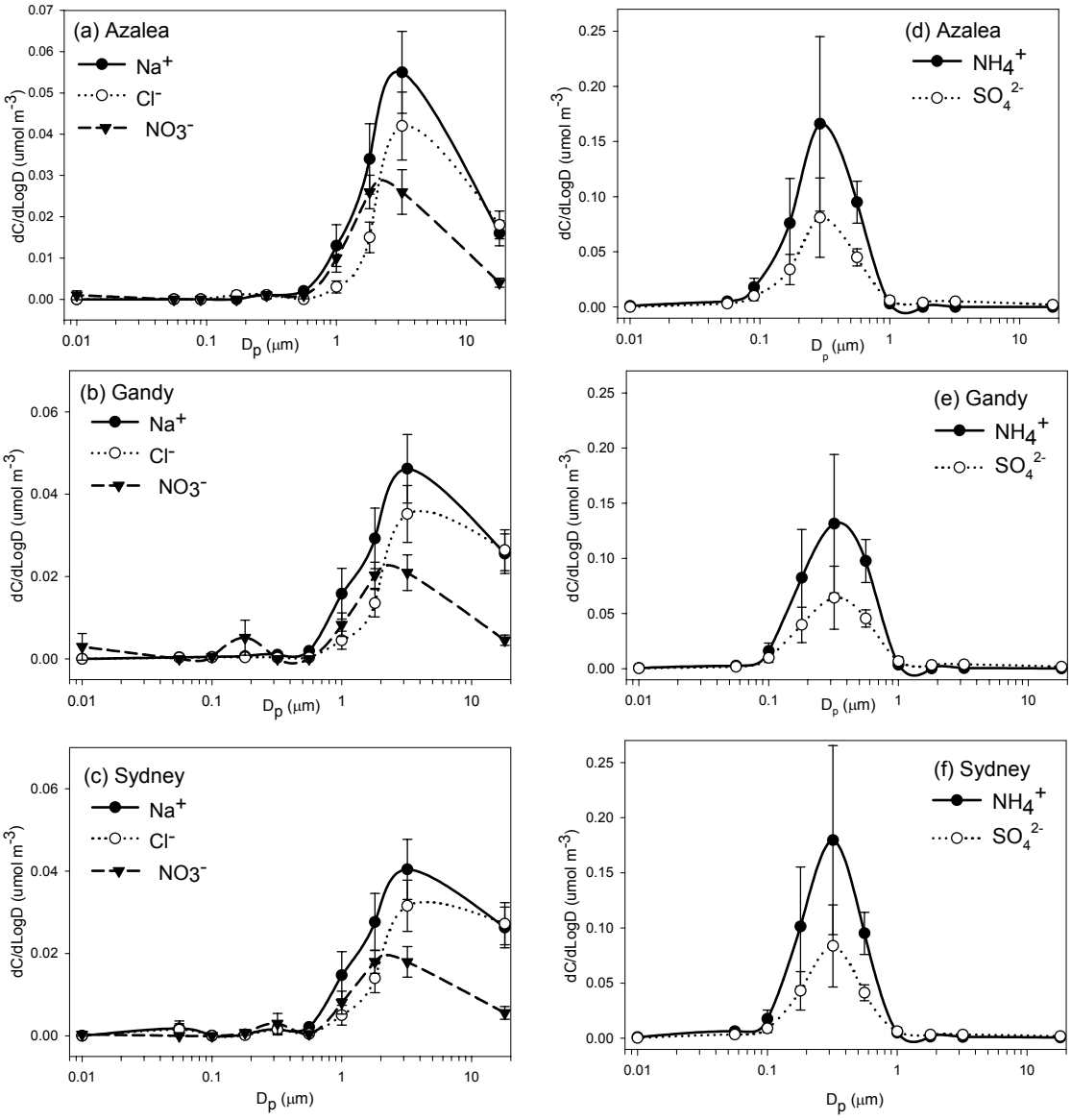

Figure 27. Size distributions for each sampling site on May 20, 2002.

	Azalea	Gandy	Sydney
Cl^-:Na^+	0.72	0.71	0.74
NO_3^-:Na^+	0.53	0.46	0.45
Cl^--dep %	39%	39%	37%
NH_4^+:SO_4^{2-}	2.1	2.0	2.2

Table 14. Ion ratios for May 20, 2002.

Upon arrival at the Sydney site, the chloride depletion had already reached 46%, steadily increasing to 55% along the prevailing wind direction (Figure 26a-c and Table 13). Coupled with increasing chloride depletion, the Cl^-:Na^+ and NO_3^-:Na^+ ratios are indicative of the nitric acid gas to particulate nitrate conversion.

On May 20, 2002, the air originated in the Atlantic Ocean area near North and South Carolina (Figure 23). NH_4^+:SO_4^{2-} ratios at all three sites are over 2.0 (Figure 27 and Table 14), indicating the arrival of an aged air mass. Chloride depletion and Cl^-:Na^+ and NO_3^-:Na^+ ratios remain nearly constant, with only a very small insignificant fraction of change between the monitoring sites.

The ammonium and nitrate particulate nitrogen flux was compared for these four sampling days (Figure 28). For each day, regardless of the air mass origin, the particulate nitrate dominated the particulate nitrogen flux. These particles were significantly larger than those of ammonium, giving them a significantly larger deposition velocity. For May 4th and 14th, when the air originated out of the west, there does not appear to be any significant trend in deposition. For May 6th and 20th, when the air originated out of the east, there does appear to be a slight trend only for nitrate. Particulate nitrate flux increased along the prevailing wind direction. In general, the air masses originating from the east were aged more than those from the west. Aging allows for the gas-to-particulate conversion of nitric acid to nitrate. In an older air mass, higher nitrate deposition fluxes would be expected. For the majority of the sampling days during May 2002, the concentration of sodium was greatest at the Azalea site.

With its proximity to the Gulf of Mexico, there appeared to be a salt gradient over land regardless of the wind direction.

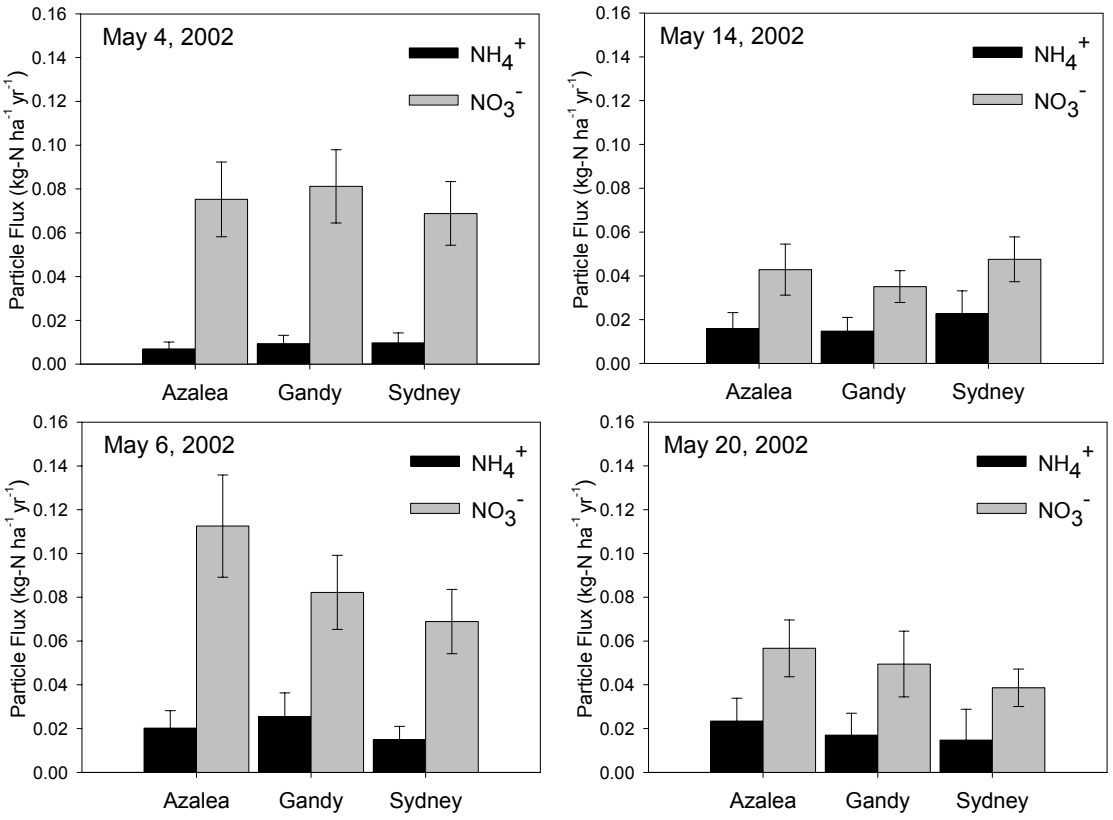

Figure 28. Nitrate and ammonium particulate flux for select days in May 2002.

Size distributions and ion ratios for the remainder of the May 2002 samples are given in Appendix 2. Meteorological data for the entire sampling period is listed in Tables 26-28 in Appendix 1.

EQUISOLV II: A Thermodynamic Model

EQUISOLV II is an aerosol thermodynamic equilibrium model, which is an updated version of EQUISOLV (Jacobson, 1999a; Jacobson, 1999b; Jacobson et al., 1996) written by Mark Jacobson from Stanford University. The original EQUISOLV model included sodium, ammonium, chloride, nitrate, and sulfate species. Advances from EQUISOLV, EQUISOLV II includes potassium, calcium, magnesium and carbonate species. The model works by solving sets of equilibrium equations, similar to aA + bB ←→ cC + dD, utilizing the temperature-dependent equilibrium coefficient, k_{eq}.

$$k_{eq}(T) = \frac{\{C\}^c \{D\}^d}{\{A\}^a \{B\}^b} \qquad \text{(Equation 24)}$$

where {X} is the thermodynamic activity of species X.

The model iteratively solves sets of equilibrium equations in a "positive-definite, mass-conserving, and charge-conserving" process using analytical equilibrium iterations and mass flux iterations (Jacobson, 1999a). After sufficient iterations and a positive solution exists to a set of equilibrium equations, EQUISOLV II converges. Species can be gases, dissolved liquids, dissolved ions or solids. Many of the equilibrium reactions and corresponding constants are listed in Jacobson (1999a).

The above equilibrium expression (Equation 24) requires the mean mixed activity coefficients. The equilibrium expression for

$NH_{3(g)} + HNO_{3(g)} \leftrightarrow NH_4^+ + NO_3^-$ is:

$$k_{eq} = \frac{\{NH_4^+\}\{NO_3^-\}}{\{NH_3\}\{HNO_3\}} = \frac{m_{NH_4^+}\, m_{NO_3^-}\, \gamma^2_{NH_4^+,NO_3^-}}{p_{NH_3}\, p_{HNO_3}} \qquad \text{(Equation 25)}$$

k_{eq} ($mol^2\ kg^{-2}\ atm^{-2}$) is the equilibrium constant, m ($mol\ kg^{-1}$) is the molality, p (atm) is the gas phase partial pressure and $\gamma_{NH_4^+,NO_3^-}$ is the mean mixed activity coefficient of NH_4NO_3. In EQUISOLV II, the mean mixed activity coefficients are calculated using the Bromley's method for the empirical mixing rule (Bromley, 1973; Jacobson, 1999b) using temperature-dependent coefficients given in Jacobson et al. (1996). The expression for the activity coefficients is as follows:

$$ln\,\gamma^0_{12b1} = B_0 + B_1\, m_{12}^{1/2} + B_2\, m_{12} + B_3\, m_{12}^{3/2} + \ldots \qquad \text{(Equation 26)}$$

where B_0, B_1, … are the fitting coefficients for each electrolyte and m_{12} the molalities of electrolytes 1 and 2. These values can be found in Table 2 of Jacobson (1999b).

The model can be used in two different modes. It can be used to solve for internal equilibrium within a single aerosol bin. Or, it can be used to determine equilibrium for species between the gas phase and multiple, internally mixed, aerosol size bins.

EQUISOLV II can be set to run under various conditions. In the default mode, aerosols are solids at relative humidity conditions below the particle's deliquescent relative humidity (DRH) and are aqueous aerosols above the DRH point. Metastable conditions are obtained by deactivating the solid formation

reactions in the program, limiting aerosols to the aqueous phase. Metastable conditions exist when the ambient relative humidity falls below the particle's DRH; and the aerosol exhibits a hysteresis effect and remains as a supersaturated droplet until the relative humidity reaches the particle's crystallization relative humidity (CRH). This is the relative humidity at which the aerosol crystallizes and becomes a solid.

Inputs

The model is initialized by creating a text file with the following data: temperature, relative humidity, pressure, number of collection stages, cut-point diameters for each collection stage, aerosol concentrations and gas concentrations. The model was altered from the original version to accept twelve input bins. Aerosol concentrations of Na^+, NH_4^+, K^+, Mg^{2+}, Ca^{2+}, Cl^-, NO_3^- and SO_4^{2-} are entered for each bin in units of ng m^{-3}. Gas concentrations of HNO_3, NH_3, HCl and SO_2 are also entered in units of ng m^{-3}. Ion imbalances were automatically corrected for using hydrogen and carbonate ions. The following is an example of an input file.

```
                  AEROSOL-COMPONENT CONCENTRATION VERSUS SIZE


DATE: 5/04 GANDY

T   = TEMPERATURE (C), EITHER SAMPLING OR AMBIENT
RH  = RELATIVE HUMIDITY (%), EITHER SAMPLING OR AMBIENT
P   = AIR PRESSURE (MB), EITHER SAMPLING OR AMBIENT
D50 = 50% CUTOFF DIAMETERS

BEGIN
SAMPLING T = 26.2 C  RH = 76.6 %;   AMBIENT T = 26.2 C; RH = 76.6 %
         P = 1019.13 MB                    P = 1019.13 MB
12  STAGES
D50(UM) 18.00 10.0  5.60  3.20  1.80  1.00  0.56  0.32  0.180 0.10  0.056 0.01
DLO, DHI (UM)     0.001  30.0

FORMAT(A1,1X,A6,12(0PF6.2))

                          AEROSOL CONCENTRATIONS (NG M-3)
BEGIN
A NA+   188.7 127.3 552.7 784.0 309.0 151.0 12.88 4.300 2.960 0.000 1.650 0.400
A NH4+  0.000 0.000 0.000 0.000 1.240 24.46 258.8 363.3 270.3 110.9 72.70 17.65
A K+    7.760 5.730 22.00 43.89 22.73 10.55 11.33 14.22 11.91 6.990 4.470 4.520
A MG2+  29.32 19.07 75.96 107.3 44.84 23.98 3.300 1.570 1.070 0.000 0.030 0.110
A CA2+  152.8 105.5 206.1 265.7 101.6 44.62 7.280 7.050 3.370 0.760 3.550 5.520
A CL-   319.6 208.8 806.3 848.5 218.1 52.06 0.000 0.000 0.000 0.000 0.000 0.000
A NO3-  115.0 89.46 550.0 1228. 604.9 238.1 0.000 0.000 0.000 2.000 2.090 20.09
A SO42- 87.74 57.89 243.6 403.0 234.2 283.8 800.0 1035. 798.0 322.2 211.6 38.16
  END
                            GAS CONCENTRATIONS (NG M-3)
BEGIN
A HNO3  395.1
A NH3   782.0
A HCL   1152.
A SO2   7421.
  END
```

Figure 29. EQUISOLV II input file example.

Upon execution, the model redistributes the volatile species between the multiple size bins and the gas phase until equilibrium is reached. The volatile species include nitrate, chloride and ammonium.

Outputs

The output for the model includes the predicted equilibrium gas, aqueous and solid particle concentrations. The list of predictable solids includes: NH_4NO_3,

NH_4Cl, NH_4HSO_4, $(NH_4)_2SO_4$, $(NH_4)_3H(SO_4)_2$, NH_4HCO_3, $NaNO_3$, NaCl, $NaHSO_4$, Na_2SO_4, $NaHCO_3$, Na_2CO_3, KNO_3, KCl, $KHSO_4$, K_2SO_4, $KHCO_3$, K_2CO_3, $Ca(NO_3)_2$, $CaCl_2$, $CaSO_4 \cdot 2H_2O$, $CaCO_3$, $MgCl_2$, $Mg(NO_3)_2$, $MgSO_4$ and $MgCO_3$. The predictable gases and liquids include: HCl, H_2O, H_2SO_4, SO_2, HNO_3, NH_3 and CO_2. The remaining analytes are constrained to the aqueous phase.

Limitations

The EQUISOLV II model is a mass and charge conserving thermodynamic model. The model cannot be used simply to predict a gas phase concentration of a species given a fixed amount in the particle phase. The model only redistributes a given amount of a substance. Multiple, iterative model runs must be completed to derive this relationship.

One benefit from using the model is that it is capable of differentiating between the solid and aqueous phases, allowing it to predict the solid phase formation. This information cannot be directly determined from aerosol measurements, which indicates the presence and size of the species but not its phase (Campbell et al., 2002).

Qualitative Analysis

Before the EQUISOLV II thermodynamic model can be used for theoretical work, it must be investigated whether it can predict size-resolved concentrations of ammonium, chloride and nitrate.

Measurements taken during the May 2002 intensive sampling period were used for the model evaluation. Samples were taken using the MOUDI sampler with 23-hour integration. Measurements were collocated with an annular denuder system for the collection of acidic and basic gas species. Meteorological data was averaged for each 23-hour period for the model input.

All ions analyzed except fluoride, nitrite and phosphate were included in the model runs. These excluded ions were only present in minute quantities, near the detection limit of the ion chromatograph, and are coincidentally not treated by the model.

The model was run in two modes, default and metastable, for analysis to see which mode gave results closest to the experimental data. In the metastable mode, analytes were constrained to the gaseous and aqueous phases.

		HNO_3 ($\mu g\ m^{-3}$)		
		Measured	Modeled (Default)	Modeled (Metastable)
5/4/02	Azalea	0.55	1.09	0.24
	Gandy	0.40	0.40	0.37
	Sydney	0.37	1.72	0.35
5/6/02	Azalea	0.89	0.39	0.13
	Gandy	1.09	1.51	0.97
	Sydney	0.63	1.46	0.10
5/10/02	Azalea	0.37	0.00	0.00
	Gandy	1.24	3.52	0.98
	Sydney	0.58	1.24	1.05
5/14/02	Azalea	0.42	0.18	0.13
	Gandy	0.88	0.88	0.84
	Sydney	0.65	0.24	0.21
5/15/02	Azalea	0.68	2.73	0.00
	Gandy	0.77	0.48	0.47
	Sydney	0.84	2.49	0.69
5/16/02	Azalea	0.69	1.09	0.37
	Gandy	0.96	1.37	0.69
	Sydney	0.28	0.70	0.34
5/17/02	Azalea	0.21	0.15	0.13
	Gandy	0.39	0.64	0.42
	Sydney	0.44	0.49	0.44
5/19/02	Azalea	0.56	0.23	0.20
	Gandy	0.23	0.20	0.18
	Sydney	0.12	0.37	0.36
5/20/02	Azalea	0.60	0.39	0.40
	Gandy	0.68	1.45	1.21
	Sydney	0.28	0.73	0.40
5/23/02	Azalea	0.60	0.57	0.37
	Gandy	0.58	0.64	0.44
	Sydney	0.39	0.01	0.01
5/24/02	Azalea	0.27	0.00	0.00
	Gandy	0.56	0.94	0.71
	Sydney	0.37	0.51	0.38
5/25/02	Azalea	0.36	0.08	0.07
	Gandy	0.57	0.97	0.76
	Sydney	0.51	0.31	0.22

Table 15. Comparison between measured HNO_3 gas concentrations and those modeled by EQUISOLV II.

		NH_3 ($\mu g\ m^{-3}$)		
		Measured	Modeled (Default)	Modeled (Metastable)
5/4/02	Azalea	2.41	1.92	2.34
	Gandy	0.78	0.75	0.82
	Sydney	1.63	1.55	1.61
5/6/02	Azalea	2.45	2.66	2.73
	Gandy	2.56	3.05	3.05
	Sydney	1.09	1.30	1.40
5/10/02	Azalea	3.54	3.78	3.80
	Gandy	1.23	1.64	1.64
	Sydney	1.73	1.97	1.94
5/14/02	Azalea	1.28	1.28	1.32
	Gandy	0.64	0.56	0.62
	Sydney	1.19	1.50	1.53
5/15/02	Azalea	2.35	2.38	2.52
	Gandy	0.84	0.75	0.84
	Sydney	1.62	1.57	1.66
5/16/02	Azalea	1.76	1.36	1.65
	Gandy	3.42	2.47	3.25
	Sydney	1.53	1.80	1.83
5/17/02	Azalea	4.51	4.38	4.43
	Gandy	1.79	1.73	1.75
	Sydney	3.38	3.40	3.39
5/19/02	Azalea	1.10	1.23	1.25
	Gandy	0.59	0.62	0.62
	Sydney	1.59	1.75	1.75
5/20/02	Azalea	2.00	1.90	1.96
	Gandy	0.62	0.58	0.55
	Sydney	1.75	1.97	1.90
5/23/02	Azalea	2.28	2.22	2.19
	Gandy	1.92	1.82	1.80
	Sydney	1.64	1.63	1.65
5/24/02	Azalea	2.43	2.52	2.53
	Gandy	2.18	2.23	2.19
	Sydney	0.91	0.79	0.76
5/25/02	Azalea	2.44	2.55	2.57
	Gandy	5.63	5.53	5.48
	Sydney	1.17	1.19	1.18

Table 16. Comparison between measured NH_3 gas concentrations and those modeled by EQUISOLV II.

		HCl (μg m^{-3})		
		Measured	Modeled (Default)	Modeled (Metastable)
5/4/02	Azalea	2.70	0.90	0.14
	Gandy	1.15	0.33	0.33
	Sydney	1.06	0.22	0.01
5/6/02	Azalea	0.58	0.09	0.04
	Gandy	1.62	0.12	0.30
	Sydney	1.01	0.66	0.05
5/10/02	Azalea	0.25	0.00	0.00
	Gandy	1.32	0.05	0.03
	Sydney	1.51	0.07	0.05
5/14/02	Azalea	0.42	0.03	0.02
	Gandy	0.82	0.11	0.05
	Sydney	0.51	0.01	0.00
5/15/02	Azalea	0.51	0.03	0.00
	Gandy	1.01	0.08	0.03
	Sydney	1.38	0.16	0.05
5/16/02	Azalea	2.17	0.89	0.16
	Gandy	4.76	2.47	0.46
	Sydney	0.94	0.90	0.38
5/17/02	Azalea	0.56	0.03	0.13
	Gandy	0.69	0.06	0.19
	Sydney	0.35	0.03	0.01
5/19/02	Azalea	0.11	0.11	0.10
	Gandy	0.07	0.11	0.11
	Sydney	0.66	0.56	0.57
5/20/02	Azalea	0.87	0.04	0.07
	Gandy	1.01	0.17	0.06
	Sydney	0.46	0.04	0.02
5/23/02	Azalea	0.72	0.04	0.03
	Gandy	0.72	0.03	0.04
	Sydney	0.43	0.01	0.01
5/24/02	Azalea	0.31	0.00	0.00
	Gandy	0.78	0.04	0.02
	Sydney	0.60	0.09	0.06
5/25/02	Azalea	0.28	0.00	0.00
	Gandy	1.00	0.01	0.02
	Sydney	0.43	0.06	0.03

Table 17. Comparison between measured HCl gas concentrations and those modeled by EQUISOLV II.

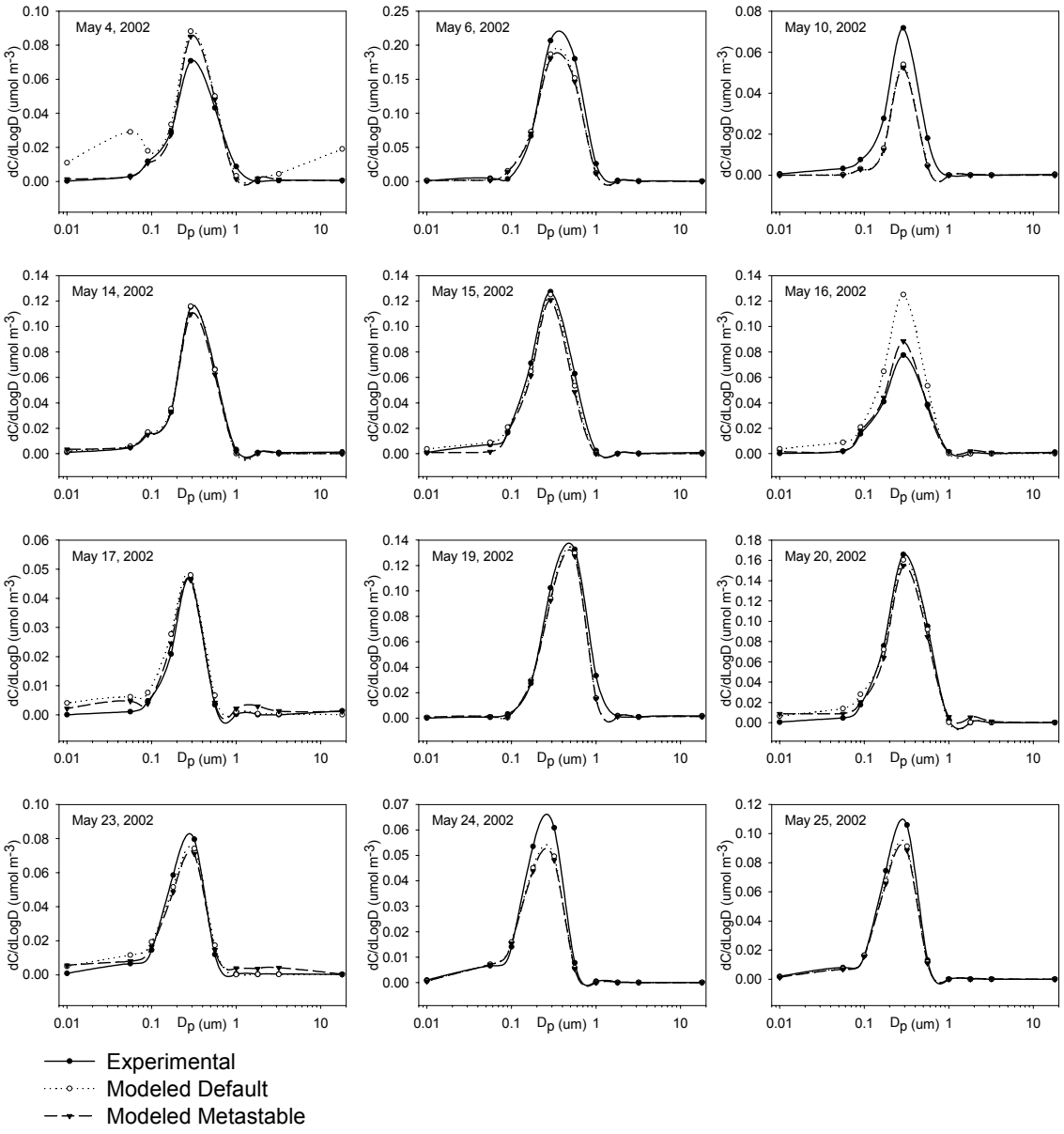

Figure 30. Comparison of experimental, EQUISOLV II default mode and EQUISOLV II metastable mode data for ammonium at the Azalea site.

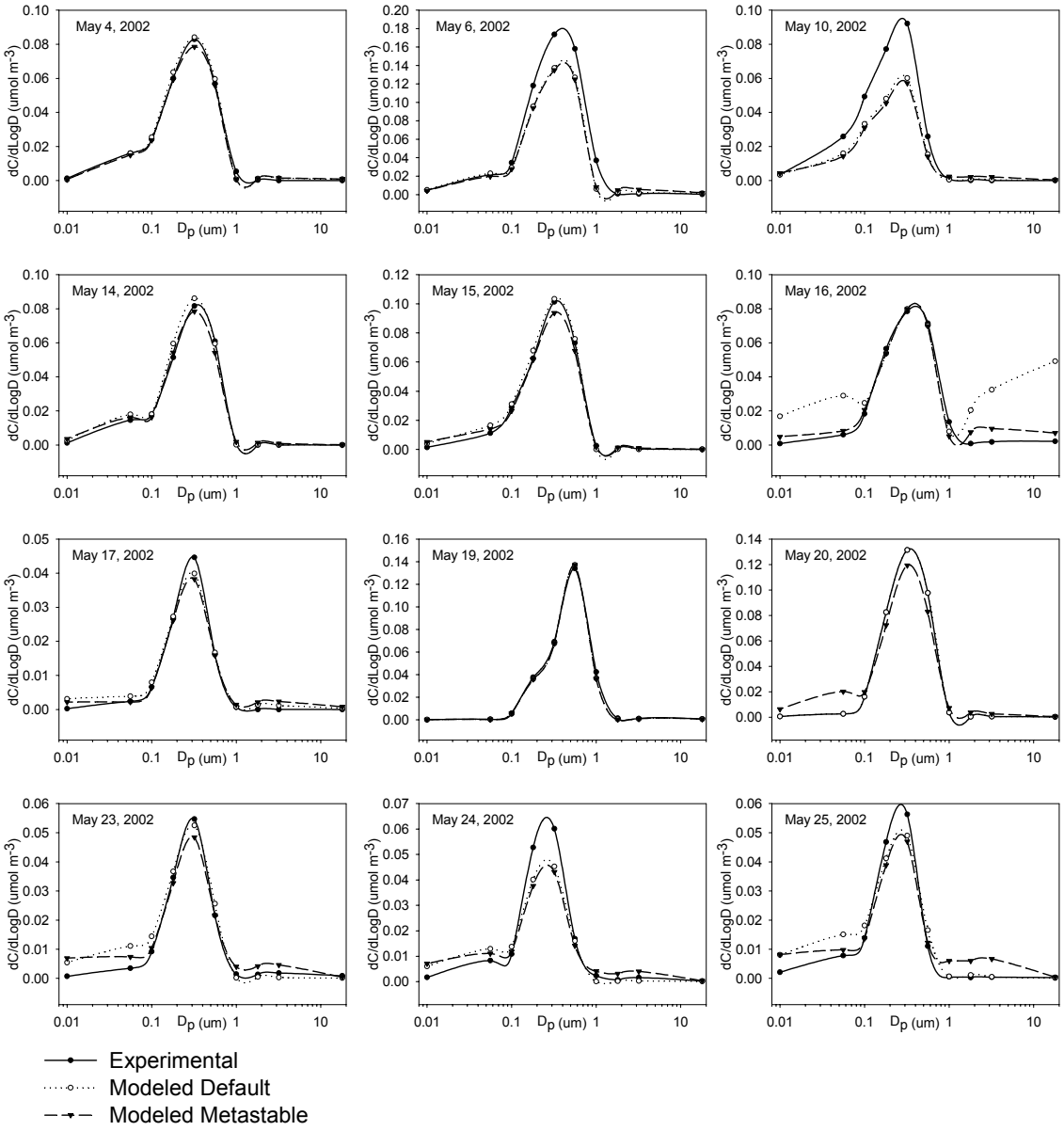

Figure 31. Comparison of experimental, EQUISOLV II default mode and EQUISOLV II metastable mode data for ammonium at the Gandy site.

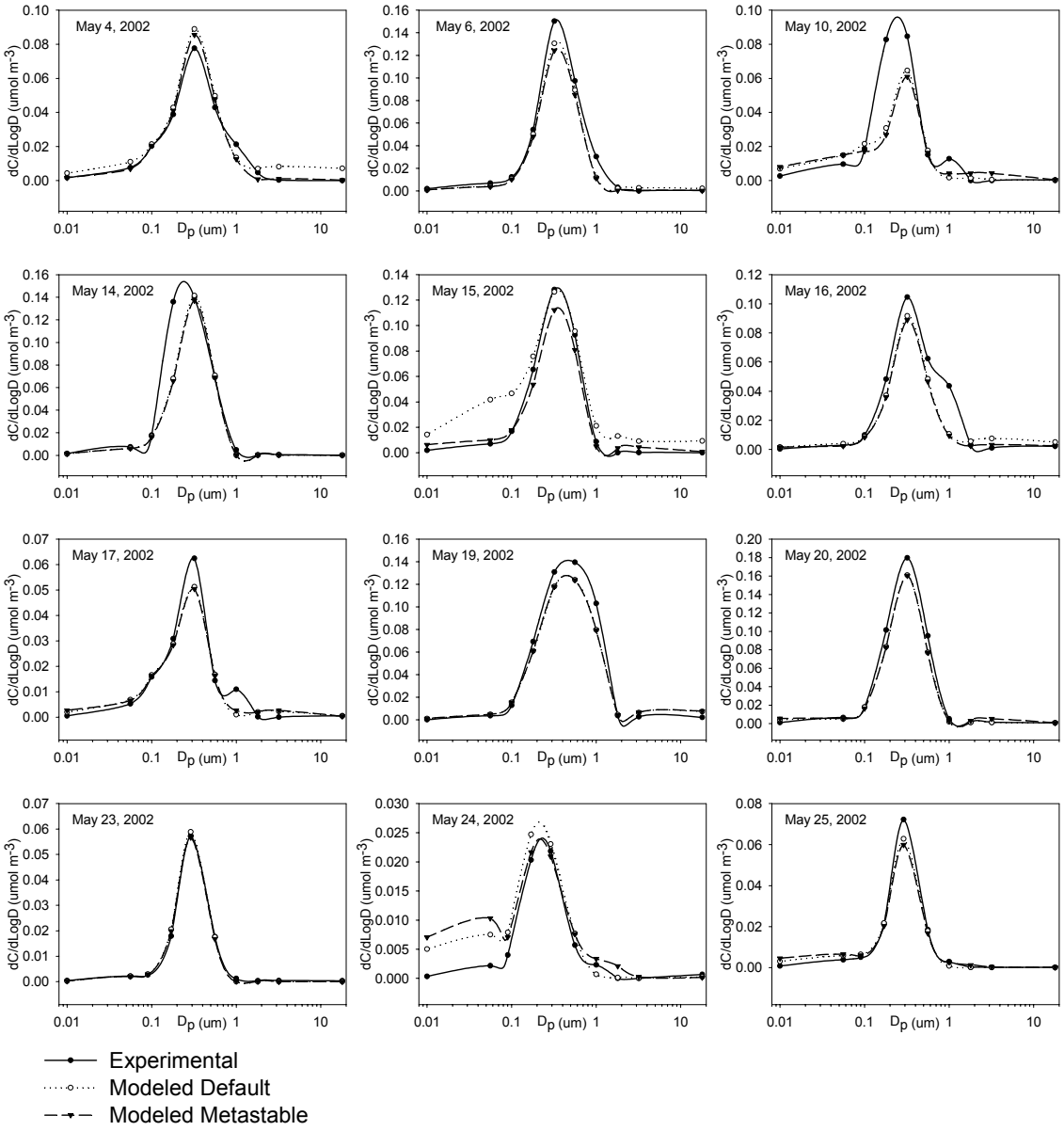

Figure 32. Comparison of experimental, EQUISOLV II default mode and EQUISOLV II metastable mode data for ammonium at the Sydney site.

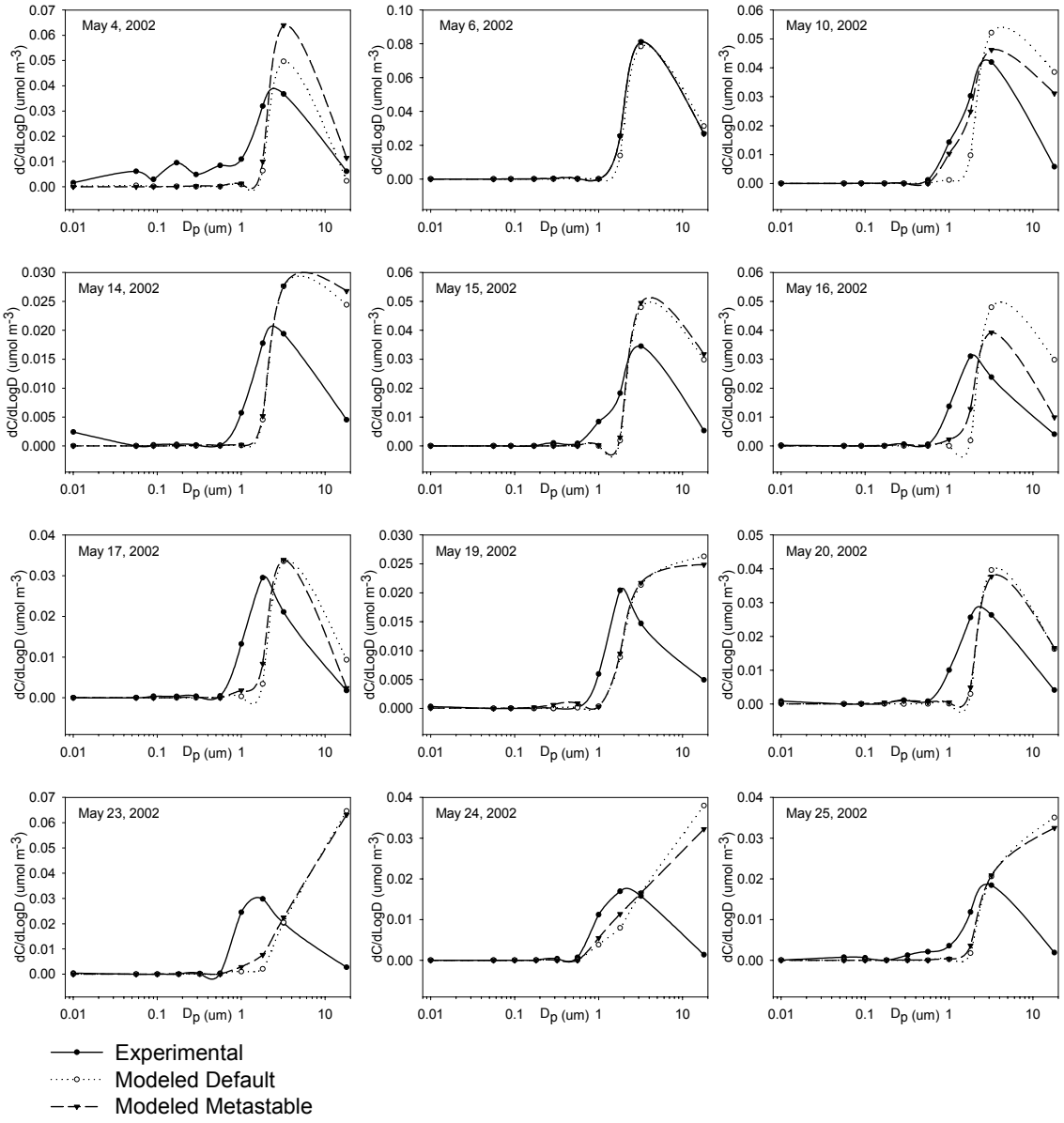

Figure 33. Comparison of experimental, EQUISOLV II default mode and EQUISOLV II metastable mode data for nitrate at the Azalea site.

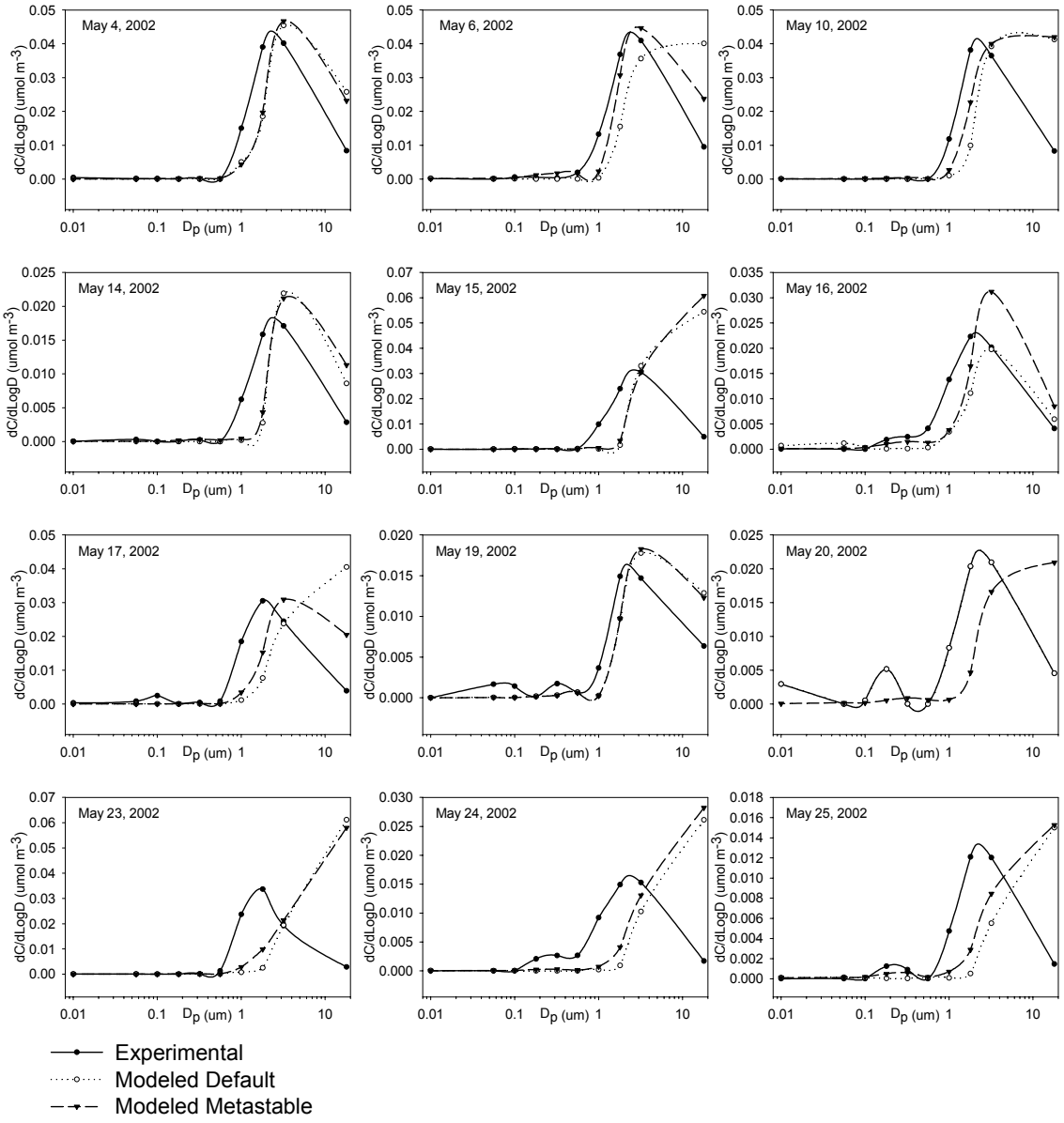

Figure 34. Comparison of experimental, EQUISOLV II default mode and EQUISOLV II metastable mode data for nitrate at the Gandy site.

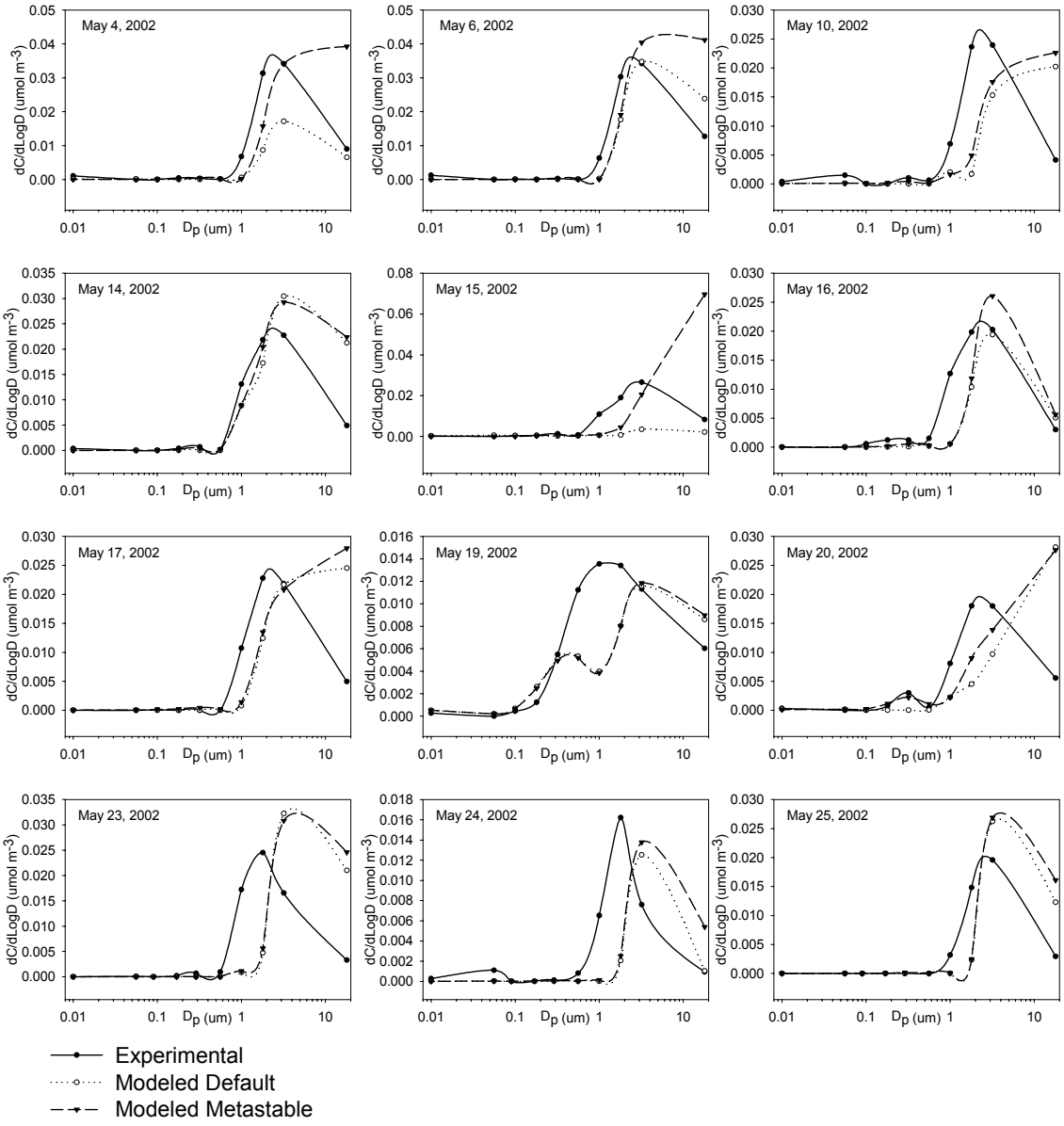

Figure 35. Comparison of experimental, EQUISOLV II default mode and EQUISOLV II metastable mode data for nitrate at the Sydney site.

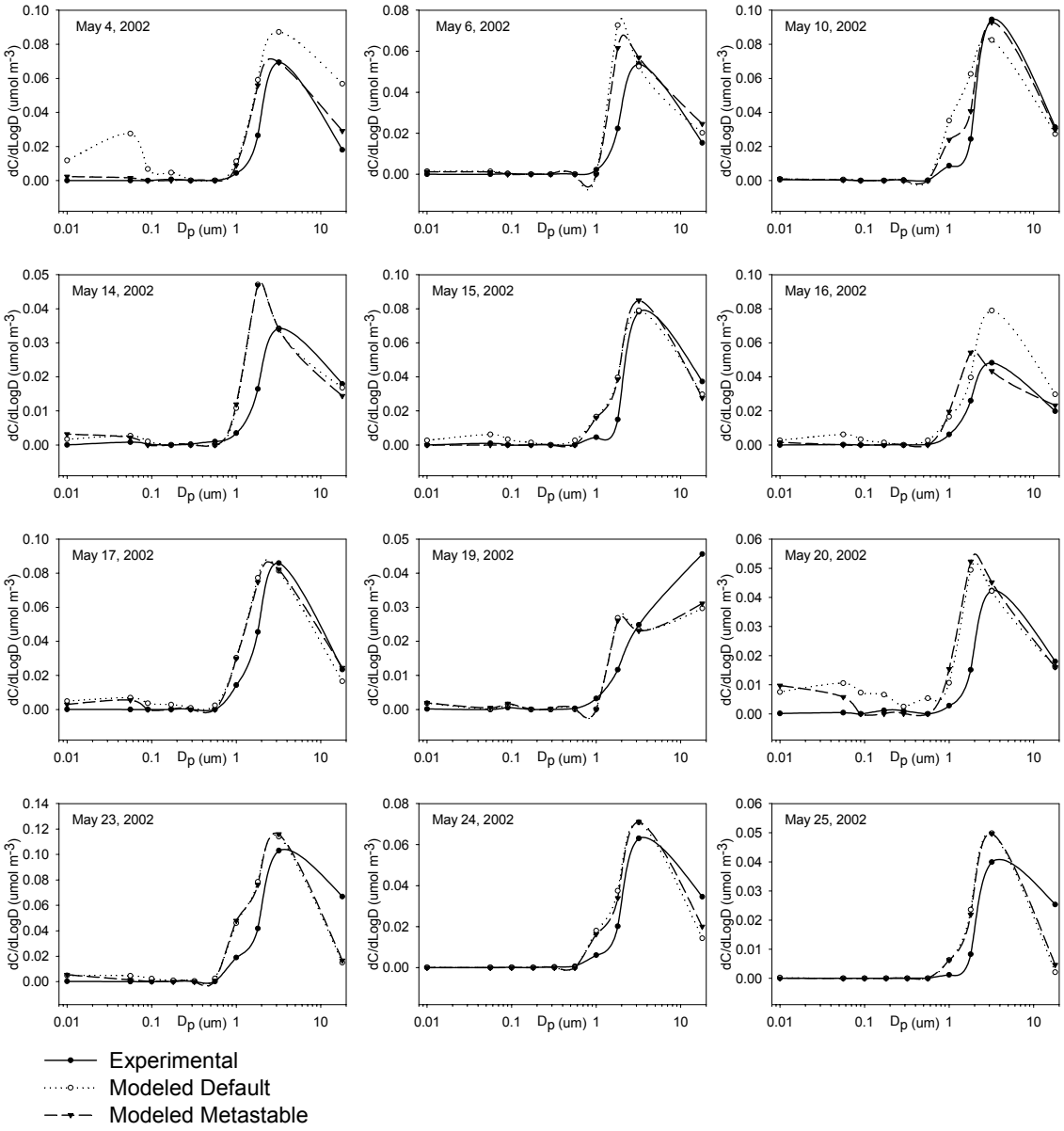

Figure 36. Comparison of experimental, EQUISOLV II default mode and EQUISOLV II metastable mode data for chloride at the Azalea site.

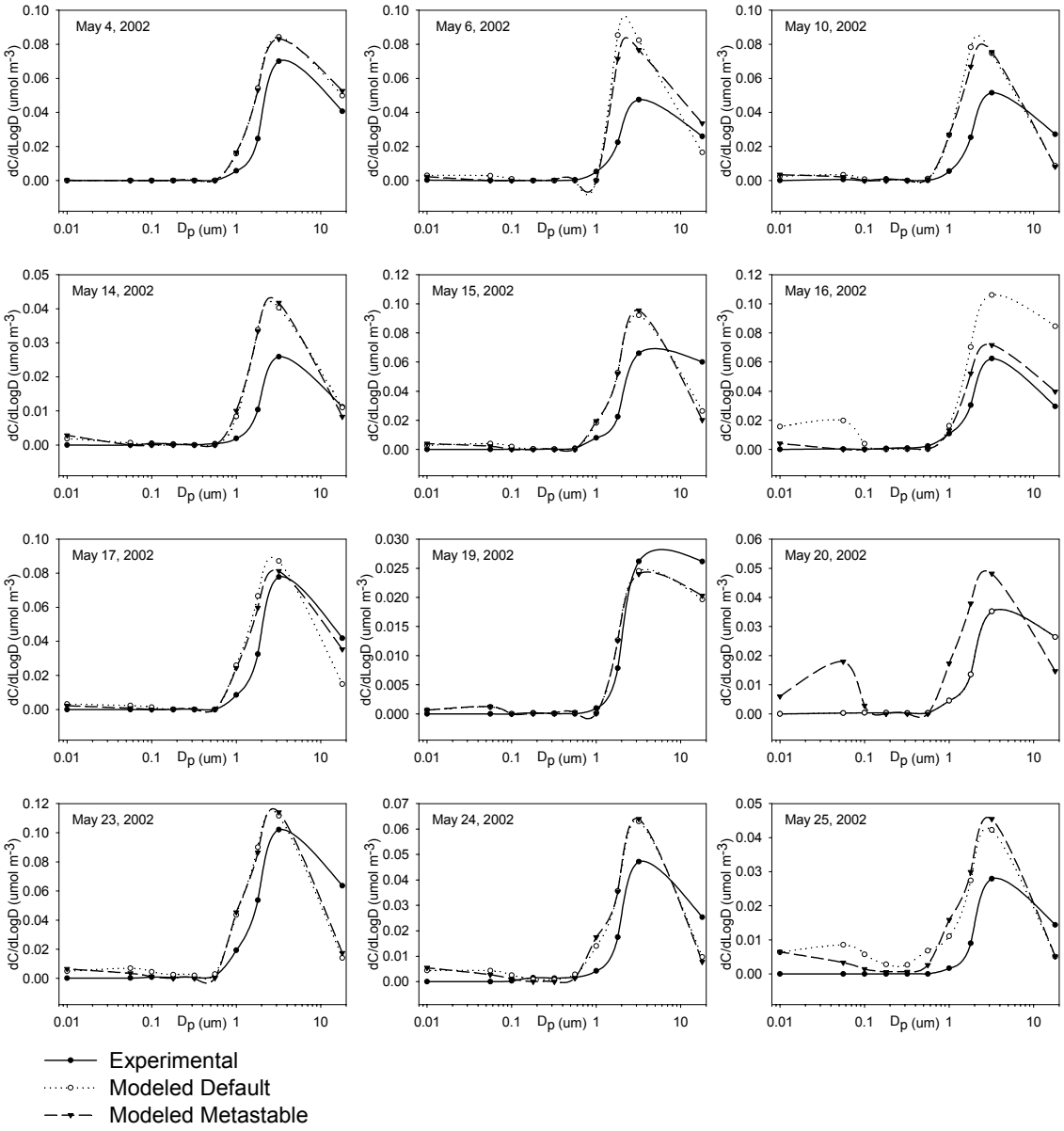

Figure 37. Comparison of experimental, EQUISOLV II default mode and EQUISOLV II metastable mode data for chloride at the Gandy site.

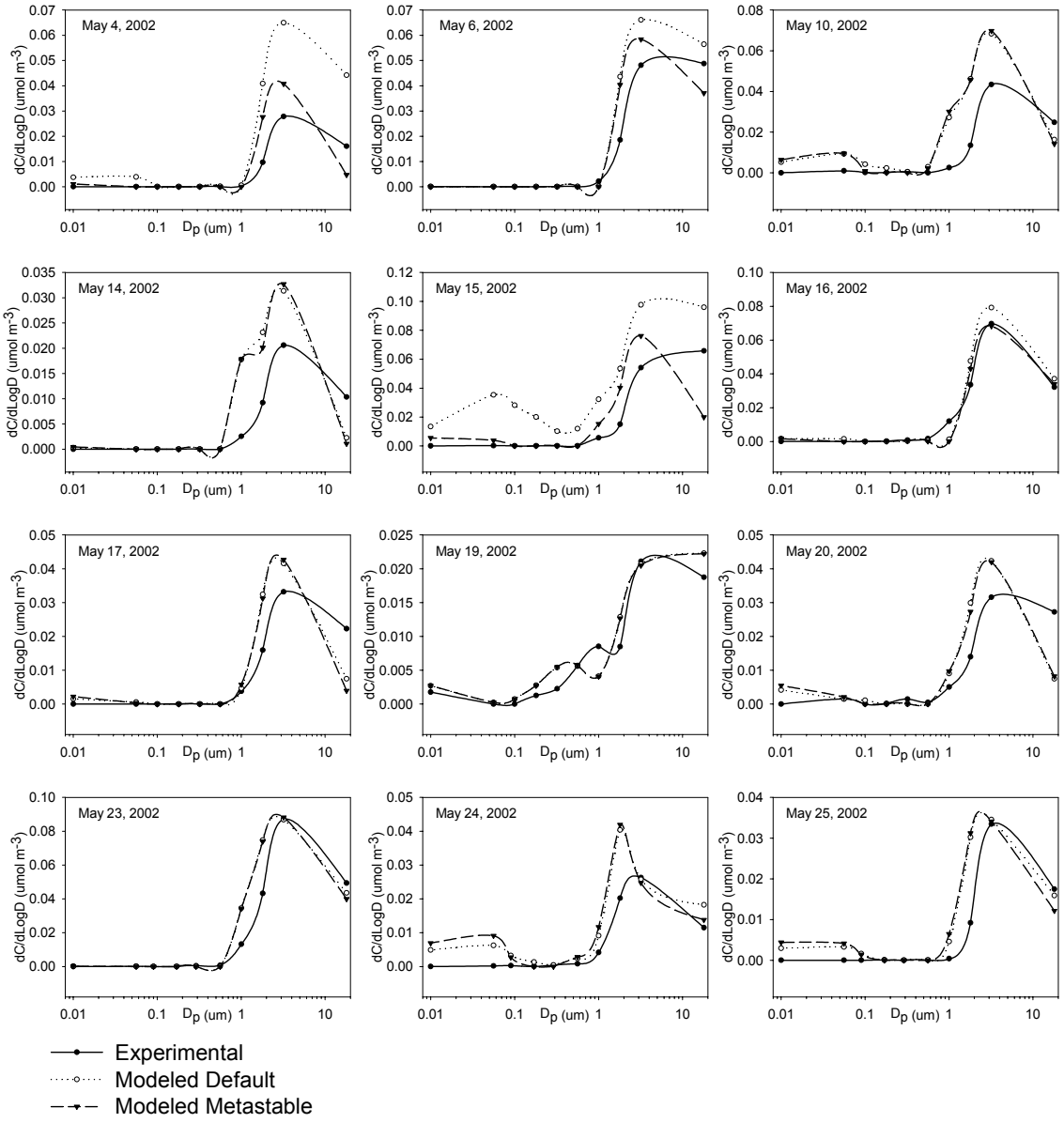

Figure 38. Comparison of experimental, EQUISOLV II default mode and EQUISOLV II metastable mode data for chloride at the Sydney site.

The comparison between the measured gaseous species and those modeled by EQUISOLV II are displayed in Tables15-17. Both the default- and metastable-modeled results agreed best for the NH_3 gas scenario. The model continually under predicted HCl and HNO_3 concentrations.

The comparisons for the particulate species are categorized by analyte and site in Figures 30-38. Of the three volatile species, ammonium had the greatest agreement between the modeled and measured values. The agreement seen for both gaseous NH_3 and particulate NH_4^+ infers that the system is in or is near an equilibrium state. These particles are primarily fine mode species, which have the potential to reach equilibrium in a relative short period of time (Campbell et al., 2002; Moya et al., 2002).

For both particulate chloride and nitrate, their situations are nearly the same. The modeled and experimental particle data showed some agreement, with the metastable mode giving better results. The model continually over predicted particle concentrations and, for nitrate, often resulted in a size distribution mode shift. From the gas results, the modeled metastable mode under predicted the gas concentration for the majority of the model runs. Since the modeled gas phase is under predicted and the modeled particle phase is over predicted, it appears that the nitrate/nitric acid and chloride/hydrochloric acid systems during May 2002 were not at thermodynamic equilibrium. This is a different scenario from the ammonium/ammonia system as chloride and nitrate are predominantly coarse mode species.

Model Comparison

The EQUISOLV II model (Jacobson, 1999a) was compared against the AIM2 – Model III thermodynamic equilibrium model (Clegg et al., 1998). The main difference between the two models lies in their method of solution. EQUISOLV II used analytical equilibrium iterations (equilibrium constants), and AIM2 uses Gibbs free energy minimization iterations. These models were run in parallel, both in default and metastable modes, to compare their predicted solid and aqueous phase concentrations. The focus of this study was to determine whether or not EQUISOLV II should be run in the metastable mode, in which the aerosols are constrained to the aqueous phase, or the default mode in which both solid and aqueous aerosols are allowed.

A simple system was developed, comprising only Na^+, Cl^- and NO_3^-. The first scenario tested was a 1:1 $NaCl:HNO_3$ molar ratio system and a 1:2 $NaCl:HNO_3$ system. The models agreed extremely well at 60% (low) and at 90% (high) relative humidities.

The systems were expanded to account for NH_4^+ and SO_4^{2-}. The models no longer agreed as they did with the simple Na^+, Cl^- and NO_3^- system in the default mode. However, the models were in closer agreement when run in the metastable mode. The compounds treated by each of the models were investigated. AIM2 was found to handle more solid compounds than EQUISOLV II. This is most likely due to the temperature limitations of the models. Data for equilibrium reactions are typically obtained under 25°C conditions. The wide

range of temperatures used by EQUISOLV II limits the number of compounds treated by the model because data for many of the equations are not available at temperatures other than 25°C.

Actual ambient concentrations of Na^+, NH_4^+, K^+, Mg^{2+}, Ca^{2+}, Cl^-, NO_3^- and SO_4^{2-} were used to compare the models under simulated environmental conditions. The AIM2 model does not treat K^+, Mg^{2+} and Ca^{2+}, so EQUISOLV II was run with and without those species. Simulations were run at the ambient relative humidity and at both the ambient temperature recorded during sampling and at 25°C. Results indicate the EQUISOLV II model is sensitive to both temperature and the presence of K^+, Mg^{2+} and Ca^{2+}. The models were most comparable at 25°C and conditions without those three species. The EQUISOLV II model predicted more aerosol nitrate and chloride than AIM2, which predicted higher gas phase concentrations of these species. Agreement was greatest in the metastable mode.

Through all of these simulations, the models best agreed in the metastable mode. Modeling in the metastable mode improved the agreement between actual and modeled results, as seen in Figures 30-38. As noted in literature, metastable aerosols are ubiquitous and are most likely the prevalent form in the Tampa Bay area (Rood et al., 1989).

Case Studies

The Partitioning of Nitric Acid to Nitrate

Atmospheric particulate nitrate is primarily formed from the transfer and/or reaction of gaseous nitric acid, HNO_3, onto existing particles' surfaces (Pakkanen et al., 1996a). The most important mechanism for coarse particulate nitrate formation is the reaction between nitric acid and sea salt (NaCl) and mineral dust ($CaCO_3$) particles.

The partitioning of gas phase nitric acid and particle phase nitrate is an important process with local environmental implications. The change from one species to another changes the residence times and removal mechanisms and rates. The partitioning from the gas phase to small particles (diameter less than 10 μm) often decreases the dry deposition locally but can increase the deposition over open waters (Pryor and Sorensen, 2000).

EQUISOLV II Model

The EQUISOLV II model was used to calculate the partitioning of nitrate between the particle and gas phases. The specified model inputs included

temperature, relative humidity and varying concentrations of sodium, chloride and calcium. The carbonate affiliated with the calcium was not directly entered into the model; instead, it was automatically accounted for by ion balance corrections. The concentration of NaCl and $CaCO_3$ used in the model were similar to ambient air concentrations seen in the Tampa Bay area. The model gave predicted gas and particle phase concentrations in its output. The EQUISOLV II model was also used to compute the hygroscopic growth and water mass fraction of the particles.

The ambient air concentrations (from annular denuder measurements) and meteorological data (NOAA, 2003a) were based on the year 2000 averages. During this time period, the averaged ambient air concentrations of nitric acid and particulate nitrate were 1.2 and 1.7 μg m^{-3}, respectively. The average sodium concentration was 1.3 μg m^{-3} (or 3.3 μg m^{-3} as NaCl), and the average calcium concentration was 0.5 μg m^{-3} (or 1.2 μg m^{-3} as $CaCO_3$).

The dry gas and particle fluxes were calculated using Equation 1 ($F = C \times V_d$). The deposition velocities for each species were calculated using the integrated NOAA Buoy – Williams model (Bhethanabotla, 2002). The particle diameter was set at 4 μm, which is the approximate modal diameter for the particles of interest. A weighted average of the values for chloride and nitrate was used based on the composition of the particle, computing the density-dependent particle deposition velocity. The deposition velocity for the gas phase was computed specifically for HNO_3.

Results and Discussion

The model results revealed that the nitric acid to nitrate partitioning was dependent on the ambient air sodium and calcium concentrations, the total nitrate in the system (Figure 39) and relative humidity (Figure 40). Increased concentrations of both NaCl and $CaCO_3$ increased the fraction of nitrate in the particulate phase (Equation 27).

$$Fraction\ of\ NO_3^-\ in\ the\ particle = \frac{[NO_3^-]_{particle}}{[NO_3^-]_{total}} \qquad \text{(Equation 27)}$$

However, increased concentration of the total available nitrate (gas plus particle phase) reduced the particulate nitrate fraction. In the NaCl example (Figure 39a), the nitrate is always divided in equilibrium between both the gas and particle phases. In the $CaCO_3$ example (Figure 39b), the fraction of particulate nitrate significantly increased with a linear slope until the nitrate was completely in the particle phase. Gas phase nitric acid was only seen when the particulate phase was completely saturated with nitrate, where the remainder was forced to the gas phase. At this saturation point, nitrate and calcium were present in equi-equivalent amounts, which is the nanoequivalents of calcium equaled the nanoequivalents of nitrate. It was observed that the particulate nitrate was preferentially formed in a calcium-rich environment.

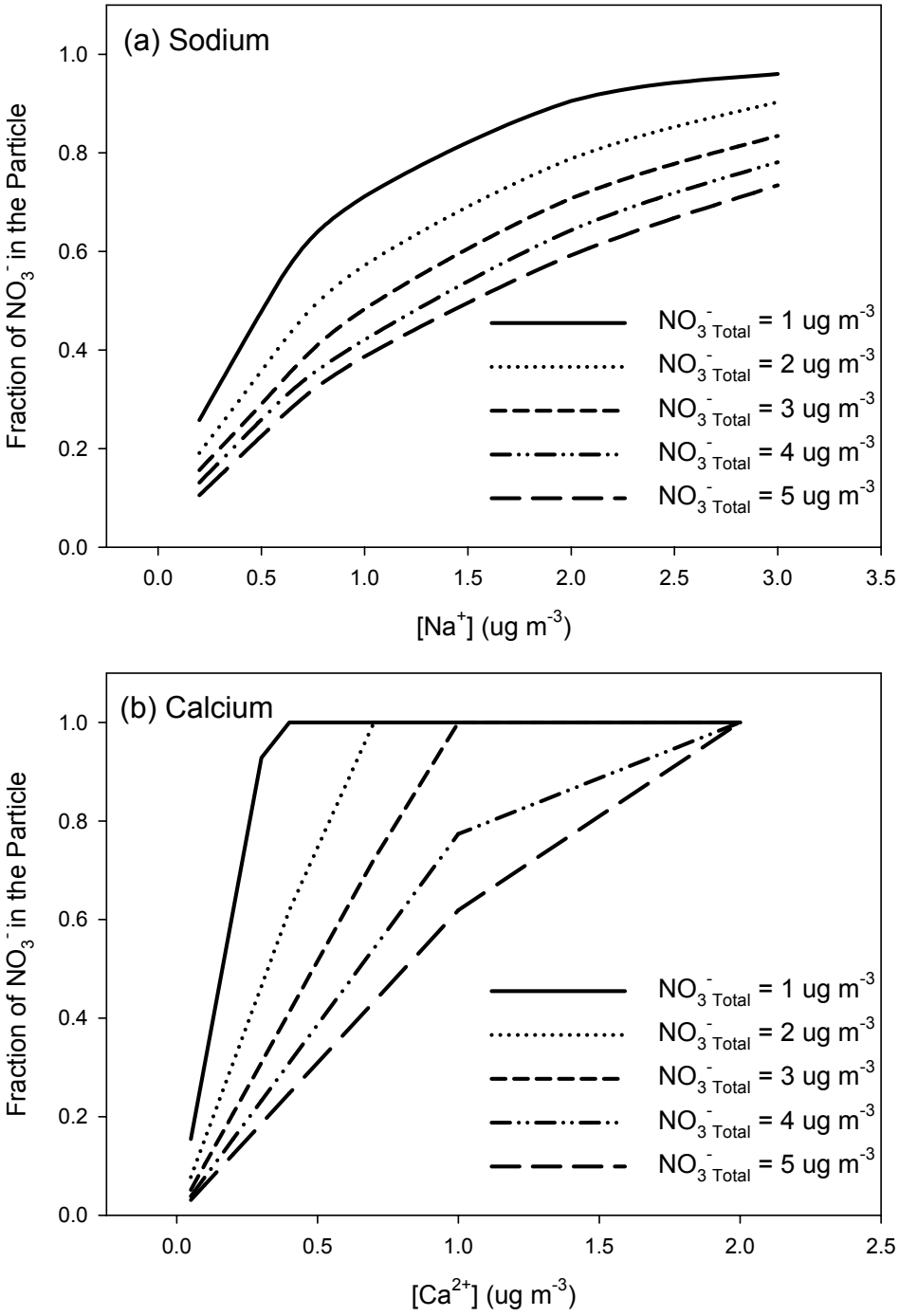

Figure 39. The partitioning of HNO_3 to nitrate by (a) NaCl and (b) $CaCO_3$ by different ambient air concentrations and total nitrate at 78% RH.

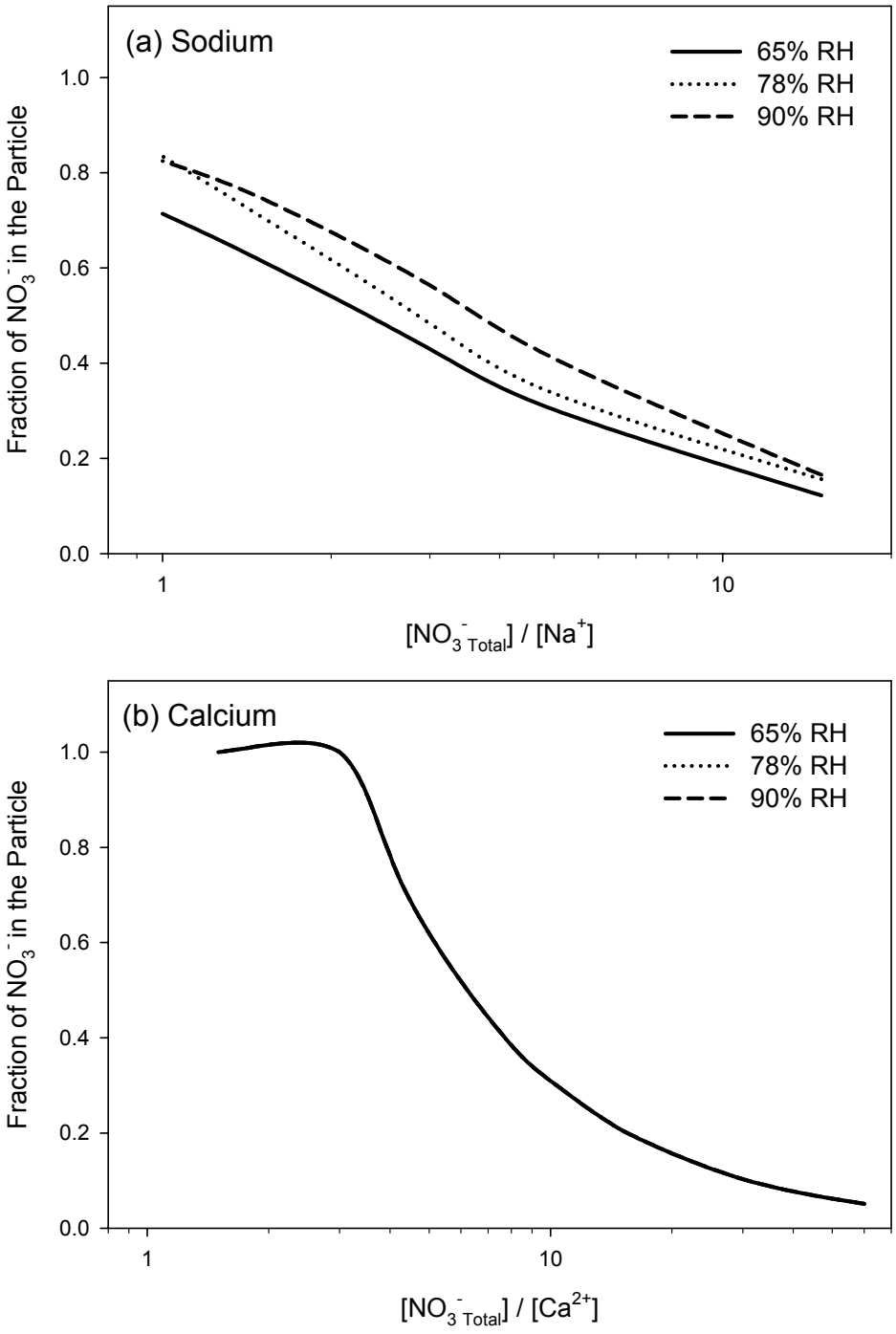

Figure 40. The effect of relative humidity on the partitioning of HNO_3 to nitrate by (a) NaCl and (b) $CaCO_3$, where the total available nitrate was 3 μg m^{-3}.

For NaCl, increased relative humidity increased the fraction of nitrate in the particle phase (Figure 40a). The hygroscopic nature of the NaCl and $NaNO_3$ particle encouraged the uptake and reaction of nitric acid with increased relative humidity. The hygroscopicity and water solubility for $CaCO_3$ are substantially lower than those of NaCl. As a result, no (or very little) change in the nitrate particle formation with changing relative humidity was seen for $CaCO_3$ (Figure 40b). In the figure, all three relative humidity scenarios are superimposed onto each other, giving one representative line for $CaCO_3$.

The concentrations and mass percent of water and the fraction of nitrate within the particle as a function of sodium and calcium concentrations for NaCl and $CaCO_3$ at 78% relative humidity are displayed in Figure 41. For NaCl and $CaCO_3$, the amount of absorbed water increased as the fraction of particulate nitrate and sodium or calcium concentrations increased (Figure 41a-d). Therefore, the formation of $NaNO_3$ and $Ca(NO_3)_2$ increased the hygroscopicity and, hence, the amount of absorbed water in the particle (Grassian, 2002). The water mass percent (Figure 41e-h) for NaCl increased as particulate nitrate formation increased. However, the water mass percent for $CaCO_3$ began to decrease as the fraction of particulate nitrate reached 1.0. As $CaCO_3$ (MW = 100 g mol^{-1}) is converted to $Ca(NO_3)_2$ (MW = 164 g mol^{-1}), the amount of adsorbed water increases or remains the same; however, the reflecting water mass percent may actually decrease due to the change in molecular weight of the salt.

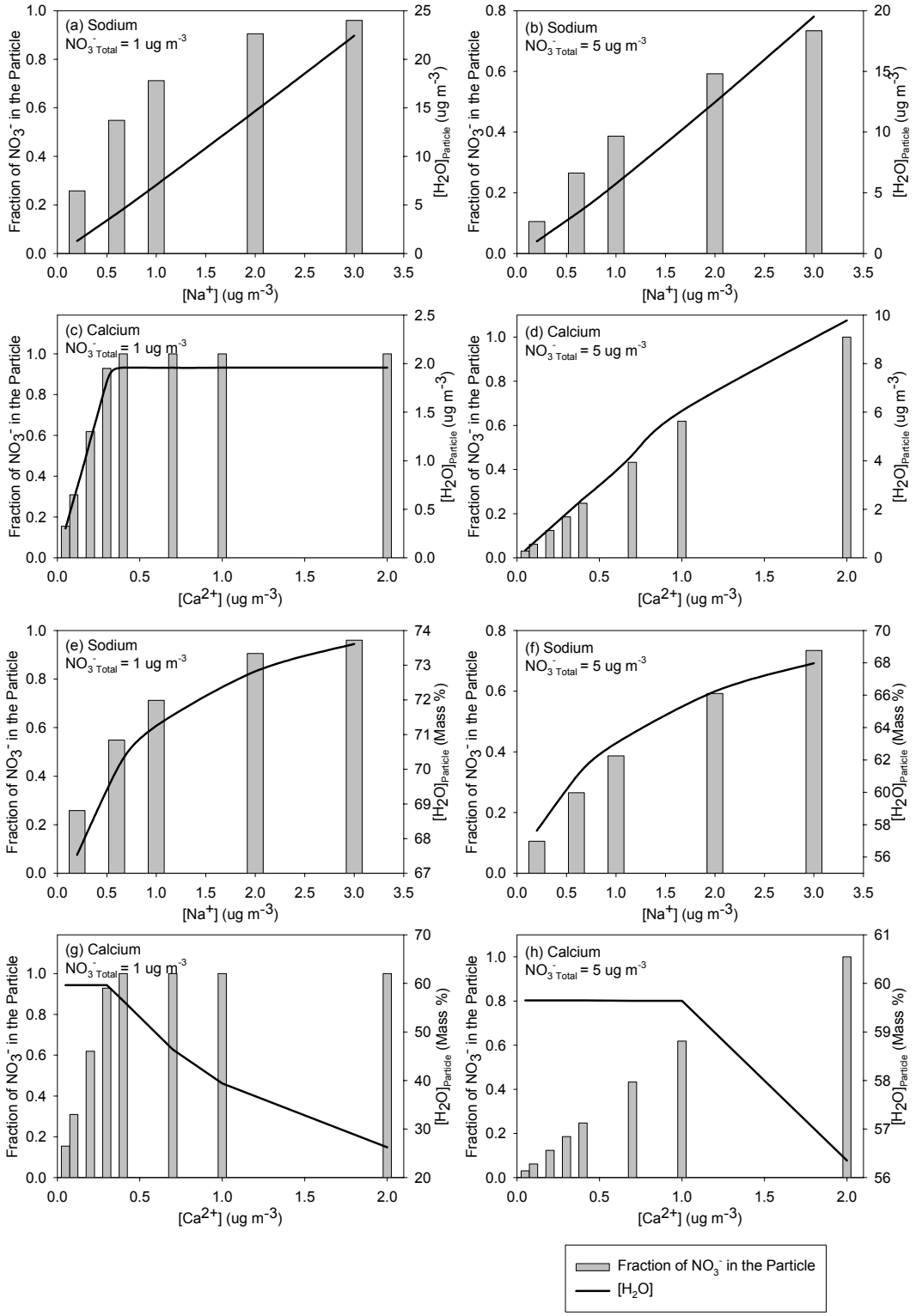

Figure 41. The concentration and mass percent of water and the fraction of total nitrate within the particle for NaCl and $CaCO_3$ at 78% RH.

Competitive Partitioning

The competitive partitioning between NaCl and $CaCO_3$ for nitrate was modeled at 78% relative humidity (Figure 42). When the total available nitrate (gas plus particle) was set at 1 μg m^{-3} for a 0% Na^+ and 100% Ca^{2+} system, the fraction of particulate nitrate was 1.0. As the percent of sodium in the particle increased, the fraction of particulate nitrate decreased. The modeled results indicated that sodium partitioned nitrate to the gas phase better than calcium, which partitioned nitrate to the particle phase.

From the previous figures, it can be concluded that both calcium and sodium play a role in the partitioning of nitric acid to nitrate. For NaCl, there was no dominant formation of one species or the other. Calcium, on the other hand, primarily partitioned nitrate to the particle phase, forming gaseous nitric acid only when the calcium was completely saturated with particulate nitrate.

The partitioning ability of sodium and calcium is directly related to the equilibrium constants for these reactions. From the EQUISOLV II code, the equilibrium constants for the NaCl and $CaCO_3$ reactions with HNO_3 were determined to be:

$$NaCl_{(s)} + HNO_{3(g)} \xrightarrow{k_{eq}} NaNO_{3(s)} + HCl_{(g)} \qquad k_{eq} = 4.0$$

$$NaCl_{(s)} + HNO_{3(g)} \xrightarrow{k_{eq}} NaNO_{3(aq)} + HCl_{(g)} \qquad k_{eq} = 48$$

$$NaCl_{(aq)} + HNO_{3(g)} \xrightarrow{k_{eq}} NaNO_{3(aq)} + HCl_{(g)} \qquad k_{eq} = 1.3$$

$$CaCO_{3(s)} + 2\,HNO_{3(g)} \xrightarrow{k_{eq}} Ca(NO_3)_{2(s)} + CO_{2(g)} + H_2O_{(l)} \qquad k_{eq} = 6.9 \times 10^{16}$$

$$CaCO_{3(s)} + 2\,HNO_{3(g)} \xrightarrow{k_{eq}} Ca(NO_3)_{2(aq)} + CO_{2(g)} + H_2O_{(l)} \quad k_{eq} = 4.6\times10^{22}$$

$$CaCO_{3(aq)} + 2\,HNO_{3(g)} \xrightarrow{k_{eq}} Ca(NO_3)_{2(aq)} + CO_{2(g)} + H_2O_{(l)} \quad k_{eq} = 9.2\times10^{30}$$

Despite the different k_{eq} values between the aqueous and solid phase reactions, the k_{eq} values for the calcium reactions are several orders of magnitude different than those for the sodium reactions. The fundamental equilibrium constant parameter explains why calcium preferentially forms particulate nitrate over gas phase nitric acid and why calcium carbonate partitions nitrate to the particulate phase better than sodium chloride.

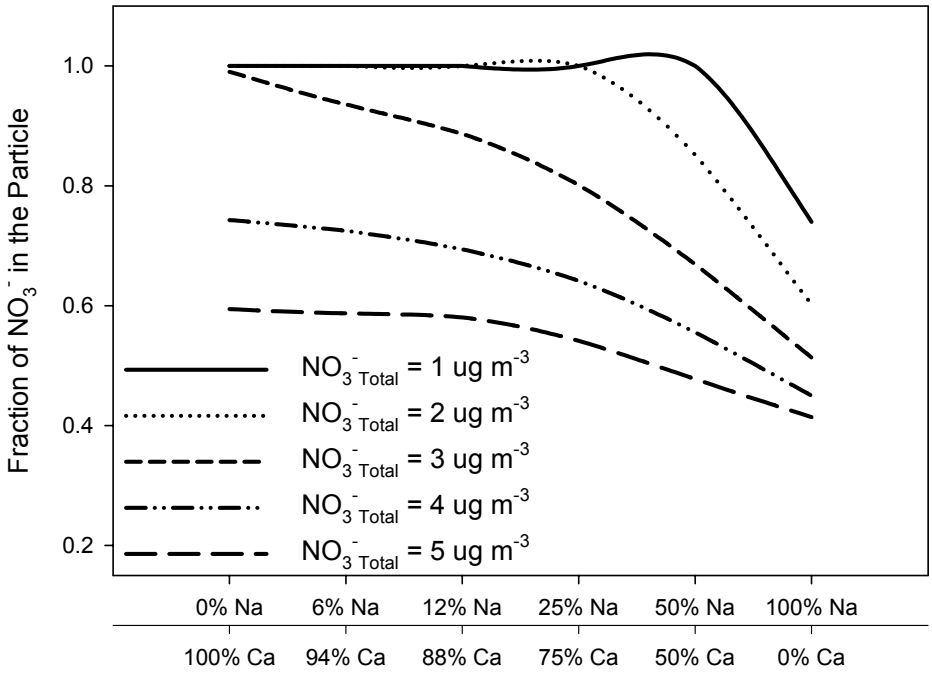

Figure 42. The competitive nitrate partitioning effect between NaCl and $CaCO_3$, in molar percentages at 78% RH.

Environmental Implications

Deposition rates were used to assess the effects of the partitioning on the local environment. Gas and particle fluxes were calculated using the respective model-predicted gas and particle phase concentrations and deposition velocities.

Gas phase nitric acid fluxes are displayed for NaCl and $CaCO_3$ in Figure 43. Particulate nitrate fluxes are displayed in Figure 44. For both NaCl and $CaCO_3$ scenarios, the gas phase nitric acid contributed to the majority of the local nitrogen deposition, with the nitrogen flux increasing as the total available nitrate increased. However, as the sodium or calcium concentration increased, the total nitrogen flux decreased (Figure 45). As a result of the presence of sodium and calcium particles, there was a decrease in the local nitrogen flux at conditions representative to the Tampa Bay area. Instead of being directly deposited as nitric acid, these 4 μm particles can travel out of the area (~250 km) when suspended to a height of 100 m. This creates a local flux divergence as the particles are subject to horizontal transport.

The gas phase nitric acid and particulate nitrate fluxes for the NaCl and $CaCO_3$ mixture are reported in Figure 46. The gas phase nitric acid flux increased with increasing percent sodium concentrations as calcium preferred to have nitrate in the particle phase. As a result, calcium played a bigger role in creating a local nitrogen flux divergence than sodium.

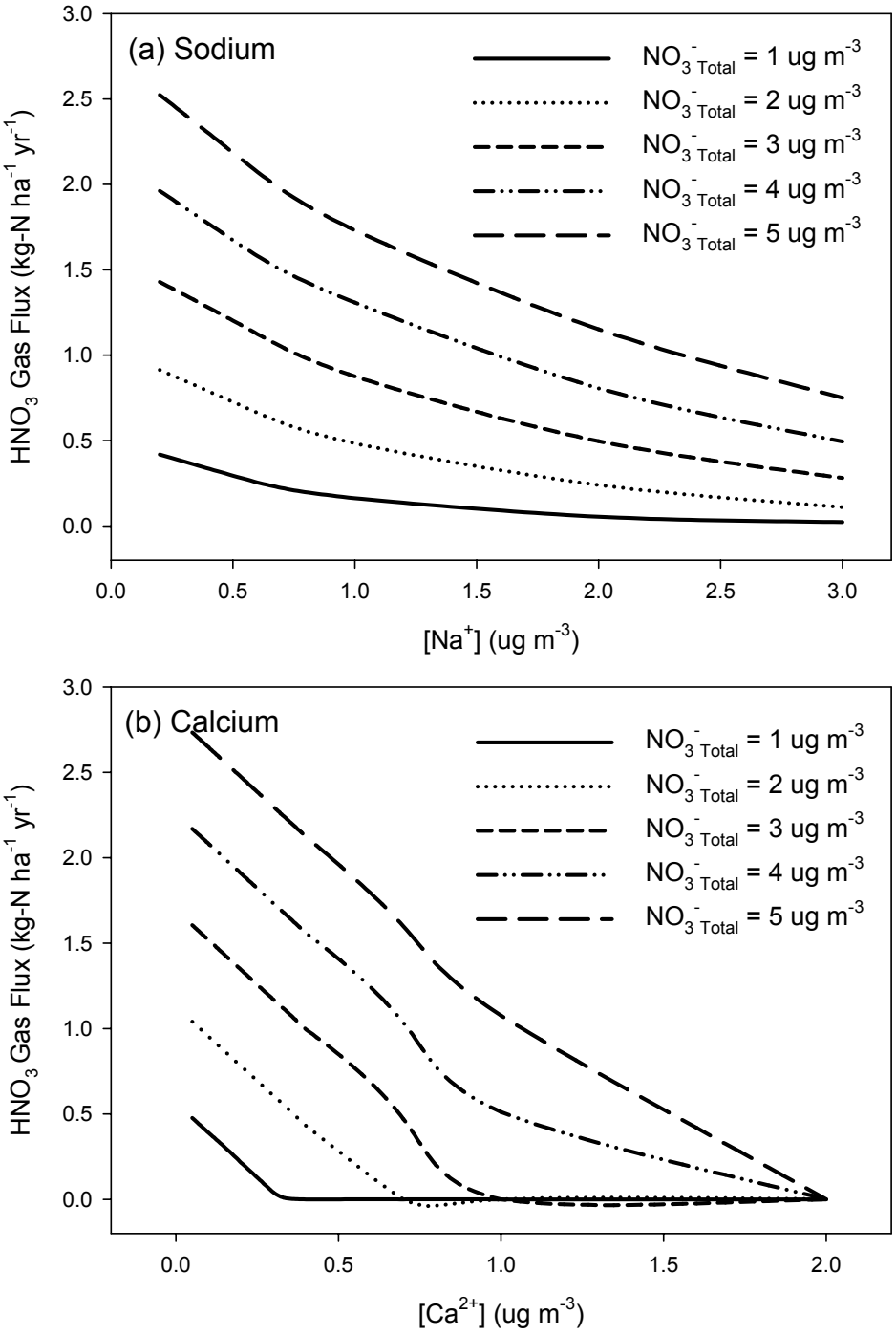

Figure 43. The predicted HNO_3 gas flux for the nitric acid partitioning by (a) NaCl and (b) $CaCO_3$ at 78% RH.

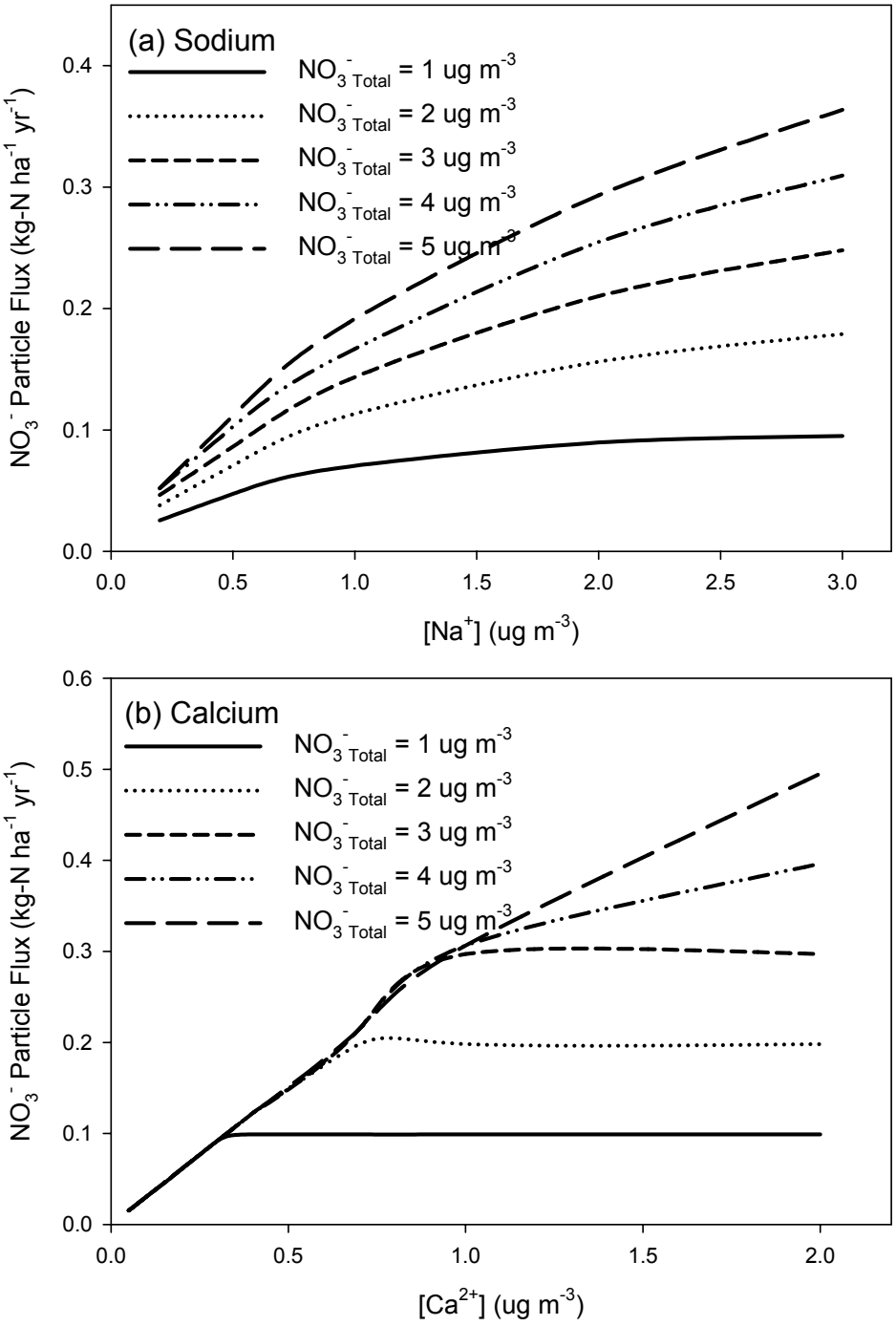

Figure 44. The predicted nitrate particle flux for the nitrate partitioning by (a) NaCl and (b) $CaCO_3$ at 78% RH.

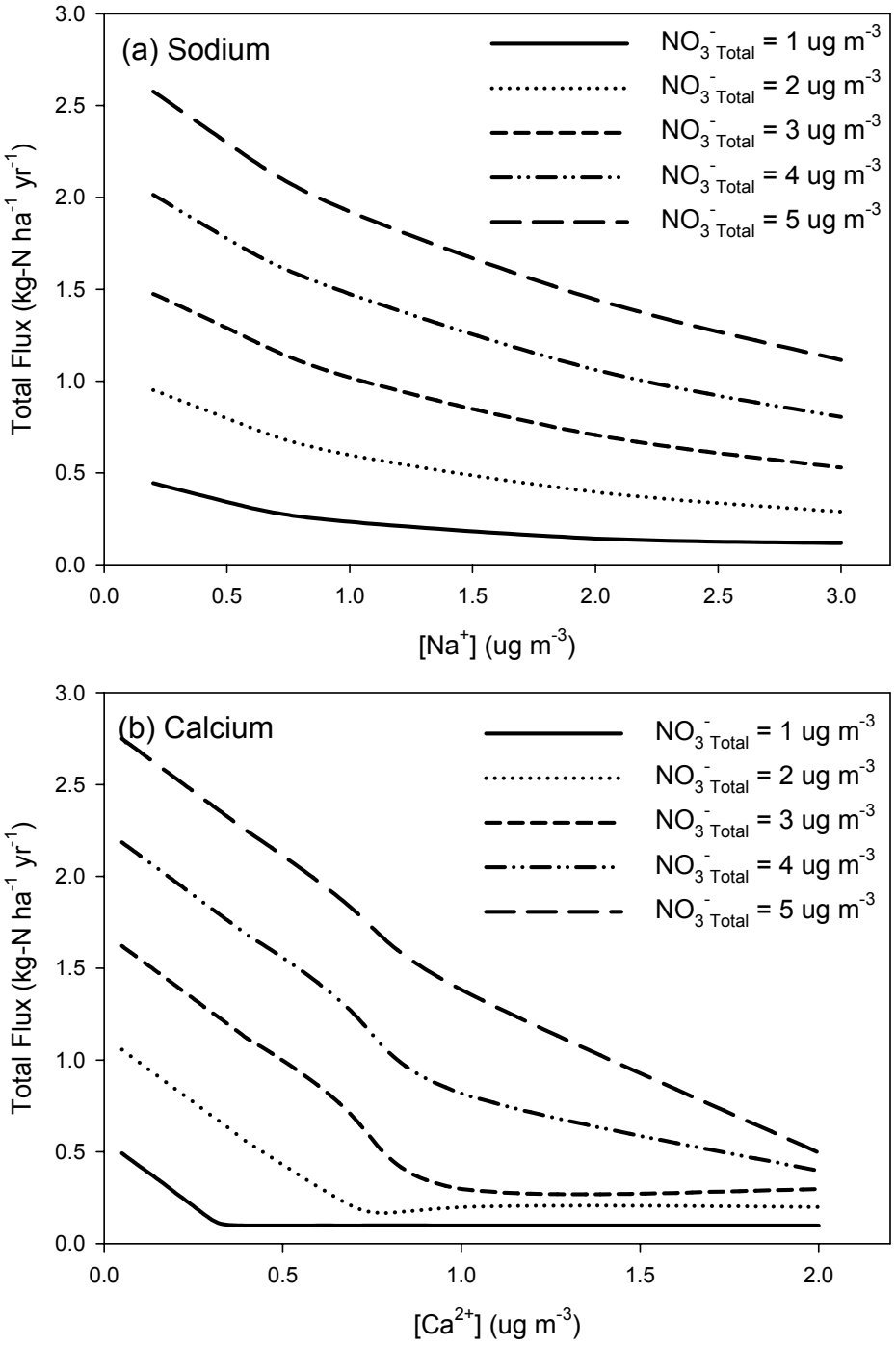

Figure 45. The total (gas + particle) predicted flux for the nitrate partitioning by (a) NaCl and (b) $CaCO_3$ at 78% RH.

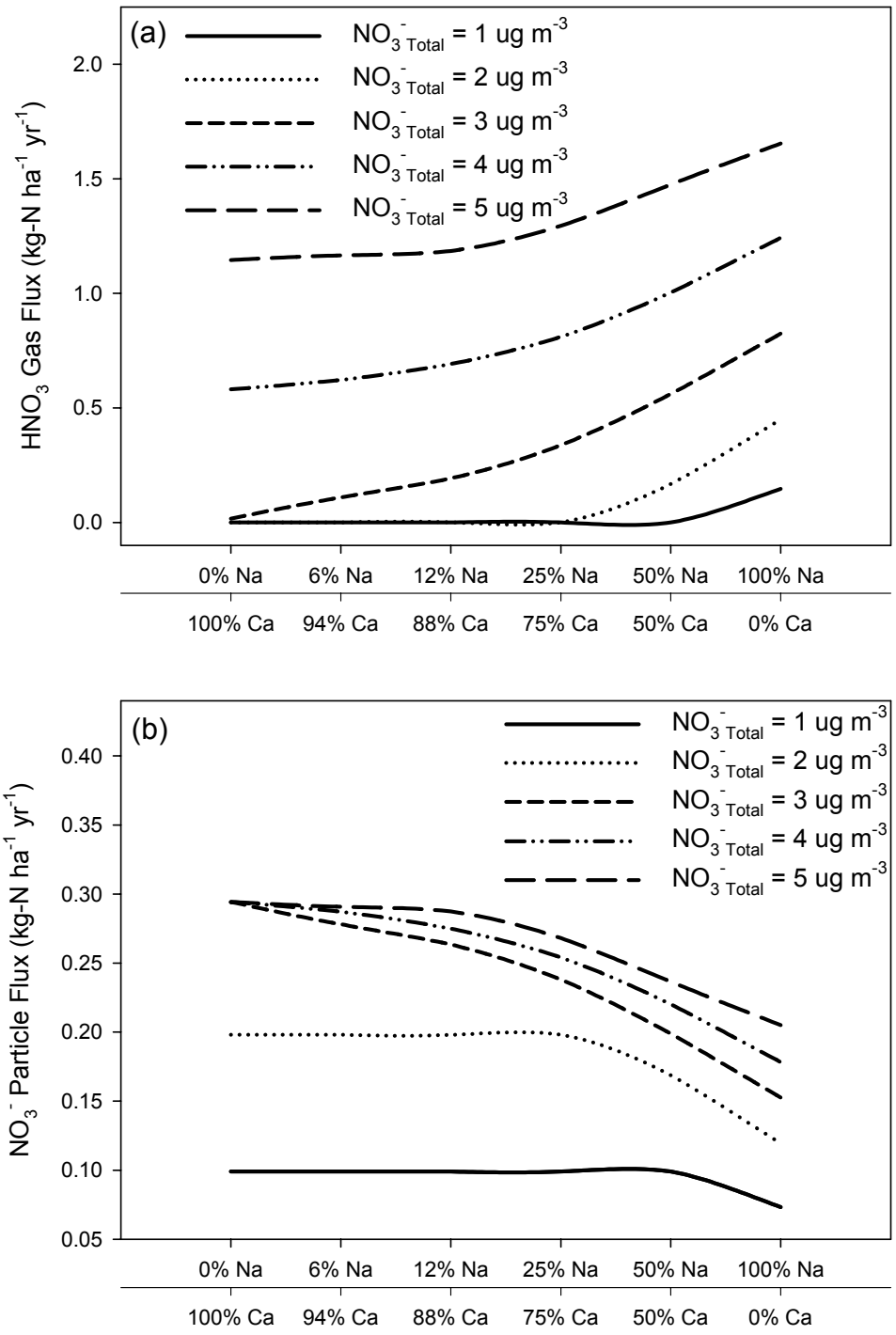

Figure 46. The predicted (a) nitric acid gas and (b) particulate nitrate flux from a molar percent mixture of NaCl and $CaCO_3$ $\left([Na^+]+[Ca^{2+}]=48\ neq\ m^{-3}\right)$ at 78% RH.

The Prediction of Coarse Mode Nitrate from Fine Mode ADS Data

Until recently, the monitoring of particulate matter around the Tampa Bay area only included fine particulate matter, having a diameter based on a cyclone inlet with a cutpoint of 2.5 μm ($PM_{2.5}$) (Poor et al., 2001). These fine particles are responsible for visibility reductions as they scatter and absorb light more efficiently than larger particles (Seinfeld and Pandis, 1998). These smaller particles are also responsible for serious health effects and mortality in humans, as well as environmental implications (Clarke et al., 1999). Coarse mode particles, however, have been found to contain nitrogen species, and they have the potential to have greater environmental implications than fine mode particles (Evans and Poor, 2001; Pryor and Barthelmie, 2000b; Pryor and Sorensen, 2000).

Direct atmospheric deposition (wet and dry) of inorganic nitrogen to Tampa Bay has been estimated from 1996-1999 to be 7.3 ± 1.3 kg-N ha^{-1} yr^{-1} or 760 ± 140 metric tons yr^{-1} (Poor et al., 2001). The dry deposition of nitrogen directly to Tampa Bay accounted for 44%, or 3.2 kg-N ha^{-1} yr^{-1}. The data used to develop these estimates included one-in-six day ambient monitoring of gaseous ammonia, nitric acid and sulfur dioxide and fine mode particulate ammonium, nitrate and sulfate. These species were collected using an annular denuder system (ADS) at the Gandy Bridge monitoring station (Poor et al., 2001).

The goal of this project was to expand the current data set by predicting the coarse mode ($PM_{10-2.5}$) nitrate concentrations from the available $PM_{2.5}$ data

set. The predicted coarse mode and total concentrations can then be used to develop new nitrogen deposition estimates.

Results and Discussion

Two approaches were used to estimate the coarse mode nitrate concentrations. The first approach estimated the coarse mode nitrate fraction from actual coarse and fine samples collected in the field. The second approach used the lognormal particle nitrate size distributions to predict the fine and coarse mode fractions.

For the first approach, three sets of fine and coarse mode data were used. Dichotomous coarse ($PM_{10-2.5}$) and fine ($PM_{2.5}$) particle samples were collected during October and November 2001 using an R&P dichotomous sampler. Total suspended particles (TSP) were also collected during this campaign using the inverted filter pack sampler. A third set of data was collected during May 2002 using an annular denuder system ($PM_{2.5}$) and an open inlet automated particle sampler ($>PM_{2.5}$) run by Texas Tech University (TTU). Both sets of data were collected at the Sydney site during the intensive May 2002 monitoring campaign.

D_p	Instrumentation	Data Collection Period
$PM_{2.5}$	Dichotomous Sampler	October 2001
$PM_{2.5}$	Annular Denuder System	May 2002
$>PM_{2.5}$*	TTU Automated Sampler	May 2002
PM_{10}	Dichotomous Sampler	October 2001
$>PM_{10}$*	Inverted Filter Pack	October 2001

* True cut point is unknown

Table 18. Particle size fraction, instrumentation and data collection periods used for predicting coarse mode nitrate fractions.

The samples were used to develop a relationship between the coarse ($>PM_{2.5}$) and fine size fractions (Figure 47). The samples were compared through direct analysis and linear regression. Figures 48-50 display the linear regressions for the dichotomous fine mode and total nitrate (Figure 48), dichotomous fine mode and inverted filter pack TSP nitrate (Figure 49), and ADS fine mode and TTU coarse mode nitrate (Figure 50).

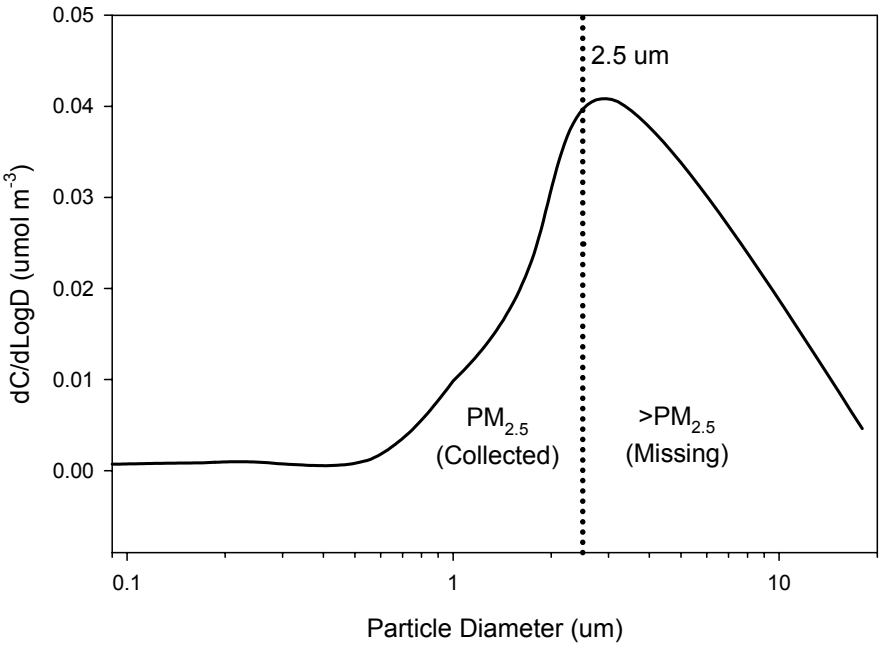

Figure 47. Nitrate particle size distribution.

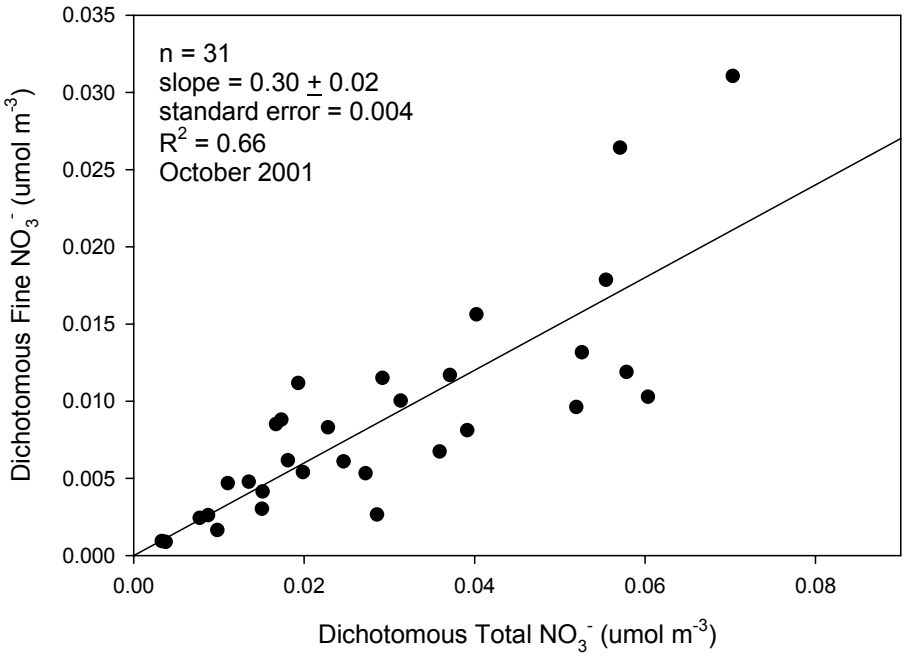

Figure 48. Linear regression for dichotomous fine mode and total nitrate.

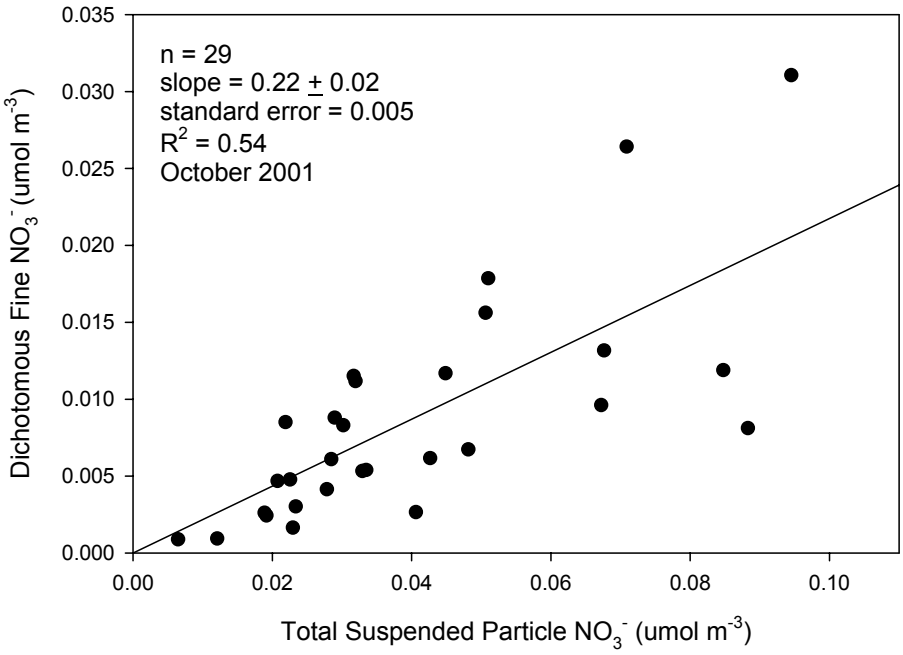

Figure 49. Linear regression for dichotomous fine and the inverted filter pack TSP nitrate.

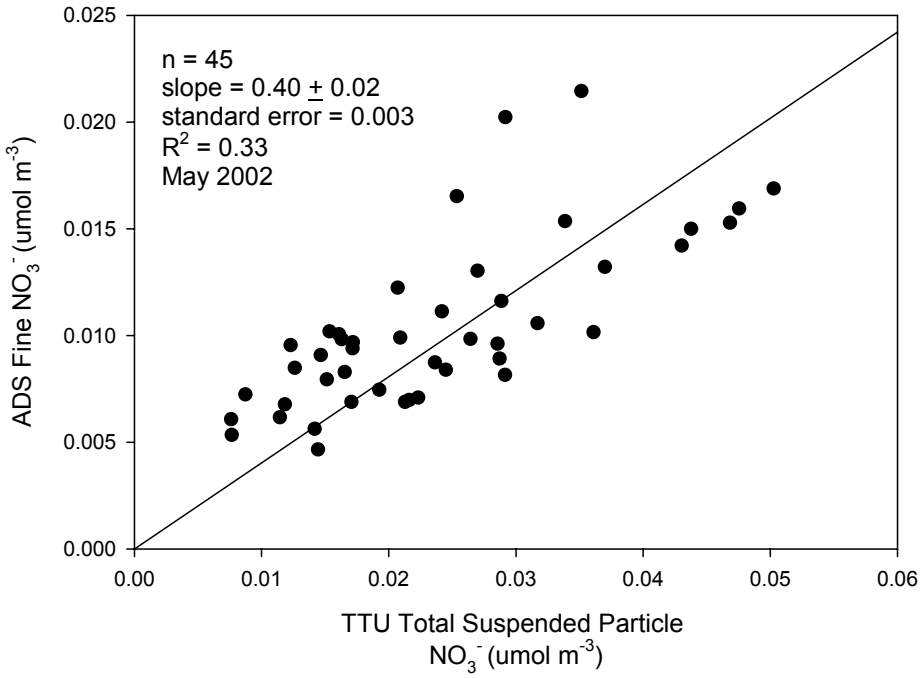

Figure 50. Linear regression for annular denuder system fine and TTU particle nitrate.

Direct comparison on a per sample basis was done using the dichotomous samples and was determined by:

$$\%\ Fine\ Mode\ Nitrate = \frac{[NO_3^-]_{PM2.5}}{[NO_3^-]_{Coarse} + [NO_3^-]_{PM2.5}} \times 100\% \qquad \text{(Equation 28)}$$

This direct daily comparison analysis resulted in a percent fine mode nitrates summarized in Table 19.

Fine Mode Nitrate Instrumentation	Coarse Mode Nitrate Instrumentation	Linear Regression Results	Direct Comparison Results
Dichot $PM_{2.5}$	Dichot $PM_{10-2.5}$	30 ± 2%	31 ± 12%
Dichot $PM_{2.5}$	Inverted FP (TSP)	22 ± 2%	21 ± 10%
ADS $PM_{2.5}$	TTU sampler	40 ± 2%	48 ± 16%

Table 19. Percent fine mode nitrate determined using actual coarse and fine mode nitrate samples.

Three different coarse mode particle samplers were used in these analyses. Of the instruments, only the dichotomous sampler had a characterized PM_{10} inlet. The others were simply open-inlet instruments with no characterized cut point. The Texas Tech University data give the greatest percentage of fine mode nitrate, whereas the inverted filter pack gives the smallest. It is apparent that the TTU instrument may have a cut diameter less than 10 μm and the inverted filter pack a cut greater than 10 μm. Due to the uncertainty of the cut diameters, only the results from the dichotomous sampler were used in the prediction of coarse mode nitrate.

The second approach was performed using lognormal analysis of size-distributed particulate nitrate, a method used by aerosol scientists for representing quantities that cannot have negative values. The width of the distribution is used to characterize the standard deviation of the distribution, and the height for the magnitude of the concentration. Figure 51 displays a typical lognormal distribution for particulate nitrate in the Tampa Bay area. The sample was collected at the Gandy site on May 4, 2002 using a MOUDI sampler.

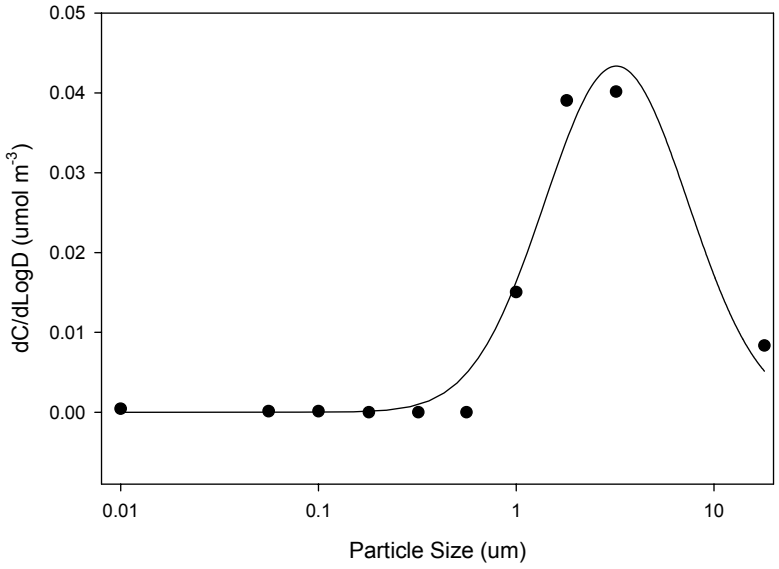

Figure 51. Typical lognormal nitrate size distribution.

The lognormal distributions were developed based on the three-parameter lognormal equation using SigmaPlot 2002 version 8.0 by SPSS Inc.:

$$y = a\, e^{\left[-0.5\left(\frac{\ln\left(\frac{x}{x_o}\right)}{b}\right)^2\right]}$$ (Equation 29)

where $a = \frac{1}{\sigma\sqrt{2\pi}}$ and $b = \sigma$, the standard deviation of the distribution. The value for x_o, the particle diameter at which the distribution peaked, was set at an averaged value of 3.15 μm. The set value of x_o and the resulting standard deviation, *b*, were used in conjunction with the lognormal function in Microsoft Excel to compute the fraction of nitrate with 2.5 μm and smaller diameter. Results are summarized in Table 20.

Method	# Samples	Percent Fine Mode Nitrate
Andersen Cascade Impactor	14	40 ± 2%
MOUDI Cascade Impactor	38	36 ± 7%

Table 20. Computed percent fine mode nitrate using lognormal analysis of cascade impactor data.

The Andersen cascade impactor is known to have poor resolution between its stages. As a result, this instrument was not used in the prediction of coarse mode nitrate.

The dichotomous sample comparison and lognormal analysis method results were averaged, giving an approximate value for the percent fine mode nitrate of 33%. This estimate was then applied to the 1996-2002 ADS data to determine the coarse mode nitrate concentrations.

The gas and particle over-water dry deposition velocities were calculated using the integrated NOAA Buoy – Williams model (Bhethanabotla, 2002) to determine the effects of coarse mode nitrate on the local nitrogen flux estimates. The averaged over-water deposition velocities for the gas and 3.15 μm diameter particulate species were 0.84 ± 0.52 and 0.034 ± 0.013 cm s^{-1}, respectively. The particulate nitrate concentrations and dry deposition fluxes ($F = C \times V_d$) as well as the gaseous nitric acid fluxes were calculated and are reported in Table 21.

Concentration (μg m^{-3})		Flux (kg-N ha^{-1} yr^{-1})	
HNO_3	1.3 ± 0.9	HNO_3	0.76 ± 0.51
Fine Mode NO_3^-	0.80 ± 0.59	CM p-NO_3^-	0.04 ± 0.03
Coarse Mode NO_3^-	1.6 ± 1.2	Total p-NO_3^-	0.06 ± 0.04
Total p-NO_3^-	2.4 ± 1.8	HNO_3 + p-NO_3^-	0.82 ± 0.52
		% CM p-NO_3^-	6.0 ± 4.4%
		% Total p-NO_3^-	8.9 ± 6.5%

Table 21. The predicted nitrate concentrations and resulting over water dry deposition fluxes.

Environmental Implications

From the 1999 dry deposition estimate, the fine mode particulate nitrate and nitric acid accounted for 1.9% (or 0.06 kg-N ha^{-1} yr^{-1}) and 19% (or 0.61 kg-N ha^{-1} yr^{-1}) of the estimated 3.2 kg-N ha^{-1} yr^{-1} nitrogen loading. The remainder resulted from gaseous ammonia (72% or 2.3 kg-N ha^{-1} yr^{-1}) and fine mode particulate ammonium (6.6% or 0.21 kg-N ha^{-1} yr^{-1}) (Poor et al., 2001).

Using the predicted PM_{10} nitrate concentrations from this study, dry nitrogen deposition from 1999 can be estimated at 3.2 kg-N ha^{-1} yr^{-1}. Total particulate nitrate accounted for 1.9% (or 0.06 kg-N ha^{-1} yr^{-1}). This value is unchanged from the original estimate, as the original estimate computed the nitrogen deposition flux using a dry deposition velocity of 0.1 cm s^{-1}, possibly overestimating the particle size. The new size-dependent particle deposition velocity (D_p = 3.15 μm) was recalculated at 0.034 cm s^{-1}. Despite the change in the particulate nitrate concentration from the previous estimate until now, the discrepancy in the particle deposition velocity results in an unchanged annual flux estimate.

The Formation of Particulate Nitrate

Experimental studies have shown that supermicron particles, those with a diameter greater than 1 μm, containing nitrogen exist in our environment (Evans et al., 2002; Pakkanen et al., 1996a; Pryor and Barthelmie, 2000b; Pryor and Sorensen, 2000). The origin of these compounds is unknown, but analysis reveals the possible affiliation with mineral dust or sea salt particles from the reactions with gaseous nitric acid (Reactions 1 and 3) (Clarke et al., 1999; de Leeuw et al., 2001; Dentener et al., 1996; Evans and Poor, 2001; Goodman et al., 2000; Pakkanen, 1996; Tabazadeh et al., 1998; Ten Brink, 1998; Zhuang et al., 1999a).

Because of their size, macroparticles have a larger deposition velocity and shorter residence time than smaller particles (Pakkanen et al., 1996a). The formation of nitrate macroparticles may cause increased local nitrogen deposition and possibly increased eutrophication problems if deposited to surface waters. Using published uptake coefficients (Abbatt and Washewsky, 1998; Guimbaud et al., 2002a; Hanisch and Crowley, 2001) and a nitrate accumulation model (Kerminen and Wexler, 1995) with our recent measurements of inorganic aerosol distribution made near Tampa Bay, the formation of $NaNO_3$ and $Ca(NO_3)_2$ is estimated from reactions of NaCl, sea salt and mineral dust ($CaCO_3$) particles with nitric acid. This was a theoretical exercise to determine the potential for nitrogen-containing coarse particles to contribute significantly to the atmospheric nitrogen deposition to the Tampa Bay estuary.

Methods

To study the theoretical formation of particulate nitrate, a closed system approach was adopted and assumed externally mixed particles of multiple size categories. Sodium and calcium were used as the non-volatile species. The system was initialized with a fixed amount of nitrogen (as gas phase nitric acid), which was allowed to distribute between the gas phase and across all particle bins. The model (described below) allowed the particulate nitrate concentrations to be calculated in a time-step process. At each time interval, the sodium, calcium and nitric acid concentrations were adjusted to account for the formation

of particulate nitrate. The time steps were allowed to continue until the particulate nitrate concentrations reached thermodynamic equilibrium with nitric acid.

Experimental values were used to initialize the system. The average annual nitric acid concentration was taken from one-in-six day annular denuder system (ADS) measurements made at the Gandy site in 2000. Average particulate sodium, calcium and nitrate size distributions and concentrations were taken from 37 micro-orifice uniform deposit impactor (MOUDI) measurements made at three (Azalea Park, Gandy and Sydney) sites in 2002. All of the nitrogen in the system (particulate nitrate plus nitric acid) was initialized as nitric acid. The geometric mean of seven MOUDI collection bins was used for the particle classification. The particle diameters compared were: 0.2, 0.49, 0.77, 1.4, 2.5, 4.3 and 7.6 μm. The species concentrations used in this modeling exercise are listed below in Table 22.

GeoMean (μm)	Bin Max (μm)	$[Na^+]$ (μmol m^{-3})	$[Ca^{2+}]$ (μmol m^{-3})	$[NO_3^-]$ (μmol m^{-3})	$[HNO_3]$ (μmol m^{-3})
0.20	0.40	5.0E-05	3.0E-04	3.0E-02	2.0E-02
0.49	0.60	8.0E-05	1.1E-04		
0.77	1.0	5.5E-04	1.5E-04		
1.4	2.0	4.0E-03	8.2E-04	Total nitrogen: 0.05 μmol m^{-3}	
2.5	3.2	9.4E-03	1.8E-03		
4.3	5.7	2.3E-02	4.0E-03		
7.6	10	1.4E-02	2.6E-03		

Table 22. Averaged concentration from 37 MOUDI experimental samples and year 2000 ADS measurements.

Deposition Velocities

The over water deposition velocities of each particle size groups and gaseous nitric acid were calculated using the integrated NOAA Buoy-Williams model (Bhethanabotla, 2002) and the year 2000 hourly meteorological data. The integrated NOAA Buoy-Williams model is a combination of a two-layer multiple-path model for dry deposition of particles to surface waters (Williams) and an iterative bulk exchange model for momentum, heat and moisture (NOAA Buoy). The model includes the effects of wave breaking, particle hygroscopic growth and turbulent heat flux. The dry deposition velocities were calculated on the basis of the turbulent heat transfer and gravitational settling of particles. The meteorological data used in the model included surface weather and water observations, which were obtained from the NOAA National Climatic Data Center (NOAA, 2003a) and the NOAA National Ocean Service's Center for Operational Oceanographic Products and Services (NOAA, 2003b), respectively. Surface weather observations were collected at the Tampa International Airport, located approximately 11 km from the Gandy sampling site. Water measurements were taken at NOAA's Clearwater Beach station, located on the Gulf of Mexico coastline approximately 30 km from the Gandy site. The meteorological data were divided into three categories based on wind speed. The low (<2.4 m s^{-1}) and high (>6.0 m s^{-1}) wind speeds were classified as the respective 25^{th} and 75^{th} percentile winds during 2000. The midrange wind speeds were those between

2.4 and 6.0 m s^{-1}. The resulting dry deposition values were averaged, giving an annual deposition velocity (Table 23).

D_p	Deposition Velocity, V_d (cm s^{-1})		
(μm)	Low WS	Mid WS	High WS
0.20	0.002 ± 0.001	0.006 ± 0.003	0.03 ± 0.02
0.49	0.003 ± 0.002	0.005 ± 0.002	0.02 ± 0.02
0.77	0.006 ± 0.004	0.007 ± 0.004	0.02 ± 0.02
1.4	0.006 ± 0.003	0.007 ± 0.003	0.02 ± 0.02
2.5	0.020 ± 0.000	0.02 ± 0.00	0.03 ± 0.02
4.3	0.06 ± 0.00	0.06 ± 0.00	0.07 ± 0.06
7.6	0.17 ± 0.00	0.17 ± 0.00	0.25 ± 0.17
HNO_3	0.28 ± 0.17	0.67 ± 0.23	1.48 ± 0.41

Table 23. Annual averaged over water dry deposition velocities with their respective standard deviations.

Residence Times and Distances Traveled

The distance a particle will travel is dependent on the particle's deposition velocity, starting height and wind speed. For all scenarios tested, the starting height was set at 100 m. The traveling distance, *TD*, was calculated using:

$$TD = \frac{Wind\ Speed \times Starting\ Height}{Deposition\ Velocity} \qquad \text{(Equation 30)}$$

The traveling distance was calculated for three different wind scenarios during 2000. Table 24 displays the distance traveled by a particle at the three wind scenarios. The residence time, *RT*, of a particle (Table 24) is the time required by a particle to deposit through dry deposition to the surface of a body of

water. It is only dependent on the starting height and the deposition velocity of the particle, and it was calculated using:

$$RT = \frac{Starting\ Height}{Deposition\ Velocity} \qquad \text{(Equation 31)}$$

D_p	Distance Traveled (km)			Residence Time (hr)		
(μm)	Low WS	Mid WS	High WS	Low WS	Mid WS	High WS
0.20	730	7100	3700	1300	470	110
0.49	4800	8600	5200	840	570	160
0.77	2800	6200	5400	480	410	170
1.41	2800	6000	5200	490	400	160
2.53	790	2000	3000	140	130	91
4.27	290	750	1200	50	49	38
7.55	94	250	350	16	16	11

Table 24. Traveling distances and residence times for low (<2.4 m s^{-1}), mid (2.4-6.0 m s^{-1}) and high (>6.0 m s^{-1}) wind speeds.

Reaction with Nitric Acid

The rate at which particulate nitrate is formed from nitric acid depends on several interacting processes (Pakkanen et al., 1996a). Under the assumption of spherical particles and surface-limited chemical reactions, the rate at which nitrate accumulates into a single particle, I_{NO_3} (mol s^{-1}) can be obtained from the relation (Kerminen and Wexler, 1995; Pakkanen et al., 1996a):

$$I_{NO_3}(d_p) = \frac{2\ \pi\ D_{HNO_3} d_p\ [HNO_{3\ (g)}]}{1+\beta} \qquad \text{(Equation 32)}$$

where $\beta = 2\ D_{HNO_3} \div k_s\ d_p$, d_p is the particle diameter, D_{HNO3} ($m^2\ s^{-1}$) is the diffusion coefficient of nitric acid, $[HNO_3]$ (mol m^{-3}) is the gas phase concentration, and k_s (m s^{-1}) is the surface rate constant for the conversion of HNO_3 to particulate nitrate ($k_s = \gamma\ \bar{c} \div 4$, where $\bar{c}$ is the molecular speed of HNO_3 and γ is the reaction uptake coefficient).

The total concentration of particulate nitrate as a result of uptake of nitric acid by sea salt over a certain size range, *j*, can be obtained by integrating I_{NO_3} over all particles in *j* and time, T_j (s) (Pakkanen et al., 1996a):

$$[NO_3]_j^{(ss)} \approx \left(\frac{6\ [Na^+]_j M_{Na} k_{s,j}^{(ss)} T_j^{(ss)}}{1000\ d_{p,j}^{(ss)} \rho_p^{(ss)} f_{Na}} \right) [HNO_{3(g)}] \qquad \text{(Equation 33)}$$

The nitrate concentration as a result of the uptake of nitric acid by calcium in mineral dust can be obtained by (Pakkanen et al., 1996a):

$$[NO_3]_j^{(md)} \approx \left(\frac{6\ [nss - Ca^{2+}]_j M_{Ca} k_{s,j}^{(md)} T_j^{(md)}}{1000\ d_{p,j}^{(md)} \rho_p^{(md)} f_{Ca}} \right) [HNO_{3(g)}] \qquad \text{(Equation 34)}$$

where $[Na^+]$ (μmol m^{-3}) is the concentration of sodium, $[nss - Ca^{2+}]$ (μmol m^{-3}) is the concentration of non-sea salt calcium (that affiliated with mineral dust), M_i (g mol^{-1}) is the molar mass of species i, $d_{p,j}$ (μm) is the representative particle diameter in the size range, ρ_p (kg m^{-3}) is the particle density and f_i is the mass fraction of sodium in sea salt and calcium in mineral dust particles.

The underlying assumptions for this model include (Pakkanen, 1996): (1) These particles consist of two externally mixed particle types on which nitrate is formed: sea salt and mineral dust. (2) The water-soluble sodium originates only from sea salt and calcium from mineral dust. (3) Particles of the same type and size have roughly the same composition. (4) The size distribution function is temporally constant over the size range. (5) The heterogeneous conversion of NO_2 and other nitrate precursor gases is negligible compared to nitric acid. (6) The nitrate accumulation in both sea salt and mineral dust particles is limited by the rate k_s.

This model considers only sodium and calcium as reactive species for nitric acid and is limited by not considering the reactions between nitric acid and other particulate matter types. However, since little or no data are available for the reactions between nitric acid and other species, they were excluded. The particle density and mass fraction were held constant for each time step. The hygroscopicity for $NaNO_3$ closely resembles that of NaCl, allowing for the assumption that the mass fraction and density remained constant.

The uptake coefficients for HNO_3 on NaCl, sea salt and $CaCO_3$ have been determined experimentally. For NaCl, the uptake coefficient was characterized by the value $\gamma > 0.2$ (Abbatt and Washewsky, 1998). This value was determined using an aerosol kinetics flow tube technique at room temperature with deliquescent NaCl at 75% relative humidity. Other uptake coefficients for NaCl have been determined using a low-pressure Knudsen cell flow reactor: $[\gamma = (1.4 \pm 0.6) \times 10^{-2}]$ (Beichert and Finlayson-Pitts, 1996) and

[$\gamma = (2.8 \pm 0.3) \times 10^{-2}$] (Fenter et al., 1994). The Knudsen cell flow reactor is limited to very low relative humidity conditions. The value determined by Abbatt and Waschewsky (1998) was used in this modeling and is considered a lower limit for the uptake of HNO_3 by NaCl as the average relative humidity for the Tampa Bay area is approximately 80%.

The uptake coefficient for deliquescent sea salt was estimated to be $\gamma = 0.50 \pm 0.20$ at 55% relative humidity (Guimbaud et al., 2002a). The difference between the coefficients for sea salt and NaCl lie in the composition of sea salt. Sea salt contains hygroscopic hydrates, such as $MgCl_2 \bullet 6H_2O$, which provide additional surface waters for the uptake and reaction of HNO_3. Other uptake coefficient values have been determined for sea salt by De Haan and Finlayson-Pitts (1997) [$\gamma \cong 0.2$] using a Knudsen cell at low relative humidity.

Uptake coefficients for $CaCO_3$ have been determined under a few conditions. At 0% and 20% relative humidities, they were estimated to be $\gamma = 2.4 \times 10^{-4}$ and $\gamma = 2.5 \times 10^{-3}$, respectively (Goodman et al., 2000; Grassian, 2002). Hanisch and Crowley (2001) determined the uptake coefficients for "dry" heated and "damp" unheated $CaCO_3$ to be $\gamma = (10 \pm 2.5) \times 10^{-2}$ and $\gamma = (18 \pm 4.5) \times 10^{-2}$, respectively. The value estimated under "damp" conditions by Hanisch and Crowley (2001) is thought to be more relevant under atmospheric conditions. Their reported value is a considered a lower limit for the uptake of HNO_3 by $CaCO_3$.

The mass fractions of sodium or calcium in the original NaCl, sea salt or mineral dust particles were estimated using the EQUISOLV II model, an aerosol thermodynamic equilibrium model (Campbell et al., 2002; Jacobson, 1999a). Input files were created using the composition of dry particles and varying temperature and relative humidity. EQUISOLV II calculated the equilibrium concentrations of the particles, including the amount of absorbed water. From a series of modeling runs, temperature was not found to have a significant effect on the mass fraction of sodium or calcium. However, the relative humidity had the greatest effect on the mass fraction. Due to the hygroscopicity of the salts, the quantity of adsorbed water depends on the relative humidity. The mass fraction was calculated for four different relative humidity scenarios. At 60% relative humidity, the particles were treated as dry solids, while those above 75% relative humidity were deliquescent aerosols. Table 25 gives the mass fraction of sodium and calcium within NaCl, sea salt and mineral dust particles at varying relative humidities.

	Mass Fraction		
RH	Na^+		Ca^{2+}
(%)	in NaCl	in sea salt	in dust
60	0.39	0.19	0.15
78	0.10	0.07	0.13
90	0.06	0.05	0.11
95	0.03	0.03	0.09

Table 25. Mass fractions of sodium and calcium in NaCl, sea salt and mineral dust.

As with the mass fraction, the density of the particles changes with the uptake of water. The densities were calculated as follows. The derivation of these equations is given in Appendix 3. The density of the aqueous phase of the particle was calculated using:

$$\rho_{aq} = \frac{1}{\frac{w_s}{\rho_s} + \frac{w_w}{\rho_w}} \qquad \text{(Equation 35)}$$

where ρ_s and ρ_w are the respective densities of the solute (salt) and water and w_s and w_w are the respective mass fractions of the solute and water. The density of the entire aerosol particle was calculated using:

$$\rho_{part} = \frac{1}{\frac{F_{aq}}{\rho_{aq}} + \frac{F_{solid}}{\rho_{solid}}} \qquad \text{(Equation 36)}$$

where F_{aq} and F_{solid} are the respective mass fractions of the aqueous and solid phases within the entire particle and ρ_{aq} and ρ_{solid} are the respective densities of the aqueous and solid phases. The resulting density values are listed in Table 26.

RH	Density (g cm^{-3})		
(%)	NaCl	Sea salt	$CaCO_3$
60	1.3	2.2	1.3
78	1.2	1.2	1.2
90	1.1	1.1	1.1
95	1.0	1.1	1.1

Table 26. Calculated densities for NaCl, sea salt and $CaCO_3$ at varying relative humidities.

The Equisolv II model was also used to compute the thermodynamic equilibrium concentrations of particle nitrate. The modeled results were dependent on the relative humidity and the composition of the particle. The reactions of NaCl and sea salt with nitric acid were greatly affected by the equilibrium, as the predicted k_{eq} is several orders of magnitude smaller than that of mineral dust. The large k_{eq} value for mineral dust did not limit the reaction between $CaCO_3$ and nitric acid, which was allowed to react until the particle was completely saturated with nitrate.

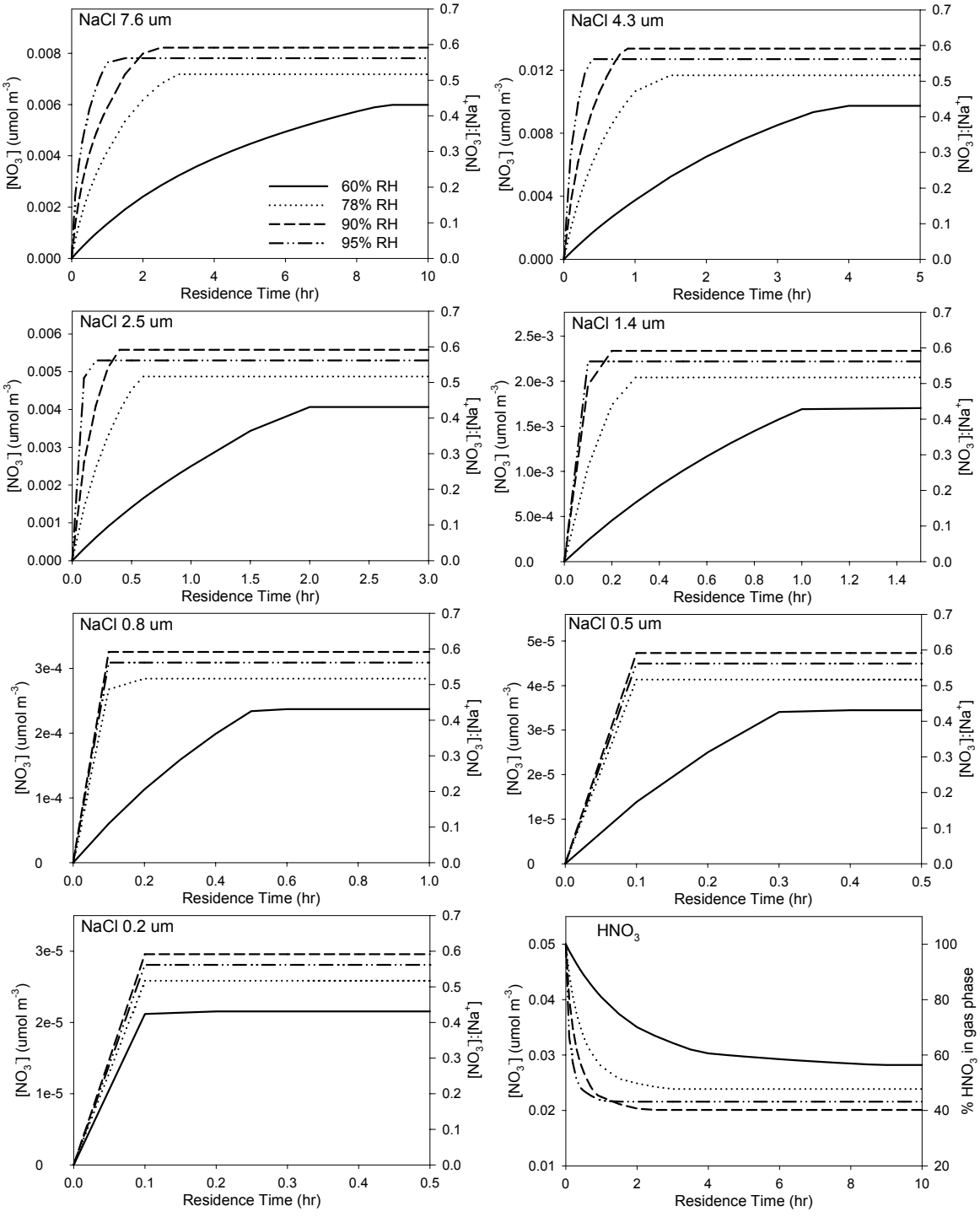

Figure 52. Time-resolved nitrate formation for NaCl.

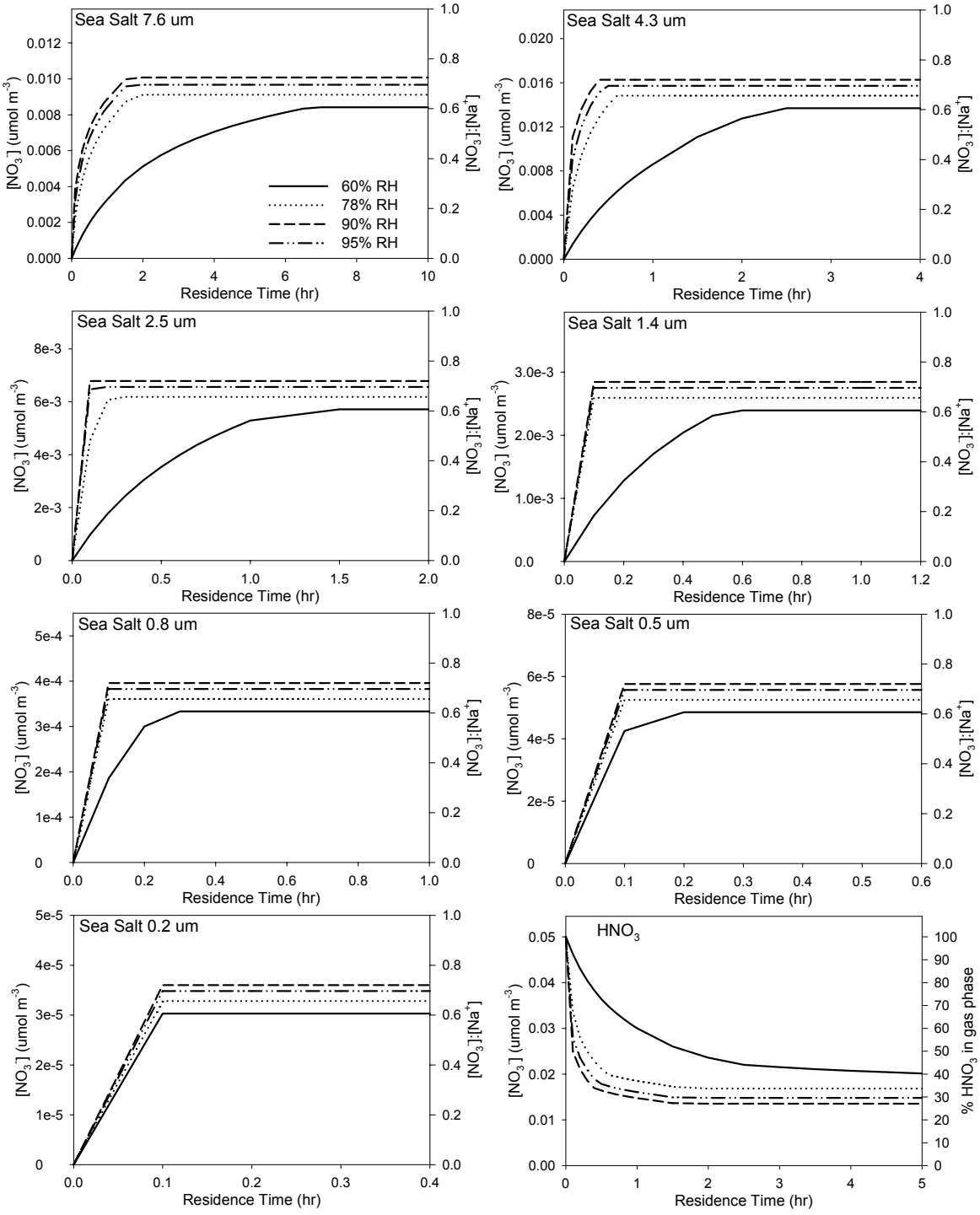

Figure 53. Time-resolved nitrate formation for sea salt.

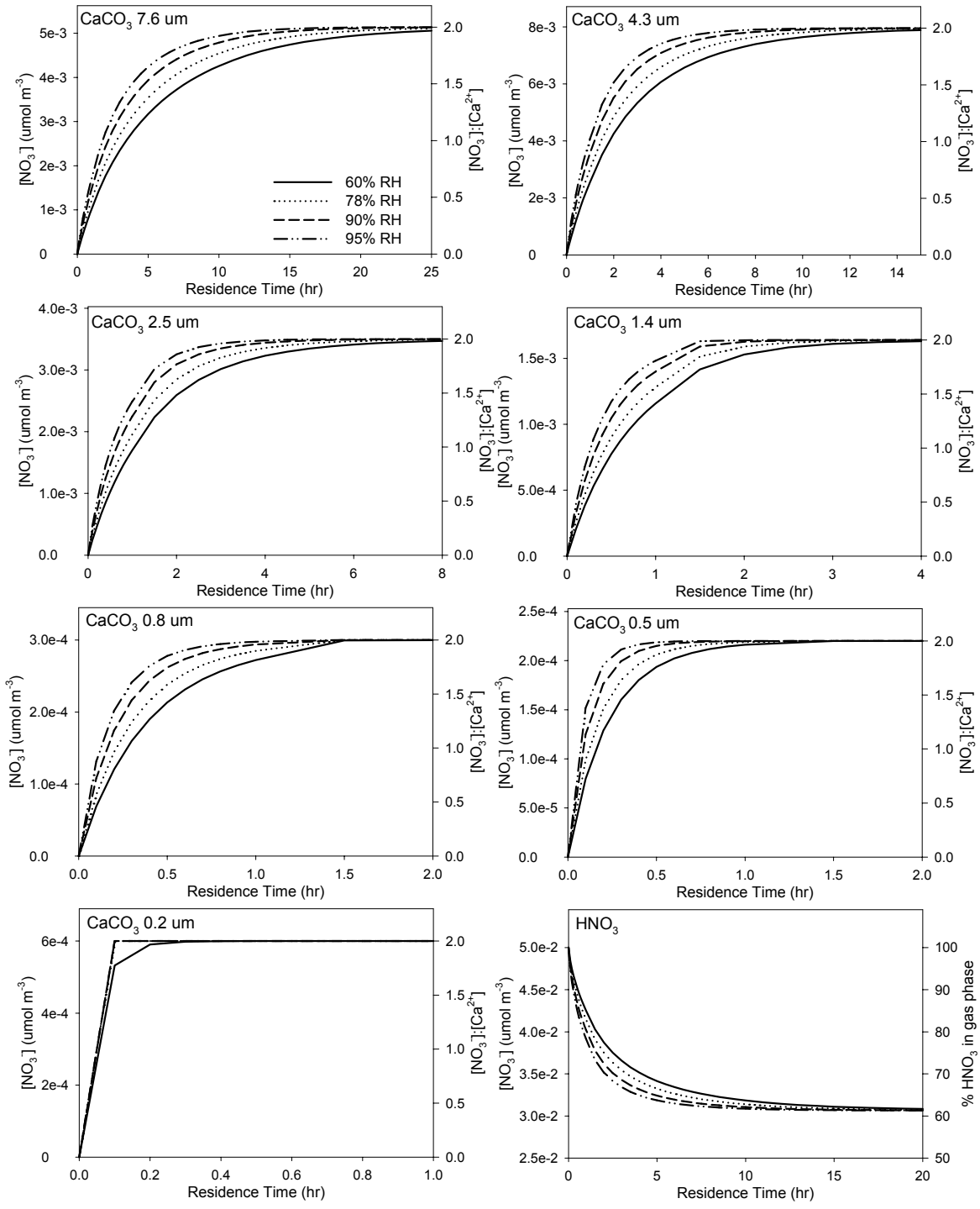

Figure 54. Time-resolved nitrate formation for $CaCO_3$.

Results and Discussions

The model was run in time steps until the particulate phase reached the thermodynamic equilibrium concentration of nitrate that was predicted by the EQUISOLV II model. The results are given in Figures 51-53 for NaCl, sea salt and $CaCO_3$, respectively.

The concentration of particulate nitrate was extrapolated at the particle residence time from the time-resolved curves given in Figures 51-53. For NaCl and sea salt, the particles reached the equilibrium nitrate concentration at speeds much faster than their residence times. For calcium, the extrapolated concentrations were compared to the saturation equation:

$$\%\text{Reacted} = ([NO_{3(\text{mod})}^{-}] \div [NO_{3(equil)}^{-}]) \times 100\% \qquad \text{(Equation 37)}$$

where $[NO_{3(\text{mod})}^{-}]$ (μmol m^{-3}) is the model-predicted nitrate concentration at a given relative humidity, and $[NO_{3(equil)}^{-}]$ (μmol m^{-3}) is the equilibrium particle nitrate concentration as predicted by the EQUISOLV II model. This was done to determine the extent of the reaction at the residence time. Those particles with a nitrate concentration less than calcium (in microequivalents) were assumed to react only partially. The results are given in Table 27.

Percent Reacted Nitrate at Residence Time (Time of Deposition)												
Ca^{2+} in mineral dust												
	Low Wind Speed				Mid Wind Speed				High Wind Speed			
D_p	60%	78%	90%	95%	60%	78%	90%	95%	60%	78%	90%	95%
0.2												
0.5						**100% Reacted**						
0.8												
1.4												
2.5												
4.3												
7.6	94%	97%	99%	99%	94%	96%	99%	99%	85%	90%	95%	97%

Table 27. The percent of particulate nitrate formation based on an initial height of 100 m at the residence time and different ambient relative humidity values.

Under the given conditions, the majority of the particles reached the nitrate equilibrium concentration at or before their residence time. The uptake of nitrate was greatest at 95% relative humidity and low wind speed conditions. The largest particle size bin collected particles up to 10 μm in diameter. According to Table 27, these particles contain a significant amount of nitrate.

Figure 55 displays the typical size distribution for sodium, calcium and nitrate in the Tampa Bay area. All three species are primarily in the coarse fraction, with the distribution beginning at ~0.5 μm. Upon reaction with sodium or calcium, particulate nitrate exhibits a similar size distribution as its parent NaCl or $CaCO_3$ particle.

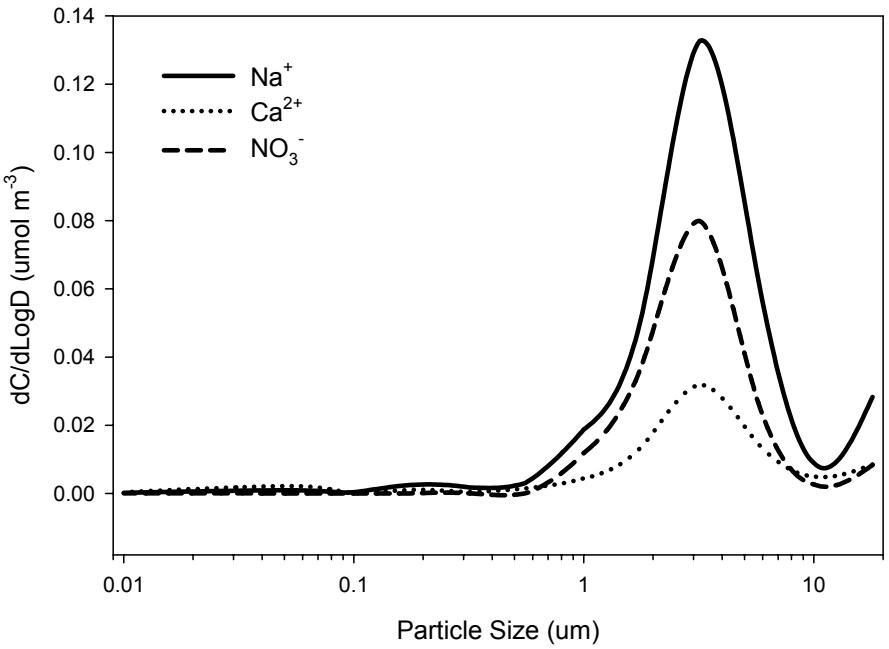

Figure 55. Typical size distribution of sodium, calcium and nitrate in the Tampa Bay area.

The aerosol sampling devices used at our bayside sampling site have an upper collection limit of 10 μm particles. Several studies have been conducted measuring the size distribution of marine aerosol (de Leeuw, 1986; Haaf and Jaenicke, 1980; Hoppel et al., 1989; Meszaros and Vissy, 1974; Seinfeld and Pandis, 1998). These studies reveal four major modes of marine aerosol: (a) 0.05-0.06, (b) 0.2-0.3, (c) 6-7 and (d) 11-15 μm. Continental aerosol size distribution has also been characterized (Jaenicke, 1993), revealing three major modes: (a) 0.01-0.02, (b) 0.15-0.25 and (c) 6-7 μm.

In Figure 55, the particle size distribution at 10 μm begins to show what may be the beginning of the largest mode (11-15 μm) of marine aerosol.

Particles with a geometric mean diameter of 15 μm have an approximate deposition velocity and residence time of 0.7 cm s^{-1} and 4 hr, respectively. From Figures 51-52, all particles in the largest size bin reached equilibrium in less than 8 hours, with the equilibrium time significantly less for deliquescent aerosols. If the modeling exercises were to continue for the largest mode of marine aerosols, results may indicate that the particles would contain a significant amount of nitrate even though they may not reach complete equilibrium before their residence time.

Impact on Nitrogen Loading

To determine if these particles could have an environmental impact, their effect on the total nitrogen loading through dry deposition was examined. Particle and gas deposition velocities were calculated using the integrated NOAA Buoy-Williams model (Bhethanabotla, 2002). The dry deposition flux was calculated using Equation 1, where $F = C \times V_d$.

During this modeling exercise, 0.05 μmol m^{-3} of nitrate was partitioned between the gas and particle phases. If all of this nitrate were to remain in the gas phase as nitric acid, the resulting fluxes for the low, mid and high wind speed conditions would be 0.61, 1.5 and 3.3 kg-N ha^{-1} yr^{-1}, respectively. However, particles have lower deposition velocities and longer residence times than nitric acid, giving them the ability to create a flux divergence as nitric acid is transferred

Nitric Acid and Particulate Nitrate Flux (kg-N ha^{-1} yr^{-1})												
Na^+ in NaCl	Low Wind Speed				Mid Wind Speed				High Wind Speed			
D_p	Relative Humidity				Relative Humidity				Relative Humidity			
(μm)	60%	78%	90%	95%	60%	78%	90%	95%	60%	78%	90%	95%
0.2	2 E-6	3 E-6	3 E-6	3 E-6	6 E-6	7 E-6	8 E-6	7 E-6	2 E-5	3 E-5	3 E-5	3 E-5
0.5	5 E-6	6 E-6	7 E-6	7 E-6	7 E-6	9 E-6	1 E-5	1 E-5	3 E-5	3 E-5	4 E-5	3 E-5
0.8	6 E-5	7 E-5	8 E-5	8 E-5	7 E-5	8 E-5	1 E-4	9 E-5	2 E-4	2 E-4	2 E-4	2 E-4
1.4	4 E-4	5 E-4	6 E-4	6 E-4	5 E-4	6 E-4	7 E-4	7 E-4	1 E-3	2 E-3	2 E-3	2 E-3
2.5	4 E-3	4 E-3	5 E-3	5 E-3	4 E-3	5 E-3	5 E-3	5 E-3	5 E-3	7 E-3	8 E-3	7 E-3
4.3	2 E-2	3 E-2	3 E-2	3 E-2	2 E-2	3 E-2	3 E-2	3 E-2	3 E-2	4 E-2	4 E-2	4 E-2
7.6	5 E-2	5 E-2	6 E-2	6 E-2	5 E-2	5 E-2	6 E-2	6 E-2	7 E-2	8 E-2	9 E-2	9 E-2
Total Particle	0.07	0.09	0.1	0.1	0.07	0.09	0.1	0.1	0.11	0.13	0.15	0.14
Gas + Particle	0.42	0.38	0.35	0.36	0.91	0.8	0.7	0.74	1.95	1.69	1.46	1.55
% Reduction	69%	62%	57%	59%	61%	53%	47%	49%	59%	51%	44%	47%
Na^+ in sea salt	Low Wind Speed				Mid Wind Speed				High Wind Speed			
D_p	60%	78%	90%	95%	60%	78%	90%	95%	60%	78%	90%	95%
0.2	3 E-6	3 E-6	4 E-6	3 E-6	8 E-6	9 E-6	9 E-6	9 E-6	3 E-5	4 E-5	4 E-5	4 E-5
0.5	7 E-6	8 E-6	8 E-6	8 E-6	1 E-5	1 E-5	1 E-5	1 E-5	4 E-5	4 E-5	4 E-5	4 E-5
0.8	9 E-5	9 E-5	1 E-4	1 E-4	1 E-4	1 E-4	1 E-4	1 E-4	2 E-4	3 E-4	3 E-4	3 E-4
1.4	6 E-4	7 E-4	7 E-4	7 E-4	7 E-4	8 E-4	9 E-4	8 E-4	2 E-3	2 E-3	2 E-3	2 E-3
2.5	5 E-3	6 E-3	6 E-3	6 E-3	5 E-3	6 E-3	6 E-3	6 E-3	8 E-3	8 E-3	9 E-3	9 E-3
4.3	3 E-2	4 E-2	4 E-2	4 E-2	3 E-2	4 E-2	4 E-2	4 E-2	4 E-2	5 E-2	5 E-2	5 E-2
7.6	6 E-2	7 E-2	8 E-2	7 E-2	6 E-2	7 E-2	8 E-2	7 E-2	9 E-2	1 E-1	1 E-1	1 E-1
Total Particle	0.1	0.11	0.12	0.12	0.1	0.11	0.12	0.12	0.15	0.16	0.18	0.17
Gas + Particle	0.34	0.32	0.29	0.3	0.68	0.61	0.53	0.56	1.41	1.26	1.07	1.14
% Reduction	56%	52%	48%	49%	45%	41%	35%	37%	43%	38%	32%	35%
Ca^{2+} in dust	Low Wind Speed				Mid Wind Speed				High Wind Speed			
D_p	60%	78%	90%	95%	60%	78%	90%	95%	60%	78%	90%	95%
0.2	6 E-5	6 E-5	6 E-5	6 E-5	2 E-4	2 E-4	2 E-4	2 E-4	7 E-4	7 E-4	7 E-4	7 E-4
0.5	3 E-5	3 E-5	3 E-5	3 E-5	5 E-5	5 E-5	5 E-5	5 E-5	2 E-4	2 E-4	2 E-4	2 E-4
0.8	8 E-5	8 E-5	8 E-5	8 E-5	9 E-5	9 E-5	9 E-5	9 E-5	2 E-4	2 E-4	2 E-4	2 E-4
1.4	4 E-4	4 E-4	4 E-4	4 E-4	5 E-4	5 E-4	5 E-4	5 E-4	1 E-3	1 E-3	1 E-3	1 E-3
2.5	3 E-3	3 E-3	3 E-3	3 E-3	3 E-3	3 E-3	3 E-3	3 E-3	5 E-3	5 E-3	5 E-3	5 E-3
4.3	2 E-2	2 E-2	2 E-2	2 E-2	2 E-2	2 E-2	2 E-2	2 E-2	3 E-2	3 E-2	3 E-2	3 E-2
7.6	4 E-2	4 E-2	4 E-2	4 E-2	4 E-2	4 E-2	4 E-2	4 E-2	5 E-2	5 E-2	6 E-2	6 E-2
Total Particle	0.06	0.06	0.06	0.06	0.06	0.06	0.06	0.06	0.09	0.09	0.09	0.09
Gas + Particle	0.44	0.44	0.44	0.44	0.97	0.97	0.97	0.97	2.12	2.11	2.1	2.1
% Reduction	72%	72%	72%	72%	65%	65%	65%	65%	64%	64%	64%	64%

Table 28. The calculated nitrogen over water dry deposition flux.

to the particle phase. The resulting particle and total flux values are reported in Table 28.

Due to their relatively higher sodium or calcium concentration and greater deposition velocity, particles 4.3 μm and greater contributed to the majority of the particle dry deposition flux, especially when the relative humidity was ≥ 90%. The gas phase nitric acid dominated the total flux and was greatest at high wind speed conditions. Low ambient concentrations of calcium resulted in lower nitrogen flux contributions from mineral dust with respect to sea salt or NaCl.

Flux divergence of HNO_3 in the marine boundary layer has been modeled by Pryor and Sorensen (2000) to determine the importance of nitric acid reactions on sea salt particles. Their results indicated that under near-neutral stability and wind speeds between 3.5 and 10 m s^{-1}, the transfer of nitric acid to the particle phase decreased the deposition velocity of nitrogen by over 50%. This transfer to the particle phase led to greater horizontal transport prior to deposition of the nitrogen particles. For low and high wind speeds (<3.5 and >10 m s^{-1}), the transfer of nitric acid to the particle phase increased the deposition rate and decreased the horizontal transport.

Conclusions

A better understanding of the characteristics and formation of particulate nitrate is essential for the development of nitrogen loading estimates and control. Nitrogen particle size distributions have been identified and investigated during the course of this study.

Through a network of ambient air sampling, a snapshot of our local environment was created giving us estimates of particle concentrations and size distributions. The data collected during a series of intensive monitoring campaigns allowed the formation and characterization of the nitrate particles to be deduced. This work researched the interaction between nitric acid and sea salt, focusing on the chemistry and its effect on the local nitrogen deposition estimates.

The partitioning of nitric acid to particulate nitrate was examined for NaCl and $CaCO_3$. Both salts exhibited an increase in particulate nitrate formation with an increase in sodium or calcium and total available nitrate concentrations in the system. The extent of particulate nitrate formation was directly related to each equation's equilibrium constant. Calcium has an equilibrium constant several orders of magnitude greater than sodium, partitioning nitrate to the particle phase until its saturation concentration. The water content of the particles was

examined. Both nitrate salts were more hygroscopic than their parent salt. As nitrate was partitioned to the particle, the amount of absorbed water increased. Nitrogen dry deposition flux estimates were calculated. For both NaCl and $CaCO_3$ scenarios, the gas phase nitric acid contributed to the majority of the local nitrogen deposition with the nitrogen flux increasing as the total available nitrate increased. However, as the sodium or calcium concentration increased, the total nitrogen flux decreased. The particles created a local nitrogen flux divergence as they have longer residence times and greater horizontal transport.

The coarse mode particulate nitrate was predicted using fine mode nitrate data and new dry deposition estimates were calculated. Analysis from dichotomous samples and lognormal distributions obtained with a cascade impactor resulted in an approximate value for percent fine mode ($PM_{2.5}$) nitrate of 33%. The coarse mode ($PM_{10-2.5}$) nitrate accounted for 0.04 of the 0.06 kg-N ha^{-1} yr^{-1} of the dry deposition flux. The gas plus particle dry deposition flux was estimated at 3.2 kg-N ha^{-1} yr^{-1}. This value is unchanged from the previous estimate, but it was calculated using coarse mode particulate concentrations and size-dependent particle deposition velocities.

The theoretical formation of particles nitrate from the reaction of nitric acid with NaCl, sea salt and mineral dust ($CaCO_3$) was estimated using a nitrate accumulation model and a thermodynamic equilibrium model. The extent of the reaction for NaCl and sea salt was limited to the predicted equilibrium nitrate concentration, as the k_{eq} values for the NaCl and sea salt reactions are relatively small when compared to that of mineral dust. The equilibrium concentration was

determined to be dependent on the relative humidity. Size distributions for marine and mineral dust aerosols were used to determine the major modes for these species. Marine aerosols were found to have a macroparticle mode greater than the cutoff of our instruments. Ambient sodium and calcium concentrations are unavailable for particles greater than 10 μm. However, the use of this modeling has inferred that these particles, when mixed with urban air, may contain a significant amount of nitrate despite their relatively short residence time. The particle contribution to the nitrogen dry deposition flux was examined. The gas phase nitric acid contributed to the majority of the nitrogen dry deposition flux, with particles only contributing a small percentage. The highest particle contribution occurred under high humidity and high wind speed conditions. However, for mineral dust, the low ambient concentrations of calcium resulted in lower particulate nitrate concentrations with respect to sodium. Our work was found to be consistent with that of others, where the transfer of nitric acid to particle phase nitrate decreased the deposition of locally produced species, as the particles have greater horizontal transport and residence times.

References

Abbatt, J.P.D., Washewsky, G.C.G., 1998. Heterogeneous interactions of HOBr, HNO3, O3, and NO2 with deliquescent NaCl aerosols at room temperature. Journal of Physical Chemistry A 102, 3719-3725.

Aherne, J., Farrell, E.P., 2002. Deposition of sulphur, nitrogen and acidity in precipitation over Ireland: chemistry, spatial distribution and long-term trends. Atmospheric Environment 36, 1379-1389.

Ali-Mohamed, A.Y., Jaffar, A.H., 2000. Estimation of atmospheric inorganic water-soluble aerosols in the western region of Bahrain by ion chromatography. Chemosphere - Global Change Science 2, 85-94.

Allegrini, I., De Sanits, F., Di Palo, V., Febo, A., Perrino, C., Possanzini, M., Liberti, A., 1987. Annular denuder method for sampling reactive gases and aerosols in the atmosphere. The Science of the Total Environment 67, 1-16.

Allegrini, I., Febo, A., Perrino, C., Masia, P., 1994. Measurement of atmospheric nitric acid in gas phase and nitrate in particulate matter by means of annular denuders. International Journal of Environmental Analytical Chemistry 54, 183-201.

Allen, A.G., Harrison, R.M., Erisman, J.W., 1989. Field measurements of the dissociation of ammonium nitrate and ammonium chloride aerosols. Atmospheric Environment 23, 1591-1599.

Allen, A.G., Miguel, A.H., 1995. Aerosol chemistry in the urban atmosphere of Sao Paulo, Brazil. Journal of Aerosol Science 26, S375-S376.

Allen, H.C., Laux, J.M., Vogt, R., Finlayson-Pitts, B.J., Hemminger, J.C., 1996. Water-induced reorganization of ultrathin nitrate films on NaCl: Implications for the tropospheric chemistry of sea salt particles. Journal of Physical Chemistry 100, 6371-6375.

Allen, H.C., Mecartney, M.L., Hemminger, J.C., 1998. Minimizing transmission electron microscopy beam damage during the study of surface reactions on sodium chloride. Microscopy and Microanalysis 4, 23-33.

Andreas, E.L., Edson, J.B., Monahan, E.C., Rouault, M.P., Smith, S.D., 1995. The spray contribution to net evaporation from the sea: A review of recent progress. Boundary-Layer Meteorology 72, 3-52.

Anlauf, K.G., Wiebe, H.A., Fellin, P., 1986. Characterization of several integrative sampling methods for nitric acid, sulphur dioxide and atmospheric particles. Journal of the Air Pollution Control Association 36, 715-723.

Ansari, A.S., Pandis, S.N., 1999. Prediction of multicomponent inorganic atmospheric aerosol behavior. Atmospheric Environment 33, 745-757.

Appel, B.R., Povard, B., Kothny, E.L., 1988. Loss of nitric acid within inlet devices intended to exclude coarse particles during atmospheric sampling. Atmospheric Environment 22, 2535-2540.

Appel, B.R., Tokiwa, Y., Haik, M., Kothny, E.L., 1984. Artifact particulate sulfate and nitrate formation on filter media. Atmospheric Environment 18, 409-416.

Appel, B.R., Wall, S.M., Tokiwa, Y., Haik, M., 1980. Simultaneous nitric acid, particulate nitrate and acidity measurements in ambient air. Atmospheric Environment 14, 549-554.

Aristarain, A.J., Delmas, R.J., 2002. Snow chemistry measurements on James Ross Island (Antarctic Peninsula) showing sea-salt aerosol modifications. Atmospheric Environment 36, 765-772.

Bassett, M.E., Seinfeld, J.H., 1983. Atmospheric equilibrium model of sulfate and nitrate aerosols. Atmospheric Environment 17, 2237-2252.

Bassett, M.E., Seinfeld, J.H., 1984. Atmospheric equilibrium model of sulfate and nitrate aerosols - II. Particle size analysis. Atmospheric Environment 18, 1163-1170.

Batterman, S., Osak, I., Gelman, C., 1997. SO2 sorption characteristics of air sampling filter media using a new laboratory test. Atmospheric Environment 31, 1041-1047.

Beichert, P., Finlayson-Pitts, B.J., 1996. Knudsen cell studies of the uptake of gaseous HNO_3 and other oxides of nitrogen on solid NaCl: The role of surface-adsorbed water. Journal of Physical Chemistry 100, 15218-15228.

Berresheim, H., Wine, P.H., Davis, D.D., 1995. Sulfur in the atmosphere. In: Singh, H.B. (Ed.), Composition, Chemistry and Climate of the Atmosphere. Van Nostrand Reinhold, New York, NY, pp. 251-307.

Bhethanabotla, V.R., 2002. NOAA Buoy - Williams Model, Web address: http://www.eng.usf.edu/~bhethana.

Binkowski, F.S., Shankar, U., 1995. The regional particulate matter model 1. Model description and preliminary results. Journal of Geophysical Research 100, 26191-26209.

Blanchard, C.L., 1999. Methods for attributing ambient air pollutants to emission sources. Annual Review of Energy and the Environment 24, 329-365.

Blanchard, C.L., Roth, P.M., Tanenbaum, S.J., Ziman, S.D., Seinfeld, J.H., 2000. The use of ambient measurements to identify which precursor species limit aerosol nitrate formation. Journal of the Air & Waste Management Association 50, 2073-2084.

Brimblecombe, P., Clegg, S.L., 1988. The solubility and behaviour of acid gases in the marine aerosol. Journal of Atmospheric Chemistry 7, 1-18.

Bromley, L.A., 1973. Thermodynamic properties of strong electrolytes in aqueous solutions. American Institute of Chemical Engineers Journal 19, 313-320.

Burian, S.J., Streit, G.E., McPherson, T.N., Brown, M.J., Turin, H.J., 2001. Modeling the atmospheric deposition and stormwater washoff of nitrogen compounds. Environmental Modelling and Software 16, 467-479.

Caffrey, P.F., Ondov, J.M., Zufall, M.J., Davidson, C.I., 1998. Determination of size-dependent dry particle deposition velocities with multiple intrinsic elemental tracers. Environmental Science & Technology 32, 1615-1622.

Caloz, F., Fenter, F.F., Tabor, K.D., Rossi, M.J., 1997. Paper I: Design and construction of a Knudsen-cell reactor for the study of heterogeneous reactions over the temperature range 130-750 K: Performances and limitations. Review of Scientific Instruments 68, 3172-3179.

Calvert, J.G., Stockwell, W.R., 1983. Acid generation in the troposphere by gas-phase chemistry. Environmental Science & Technology 17, A428-A443.

Campbell, S.W., Evans, M.C., Poor, N.D., 2002. Predictions of size-resolved aerosol concentrations of ammonium, chloride and nitrate at a bayside site using EQUISOLV II. Atmospheric Environment 36, 4299-4307.

Chameides, W.L., Stelson, A.W., 1992. Aqueous-phase chemical processes in deliquescent sea-salt aerosols: A mechanism that couples the atmospheric cycles of S and sea salt. Journal of Geophysical Research 97, 20565-20580.

Chang, J.-S., Urashima, K., Tong, Y.X., Liu, W.P., Wei, H.Y., Yang, F.M., Liu, X.J., 2003. Simultaneous removal of NOx and SO2 from coal boiler flue gases by DC corona discharge ammonia radical shower systems: pilot plant tests. Journal of Electrostatics 57, 313-323.

Cheng, Z.L., Lam, K.S., Chan, L.Y., Wang, T., Cheng, K.K., 2000. Chemical characteristics of aerosols at coastal station in Hong Kong. I. Seasonal variation of major ions, halogens and mineral dusts between 1995 and 1996. Atmospheric Environment 34, 2771-2783.

Clarke, A.G., Azadi-Boogar, G.A., Andrews, G.E., 1999. Particle size and chemical composition of urban aerosols. The Science of the Total Environment 235, 15-24.

Clegg, N.A., Toumi, R., 1998. Non-sea-salt-sulphate formation in sea-salt aerosols. Journal of Geophysical Research 103, 31095-31102.

Clegg, S.L., Brimblecombe, P., Wexler, A.S., 1998. Thermodynamic model of the system H^+-NH_4^+-Na^+-SO_4^{2-}-NO_3^--Cl^--H_20 at 298.15 K. Journal of Physical Chemistry A 102, 2155-2171.

Conley, D.J., 2000. Biogeochemical nutrient cycles and nutrient management strategies. Hydrobiologia 410, 87-96.

Cooper, D.W., Spielman, L.A., 1976. Data inversion using nonlinear programming with physical constraints: Aerosol size distribution measurement by impactors. Atmospheric Environment 10, 723-730.

Dasch, J.M., Cadle, S.H., Kennedy, K.G., Mulawa, P.A., 1989. Comparison of annular denuders and filter packs for atmospheric sampling. Atmospheric Environment 23, 2775-2782.

Davies, J.A., Cox, R.A., 1998. Kinetics of the heterogeneous reaction of HNO_3 with NaCl: Effect of water vapor. Journal of Physical Chemistry A 102, 7631-7642.

De Haan, D.O., Finlayson-Pitts, B.J., 1997. Knudsen cell studies of the reaction of gaseous nitric acid with synthetic sea salt at 298 K. Journal of Physical Chemistry A 101, 9993-9999.

de Leeuw, G., 1986. Vertical profiles of giant particles close above the sea surface. Tellus 38B, 51-61.

de Leeuw, G., Cohen, L., Frohn, L.M., Geernaert, G., Hertel, O., Jensen, B., Jickells, T., Klein, L., Kunz, G.J., Lund, S., 2001. Atmospheric input of nitrogen into the North Sea: ANICE project overview. Continental Shelf Research 21, 2073-2094.

de Wit, M., Bendoricchio, G., 2001. Nutrient fluxes in the Po basin. The Science of the Total Environment 273, 147-161.

Dentener, F.J., Carmichael, G.R., Zhang, Y., Crutzen, P.J., 1996. Role of mineral aerosol as a reactive surface in the global troposphere. Journal of Geophysical Research 101, 22869-22889.

Dentener, F.J., Crutzen, P.J., 1994. A three-dimensional model of the global ammonia cycle. Atmospheric Environment 19, 331-369.

Draxler, R.R., Hess, G.D., 1998. An overview of the HYSPLIT_4 modelling system for trajectories, dispersion and deposition. Australian Meteorological Magazine 47, 295-308.

Ebert, M., Weinbruch, S., Hoffmann, P., Ortner, H.M., 2000. Chemical characterization of North Sea aerosol particles. Journal of Aerosol Science 31, 613-632.

Erickson III, D.J., Seuzaret, C., Keene, W.C., Gong, S.L., 1999. A general circulation model based calculation of HCl and $ClNO_2$ production from sea salt dechlorination: Reactive chlorine emissions inventory. Journal of Geophysical Research 104, 8347-8372.

Erisman, J.W., Brydges, T., Bull, K., Cowling, E., Grennfelt, P., Nordberg, L., Satake, K., Schneider, T., Smeulders, S., Van der Hoek, K.W., Wisniewski, J.R., Wisniewski, J., 1998. Nitrogen, the Confer-N-s, First International Nitrogen Conference 1998: Summary Statement.

Evans, M.C., Hendrix-Holmes, H., Poor, N.D., 2002. Do macroparticles contain nitrogen? Proceedings of the 95th Annual Air and Waste Management Conference and Exhibition, June 23-27, Baltimore, MD. A&WMA, Pittsburgh, PA.

Evans, M.C., Poor, N.D., 2001. Scrubbing of atmospheric nitric acid and sulfuric acid by marine air. Proceedings of the 94th Annual Air and Waste Management Conference and Exhibition, June 24-28, Orlando, FL. A&WMA, Pittsburgh, PA.

Febo, A., De Sanits, F., Perrino, C., Giusto, M., 1989. Evaluation of laboratory and field performance of denuder tubes: a theoretical approach. Atmospheric Environment 23, 1517-1530.

Fenter, F.F., Caloz, F., Rossi, M.J., 1994. Kinetics of nitric acid uptake by salt. Journal of Physical Chemistry 98, 9801-9810.

Fenter, F.F., Caloz, F., Rossi, M.J., 1997. Paper II: Simulation of flow conditions in low-pressure flow reactors (Knudsen cells) using a Monte Carlo technique. Review of Scientific Instruments 68, 3180-3186.

Finlayson-Pitts, B.J., Hemminger, J.C., 2000. Physical chemistry of airborne sea salt particles and their components. Journal of Physical Chemistry A 104, 11463-11477.

Finlayson-Pitts, B.J., Pitts Jr., J.N., 2000. Chemistry of the Upper and Lower Atmosphere: Theory, Experiments, and Applications. Academic Press, New York, NY, pp. 969.

Fitzgerald, J.W., 1991. Marine aerosols: A review. Atmospheric Environment 25A, 533-545.

Forrest, J., Spandau, D.J., Tanner, R.L., Newman, L., 1982. Determination of atmospheric nitrate and nitric acid employing a diffusion denuder with a filter pack. Atmospheric Environment 16, 1473-1584.

Forrest, J., Tanner, R.L., Spandau, D.J., D'Ottavio, T., Newman, L., 1980. Determination of total inorganic nitrate utilizing collection of nitric acid on NaCl-impregnated filters. Atmospheric Environment 14, 137-144.

Ghosal, S., Hemminger, J.C., 1999. Effect of water on the HNO_3 pressure dependence of the reaction between gas-phase HNO_3 and NaCl surfaces. Journal of Physical Chemistry A 103, 4777-4781.

Gilliland, A.B., Pierce, T.E., Dennis, R.L., Roselle, S., Inverse Modeling to Estimate Seasonal Ammonia Emissions. USEPA Atmospheric Modeling Division, Research Triangle Park, NC, pp.

Glover, T., Mitchell, K., 2002. An Introduction to Biostatistics. McGraw Hill, Boston, MA, pp. 416.

Goodman, A.L., Underwood, G.M., Grassian, V.H., 2000. A laboratory study of the heterogeneous reaction of nitric acid on calcium carbonate particles. Journal of Geophysical Research 105, 29053-29064.

GraphPad Software, 2000. GraphPad Software, Web address: http://www.graphpad.com.

Grassian, V.H., 2002. Chemical reactions of nitrogen oxides on the surface of oxide, carbonate, soot, and mineral dust particles: Implications for the chemical balance of the troposphere. Journal of Physical Chemistry A 106, 860-877.

Grosjean, D., 1982. The stability of particulate nitrate in the Los Angeles atmosphere. The Science of the Total Environment 25, 263-275.

Guimbaud, C., Arens, F., Gutzwiller, L., Gaggeler, H.W., Ammann, M., 2002a. Uptake of HNO_3 to deliquescent sea-salt particles. Atmospheric Chemistry and Physics Discussions 2, 739-763.

Guimbaud, C., Arens, F., Gutzwiller, L., Gaggeler, H.W., Ammann, M., 2002b. Uptake of HNO_3 to deliquescent sea-salt particles: a study using the short-lived radioactive isotope tracer ^{13}N. Atmospheric Chemistry and Physics Discussions 2, 249-257.

Haaf, W., Jaenicke, R., 1980. Results of improved size distribution measurements in the Aitken range of atmospheric aerosols. Journal of Aerosol Science 11, 321-330.

Hanisch, F., Crowley, J.N., 2001. Heterogeneous reactivity of gaseous nitric acid on Al_2O_3, $CaCO_3$, and atmospheric dust samples: A Knudsen cell study. Journal of Physical Chemistry A 105, 3096-3106.

Harrison, R.M., 1993. The Chemistry and Deposition of Particulate Nitrogen-containing Species. In: Cocks, A.T. (Ed.), The Chemistry and Deposition of Nitrogen Species in the Troposphere. The Royal Society of Chemistry, Cambridge, pp. 95-105.

Harrison, R.M., Kitto, A.-M.N., 1990. Field inter-comparison of filter pack and denuder sampling methods for reactive gaseous and particulate pollutants. Atmospheric Environment 24A, 2633-2640.

Hering, S.V., Lawson, D.R., Allegrini, I., Febo, A., Perrino, C., Possanzini, M., Sickles II, J.E., Anlauf, K.G., Wiebe, A., Appel, B.R., John, W., Ondo, J.L., Wall, S.M., Braman, R.S., Sutton, R., Cass, G.R., Solomon, P.A., Eatough, D.J., Eatough, N.L., Ellis, E.C., Grosjean, D., Hicks, B.B., Womack, J.D., Horrocks, J., Knapp, K.T., Ellestad, T.G., Paur, R.J., Mitchell, W.J., Pleasant, M., Peake, E., MacLean, A., Pierson, W.R., Brachaczek, W., Schiff, H.I., Mackay, G.I., Spicer, C.W., Stedman, D.H., Winer, A.M., Biermann, H.W., Tuazon, E.C., 1988. The nitric acid shootout: Field comparison of measurement methods. Atmospheric Environment 22, 1519-1539.

Hinds, W.C., 1999. Aerosol Technology: Properties, Behavior, and Measurements of Airborne Particles. John Wiley & Sons, Inc., New York, NY, pp. 483.

Hoppel, W.A., Fitzgerald, J.W., Frick, G.M., Larson, R.E., Mack, E.J., 1989. Atmospheric Aerosol Size Distributions and Optical Properties in the Marine Boundary Layer over the Atlantic Ocean. NRL Report 9188, Washington, DC.

Hu, J.H., Abbatt, J.P.D., 1997. Reaction probabilities for N_2O_5 hydrolysis on sulfuric acid and ammonium sulfate aerosols at room temperature. Journal of Physical Chemistry A 101, 871-878.

Huebert, B.J., Lazrus, A.L., 1980. Tropospheric gas-phase and particulate nitrate measurements. Journal of Geophysical Research 85, 7322-7328.

HYSPLIT4, 1997. HYSPLIT4 (HYbrid Single-Particle Lagrangian Integrated Trajectory) Model, NOAA Air Resources Laboratory, Silver Spring, MD. Web address: http://www.arl.noaa.gov/ready/hysplit4.html.

Jacobson, M., 1999a. Studying the effects of calcium and magnesium on size-distributed nitrate and ammonium with EQUISOLV II. Atmospheric Environment 33, 3635-3649.

Jacobson, M.Z., 1997. Development and application of a new air pollution modeling system - Part III. Aerosol-phase simulations. Atmospheric Environment 31, 587-608.

Jacobson, M.Z., 1999b. Fundamentals of Atmospheric Modeling. Cambridge University Press, New York, NY, pp. 656.

Jacobson, M.Z., Tabazadeh, A., Turco, R.P., 1996. Simulating equilibrium within aerosols and nonequilibrium between gases and aerosols. Journal of Geophysical Research 101, 9079-9091.

Jaenicke, R., 1993. Tropospheric aerosols. In: Hobbs, P.V. (Ed.), Aerosol-Cloud-Climate Interactions. Academic Press, San Diego, CA, pp. 1-31.

Jordan, C.E., Talbot, R.W., Keim, B.D., 2000. Water-soluble nitrogen at the New Hampshire sea coast: HNO_3, aerosols, precipitation, and fog. Journal of Geophysical Research 105, 26403-26431.

Karakas, D., Tuncel, S.G., 1997. Optimization and field application of a filter pack system for the simultaneous sampling of atmospheric HNO_3, NH_3 and SO_2. Atmospheric Environment 31, 1657-1666.

Kerminen, V.-M., Wexler, A.S., 1995. Growth laws for atmospheric aerosol particles: An examination of the bimodality of the accumulation mode. Atmospheric Environment 29, 3263-3275.

Kim, J.C., Allen, E.R., 1997. Effects of filter pack sampling conditions on observed ambient concentrations of dry acid deposition species. Chemosphere 34, 587-610.

Kim, Y.P., Seinfeld, J.H., 1995. Atmospheric gas-aerosol equilibrium: III. Thermodynamics of crustal elements Ca^{2+}, K^{+}, and Mg^{2+}. Aerosol Science and Technology 22, 93-110.

Kim, Y.P., Seinfeld, J.H., Saxena, P., 1993a. Atmospheric gas-aerosol equilibrium I. Thermodynamic model. Aerosol Science and Technology 19, 157-181.

Kim, Y.P., Seinfeld, J.H., Saxena, P., 1993b. Atmospheric gas-aerosol equilibrium II. Analysis of common approximations and activity coefficient calculation methods. Aerosol Science and Technology 19, 182-198.

Kitto, A.-M.N., Colbeck, I., 1999. Filtration and Denuder Sampling Techniques. In: Spurny, K.R. (Ed.), Analytical Chemistry of Aerosols. Lewis Publishers, Boca Raton, FL, pp. 103-132.

Kolb, C.E., Worsnop, D.R., Zahniser, M.S., Davidovits, P., Keyser, L.F., Leu, M.T., Molina, L.T., Hanson, D.R., Ravishankara, A.R., 1995. Laboratory studies of atmospheric heterogeneous chemistry. In: Barker, J.R. (Ed.), Progress and Problems in Atmospheric Chemistry. World Scientific, New Jersey, pp. 771-875.

Langer, S., Pemberton, R.S., Finlayson-Pitts, B.J., 1997. Diffuse reflectance infrared studies on the reaction of synthetic sea salt mixtures with NO_2: A key role for hydrates in the kinetics and mechanism. Journal of Physical Chemistry A 101, 1277-1286.

Laskin, A., Iedema, M.J., Cowin, J.P., 2002. Quantitative time-resolved monitoring of nitrate formation in sea salt particles using a CCSEM/EDX single particle analysis. Environmental Science & Technology 36, 4948-4955.

Laux, J.M., Hemminger, J.C., Finlayson-Pitts, B.J., 1994. X-ray photoelectron spectroscopic studies of the heterogeneous reaction of gaseous nitric acid with sodium chloride: Kinetics and contribution to the chemistry of the marine troposphere. Geophysical Research Letters 21, 1623-1626.

Lide, D.R., 1991. Handbook of Chemistry and Physics. CRC Press, Boca Raton, FL, pp.

Li-Jones, X., Savoie, D.L., Prospero, J.M., 2001. HNO_3 losses within the cyclone inlet of a diffusion-denuder system under simulated marine environments. Atmospheric Environment 35, 985-993.

Lovett, R.F., 1978. Quantitative measurement of airborne sea-salt in the North Atlantic. Tellus 30, 358-364.

Luo, Y., Yang, X., Carley, R.J., Perkins, C., 2003. Effects of geographical location and land use on atmospheric deposition of nitrogen in the State of Connecticut. Environmental Pollution 124, 437-448.

Mamane, Y., Mehler, M., 1987. On the nature of nitrate particles in a coastal urban area. Atmospheric Environment 21, 1989-1994.

Markowski, G.R., 1987. Improving Twomey's algorithm for inversion of aerosol measurement data. Aerosol Science and Technology 7, 127-141.

Marple, V.A., Rubow, K.L., Behm, S.M., 1991. A microorifice uniform deposit impactor (MOUDI): description, calibration and use. Aerosol Science and Technology 14, 434-446.

Masia, P., Di Palo, V., Possanzini, M., 1994. Uptake of ammonia by nylon filters in filter pack systems. Atmospheric Environment 28, 365-366.

McCulloch, R.B., Shendrikar, A.D., 2000. Concurrent atmospheric ammonia measurements using citric-acid-coated diffusion denuders and a chemiluminescence analyzer. Atmospheric Environment 34, 4957-4958.

McMurry, P.H., 2000. A review of atmospheric aerosol measurements. Atmospheric Environment 34, 1959-1999.

Mehlmann, A., Warneck, P., 1995. Atmospheric gaseous HNO_3, particulate nitrate, and aerosol size distributions of major ionic species at a rural site in western Germany. Atmospheric Environment 29, 2359-2373.

Meng, Z., Seinfeld, J.H., Saxena, P., Kim, Y.P., 1995. Atmospheric gas-aerosol equilibrium: IV. Thermodynamics of carbonates. Aerosol Science and Technology 23, 131-154.

Meszaros, A., Vissy, K., 1974. Concentration, size distribution and chemical nature of atmospheric aerosol particles in remote ocean areas. Journal of Aerosol Science 5, 101-109.

Moya, M., Pandis, S.N., Jacobson, M.Z., 2002. Is the size distribution of urban aerosols determined by thermodynamic equilibrium? An application to Southern California. Atmospheric Environment 36, 2349-2365.

Murphy, D.M., Anderson, J.R., Quinn, P.K., McInnes, L.M., Brechtel, F.J., Kreidenweis, S.M., Middlebrook, A.M., Posfai, M., Thompson, D.S., Buseck, P.R., 1998. Influence of sea-salt on aerosol radiative properties in the Southern Ocean marine boundary layer. Nature 392, 62-65.

Nenes, A., Pilinis, C., Pandis, S.N., 1998. ISORROPIA: a new thermodynamic model for inorganic multicomponent atmospheric aerosols. Aquatic Geochemistry 4, 123-152.

Nixon, S.W., Ammerman, J.W., Atkinson, L.P., Berounsky, V.M., Billen, G., Boicourt, W.C., Boynton, W.R., Church, T.M., Ditoro, D.M., Elmgren, R., Garber, J.H., Giblin, A.E., Jahnke, R.A., Owens, N.J.P., Pilson, M.E.Q., Seitzinger, S.P., 1996. The fate of nitrogen and phosphorus at the land sea margin of the North Atlantic Ocean. Biogeochemistry 35, 141-180.

NOAA, 2003a. NOAA National Climatic Data Center, Web address: http://ncdc.noaa.gov.

NOAA, 2003b. NOAA National Ocean Service, Center for Operational Oceanographic Products and Services, Web address: http://www.co-ops.nos.noaa.gov.

Nodop, K., Hanssen, J.E., 1986. Field intercomparison of sampling and analytical methods for SO_2 and SO_4 in ambient air. In: Angeletti, G., Restelli, G. (Ed.), Physico-chemical Behaviour of Atmospheric Pollutants. D. Reidel Publishing Company, Dordrecht, Holland, pp.

O'Dowd, C.D., Smith, M.H., Consterdine, I.E., Lowe, J.A., 1997. Marine aerosol, sea-salt, and the marine sulphur cycle: A short review. Atmospheric Environment 31, 73-80.

Okita, T., Morimoto, S., Izawa, S., Konno, W., 1976. Measurement of gaseous and particulate nitrates in the atmosphere. Atmospheric Environment 10, 1085-1089.

Ooki, A., Uematsu, M., Miura, K., Nakae, S., 2002. Sources of sodium in atmospheric fine particles. Atmospheric Environment 36, 4367-4374.

O'Shaughnessy, P.T., Raabe, O.G., 2003. A comparison of cascade impactor data reduction methods. Aerosol Science and Technology 37, 187-200.

Ott, R.L., 1993. An Introduction to Statistical Methods and Data Analysis. Duxbury Press, Belmont, CA, pp. 1051.

Paerl, H.W., 2001. Atmospheric Deposition of Nitrogen in Coastal Waters: Biogeochemical and Ecological Implications. In: Valigura, R.A., Alexander, R.B., Castro, M.S., Meyers, T.P., Paerl, H.W., Stacey, P.E., Turner, R.E. (Ed.), Coastal and Estuarine Studies. American Geophysical Union, Washington, D.C., pp. 11-52.

Pagano, M., Gauvreau, K., 2000. Principles of Biostatistics. Duxbury, Pacific Grove, CA, pp.

Pakkanen, T.A., 1996. Study of formation of coarse particle nitrate aerosol. Atmospheric Environment 30, 2475-2482.

Pakkanen, T.A., Kerminen, V.-M., Hillamo, R.E., Makinen, M., Makela, T., Virkkula, A., 1996a. Distribution of nitrate over sea-salt and soil derived particles - Implications from a field study. Journal of Atmospheric Chemistry 24, 189-205.

Pakkanen, T.A., Kerminen, V.-M., Hillamo, R.E., Makinen, M., Makela, T., Virkkula, A., 1996b. Erratum: Distribution of nitrate over sea-salt and soil

derived particles - implications from a field study. Journal of Atmospheric Chemistry 25, 227.

Patwardhan, A.S., Donigian Jr., A.S., 1995. Assessment of Nitrogen Loads to Aquatic Systems. USEPA, Prepared by AQUA TERRA Consultants, Mountain View, CA.

Perrino, C., De Sanits, F., Febo, A., 1990. Criteria for the choice of a denuder sampling technique devoted to the measurement of atmospheric nitrous and nitric acids. Atmospheric Environment 24A, 617-626.

Perrino, C., De Sanits, F., Febo, A., 1988. Uptake of nitrous acid and nitrogen oxides by nylon surfaces: Implications for nitric acid measurement. Atmospheric Environment 22, 1925-1930.

Perrino, C., Gherardi, M., 1999. Optimization of the coating layer for the measurement of ammonia by diffusion denuders. Atmospheric Environment 33, 4579-4587.

Perrino, C., Ramirez, D., Allegrini, I., 2001. Monitoring acidic air pollutants near Rome by means of diffusion lines: development of a specific quality control procedure. Atmospheric Environment 35, 331-341.

Pilinis, C., Seinfeld, J.H., 1987. Continued development of a general equilibrium model for inorganic multicomponent atmospheric aerosols. Atmospheric Environment 21, 2453-2466.

Pilinis, C., Seinfeld, J.H., Grosjean, D., 1989. Water content of atmospheric aerosols. Atmospheric Environment 23, 1601-1606.

Pio, C.A., Harrison, R.M., 1987. The equilibrium of ammonium chloride aerosol with gaseous hydrochloric acid and ammonia under tropospheric conditions. Atmospheric Environment 21, 1243-1246.

Plate, E., Schulz, M., 1997. Coarse nitrate formation in a coastal area of the North Sea. Journal of Aerosol Science 28, S333-S334.

Platt, U., Perner, D., Harris, G.W., Winer, A.M., Pitts, J.N., 1980. Observations of nitrous acid in an urban atmosphere by differential optical absorption. Nature 285, 312-314.

Poor, N., Pribble, R., Greening, H., 2001. Direct wet and dry deposition of ammonia, nitric acid, ammonium and nitrate to the Tampa Bay Estuary, FL, USA. Atmospheric Environment 35, 3947-3955.

Poor, N.D., Clark, T., Nye, L., Tamanini, T., Tate, K., Stevens, R.K., Atkeson, T., 2002. Field performance of dichotomous sequential PM air samplers. Atmospheric Environment 36, 3289-3298.

Possanzini, M., Febo, A., Liberti, A., 1983. New design of high-performance denuder for sampling of atmospheric pollutants. Atmospheric Environment 17, 2605-2610.

Pryor, S.C., Barthelmie, R.J., 2000a. Particle dry deposition to water surfaces: Processes and consequences. Marine Pollution Bulletin 41, 220-231.

Pryor, S.C., Barthelmie, R.J., 2000b. Particle dry deposition to water surfaces: processes and consequences. In: Sheppard, C. (Ed.), Seas at the Millennium: An Environmental Evaluation. Elsevier Science Ltd., New York, NY, pp. 197-209.

Pryor, S.C., Sorensen, L.L., 2000. Nitric acid-sea salt reactions: Implications for nitrogen deposition to water surfaces. Journal of Applied Meteorology 39, 725-731.

Puttock, J.S., 1981. Data inversion for cascade impactors: Fitting sums of log-normal distributions. Atmospheric Environment 15, 1709-1716.

Ramachandran, G., Johnson, E.W., Vincent, J.H., 1996. Inversion techniques for personal cascade impactor data. Journal of Aerosol Science 27, 1083-1097.

Ramachandran, G., Kandlikar, M., 1996. Bayesian analysis for inversion of aerosol size distribution data. Journal of Aerosol Science 27, 1099-1112.

Rood, M.J., Shaw, M.A., Larson, R.V., Covert, D.S., 1989. Ubiquitous nature of ambient metastable aerosol. Nature 337, 537-539.

Roth, B., Okada, K., 1998. On the modification of sea-salt particles in the coastal atmosphere. Atmospheric Environment 32, 1555-1569.

Russell, A.G., Cass, G.R., 1984. Acquisition of regional air quality model validation data for nitrate, sulfate, ammonium ion and their precursors. Atmospheric Environment 18, 1815-1827.

Saxena, P., Hudischewskyj, A.B., Seigneur, C., Seinfeld, J.H., 1986. A comparative study of equilibrium approaches to the chemical characterization of secondary aerosols. Atmospheric Environment 20, 1471-1483.

Saxena, P., Mueller, P.K., Hildemann, L.M., 1994. Sources and chemistry of chloride in the troposphere: a review. In: Chow, W., Connor, K.K. (Ed.), Managing Hazardous Air Pollutants: State of the Art. CRC Press, Boca Raton, FL, pp. 173-190.

Seinfeld, J.H., Pandis, S.N., 1998. Atmospheric Chemistry and Physics: From Air Pollution to Climate Change. John Wiley & Sons, Inc., New York, NY, pp. 1326.

Sickles II, J.E., Hodson, L.L., 1999. Short communication retention of sulfur dioxide by nylon filters. Atmospheric Environment 33, 2423-2426.

Sievering, H., Gorman, E., Ley, T., Pszenny, A.A.P., Spring-Young, M., Boatman, J.F., Kim, Y.P., Nagamoto, C., Wellman, D.L., 1995. Ozone oxidation of sulfur in sea-salt aerosol particles during the Azores marine aerosol and gas exchange experiment. Journal of Geophysical Research 100, 23075-23081.

Spicer, C.W., 1986. Patterns of atmospheric nitrates, sulfate, and hydrogen chloride in the central Ohio River valley over a one-year period. Environmental International 12, 513-518.

Spicer, C.W., Howes Jr., J.E., Bishop, T.A., Arnold, L.H., Stevens, R.K., 1982. Nitric acid measurement methods: An intercomparison. Atmospheric Environment 16, 1487-1500.

Spurny, K.R., 1999. New Concepts for Sampling, Measurement, and Analysis of Atmospheric Anthropogenic Aerosols. In: Spurny, K.R. (Ed.), Analytical Chemistry of Aerosols. Lewis Publishers, Boca Raton, FL, pp. 49-99.

Stelson, A.W., Friedlander, S.K., Seinfeld, J.H., 1979. A note on the equilibrium relationship between ammonia and nitric acid and particulate ammonium nitrate. Atmospheric Environment 13, 369-371.

Stelson, A.W., Seinfeld, J.H., 1982. Relative humidity and temperature dependence of the ammonium nitrate dissociation constant. Atmospheric Environment 16, 983-992.

Tabazadeh, A., Jacobson, M.Z., Singh, H.B., Toon, O.B., Lin, J.S., Chatfield, R.B., Thakur, A.N., Talbot, R.W., Dibb, J.E., 1998. Nitric acid scavenging by mineral and biomass burning aerosols. Geophysical Research Letters 25, 4185-4188.

Tampa Bay National Estuary Program, 1996. Charting the Course for Tampa Bay. St. Petersburg, FL, pp. 263.

Tang, I.N., 1980. Deliquescence properties and particle size change of hygroscopic aerosols. In: Willeke, K. (Ed.), Generation of Aerosols. Ann Arbor Publications, Ann Arbor, MI, pp. 153-170.

Ten Brink, H.M., 1998. Reactive uptake of HNO_3 and H_2SO_4 in sea-salt (NaCl) particles. Journal of Aerosol Science 29, 57-64.

Ten Brink, H.M., Spoelstra, H., 1998. The dark decay of HONO in environmental (SMOG) chambers. Atmospheric Environment 32, 247-251.

Torseth, K., Semb, A., Schaug, J., Hanssen, J.E., Aamlid, D., 2000. Processes affecting deposition of oxidised nitrogen and associated species in the coastal areas of Norway. Atmospheric Environment 34, 207-217.

Tsai, C.-J., Perng, S.-B., Chiou, S.-F., 2000. Use of two different acidic aerosol samplers to measure acidic aerosols in Hsinchu, Taiwan. Journal of the Air & Waste Management Association 50, 2120-2128.

Valigura, R.A., 2001. An Introduction to the First Assessment of Nitrogen Loads to US Estuaries with an Atmospheric Perspective. In: Valigura, R.A., Alexander, R.B., Castro, M.S., Meyers, T.P., Paerl, H.W., Stacey, P.E., Turner, R.E. (Ed.), Coastal and Estuarine Studies. American Geophysical Union, Washington, D.C., pp. 1-10.

Vogt, R., Elliott, C., Allen, H.C., Laux, J.M., Hemminger, J.C., Finlayson-Pitts, B.J., 1996. Some new laboratory approaches to studying tropospheric heterogeneous reactions. Atmospheric Environment 30, 1729-1737.

Vogt, R., Finlayson-Pitts, B.J., 1994. A diffuse reflectance infrared Fourier transform spectroscopic (DRIFTS) study of the surface reaction of NaCl with gaseous NO_2 and HNO_3. Journal of Physical Chemistry 98, 3747-3755.

Vossler, T.L., Stevens, R.K., Paur, R.J., Baumgardner, R.E., Bell, J.P., 1988. Evaluation of improved inlets and annular denuder systems to measure inorganic air pollutants. Atmospheric Environment 22, 1729-1736.

Wall, S.M., John, W., Ondo, J.L., 1988. Measurement of aerosol size distributions for nitrate and major ionic species. Atmospheric Environment 22, 1649-1656.

Watson, J.G., Chow, J.C., Lurmann, F.W., Musarra, S.P., 1994. Ammonium nitrate, nitric acid, and ammonia equilibrium in wintertime Phoenix, Arizona. Journal of the Air & Waste Management Association 44, 405-412.

Wayne, R.P., 2000. Chemistry of Atmospheres. Oxford University Press, New York, NY, pp.

Weis, D.D., Ewing, G.E., 1999. The reaction of nitrogen dioxide with sea salt aerosol. Journal of Physical Chemistry A 103, 4865-4873.

Wexler, A.S., Seinfeld, J.H., 1991. Second-generation inorganic aerosol model. Atmospheric Environment 25A, 2731-2748.

Williams, R.M., 1982. A model for the dry deposition of particles to natural water surfaces. Atmospheric Environment 16, 1933-1938.

Yeatman, S.G., Spokes, L.J., Jickells, T.D., 2001. Comparisons of coarse-mode aerosol nitrate and ammonium at two polluted coastal sites. Atmospheric Environment 35, 1321-1335.

Zangmeister, C.D., Pemberton, J.E., 1998. In situ monitoring of the NaCl + HNO_3 surface reaction: The observation of mobile surface strings. Journal of Physical Chemistry B 102, 8950-8953.

Zangmeister, C.D., Pemberton, J.E., 2001. Raman spectroscopy of the reaction of sodium chloride with nitric acid: Sodium nitrate growth and effect of water exposure. Journal of Physical Chemistry A 105, 3788-3795.

Zarbock, H.W., Janicki, A.J., Janicki, S.S., 1996. Estimates of Total Nitrogen, Total Phosphorus, and Total Suspended Solids to Tampa Bay, Florida. Technical Appendix: 1992-1994 total nitrogen loadings to Tampa Bay, Florida. Tampa Bay National Estuary Program, Prepared by Coastal Environmental, Inc., St. Petersburg, FL.

Zhuang, H., Chan, C.K., Fang, M., Wexler, A.S., 1999a. Formation of nitrate and non-sea-salt sulfate on coarse particles. Atmospheric Environment 33, 4223-4233.

Zhuang, H., Chan, C.K., Fang, M., Wexler, A.S., 1999b. Size distributions of particulate sulfate, nitrate, and ammonium at a coastal site in Hong Kong. Atmospheric Environment 33, 843-853.

Appendices

	Temp (°C)			RH (%)				Temp (°C)			RH (%)		
	Avg	Min	Max	Avg	Min	Max		Avg	Min	Max	Avg	Min	Max
10/10/01	26	21	30	69	46	84	11/1/01	25	21	29	73	51	90
10/11/01	27	22	31	68	42	87	11/2/01	25	21	29	84	65	96
10/12/01	26	21	31	68	50	87	11/3/01	26	21	31	76	51	94
10/13/01	27	22	31	68	51	84	11/4/01	24	21	27	78	62	91
10/14/01	27	23	30	87	72	97	11/5/01	20	17	23	73	59	87
10/15/01	26	21	30	71	51	94	11/6/01	20	14	26	60	43	78
10/16/01	25	21	29	74	50	87	11/7/01	19	13	24	67	50	87
10/17/01	19	14	24	57	44	75	11/8/01	19	13	25	73	54	90
10/18/01	22	14	29	65	46	81	11/9/01	19	14	24	78	55	100
10/19/01	25	19	31	75	57	91	11/11/01	19	13	25	74	45	97
10/20/01	27	23	31	80	57	94	11/12/01	21	16	27	65	45	84
10/21/01	27	23	30	88	72	97	11/13/01	21	16	27	82	50	96
10/24/01	27	24	30	89	72	97	11/14/01	20	18	22	83	68	91
10/26/01	20	15	25	47	32	91	11/15/01	20	18	22	79	73	90
10/27/01	16	12	20	42	28	62	11/16/01	21	16	27	65	49	81
10/28/01	16	10	21	56	42	77	11/17/01	22	15	28	68	53	87
10/30/01	21	16	26	72	58	81	11/18/01	23	18	27	76	50	93
10/31/01	22	17	27	72	54	87	11/19/01	23	18	27	81	52	93

Table 29. Temperature and relative humidity data for October - November 2001.

	Temp (°C)			RH (%)		
	Avg	Min	Max	Avg	Min	Max
5/2/02	27	24	31	76	59	97
5/4/02	28	23	32	70	52	91
5/6/02	28	24	33	68	41	90
5/10/02	28	24	31	61	44	84
5/14/02	26	22	30	60	48	71
5/15/02	26	22	32	53	39	76
5/16/02	27	24	33	71	40	94
5/17/02	28	25	32	69	46	89
5/19/02	22	18	26	79	63	100
5/20/02	23	18	28	55	45	71
5/23/02	26	20	31	54	35	80
5/24/02	26	20	31	50	32	78
5/25/02	26	21	30	53	37	78
5/31/02	27	23	32	70	47	91

Table 30. Temperature and relative humidity data for May 2002 Azalea Park sampling site.

	Temp (°C)			RH (%)		
	Avg	Min	Max	Avg	Min	Max
5/4/02	26	24	30	76	56	86
5/6/02	28	24	33	67	44	88
5/10/02	28	24	32	61	42	82
5/14/02	25	21	29	63	55	70
5/15/02	27	22	31	50	35	76
5/16/02	26	23	32	74	43	91
5/17/02	27	24	31	71	48	87
5/19/02	21	17	25	81	74	87
5/20/02	22	18	28	58	45	72
5/23/02	25	21	30	54	33	74
5/24/02	25	20	31	52	30	78
5/25/02	26	22	29	50	37	68
5/31/02	26	22	31	73	54	89

Table 31. Temperature and relative humidity data for May 2002 Gandy sampling site.

	Temperature (ºC)			Relative Humidity (%)		
	Avg	Min	Max	Avg	Min	Max
5/6/02	27	22	35	77	44	99
5/10/02	29	21	35			
5/14/02	25	19	36	66	53	77
5/15/02	26	20	32	62	39	89
5/16/02	27	23	33	79	51	99
5/17/02	28	22	35	75	38	99
5/19/02	22	16	28	88	70	97
5/20/02	21	16	28	69	53	81
5/23/02	25	19	31	64	39	93
5/24/02	25	17	31	63	35	98
5/25/02	25	18	30	65	41	95

Table 32. Temperature and relative humidity for May 2002 Sydney sampling site.

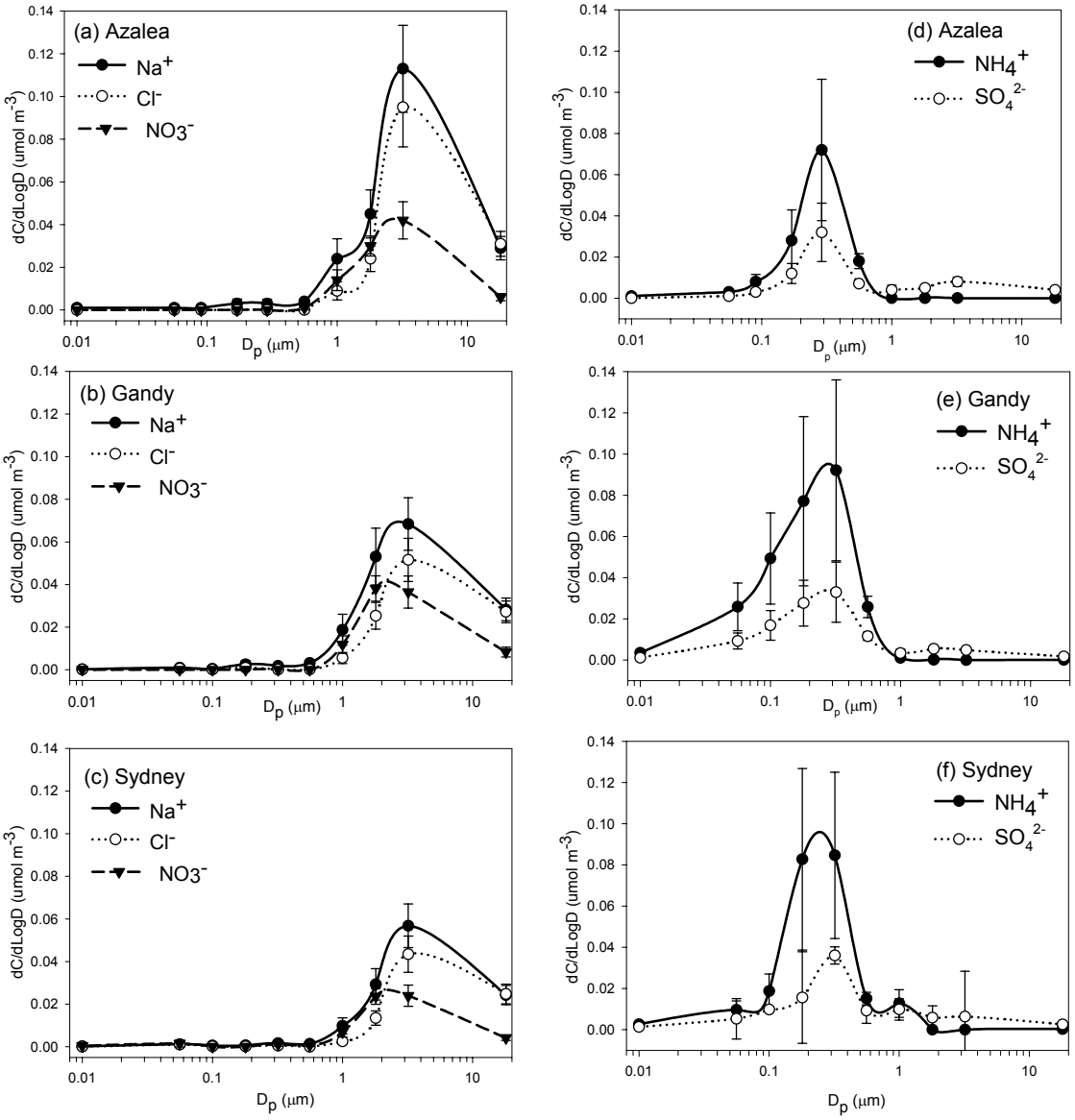

Figure 56. Size distributions for May 10, 2002.

	Azalea	Gandy	Sydney
$Cl^-:Na^+$	0.79	0.69	0.73
$NO_3^-:Na^+$	0.41	0.55	0.46
Cl^--dep %	32%	41%	38%
$NH_4^+:SO_4^{2-}$	2.3	2.8	2.7

Table 33. Ion ratios for May 10, 2002.

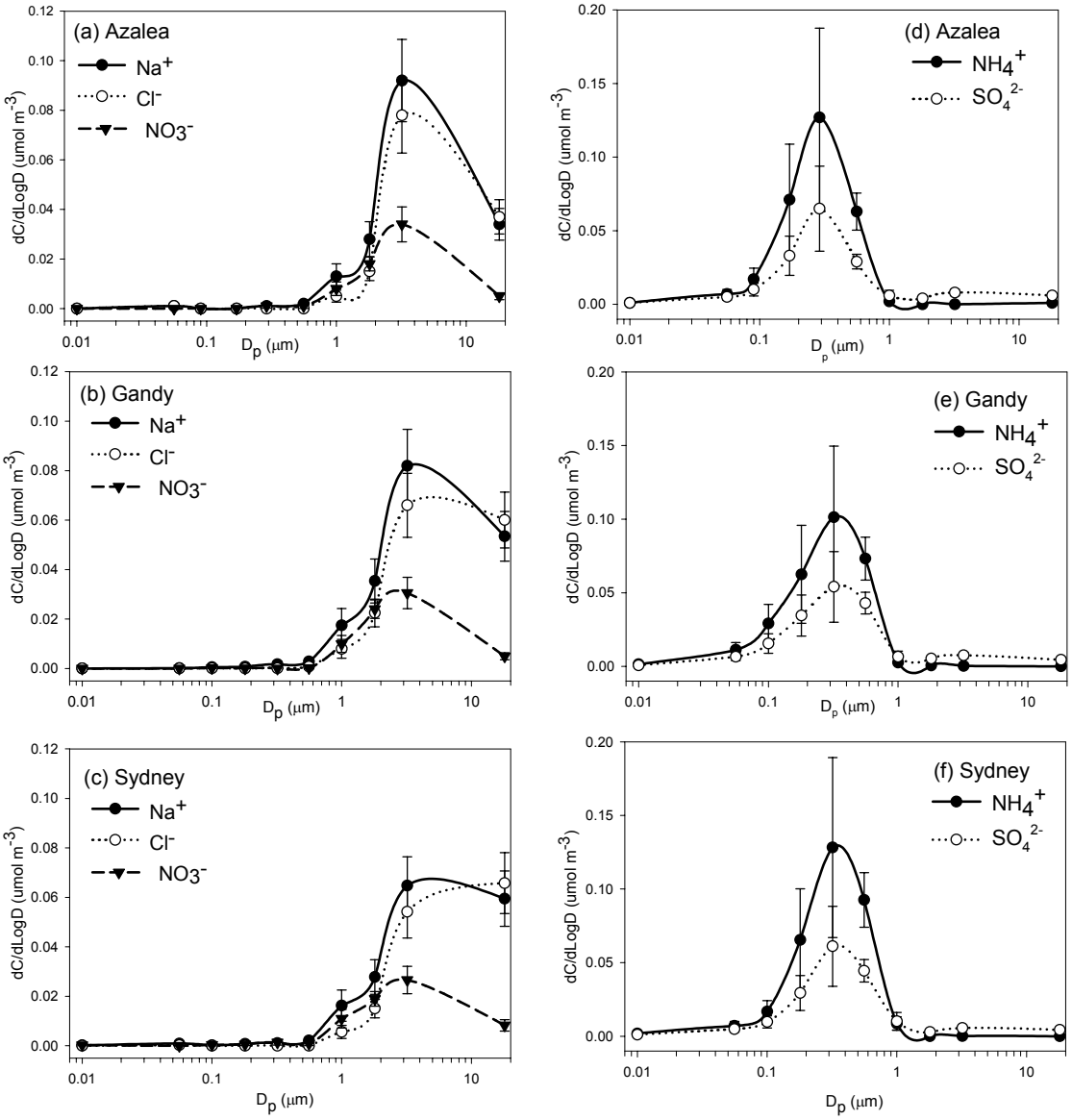

Figure 57. Size distributions for May 15, 2002.

	Azalea	Gandy	Sydney
$Cl^-:Na^+$	0.83	0.81	0.83
$NO_3^-:Na^+$	0.39	0.38	0.40
Cl^--dep %	30%	31%	29%
$NH_4^+:SO_4^{2-}$	2.0	1.8	2.1

Table 34. Ion ratios for May 15, 2002.

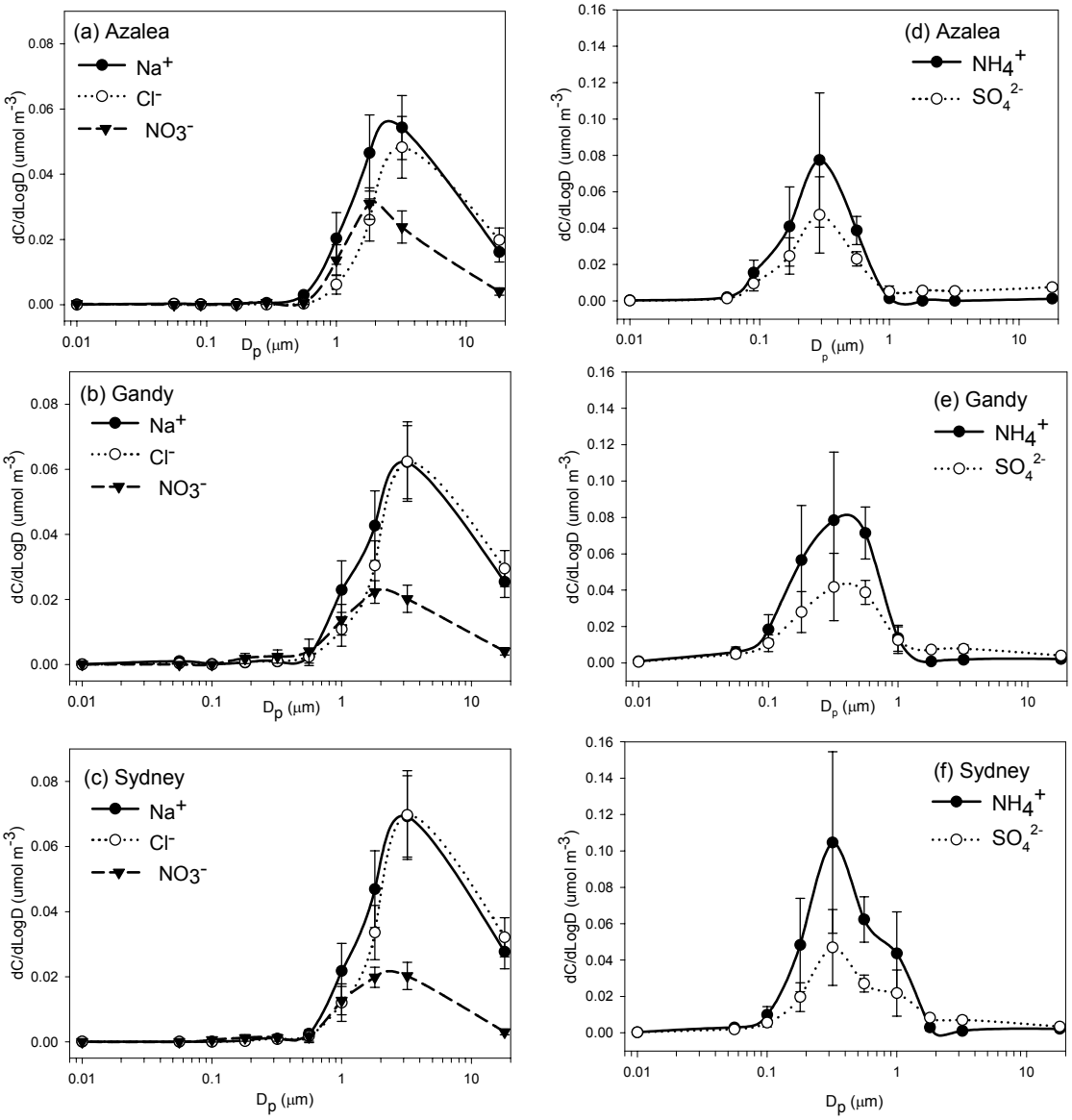

Figure 58. Size distributions for May 16, 2002.

	Azalea	Gandy	Sydney
Cl^-:Na^+	0.80	0.93	0.94
NO_3^-:Na^+	0.49	0.37	0.32
Cl^--dep %	32%	21%	20%
NH_4^+:SO_4^{2-}	1.7	1.9	2.3

Table 35. Ion ratios for May 16, 2002.

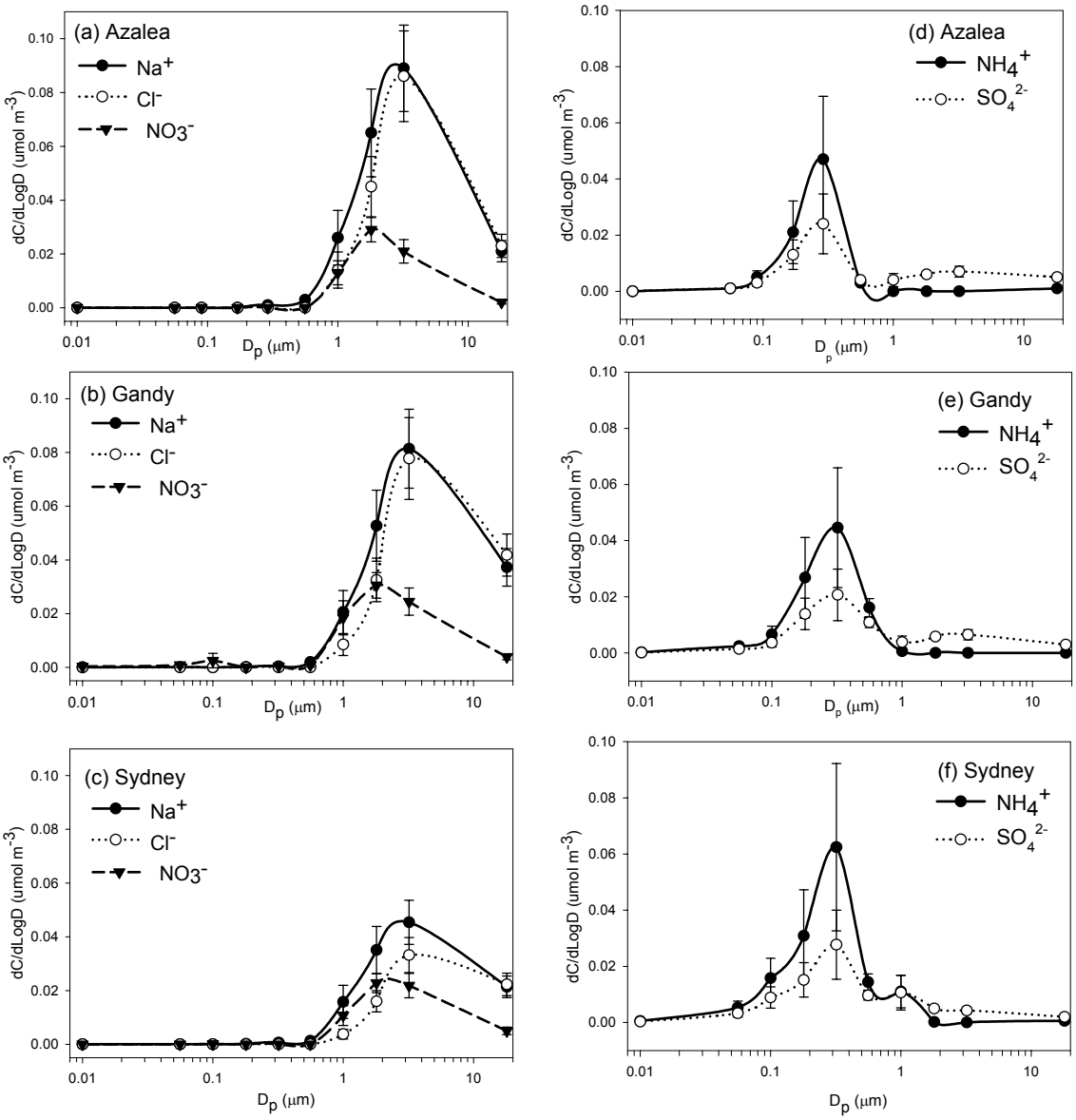

Figure 59. Size distributions for May 17, 2002.

	Azalea	Gandy	Sydney
Cl^-:Na^+	0.90	0.89	0.67
NO_3^-:Na^+	0.29	0.36	0.50
Cl^--dep %	23%	24%	43%
NH_4^+:SO_4^{2-}	1.7	1.9	2.0

Table 36. Ion ratios for May 17, 2002.

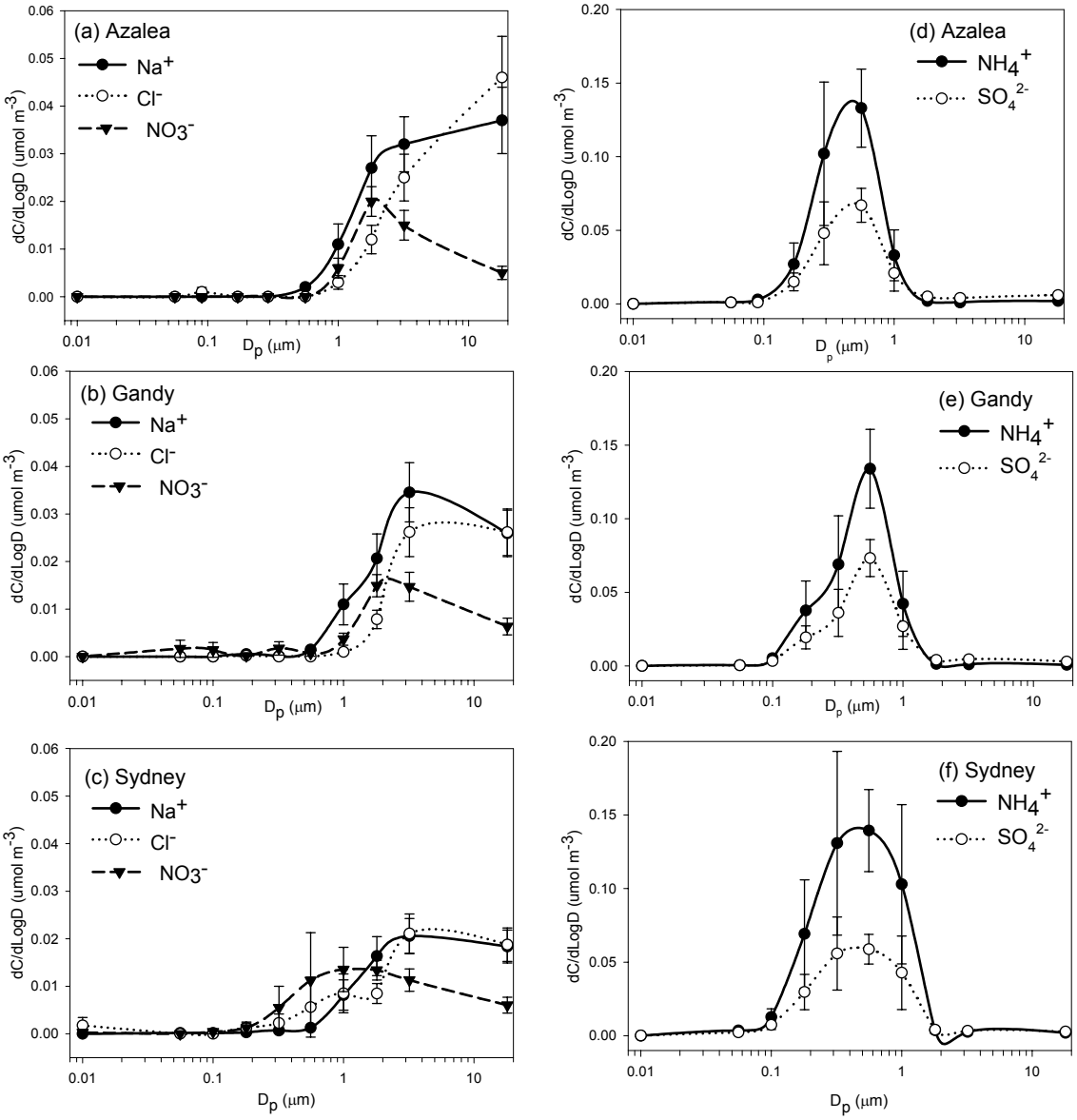

Figure 60. Size distributions for May 19, 2002.

	Azalea	Gandy	Sydney
Cl^-:Na^+	0.77	0.70	0.95
NO_3^-:Na^+	0.45	0.43	0.65
Cl^--dep %	34%	41%	20%
NH_4^+:SO_4^{2-}	2.0	1.9	2.3

Table 37. Ion ratios for May 19, 2002.

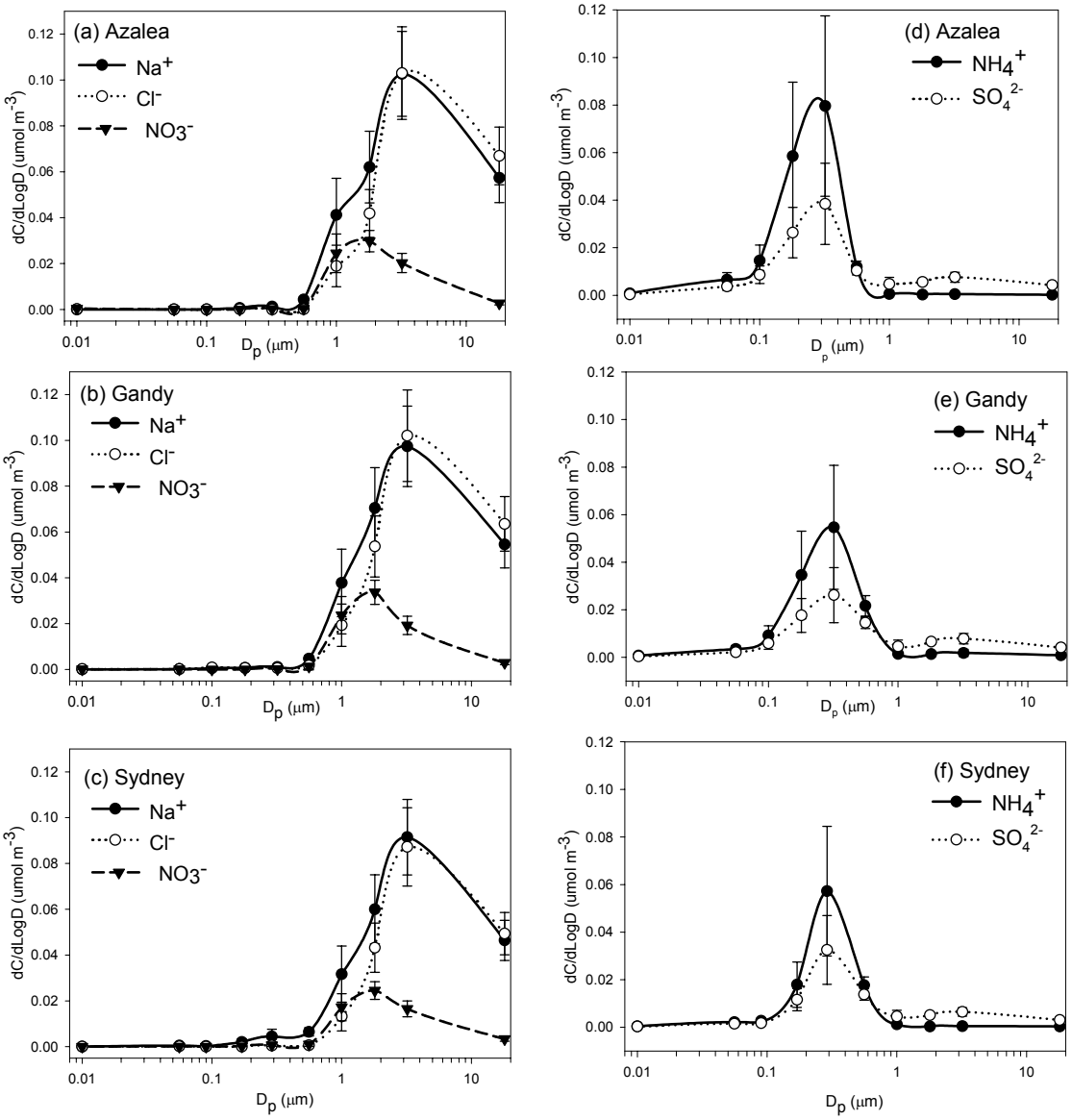

Figure 61. Size distributions for May 23, 2002.

	Azalea	Gandy	Sydney
Cl^-:Na^+	0.93	0.97	0.89
NO_3^-:Na^+	0.26	0.26	0.23
Cl^--dep %	21%	17%	24%
NH_4^+:SO_4^{2-}	2.0	1.9	1.6

Table 38. Ion ratios for May 23, 2002.

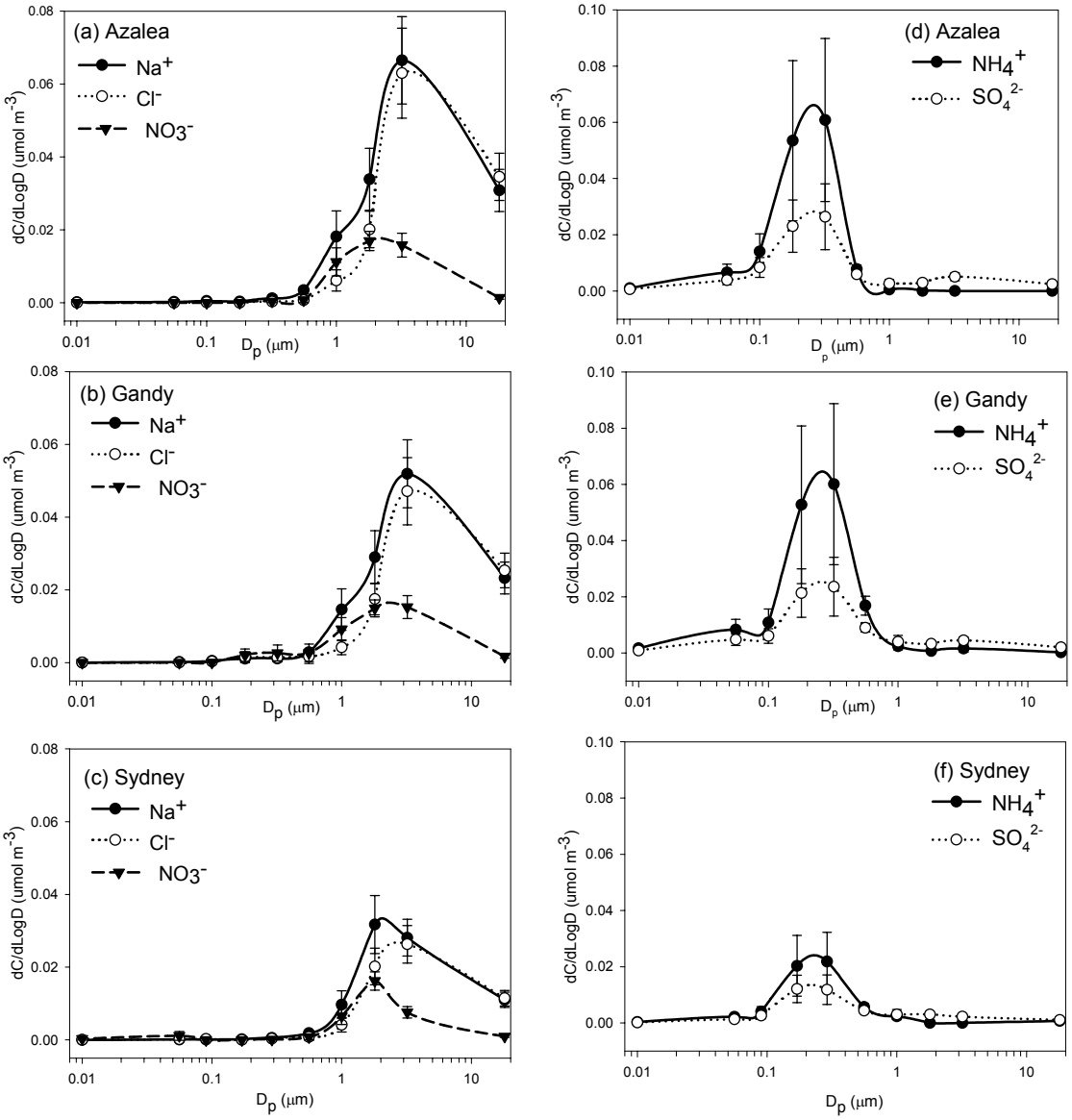

Figure 62. Size distributions for May 24, 2002.

	Azalea	Gandy	Sydney
Cl^-:Na^+	0.88	0.84	0.84
NO_3^-:Na^+	0.28	0.33	0.34
Cl^--dep %	25%	28%	29%
NH_4^+:SO_4^{2-}	2.1	2.3	1.7

Table 39. Ion ratios for May 24, 2002.

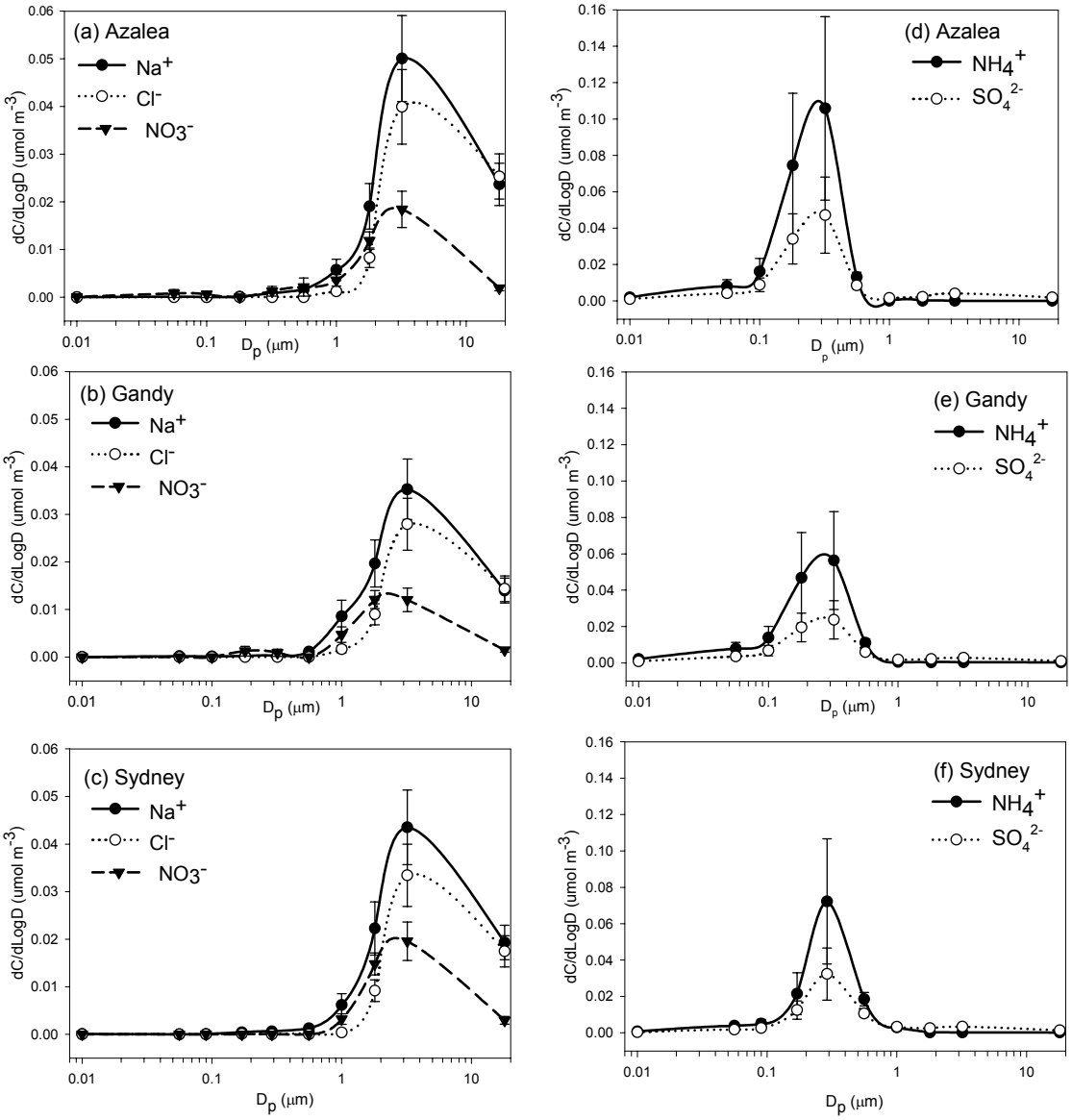

Figure 63. Size distributions for May 25, 2002.

	Azalea	Gandy	Sydney
Cl^-:Na^+	0.77	0.73	0.71
NO_3^-:Na^+	0.37	0.37	0.45
Cl^--dep %	34%	38%	39%
NH_4^+:SO_4^{2-}	2.1	2.3	2.1

Table 40. Ion ratios for May 25, 2002.

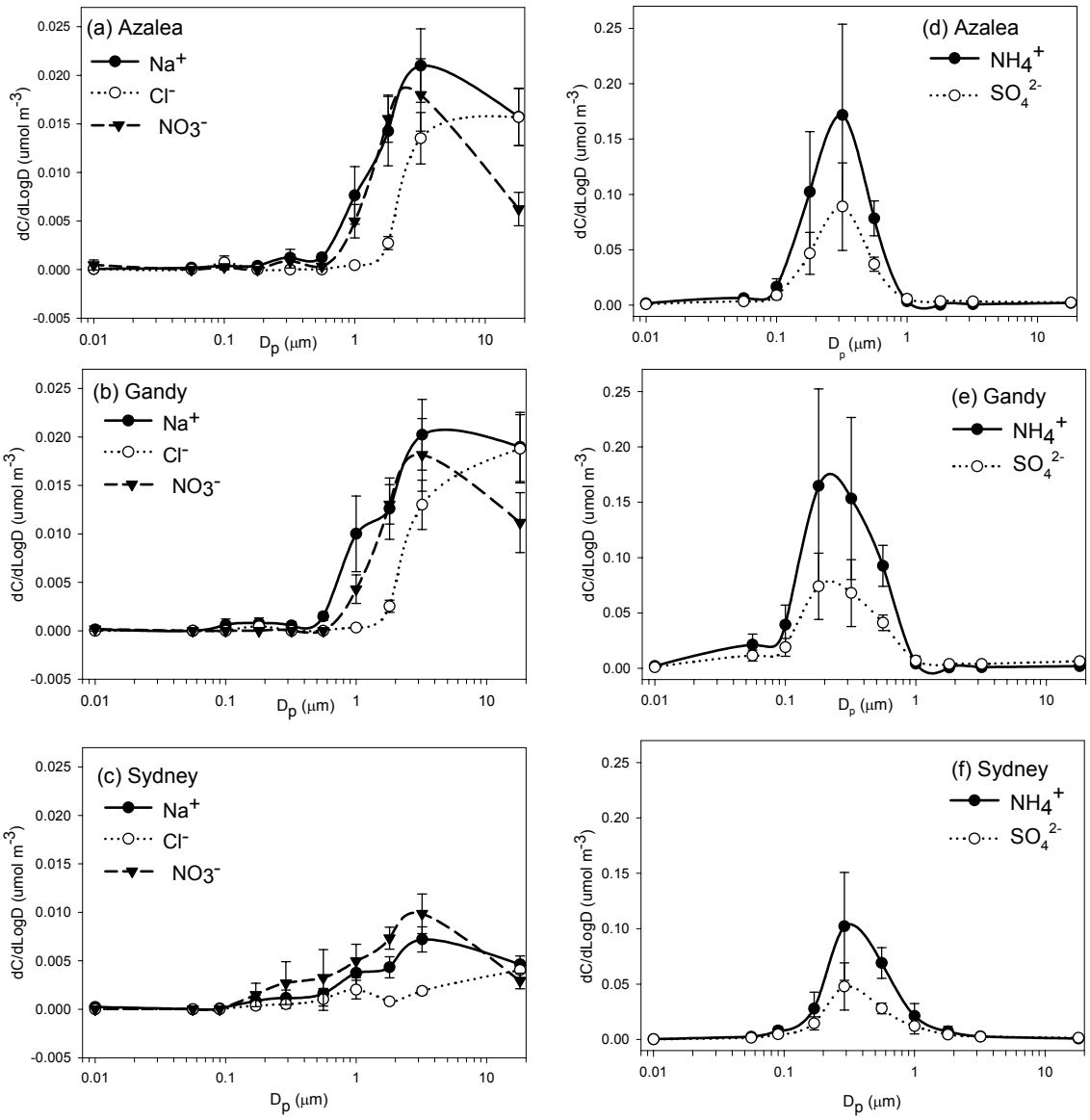

Figure 64. Size distributions for May 31, 2002.

	Azalea	Gandy	Sydney
Cl^-:Na^+	0.58	0.58	0.36
NO_3^-:Na^+	0.81	0.82	1.32
Cl^--dep %	50%	50%	70%
NH_4^+:SO_4^{2-}	2.0	2.2	2.2

Table 41. Ion ratios for May 31, 2002.

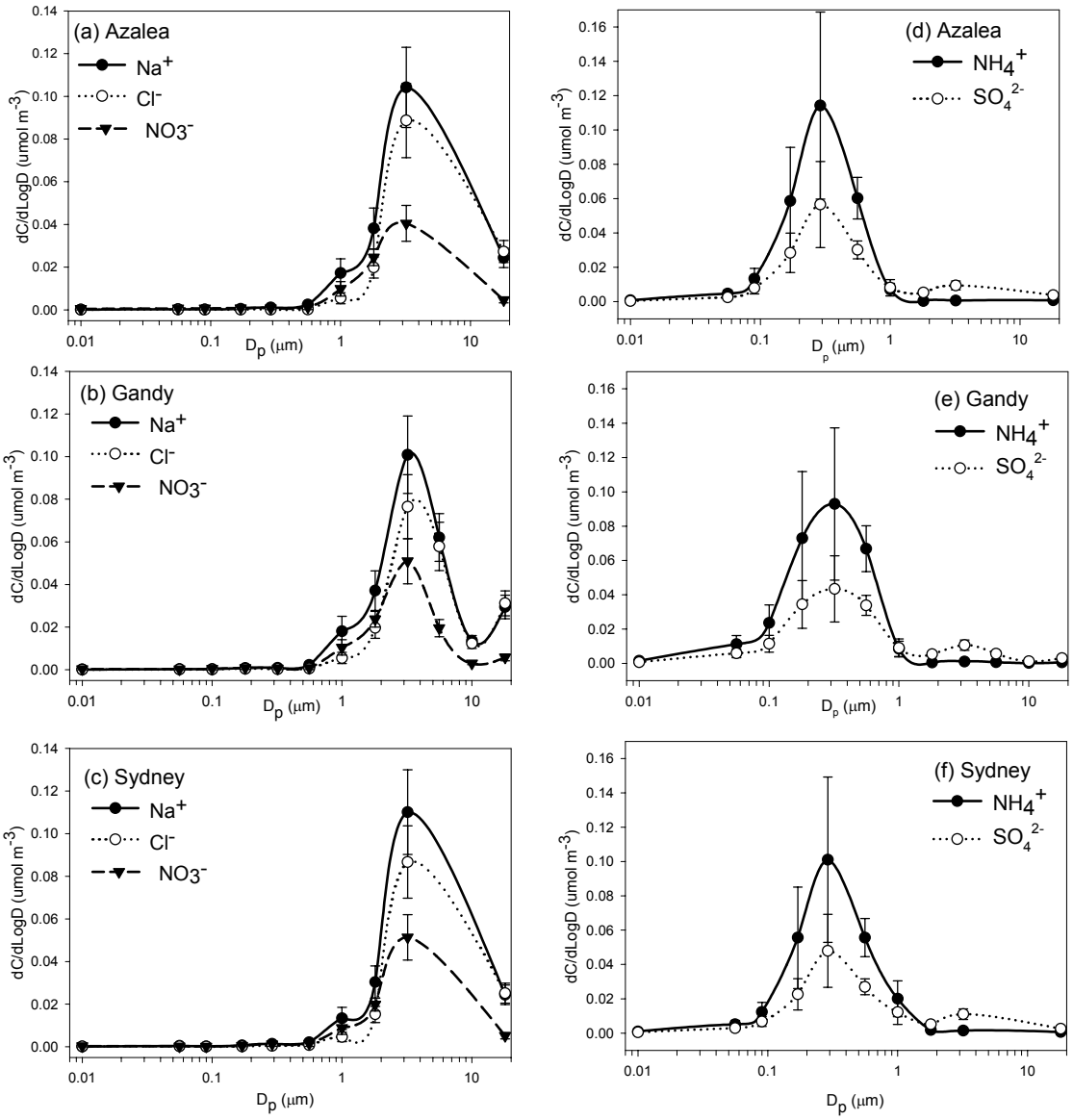

Figure 65. Average size distributions for May 2002.

	Azalea	Gandy	Sydney
Cl^-:Na^+	0.78	0.76	0.72
NO_3^-:Na^+	0.45	0.45	0.54
Cl^--dep %	34%	36%	39%
NH_4^+:SO_4^{2-}	2.0	2.1	2.1

Table 42. Overall ion ratios for May 2002.

Appendix 3. Density Calculation for Aqueous Aerosol

Variables defined:

V_i	molar volume of *i*
X_i	mole fraction of *i*
M_i	molar mass of *i*
ρ_i	density of *i*
w_i	mass fraction of *i* in aqueous phase
F_i	mass fraction of *i* in total particle
soln	solution
s	solute (salt) in aqueous phase of the particle
w	water
solid	solid or crystalline phase of the particle

Aqueous phase:

$$V_{aq} = X_s V_s + X_w V_w$$

$$\frac{M_{aq}}{\rho_{aq}} = X_s \frac{M_s}{\rho_s} + X_w \frac{M_w}{\rho_w}$$

$$M_{aq} = X_s M_s + X_w M_w$$

$$\frac{1}{\rho_{aq}} = \left(\frac{M_s X_s}{M_s X_s + M_w X_w} \right) \frac{1}{\rho_s} + \left(\frac{M_w X_w}{M_s X_s + M_w X_w} \right) \frac{1}{\rho_w}$$

$$\frac{1}{\rho_{aq}} = \frac{w_s}{\rho_s} + \frac{w_w}{\rho_w}$$

$$\rho_{aq} = \frac{1}{\frac{w_s}{\rho_s} + \frac{w_w}{\rho_w}}$$

Overall particle phase:

$$V_{part} = V_{aq} + V_{solid}$$

$$Mass_{part} = Mass_{aq} + Mass_{solid}$$

$$\rho_{part} = \frac{Mass_{aq} + Mass_{solid}}{V_{aq} + V_{solid}} = \frac{Mass_{aq} + Mass_{solid}}{\frac{Mass_{aq}}{\rho_{aq}} + \frac{Mass_{solid}}{\rho_{solid}}}$$

$$F_{aq} = \frac{Mass_{aq}}{Mass_{aq} + Mass_{solid}}$$

$$\rho_{part} = \frac{1}{\frac{F_{aq}}{\rho_{aq}} + \frac{F_{solid}}{\rho_{solid}}}$$

Appendix 4. Size Distributions and Data Inversion

Cascade impactors are the standard instruments for measuring particle size distributions (Puttock, 1981). They separate particles by size according to their inertial properties (O'Shaughnessy and Raabe, 2003). The size distributions result from either directly assigning the collected mass or concentration to the given size on each stage or indirectly through the reduction of the impactor data (O'Shaughnessy and Raabe, 2003).

The direct application of the data assumes that the instrument response is ideal, that the deposition step functions of each stage are perfectly sharp (Cooper and Spielman, 1976; Ramachandran et al., 1996). This is the most widely used approach for treating cascade impactor data (Cooper and Spielman, 1976). The ideal or perfect step function efficiency curve assumption says that all particles greater than a certain size are collected on a particular stage and all particles smaller than that size pass through (Hinds, 1999; Puttock, 1981). This allows the mass or concentration on a stage to be directly assigned to a given particle size. Most well defined impactors can be assumed to be ideal, in that they have a sharp cut-off curve that approaches the ideal curve (Cooper and Spielman, 1976; Hinds, 1999). The following displays the collection efficiencies as a function of particle diameter for the MOUDI sampler (Figure 66).

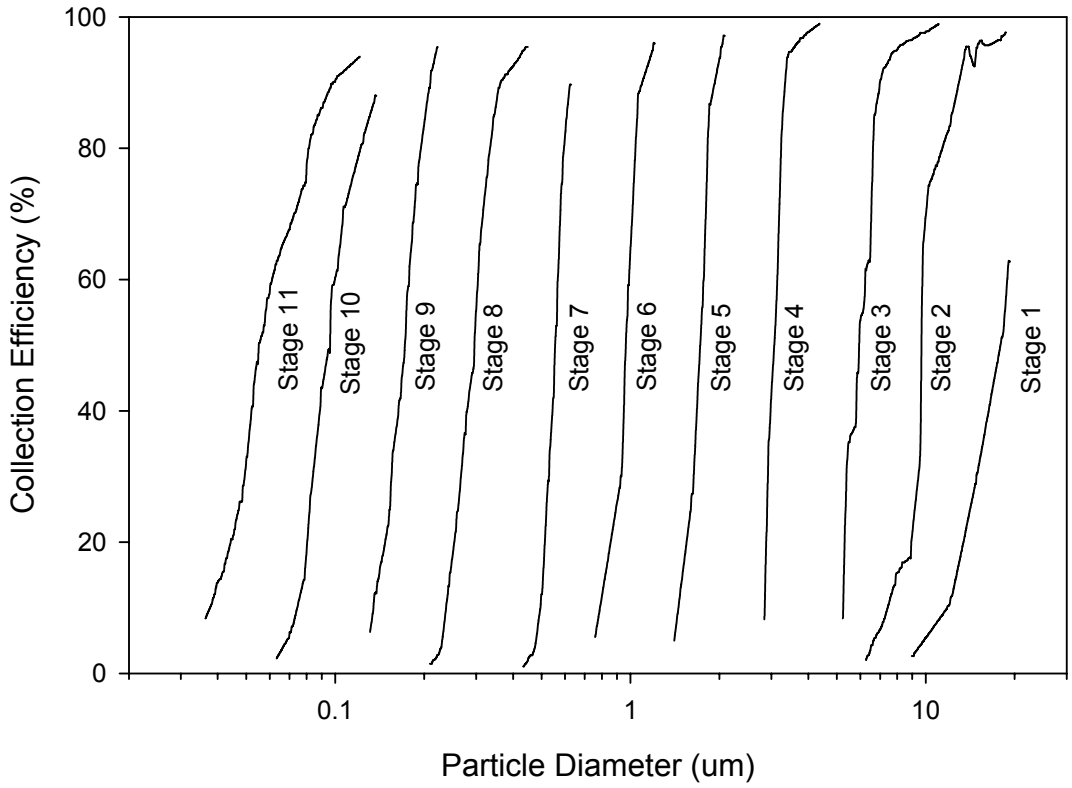

Figure 66. Collection efficiencies as a function of particle diameter for the MOUDI sampler (adapted from Marple et al., 1991).

The cutpoint for each collection stage of a cascade impactor is determined by the 50% collection efficiency point (Hinds, 1999). Each collection stage, or particle bin, has a range of particle sizes collected. The range is determined by the cutpoint characteristics of the adjacent stages.

For cascade impactors with non-ideal, broad responses, the measured data must be reduced through a process known as inversion (Markowski, 1987). Data inversion is the “inference of the particle size distribution function from the

measured stage loadings" (Puttock, 1981). Data inversion is used when the collection characteristics of cascade impactors deviate from ideal and when the impactors provide too few size separations to accurately resolve the complex size distributions occurring in the atmosphere (Puttock, 1981; Ramachandran and Kandlikar, 1996).

The mass on each stage loading is related to the kernel function, which is the fraction of particles that enters the instrument and is collected on a particular stage (Ramachandran et al., 1996; Ramachandran and Kandlikar, 1996). Kernel functions are determined for each stage of the instrument and are a function of the collection efficiency curves. For non-ideal response impactors, kernel functions overlap as particles of a given size are collected on more than one stage (Ramachandran and Kandlikar, 1996). The kernel function can be calculated using:

$$K_i(D_a) = E_i(D_a)\left[1 - E_{i-1}(D_a)\right]\left[1 - E_{i-2}(D_a)\right]\ldots\left[1 - E_1(D_a)\right] \qquad \text{(Equation 38)}$$

where $E_i(D_a)$ is the collection efficiency of the i^{th} stage as a function of the particle aerodynamic diameter. The following shows the kernel functions for the eight stages of the MOUDI sampler used in these studies (Figure 67).

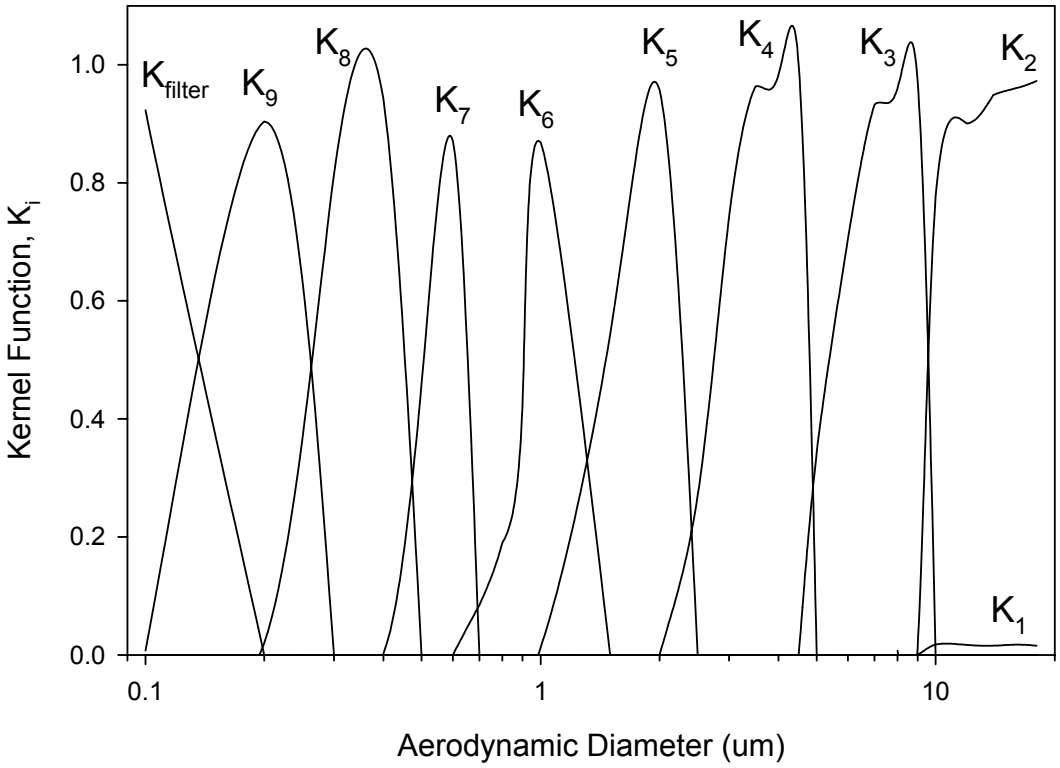

Figure 67. Deposition kernel functions for the MOUDI as functions of particle aerodynamic diameter.

The kernel functions are not strictly independent; there is overlap between them (Ramachandran and Kandlikar, 1996). For stage one of the MOUDI sampler, the kernel function shows poor efficiency for particle collection. The inlet of this instrument was designed for high efficiency for particles less than 10 μm. The top two stages result in less than perfect collection and need to be taken under consideration.

The data inversion process takes the kernel functions and uses them in algorithms. The results are often of poorer quality than those obtained from a direct application of the data, as the inversion problem is ill defined and results in multiple iterations and solutions (Ramachandran and Kandlikar, 1996).

About the Author

Melissa Cheryl Foster Evans was born October 11, 1978 in Michigan. She graduated from Indian Rocks Christian High School as co-valedictorian in 1995. In 1999, she earned a Bachelor of Arts degree in Chemistry from the University of South Florida, graduating cum laude from the University Honors Program. She continued her education at that institution, where she completed her requirements for a Doctor of Philosophy degree in Physical Chemistry in December 2003.